STAGED SURGICAL PALLIATION AND VENTRICULAR PERFORMANCE IN FUNCTIONALLY SINGLE VENTRICLE ANATOMY

by

SIMON PROSSER MCGUIRK

A thesis submitted to
the Faculty of Medicine and Dentistry of
The University of Birmingham
for the degree of
DOCTOR OF PHILOSOPHY

School of Clinical and Experimental Medicine
College of Medical and Dental Sciences
The University of Birmingham.
October 2009.

ABSTRACT

This thesis reports a series of laboratory and clinical studies designed to investigate the acute effect of surgical palliation on ventricular function in children with functionally single ventricle anatomy. Ventricular volume and pressure were measured using a combined pressure-conductance catheter.

Initial laboratory-based experiments were performed using a physical model of the left ventricle, which allowed examination of the measurement techniques used in the clinical studies but under controlled conditions. These experiments identified a non-linear conductance-absolute volume relationship and demonstrated for the first time that the calibration coefficient, α_{SV} produced a significant, volume-dependent measurement error. These experiments also demonstrated that conductance volume measurements were adversely influenced by other electrical signals. The ventricular electrogram produced clinically important measurement error that has not previously been described..

Two clinical studies were then undertaken to investigate the separate effects of the bidirectional cavo-pulmonary anastomosis (BCPA) and the completion total cavo-pulmonary connection (TCPC). These studies represent the core of the thesis. Both procedures were associated with significant changes in the pressure and volume conditions of the dominant ventricle. In addition, the BCPA was associated with a substantial and immediate improvement in ventricular systolic function but this was accompanied by an increase in diastolic chamber stiffness. By contrast, the TCPC was not associated with a significant change ventricular systolic or diastolic function in spite of the changes in ventricular load. Comparable changes were observed in patients with a dominant ventricle of either left or right ventricular morphology.

These studies provide a more detailed understanding about the acute events that accompany surgical palliation in children with functionally single ventricle anatomy. These findings confirm the validity of staged surgical palliation in the management of these children.

DEDICATION

To Becky, Harry, Ethan and Jessica with all my love.

ACKOWLEDGEMENTS

I would like to thank a number of people that have helped make this project possible. I would particularly like to thank my supervisors, Professor John Coote and Mr David Barron, for their repeated encouragement, considered advice and general support. I would also like to thank Mr William Brawn, Dr Oliver Stumper and Dr Monica Stokes and all the other clinical staff at Birmingham Children's Hospital for their help with the clinical aspects of the study.

The research undertaken in this thesis was supported by a British Heart Foundation Project Grant (FS/03/102) and I would like to the British Heart Foundation and their sponsors for this support.

PERSONAL CONTRIBUTION

This thesis details the work undertaken during a period of dedicated research in the Department of Cardiac Services at Birmingham Children's Hospital. While the work contained in the thesis is wholly my own, the projects described could not have been achieved without the help of others.

The experimental studies described in Chapters 4 and 5 utilised a physical model developed by Dr HA Al-Khalidi at the University of Birmingham. These experiments would not have been possible without the help and support of Professor John H Coote (supervisor). The design and data collection used in these studies was my own responsibility.

Data analysis required the development of custom-made software developed in Matlab® (The MathWorks, Cambridge, UK). This was only possible with the help of Dr Dan Ewert and his team at the Department of Electrical and Computer Engineering, North Dakota State University, ND, USA. Additional custom-made software was subsequently developed in Delphi (Borland Software Corporation, Austin, TX, USA) with Mr John Stickley at Birmingham Children's Hospital.

All of the human studies were conducted at Birmingham Children's Hospital. I consented all of the patients and dealt with the organisational matters relating to this study. Patients were anaesthetised by the consultant anaesthetist of the day. All surgical procedures were performed by Mr William J Brawn or Mr David J Barron (co-supervisor). All of the procedures used in this study (insertion of the conductance catheter; application of the aortic flow probe; and transient inferior vena caval occlusion) were performed by the primary surgeon. I was responsible for data collection, post-processing, analysis and interpretation. I also took the lead role in publications resulting from this work.

PERSONAL PUBLICATIONS ARISING FROM THIS RESEARCH

1. McGuirk, S.P., Winlaw, D.S., Langley, S.M., Stumper, O.F., de Giovanni, J.V., Wright, J.G., Brawn, W.J. and Barron, D.J. The impact of ventricular morphology on midterm outcome following completion total cavopulmonary connection. *European Journal of Cardio-Thoracic Surgery*. 2003;24:37-46.
   (Cited but not discussed in this thesis)

2. McGuirk, S.P., Barron, D.J., Ewert, D. and Coote, J.H. Calibrating volume measurements made using the dual-field conductance catheter. *Journal of Biomedical Science and Engineering*. 2009;2:484-490.

3. McGuirk, S.P., Barron, D.J., Ewert, D. and Coote, J.H. Electrocardiographic interference and conductance volume measurements. *Journal of Biomedical Science and Engineering*. 2009;2;491-498.

TABLE OF CONTENTS

CHAPTER 2 (continued)

LIST OF ILLUSTRATIONS

CHAPTER 2. GENERAL INTRODUCTION

CHAPTER 2 (continued)

CHAPTER 3. GENERAL METHODS

CHAPTER 4. CALIBRATING VOLUME MEASUREMENTS MADE USING THE DUAL-FIELD CONDUCTANCE CATHETER

CHAPTER 5. ELECTROCARDIOGRAPHIC INTERFERENCE AND CONDUCTANCE VOLUME MEASUREMENTS

CHAPTER 6. ACUTE CHANGES IN VENTRICULAR PERFORMANCE FOLLOWING BIDIRECTIONAL CAVO-PULMONARY ANASTOMOSIS

CHAPTER 7. ACUTE CHANGES IN VENTRICULAR PERFORMANCE FOLLOWING TOTAL CAVO-PULMONARY CONNECTION

LIST OF TABLES

LIST OF ABBREVIATIONS

A	cross-sectional area
α	chamber stiffness and scaling coefficient (assessment of ventricular compliance)
	dimensionless calibration coefficient (conductance volume measurements)
α_{SV}	stroke conductance-stroke volume calibration coefficient
$\alpha_{V(t)}$	conductance-volume calibration coefficient
α_{VV}	calibration coefficient based on the $\alpha_{V(t)}$-volume relation
ACT	activated clotting time
ANOVA	analysis of variance
Atm	atmosphere
ATP	adenosine triphosphate
AoP	aortic pressure
AV	atrio-ventricular
AV	atrio-ventricular valve
β	chamber stiffness coefficient (assessment of ventricular compliance)
	damping coefficient (characterisation of catheter-manometer system)
B	magnetic field strength
β_0	damping constant
BCPA	bidirectional cavo-pulmonary anastomosis
BDG	bidirectional Glenn
BSA	body surface area
C	arterial compliance
	velocity of ultrasound in blood (ultrasound flow measurement only)
Ca	arterial concentration of substance
CHD	congenital heart disease
cm	centimetre
cmH_2O	centimetre of water
CO	cardiac output
CO_2	carbon dioxide
cos	cosine
CPA	central pulmonary arteries
CPB	cardio-pulmonary bypass

$C(t)$	time varying concentration of substance
Cv	venous concentration of substance
CVP	central venous pressure
d	slice thickness
$DILV$	double inlet left ventricle
DKS	Damus-Kaye-Stansel
ΔL	instantaneous change in muscle length
dl/dt	rate of muscle shortening (isotonic contraction)
d_n	nth pressure overshoot
$DOLV$	double outlet left ventricle
dP	instantaneous change in pressure
dP/dt	first-derivative of pressure with respect to time
dP/dt_{max}	maximal first-derivative of pressure with respect to time
dP/dt_{min}	maximal negative first-derivative of pressure with respect to time
dt	change in time
dV	instantaneous change in volume
dV/dt	first-derivative of volume with respect to time
ΔV_{ECG}	Difference in conductance volume associated with ECG interference (%)
e	electromagnetic force
E	elastance
Ea	arterial elastance
ECG	electrocardiogram
$ECGc$	intracavitary electrogram
$EDPVR$	end-diastolic pressure-volume relation
ED	end-diastole
EDV	end-diastolic volume
EDV'	estimated end-diastolic volume
$EDVI$	indexed end-diastolic volume
E_{ES}	end-systolic elastance
EEV	end-ejection volume
EF	ejection fraction
E_{max}	maximal elastance

ES	end-systole
ESPVR	end-systolic pressure-volume relation
ESV	end-systolic volume
E(t)	time-varying elastance
f_0	undamped natural frequency
f_d	damped natural frequency
F_iO_2	inspired oxygen concentration
γ	relative frequency
g	gram
$G_i(t)$	time-varying conductance signal
$G_i^+(t)$	time-varying conductance signal with ECG interference
$G_i^-(t)$	time-varying conductance signal without ECG interference
$G_{ECG}(t)$	time-varying ECG interference
Abbrev	meaning
G_P	parallel conductance
h	ventricular wall thickness
HLHS	hypoplastic left heart syndrome
HR	heart rate
Hz	hertz
IABP	intra-aortic balloon pump
IPCCC	International Paediatric and Congenital Cardiac Code
IVC	inferior vena cava
IVCO	inferior vena caval occlusion
kg	kilogram
kHz	kilohertz
Λ	logarithmic decrement of pressure
L	inter-electrode distance
	distance between crystals (ultrasound flow measurement only)
L_0	Muscle length at which resting and active tension are both approximately zero (isometric contraction)
L_{max}	Muscle length at which active tension is maximal (isometric contraction)
LA	left atrium

LAP	left atrial pressure
LV	left ventricle
LVP	left ventricular pressure
LVEDV	left ventricular end-diastolic volume
LVEF	left ventricular ejection fraction
μA	micro amp
mA	milliamp
MA	mitral atresia
m	metre
	amount of indicator injected (indictor-dilution estimate of blood flow only)
μg	microgram
mg	milligram
min	minute
ml	millilitre
mLA	morphological left atrium
mLV	morphological left ventricle
mm	millimetre
mmHg	millimetres of mercury
MPA	main pulmonary artery
mRA	morphological right atrium
MRI	magnetic resonance imaging
mRV	morphological right ventricle
MS	mitral stenosis
M(t)	amount of indicator taken up
%N-EDV	end-diastolic volume as a percentage of the expected end-diastolic volume in normal children
%N-EF	ejection fraction as a percentage of the expected left ventricular ejection fraction in normal children
NaCl	sodium chloride
n	number
NYHA	New York Heart Association
Ω	ohms

ϕ	angle of ultrasound beam
P	total load (isotonic and isometric contraction)
	intraventricular pressure (*in vivo* measurements)
P_0	maximum isometric tension (isotonic contraction)
	pressure at time, t=0 (*in vivo* measurements)
P_∞	non-zero pressure asymptote
$P(t)$	time-varying pressure
PA	pulmonary artery
PAt	pulmonary atresia
$PAt\text{-}IVS$	pulmonary atresia with intact ventricular septum
P_aCO_2	partial pressure of carbon dioxide
PAP	pulmonary arterial pressure
$PCWP$	pulmonary capillary wedge pressure
P_aO_2	partial pressure of oxygen
P_{ED}	end-diastolic pressure
P_{ES}	end-systolic pressure
$PRSW$	preload-recruitable stroke work
PS	pulmonary stenosis
$PTFE$	polytetrafluoroethylene
PVA	pressure-volume area
PVR	pulmonary vascular resistance
$\dot{Q}$	blood flow
Q_{ED}	end-diastolic conductance
Q_{ES}	end-systolic conductance
$\dot{Q}p$	pulmonary blood flow
$\dot{Q}s$	systemic blood flow
Q_{SV}	stroke conductance
$\overline{Q}_{SV}$	average stroke conductance
$Q(t)$	time-varying conductance volume
ρ	specific resistivity of blood (conductance volume measurements)
R	arterial resistance
RA	right atrium

RMS	root mean square
RMBTS	right modified Blalock-Taussig shunt
R_T	total mean vascular resistance
RV	right ventricle
RVEDV	right ventricular end-diastolic volume
RVOTO	right ventricular outflow tract obstruction
RVP	right ventricular pressure
RV-PA	right ventricle-pulmonary artery
s	second
SA	sino-atrial
SaO_2	systemic arterial oxygen saturation
$SpaO_2$	pulmonary arterial oxygen saturation
$SpvO_2$	pulmonary venous oxygen saturation
$SsvO_2$	systemic venous oxygen saturation
SV	stroke volume
$\overline{SV}_{AoF}$	average stroke volume calculated using aortic flow probe
SVC	superior vena cava
SVR	systemic vascular resistance
SW	stroke work
τ	tau, time constant of pressure decay
t	time
t_1	time after which indicator has completely passed
T	wall tension (Laplace's law)
$T_{1/2}$	time for pressure to decline by 50% of starting value
TA	tricuspid atresia
T_c	cardiac cycle length
^{99m}Tc	technetium-99m
TCPC	total cavo-pulmonary connection
T_d	time period of each complete cycle
TGA	transposition of the great arteries
t_{max}	time to maximal elastance
TVR	total vascular resistance

u	flow velocity
$\bar{u}$	average flow velocity
$U(x)$	blood flow velocity in the axial direction
$uAVSD$	unbalanced atrio-ventricular septal defect
v	rate of muscle shortening (isotonic contraction)
v_{max}	velocity of shortening of muscle fibres at zero load (isotonic contraction)
V	volume
V_0	equilibrium volume (assessment of time-varying elastance)
	volume of heart at zero end-diastolic pressure (assessment of ventricular compliance)
VSD	ventricular septal defect
$V(t)$	time-varying volume
$V(t)$	time-varying calibrated conductance volume
ω_0	angular frequency of undamped motion
ζ	measurement error
ζ_{SV}	measurement error associated with α_{SV}
$\zeta_{V(t)}$	measurement error associated with $\alpha_{V(t)}$
Z	impedance
Z_c	characteristic impedance

PERSONAL CONTRIBUTION

This thesis details the work undertaken during a period of dedicated research in the Department of Cardiac Services at Birmingham Children's Hospital. While the work contained in the thesis is wholly my own, the projects described could not have been achieved without the help of others.

The experimental studies described in Chapters 4 and 5 utilised a physical model developed by Dr HA Al-Khalidi at the University of Birmingham. These experiments would not have been possible without the help and support of Professor John H Coote (supervisor). The design and data collection used in these studies was my own responsibility.

Data analysis required the development of custom-made software developed in Matlab® (The MathWorks, Cambridge, UK). This was only possible with the help of Dr Dan Ewert and his team at the Department of Electrical and Computer Engineering, North Dakota State University, ND, USA. Additional custom-made software was subsequently developed in Delphi (Borland Software Corporation, Austin, TX, USA) with Mr John Stickley at Birmingham Children's Hospital.

All of the human studies were conducted at Birmingham Children's Hospital. I consented all of the patients and dealt with the organisational matters relating to this study. Patients were anaesthetised by the consultant anaesthetist of the day. All surgical procedures were performed by Mr William J Brawn or Mr David J Barron (co-supervisor). All of the procedures used in this study (insertion of the conductance catheter; application of the aortic flow probe; and transient inferior vena caval occlusion) were performed by the primary surgeon. I was responsible for data collection, post-processing, analysis and interpretation. I also took the lead role in publications resulting from this work.

CHAPTER 1

GENERAL OVERVIEW

CHAPTER 1. GENERAL OVERVIEW

Congenital heart disease is the single most common form of birth defect, which affects approximately 1% of all children born in the United Kingdom. The term *functionally single ventricle anatomy* refers to a heterogeneous group of complex heart malformations, in which one of the two ventricular chambers is either absent or severely underdeveloped. These heart defects preclude the establishment of a normal, biventricular circulation because the hypoplastic ventricular cavity is unable to support either the systemic or the pulmonary circulation.

Without surgical intervention, children with functionally single ventricle anatomy have a very poor prognosis. Long-term survival is dependent on a series of palliative operations, which culminate in the Fontan procedure. This procedure involves the direct connection of the central veins to the central pulmonary arteries, which creates a circulation in which the systemic and pulmonary circulations are connected in series, without an intervening ventricle. The single ventricle acts as a systemic ventricle only while blood flow through the pulmonary circulation is maintained by the venous pressure in the systemic veins.

The successful management of functionally single ventricle anatomy is thus fundamentally dependent on the performance of the dominant ventricle. Unfortunately, the children with functionally single ventricle anatomy are characterised by abnormal circulatory haemodynamics, which change during the course of surgical palliation. These abnormal circulatory haemodynamics may profoundly influence the performance of the ventricle and hence could potentially influence the clinical outcome of children with functionally single ventricle anatomy. For that reason, accurate measurements of cardiac volume, pressure and blood flow are critically important to allow a comprehensive evaluation of changes in ventricular function that may accompany each stage of surgical palliation and the subsequent post-operative period.

The main purpose of the experimental and clinical studies described in this thesis was to measure critical indices of ventricular performance to help determine the effect of surgical palliation in children with functionally single ventricle anatomy. As a necessary framework to these studies,

Chapter 2 traces the history of present knowledge and basic physiology of normal cardiac function and its assessment together with an outline of congenital heart disease. This is followed in Chapter 3 by a detailed consideration of the methods that have been used to measure cardiac function in man for the assessment of pressure, volume and flow within the heart. This leads to the aims and objectives of the subsequent investigations.

The results of the research are described in four separate chapters. In order to gain a more accurate assessment of ventricular performance in children with functional single ventricle anatomy, a pressure-conductance catheter was used to invasively measure the intraventricular pressure and volume. This is the first clinical study that has used this catheter in these children. Therefore, the performance of this catheter was thoroughly investigated in a series of laboratory-based experiments using different sized balloons to simulate the functional single ventricle. The results of these experiments are described in Chapters 4 and 5. The final two results chapters describe the use of the pressure-conductance catheter in two separate clinical studies. These studies were designed to investigate the changes in ventricular function that accompany two surgical procedures performed at Birmingham Children's Hospital.

The overall aim of this thesis was to provide important new information about ventricular function and the effects of surgical palliation in children with functionally single ventricle anatomy. This information may help inform the post-operative care of these children as well as establishing a benchmark for any subsequent investigation.

CHAPTER 2

GENERAL INTRODUCTION

CHAPTER 2. GENERAL INTRODUCTION

2.1 NORMAL CARDIOVASCULAR SYSTEM

The normal adult human cardiovascular system consists of two separate circulations, the systemic circulation and pulmonary circulation. The systemic circulation delivers oxygenated blood to the organs of the body. The pulmonary circulation transports blood to the lungs for gas exchange with oxygen uptake and release of carbon dioxide. The two circulations are connected in series; blood flows through the systemic circulation then the pulmonary circulation before returning to the systemic circulation, Figure 2.1 [1]. Blood flow is maintained by the function of the heart, which acts as an integral pump within the cardiovascular system. In particular, intermittent contraction of the left ventricle supports blood flow through the systemic circulation and synchronous contraction of the right ventricle supports blood flow through the pulmonary circulation.

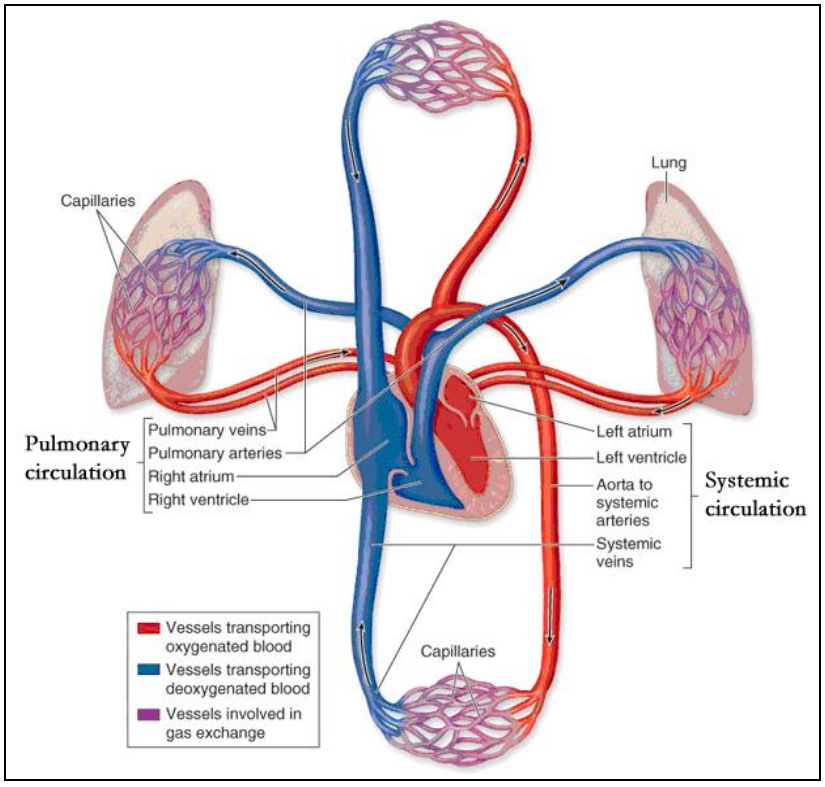

Figure 2.1 *Schematic illustration of the normal cardiovascular system. This includes the heart together with the arteries, veins and capillaries that form both the systemic and pulmonary circulations. Reproduced from http://academic.kellogg.cc.mi.us/herbrandsonc/bio201_McKinley/f22-1_cardiovascular_sy_c.jpg*

The normal human heart consists of four separate chambers and two arterial trunks that are connected sequentially. The left atrium connects to the left ventricle through the mitral valve and the left ventricle is connected to the aorta through the aortic valve. Oxygenated pulmonary venous blood flows from the pulmonary veins through the left atrium, left ventricle and then into the aorta (the systemic circulation). Similarly, the right atrium connects to the right ventricle through the tricuspid valve and the right ventricle is connected to the pulmonary trunk through the pulmonary valve. Deoxygenated systemic venous blood flows from the superior and inferior vena cavae into the right atrium, right ventricle and then into the pulmonary trunk (the pulmonary circulation), Figure 2.2 [1].

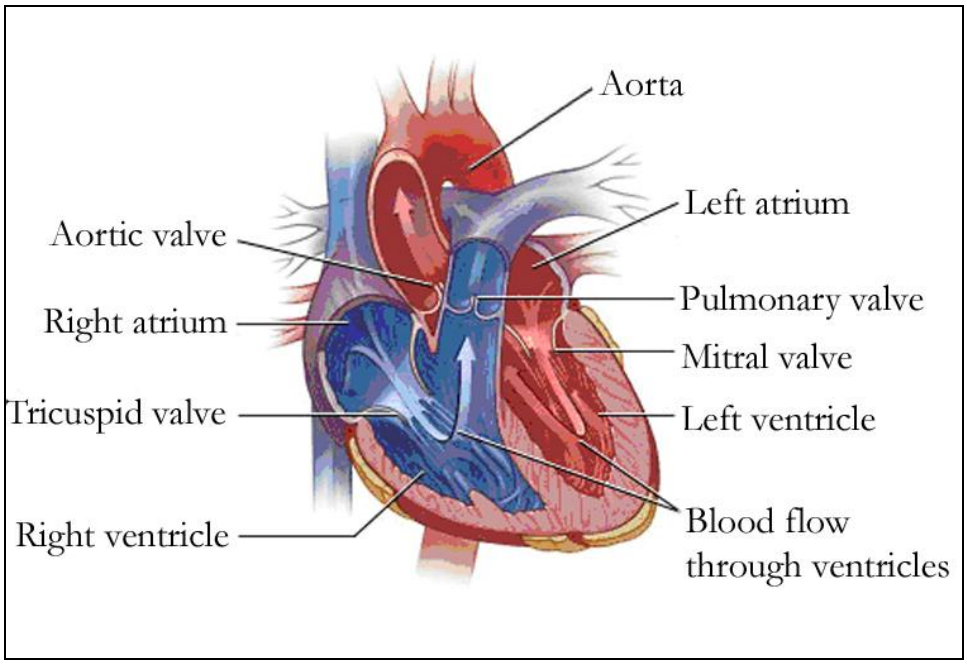

Figure 2.2 *Schematic illustration of the inside of the normal human heart, including the four chambers, four valves and two outflow tracts. The arrows indicate the direction of blood flow through the heart. Reproduced from http://www.nhlbi.nih.gov/health/dci/images/heart_interior.gif.*

2.2 THE PUMP FUNCTION OF NORMAL MYOCARDIUM

The ability of the heart to function as a pump is determined, firstly, by events at the level of the individual cardiac myocyte and, secondly, by how these myocytes function together within the cardiac chambers.

2.2.1 Cardiac myocyte anatomy

The myocardium of the mammalian heart consists of a three-dimensional branching network of myocytes embedded within a supporting connective tissue matrix [2,3]. The myocytes are organised into bundles, called myofibres that are arranged in a series of layers around the chambers of the heart [2,3]. The myocytes are connected end to end with one another by specialised domains within the plasma membrane, called intercalated discs. Intercalated discs mediate electrical and structural coupling between adjacent cells [4], allowing the myocardium to operate as a functional syncitium.

2.2.2 The sliding filament model of contraction

The sarcomere represents the fundamental contractile unit within the myocyte. Each sarcomere is composed of two sets of parallel and partly overlapping filaments. The thin filaments are composed mainly of actin and the thick filaments are made of myosin. During muscle contraction, the actin filaments at each end of the sarcomere slide between the myosin filaments towards the middle of the sarcomere. Consequently, the sarcomere shortens without any change in the lengths of the filaments themselves. This is known as the sliding filament model of contraction [5,6].

The force produced by myocyte contraction is dependent on a number of factors, including the length of the sarcomere [7]. In isolated cardiac muscle preparations, there is a rapid rise in the active force developed as the sarcomere length is increased from 1.8μm to 2.2μm, Figure 2.3. The force developed then declines rapidly as the sarcomere length is increased beyond 2.2 μm.

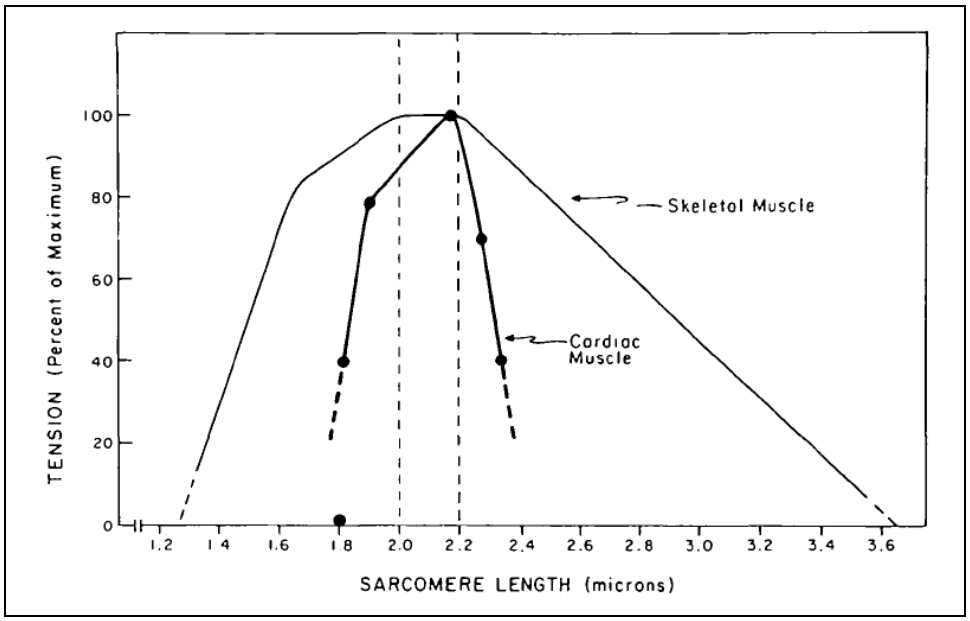

Figure 2.3 *The relation between tension development and sarcomere length in cat papillary muscle. The relation in skeletal muscle fibres has been superimposed for comparison. Reproduced from Sonnenblick & Skelton* [7].

Most of the features observed in Figure 2.3 can be accounted for by the sliding filament model of contraction [8]. Maximum force is developed when sarcomere length produces optimum overlap of filaments, as this enables maximal cross-bridge formation. The decreased force generated at smaller lengths has been attributed to progressive penetration of the thin filaments across the midline and into the other half of the sarcomere. These additional thin filaments causes a steric interference of the normal thick-thin filament interaction, which inhibits cross-bridge formation [9]. The decreased force generated at higher sarcomere lengths occurs because there are a diminishing number of potential sites for cross-bridge formation.

2.2.3 Myocardial function in isolated muscle preparations

Much of our understanding about the mechanical behaviour of the heart has been obtained from in vitro experiments with isolated cardiac muscle specimens. The muscle specimen, placed in an oxygenated physiologic saline solution, is suspended within a myograph that allows simultaneous measurements of the tension and length of the muscle [8]. A simplified diagram of the myograph is illustrated in Figure 2.4. The lower end of the muscle is attached to a strain gauge and the upper end is connected to an isotonic lever. A series of weights can be attached to the other end

of the lever. This mechanical load is subdivided into preload and afterload. The term preload describes the small load that stretches the quiescent muscle to an initial pre-contracted length. A mechanical stop above the lever prevents further stretching of the muscle if additional load is added to the lever. This additional load is termed afterload and is only encountered by the muscle when it attempts to shorten. The muscle is then activated with a suprathreshold electrical stimulus. Contracting muscle may develop a force without shortening; shorten at various velocities; or may lengthen if the load is greater than the force that the muscle can generate.

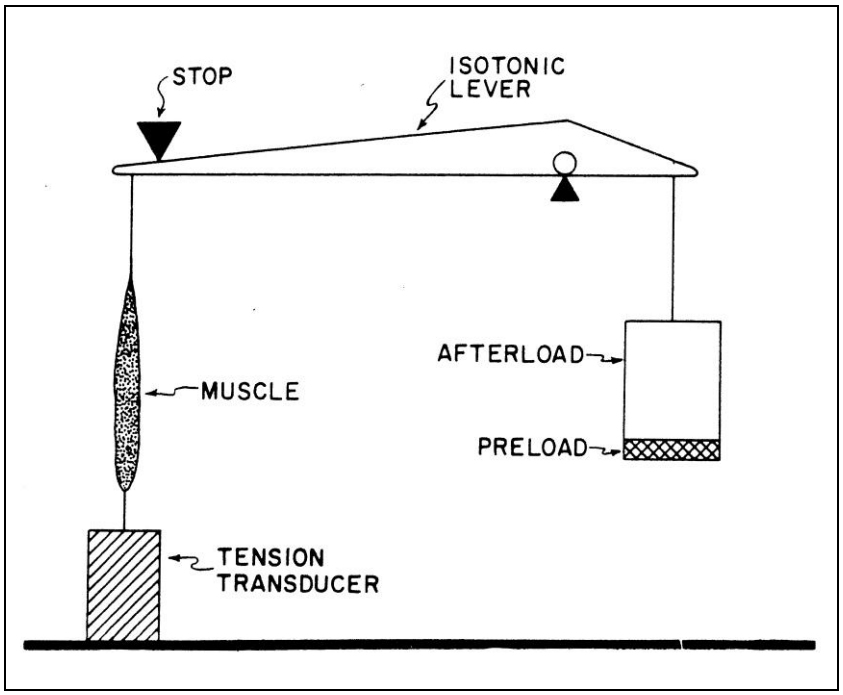

Figure 2.4 *Diagrammatic illustration of the myograph. The papillary muscle is suspended in a physiological bath (not shown). The lower end of the papillary muscle is attached to a tension transducer and the upper end is attached to a lever system, which is free to move. The fulcrum of the lever system is shown on the right. Load (preload and afterload) is placed on the opposite end of the lever. The mechanical 'stop' limits lever movement and thus determines the maximal length of the muscle specimen. Reproduced from Braunwald et al.* [10]*, pp. 45.*

In isolated muscle preparations, the output of a muscle is described by three interrelated and interdependent variables, namely tension, length and time. The analysis of muscle performance is simplified by experimentally holding one variable constant and determining the relationship between the other two variables. This approach yields two types of muscle contraction: isometric

(same length) and isotonic (same tension) contraction. Analysis of these two types of contraction allows a complete evaluation of the mechanical properties of isolated muscle.

Most of the original studies that investigated the behaviour of isolated cardiac muscle were performed with isolated papillary muscles obtained from the right ventricle of the cat. The muscle fibres in the feline papillary muscle are arranged in a longitudinal, parallel fashion. These muscles are also sufficiently thin to allow oxygen diffusion in vitro, thus avoiding potentially deleterious hypoxic damage to the muscle specimen under experimental conditions [9]. However, the muscle fibres do not have the geometric complexity observed in the intact ventricle.

2.2.3*a* *Isometric contraction and the length-tension relationship*

During isometric contraction, the muscle is stretched to a chosen resting length and both ends are then fixed. This prevents any external shortening of the muscle. When stimulated, the muscle develops tension, which rises to a peak before returning to the quiescent level [11]. The maximal tension and time to peak tension developed during isometric contraction are primarily influenced by changes in either the resting muscle length or the level of inotropy [11].

The length-tension curve provides a more complete description of the relationship between muscle length and tension in isolated muscle [11,12]. This curve is obtained by measuring the muscle tension, both at rest and during isometric contraction, as the resting muscle length is increased. The force generated by contraction (active tension) represents the difference between total tension and resting tension. Typical length-tension curves from feline papillary muscle are shown in Figure 2.5. In this example, the starting length, L_0 was defined as the muscle length where resting tension was zero and active tension was approximately zero [12].

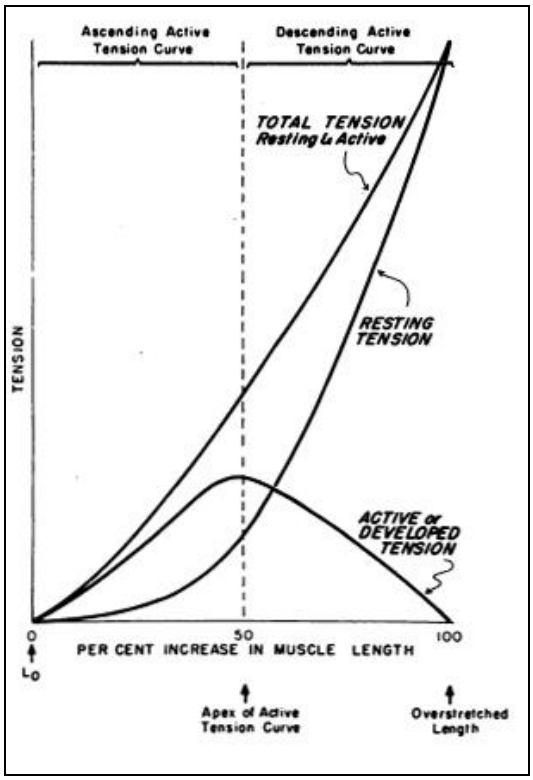

Figure 2.5 *Length-tension relation of cat papillary muscle. Total tension = resting (or passive) plus active (or developed) tension. Reproduced from Sonnenblick et al.* [12].

Active length-tension relationship

In cardiac muscle, like all forms of striated muscle, the force generated during isometric contraction varies as a function of muscle length. There is a rise in active tension as muscle length is increased from L_0. Active tension reaches a maximum when the resting muscle length is increased by approximately 45%. This muscle length, L_{max} marks the apex of the active length-tension curve. Further increases in muscle length are associated with a decline in active tension. Active tension developed is almost zero when the resting muscle length is increased by approximately 100% (Figure 2.5) [12]. By convention, the active length-tension relation is described as two separate parts; the active length-tension relation between L_0 and L_{max} is called the ascending limb of the curve while the relation beyond L_{max} is termed the descending limb of the curve [13].

Under physiological conditions, the myocardium normally functions only on the ascending limb of the active length-tension relation [12]. The upper limit of end-diastolic pressure in the normal

heart is about 12 mmHg. This pressure corresponds with a sarcomere length of 2.2μm [14], the sarcomere length at which active tension is maximal. Therefore, in the intact heart, increasing muscle length produces a greater force of contraction. This relationship forms the basis of the Frank-Starling law [15,16] in which, "the larger the diastolic volume of the heart … the greater is the energy of its contraction" [16].

Resting length-tension relationship

The resting length-tension curve in cardiac muscle is characterised by a non-linear length-tension relation, Figure 2.5. The resting tension is zero at L_0 [13] but rises exponentially as the muscle length is increased [17]. As a result, resting tension contributes between 15 to 50% of the total muscle tension at L_{max} [7,18].

The relatively high resting tension in cardiac muscle is due to passive elastic elements within the heart muscle [19]. These include collagen and elastin fibres found primarily in the extracellular matrix of the myocardium [18,20] but also ultrastructural components within the myocyte [21]. These passive elastic elements prevent excessive lengthening of cardiac muscle and ensure that the cardiac muscle operates on the ascending limb of the length-tension relation under physiological conditions [22].

2.2.3*b* *Isotonic contraction and the force-velocity relationship*

The complete assessment of the mechanical properties of cardiac muscle involves the analysis of muscle shortening and shortening velocity, as well as the force-generating characteristics of the muscle. The shortening characteristics are measured during isotonic contraction.

During simple isotonic contraction, one end of the muscle is fixed while the other end is attached to the mobile isotonic lever. Preload attached to the other end of the lever determines the initial muscle length. Stimulation causes the muscle shortens to a minimum length (ΔL) before elongating to the resting length. The shortening velocity (dl/dt, v) rises to a peak during early contraction and then declines as shortening ensues. The muscle tension remains constant

throughout simple isotonic contraction [23]. When afterload is also added to the lever (afterloaded isotonic contraction), the muscle must initially contract isometrically until the muscle tension equals the total load (P, i.e. preload plus afterload), after which isotonic muscle shortening can begin [11]. Increments in afterload are associated with a delay in the time to peak velocity and a progressive fall in both the peak velocity and extent of shortening.

There is an inverse relationship between the velocity of shortening and the total load, as illustrated in the force-velocity curve (Figure 2.6). When the afterload is increased until no shortening occurs, the maximum isometric tension (P_0) is developed. As the load is reduced, there is a progressive increase in the shortening velocity, which is greatest when the load is smallest. The velocity of shortening at zero load (unloaded shortening, v_{max}) cannot be measured directly but can be estimated by extrapolation of the force-velocity curve to zero load. The parameters, P_0 and v_{max} define the limits for a given force-velocity curve and reflect the contractile properties of the muscle specimen [11].

In cardiac muscle, the force-velocity relation is not fixed but varies with changes in the initial muscle length (i.e. preload) and the level of inotropy. Increments in the initial muscle length are accompanied by an increase in P_0 and a rise in the shortening velocity at each individual load. This results in a rightward shift in the force-velocity curve. However, v_{max} remains essentially unchanged. By contrast, inotropic stimuli are associated with an increase in both P_0 and v_{max}. This, in turn, results in a rightward and upward shift in the force-velocity curve [11].

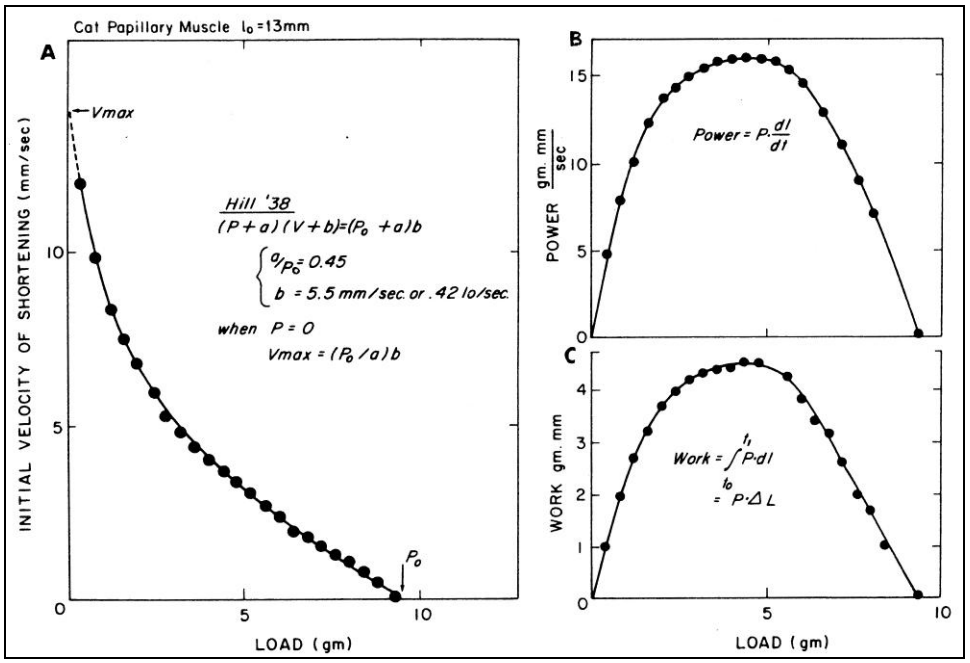

Figure 2.6 *Force-velocity relations obtained during afterloaded isotonic contractions.* A, *Velocity of shortening is plotted as a function of load. As the load increases, the velocity of shortening decreases. When velocity is zero, the force is equivalent to the isometric contraction* (P_0). *When the curve is extrapolated to zero load,* v_{max} *is obtained.* B *and* C, *Power and work are shown as a function of increasing afterload. Power and work are zero at both zero load and isometric contraction; both peak at an intermediate load. Reproduced from Braunwald et al.* [10], *pp. 45.*

Sonnenblick proposed that v_{max} may represent an index of cardiac contractility, since it was apparently unchanged by changes in preload but was altered by changes in the contractile state [11]. However, the number of assumptions and uncertainties involved in the calculation has limited the value of v_{max} in routine practice [24]. In addition, it has been demonstrated that v_{max} varies somewhat with preload and the model used to calculate it [24,25].

In addition to the assessment of contractile properties, force-velocity relation obtained from afterloaded isotonic contractions allow quantification of *work* and rate of work, i.e. *power* produced by the heart muscle (Equations 2.1 and 2.2, respectively).

Equation 2.1 $$Work = \Delta L \cdot P$$

Equation 2.2 $$Power = v \cdot P$$

For a given muscle length in a constant physicochemical environment, work and power vary as a function of the total load (Figure 2.6). Work increases with increasing afterload and reaches a peak at a load approximately 40% of P_0. Further increases in afterload result in a decline in work, which is zero when the load is too great to allow shortening. Increases in preload and inotropy are associated with an increase in maximal work and the load at which maximal work was performed. However, the shape of the workload curve remains essentially unchanged. Work per contraction is thus a complex function of the initial muscle length, the load and the force-velocity curve on which the muscle operates. A similar relationship also exists for muscle power (Figure 2.6).

2.3 MYOCARDIAL FUNCTION IN THE INTACT HEART

Early studies of cardiac function attempted to extrapolate the behaviour of isolated cardiac muscle to the function of the intact heart as a whole [26,27]. However, the complex three-dimensional arrangement of muscle fibres [3] means that it is very difficult to accurately measure the tension or length of individual myofibres within the ventricular mass [28]. For example, the length of the sarcomere also varies according to the position within the ventricular wall; sarcomeres in the subendocardial layer are generally longer than those in the subepicardial layer [29]. In addition, the normal pattern of ventricular contraction is characterised by marked regional heterogeneity, with more pronounced deformation and wall motion in the left ventricular free wall than the interventricular septum [30]. These factors have limited the applicability of the length-tension relation to the assessment of ventricular function, particularly the assessment *in vivo*.

2.3.1 Changes in ventricular pressure and volume in the intact heart

At the turn of the twentieth century, Frank established the basis of modern cardiodynamics [28]. He postulated that the performance of the ventricle could be defined, like a mechanical pump, by changes in pressure, volume and flow within the ventricle [31]. This approach involves the assessment of the ventricle as a *system* rather than the analysis of the *individual* muscle properties.

However, the two approaches are interrelated. Ventricular volume (V) varies as a function of the dimensions of the heart (i.e. radius) and, by extension, the sarcomere length [32]. Similarly, the intraventricular pressure is related to wall tension by Laplace's law (Equation 2.3).

Equation 2.3 $$P = \frac{T \cdot 2h}{r}$$

where P is the intraventricular pressure; T is wall tension; h is the ventricular wall thickness; and r is the radius of the spheroid.

2.3.1*a* *Changes in ventricular pressure*

In a series of experiments using isolated, perfused ranine hearts, Frank recorded the active and passive pressure within the frog ventricle during isovolumic and isobaric contractions [15] (Figure 2.7). The passive intraventricular pressure increased with increments in the ventricular volume (Figure 2.7A). There was a progressive rise in the isovolumic pressure as the ventricular volume is increased (curves 1 – 6; Figure 2.7A). However, beyond a certain level of filling, the isovolumic pressure declined (curves 3 – 4; Figure 2.7B).

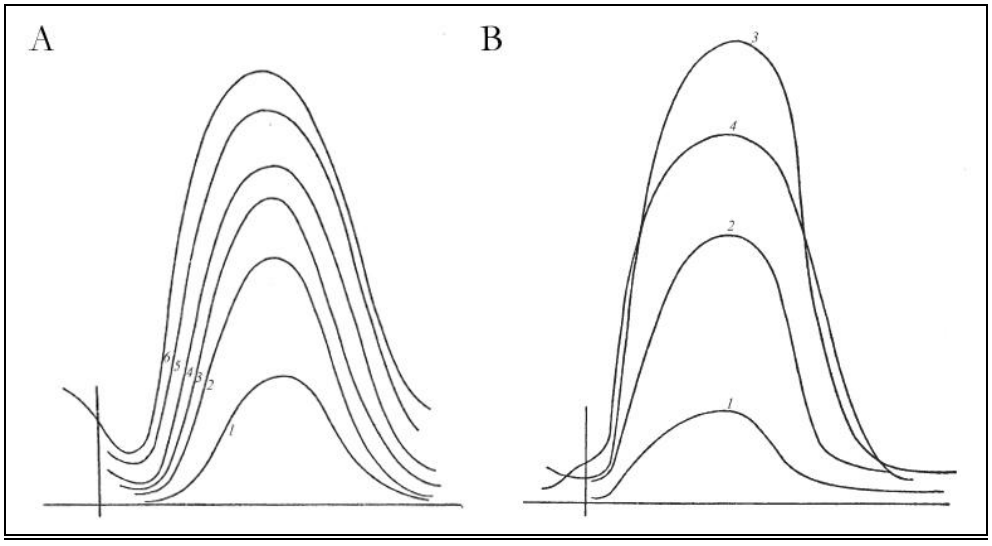

Figure 2.7 *Effect of increasing initial filling on the isovolumic pressure curve.* A*, The peak isovolumic pressure and passive pressure both increased with increments in initial filling.* B*, Beyond a certain level of filling, peak isovolumic pressure declined. Reproduced from Zimmer* [33].

2.3.1*b* *Changes in the pressure-volume relations of the intact heart*

Frank devised a schematic diagram to characterise contractions of the frog ventricle in a pressure-volume diagram [28] (Figure 2.8). The top curve, labelled "Isomet. maxima" represents the peak pressure developed during isovolumic contraction at various ventricular volumes. Frank called this curve the maximal isometric pressure curve, although we now know that the wall fibre length is not constant during isovolumic contraction [34]. The maximal pressure curve rises rapidly with the increase in volume. Beyond a certain volume, the curve levels off and then falls to a final point where it meets the passive pressure-volume curve ("Isomet. minima"). These two curves are equivalent to the active and passive length-tension curves obtained in isolated muscle specimens, as previously described (Figure 2.5).

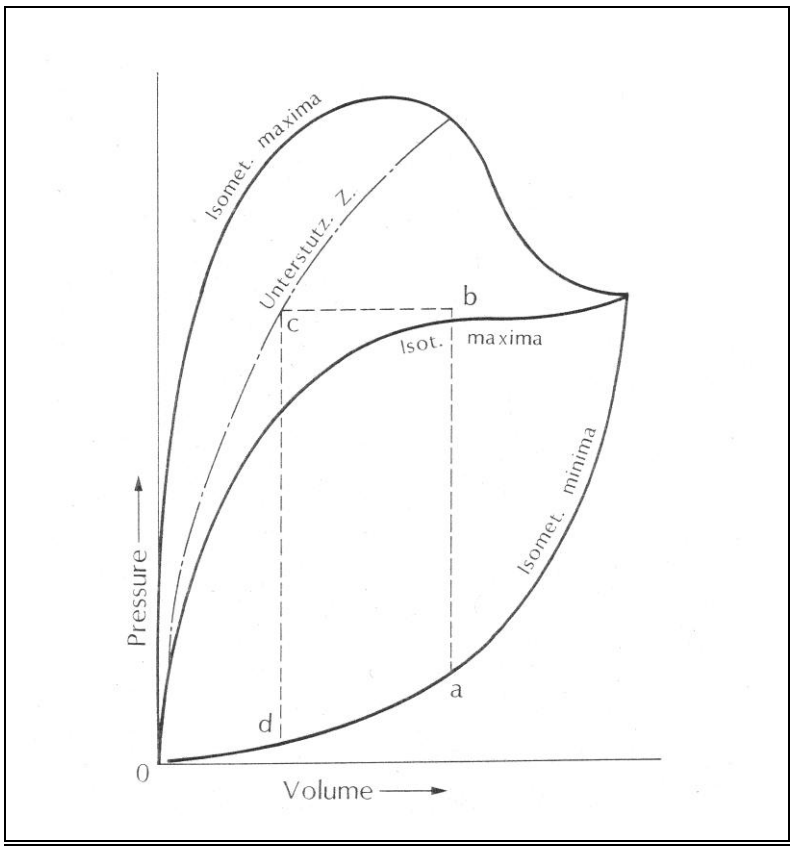

Figure 2.8 *Schematic pressure-volume diagram based on data observed in the isolated frog ventricle. The "isometrische minima" reflects the pressure-volume curve of the resting ventricle. The "isometrische maxima" and "isotonische maxima" reflects the active pressure-volume curves during isovolumic and isotonic contractions, respectively. Reproduced from Sagawa et al.* [35], *pp 8.*

Frank also demonstrated that the pressure-volume curve obtained during isobaric contraction ("Isoton. maxima") was quite different from the isovolumic pressure-volume curve (Figure 2.8). The maximal isobaric pressure-volume curve is positioned to the right of the isovolumic pressure-volume curve. While both curves are non-linear, the maximal isobaric pressure-volume curve is less curvilinear than the corresponding isovolumic pressure-volume curve.

As will be discussed in more detail in the following section, left ventricular contraction *in vivo* begins with an isovolumic phase and becomes quasi-isobaric during the ejection phase. Frank inferred that the end-systolic points of physiological ventricular contraction would be found on a line somewhere in the area bounded by the isovolumic and isobaric pressure-volume curves. The "Unterstütz. Z." curve represents one possible example of the end-systolic pressure-volume curve that may be obtained (Figure 2.8).

The end-systolic pressure-volume curve, together with the passive pressure-volume curve, defines the limits of the pressure-volume diagram of the ventricle under constant physicochemical conditions [35]. Frank included the pressure-volume diagram of an engine (points a – d; Figure 2.8) to illustrate this concept. During filling of the ventricle (points d – a), Frank assumed that the pressure and volume within the ventricle would follow the passive pressure-volume curve ("Isomet. minima"). During contraction, the ventricle would undergo periods of pressure generation (points a – b) and change in volume (points b – c). Frank concluded that, at the end of these processes, the pressure and volume would lie at some point along the end-systolic pressure-volume relation ("Unterstütz. Z."). The ventricle would then undergo a period of pressure decline (points c – d) before filling resumed.

Volume measurements were originally obtained using a cardiometer, in which the heart was hermetically sealed in a cup. Changes in the air pressure within the cup reflected changes in the ventricular volume. In 1955, Katz described an improved cardiometer that allowed more accurate measurements, so that the ventricular volume could be measured throughout the cardiac cycle [36]. This demonstrated that the shape of the pressure-volume loop in the normal left ventricle

has a characteristic quadrilateral shape (Figure 2.9), which is qualitatively similar to the pressure-volume diagram from an engine, which Frank had used to express the stroke work.

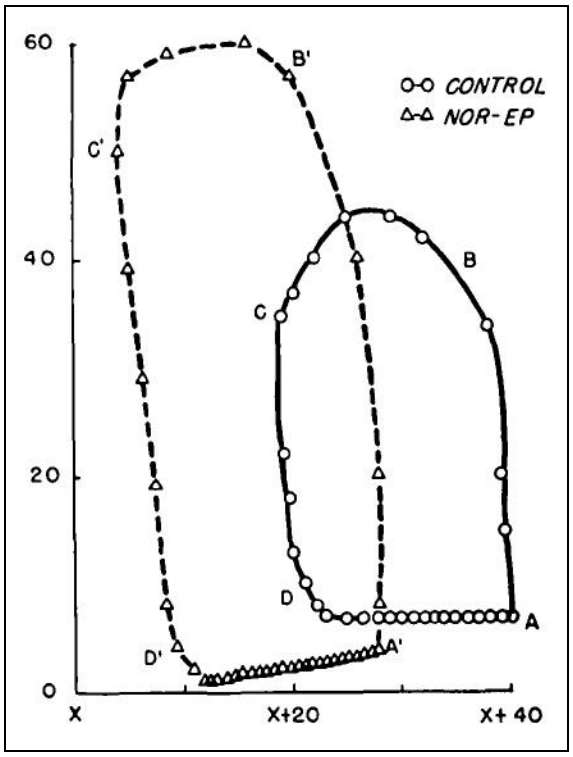

Figure 2.9 *Pressure-volume loop diagrams obtained in the canine left ventricle before and after norepinephrine infusion. Reproduced from* [36].

During the early part of the twentieth century, the studies of Frank were re-examined by a number of separate groups [36-44]. The studies of Sulzer [39] and Reichel & Kapel [40] identified comparable results in the isolated ranine ventricle. Studies in the canine ventricle were also broadly similar. The end-systolic pressure-volume relation also remained essentially linear over the physiological range [43,45]. Furthermore, these studies did not find wide separation between the end-systolic pressure-volume curves of isovolumic and ejecting contractions. As an approximation, the two curves could be superimposed on top of one another [46]. This is in clear contrast with the studies in the isolated frog ventricle.

2.4 THE NORMAL CARDIAC CYCLE

The cardiac cycle defines the period from the beginning of one heartbeat to the beginning of the next heartbeat. Each cycle consists of a complex sequence of electrical and mechanical events that determine the characteristic pattern of pressure and volume within each cardiac chamber, as well as well as the timing of heart sounds and murmurs [47]. A comprehensive illustration of the changes that occur during the cardiac cycle is shown in Figure 2.10, in which the surface electrocardiogram (ECG) serves as a useful time reference [48].

2.4.1 Electrical activity and the electrocardiogram

Each cycle begins with the rhythmic, automatic generation of action potentials within the sino-atrial (SA) node. The sino-atrial node, lying in the terminal groove formed between superior vena cava (SVC) and the right atrium [49], acts as the natural pacemaker for the mammalian heart [50]. Action potentials generated in the sino-atrial node to spread rapidly across the atria and results in the almost simultaneous contraction of the right and left atria. Electrical activity then spreads to the ventricle through the atrio-ventricular (AV) node [49]. The atrio-ventricular node produces a short temporal delay in the wave of depolarisation (approximately 150 – 200 ms), which ensures that atrial contraction precedes ventricular activation. After the short delay, the wave of activation passes rapidly along the His-Purkinje system and results in the coordinated depolarisation of the left ventricle and, shortly thereafter, the right ventricle [51,52].

The overall pattern of electrical depolarisation and subsequent repolarisation within the heart can be non-invasively recorded using pairs of electrodes positioned on the skin surface. The typical ECG consists of a P wave, QRS complex and T wave that correspond with atrial depolarisation, ventricular depolarisation and ventricular repolarisation, respectively. The PR interval equates to the time delay between atrial and ventricular excitation and the RT interval corresponds to the ventricular action potential duration (Figure 2.10). This normal pattern of electrical excitation may be altered in patients with congenital heart disease [53].

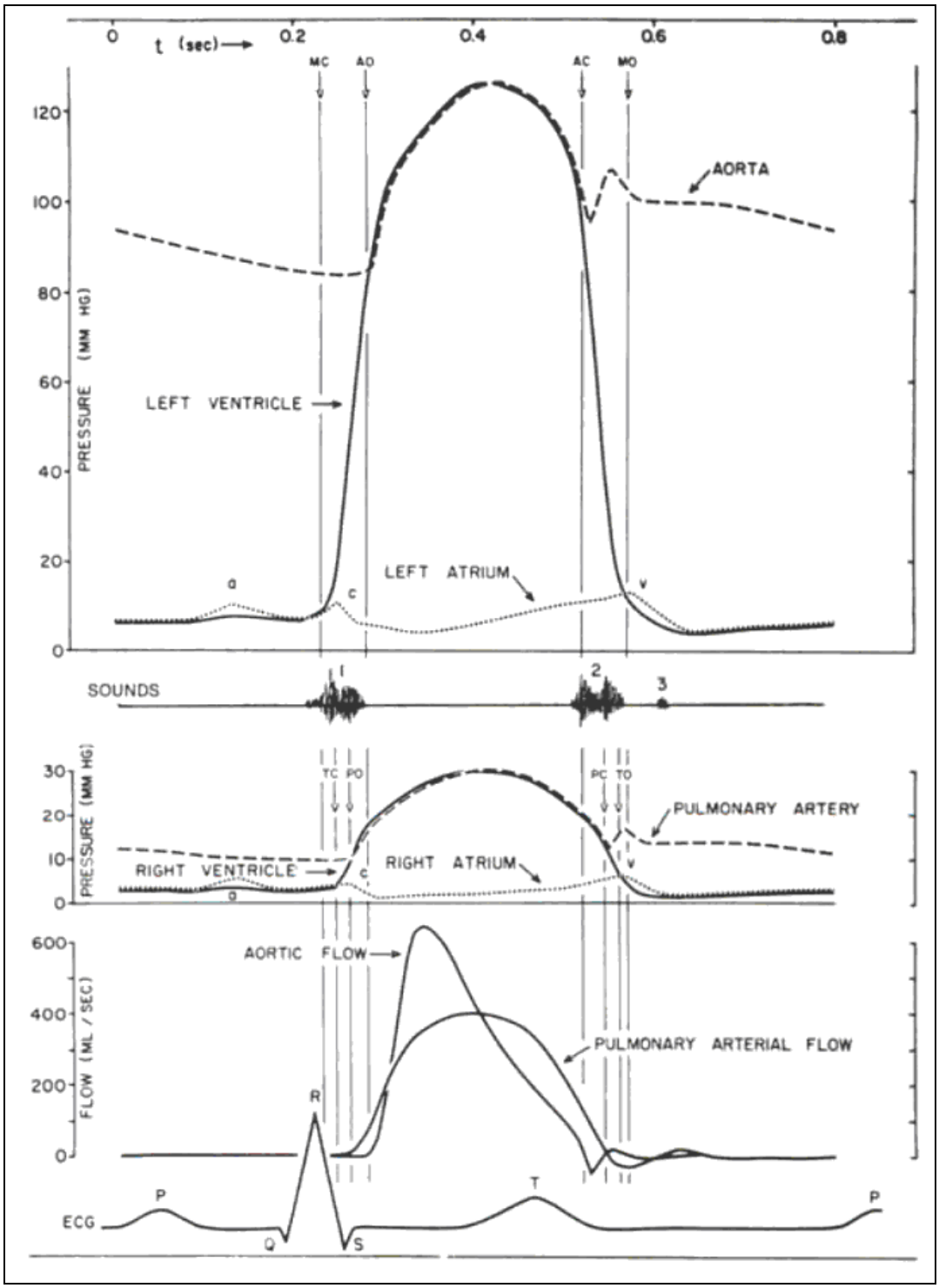

Figure 2.10 *Events in the normal human cardiac cycle. From top to bottom, pressure in the aorta, left ventricle and left atrium; heart sounds; pressure in the pulmonary artery, right ventricle and right atrium; blood flow in the aorta and pulmonary artery; and ECG. Valve opening and closure for the aortic valve are indicated by AO and AC, respectively; MO and MC for the mitral valve; PO and PC for the pulmonary valve and TO and TC for the tricuspid valve. Reproduced from Milnor* [48], *pp. 112.*

2.4.2 Mechanical events within the cardiac cycle

The ventricular cycle consists of two separate phases; an active contraction phase called systole followed by a filling phase called diastole [54]. Three distinct definitions of systole and diastole have been proposed [45,47,55], which can be differentiated from one another primarily according to the definition of end-systole.

Wiggers defined systole as the period that begins with the rise in ventricular pressure and ends with the, "cessation of tension development", which occurred during the finite period immediately preceding closure of the semi-lunar valve. This point could conveniently be identified by the end of ejection [47].

Brutsaert *et al.* proposed an alternative definition, in which systole was extended to include the period of active ventricular relaxation (i.e. isovolumic relaxation phase and period of rapid ventricular filling). Accordingly, diastole was limited to the period when the ventricle was completely relaxed (i.e. diastasis and atrial filling only) [55]. This definition was based on the observation that early muscle relaxation is load-dependent, just as muscle function during contraction is load-dependent. Nevertheless, this definition is not suitable for studying contractility using the end-systolic pressure-volume relation approach that will be discussed in the following sections.

For the purposes of this thesis, I have used the definition of systole proposed by Suga *et al.* This definition, like Wiggers' definition, considered systole as a phase of active force development [45]. However, Suga *et al.* defined end-systole as the period where force of contraction (or elastance) is maximal rather than the end of ejection. Elastance (E) was defined by the incremental pressure-volume ratio of the ventricle (dP/dV), Equation 2.4:

Equation 2.4 $$E = dP/dV$$

Elastance represents the reciprocal of the ventricular compliance (dV/dP).

In the normal left ventricle, the end of ejection and end-systole occur effectively simultaneously [56]. However, changes in the pressure loading conditions loading can alter the relative timing of these two events; a rise in afterload causes ejection to end relatively early and vice versa. By contrast, end-systole remains relatively constant [57,58].

2.4.2*a* *Normal left ventricular cycle*

In the left ventricle (LV), there is a rapid rise in pressure (LVP) following ventricular excitation (i.e. the QRS complex on the ECG). When LVP exceeds the pressure in the left atrium (LAP), the mitral valve closes and the *isovolumic contraction phase* begins. As the name suggests, this phase is not associated with any change in the intraventricular volume as both mitral and aortic valves are closed. Isovolumic contraction in vivo is considered broadly equivalent to isometric contraction in vitro [34].

When LVP rises above aortic blood pressure (AoP), the aortic valve opens and blood is rapidly ejected from the ventricle into the aorta (*ejection phase*). Approximately 70% of ejection occurs during the initial third of the ejection phase. Ventricular pressure rises to a peak and then declines with a reduction in the rate of ejection. During the latter part of ejection, the momentum of blood maintains forward flow into the aorta, even though LVP may be slightly lower than AoP. Eventually, LVP falls more sharply and the aortic valve closes.

Closure of the aortic valve is followed by the *isovolumic relaxation phase*, during which there is no change in the intraventricular volume. When LVP falls below LAP, the mitral valve opens and the ventricle begins to fill (*filling phase*). During the initial period of filling, LVP continues to fall as the ventricular volume increases. This reflects the effects of continued active relaxation, which produce a 'suction' effect that actively fills the ventricle [59,60]. This period of rapid ventricular filling lasts for approximately the first third of diastole and accounts for most of ventricular filling [61]. The middle third is characterised by a very small flow of blood into the ventricles as blood continues to drain from the central veins into the atria (diastasis). Atrial systole occurs during the final third of ventricular diastole and this is accompanied by a secondary increase in the rate of

ventricular filling. During the filling phase, the ventricular volume is increased from the end-systolic residual volume to the end-diastolic volume, in preparation for the next ventricular cycle.

The length of ventricular diastole and systole vary with heart rate. At a resting heart rate of 75 beats per minute, diastole occupies approximately two thirds of the cardiac cycle. Both periods shorten at faster heart rates, but the effect upon diastole is proportionately greater.

2.4.2*b* *Normal right ventricular cycle*

The changes that occur in the normal right ventricle (RV) are qualitatively similar to the changes that occur in the LV (Figure 2.10). However, there are important differences, which primarily reflect differences in the pressure loading characteristics of the two ventricles [62]. In the left and right ventricles, the rate of pressure rise (dP/dt) at the start of contraction is essentially the same. However, since pulmonary artery pressure (PAP) is approximately one-fifth the level of aortic pressure, ejection commences earlier in the RV. The isovolumic contraction time in the RV is correspondingly shortened. Similarly, the low hydraulic impedance of the normal pulmonary circulation means that the RV continues to eject for a considerable time after right ventricular pressure begins to decline [63,64]. In the LV, by comparison, the end of ejection and end-systole are effectively simultaneous [56].

2.4.3 The normal ventricular pressure-volume loop

The changes in ventricular cycle can be summarised in the pressure-volume curve. This is obtained by plotting the instantaneous ventricular pressure against the corresponding ventricular volume; this effectively integrates the separate ventricular pressure-time and volume-time traces (Figure 2.11).

2.4.3*a* *The normal left ventricular pressure-volume loop*

As previously illustrated, the normal LV pressure-volume curve has a characteristic quadrilateral shape or loop (Figure 2.11A). The bottom right-hand corner corresponds with end-diastole. Starting from this point, the curve passes in an anti-clockwise direction. Each side of the curve

corresponds with one of the four phases of the cardiac cycle. The right-hand side (points A-B) represents the isovolumic contraction phase; the upper surface (points B-C) represents the isotonic, ejection phase; the left-hand side (points C-D) represents isovolumic relaxation; and the lower surface (points D-A) represents ventricular filling. The upper left-hand corner (point C, Figure 2.11A) corresponds with end-systole, as defined by Suga *et al.* [45].

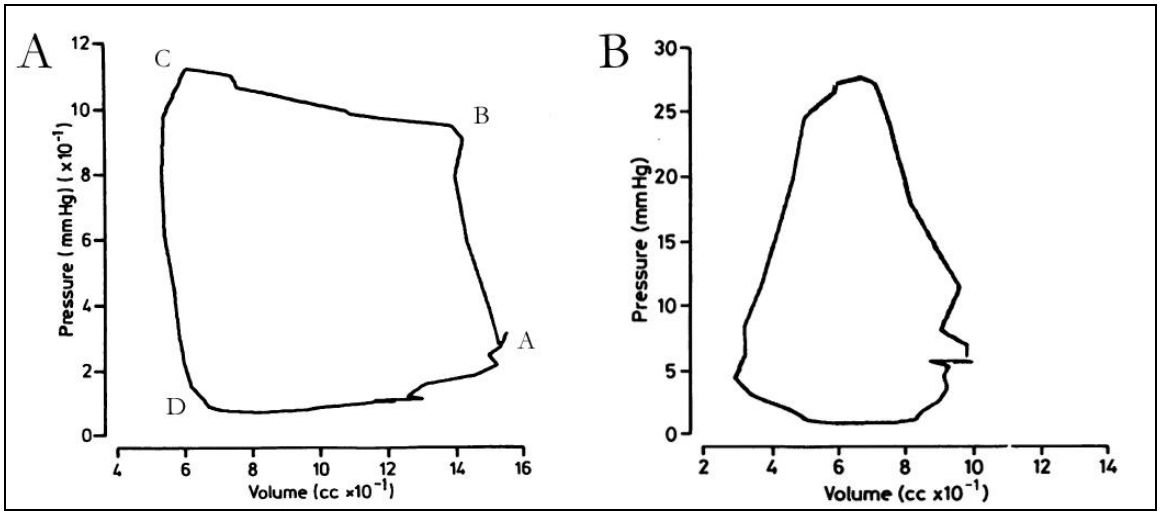

Figure 2.11 *Typical examples of left and right ventricular pressure-volume loops.* A*, the left ventricular pressure-volume loop has a characteristic quadrilateral shape. Points A – D represent end-diastole, start of ejection, end-ejection and start of ventricular filling, respectively.* B, *The normal right ventricular pressure-volume loop has a broadly triangular shape.*
Reproduced from Redington et al. [64].

A number of basic haemodynamic indices are evident from the pressure-volume curve. The horizontal width corresponds with the stroke volume, *SV*. This is the difference between the ventricular volume at end-diastole (*EDV*; lower right-hand corner, A) and end-systole (*ESV*; Equation 2.5):

Equation 2.5 $$SV = EDV - ESV$$

From this, the ejection fraction (*EF*) can be calculated (Equation 2.6):

Equation 2.6 $$EF = SV/EDV$$

In addition, the area subtended by the pressure-volume curve, the pressure-volume area (*PVA*) gives a measure of energy used by the heart to pump blood into the systemic circulation; this is known as the stroke work, *SW* (Equation 2.7):

Equation 2.7 $$SW = -\int_{EDV}^{EEV} P(t)\,dV$$

where *EDV* and *EEV* represent the end-diastolic and end-ejection volume, respectively; $P(t)$ represents the time-varying pressure; and dV is the instantaneous change in volume [65].

Changes in either the *SV* or the maximal pressure developed (i.e. the vertical height of the pressure-volume curve) will alter pressure-volume area, thus indicating a change in the work performed by the heart.

2.4.3*b* *The normal right ventricular pressure-volume loop*

The normal RV pressure-volume curve is substantially different from that of the LV, Figure 2.11B. It has a triangular or trapezoidal in shape, with poorly defined periods of isovolumic contraction and relaxation.

Although the shape of the RV pressure-volume loop may reflect differences in the performance of the two ventricles, the shape is also a reflection of acute or chronic changes in the loading conditions. For example, in patients with transposition of the great arteries following an atrial switch procedure (i.e. Mustard or Senning operation), the RV supports the systemic circulation while the LV supports blood flow through the pulmonary circulation. Pressure-volume loops obtained in these patients are distinctly different from normal. The LV pressure-volume loop has a trapezoidal shape (like the normal RV) whereas the RV pressure-volume loop has a quadrilateral shape (like the normal LV; Figure 2.12).

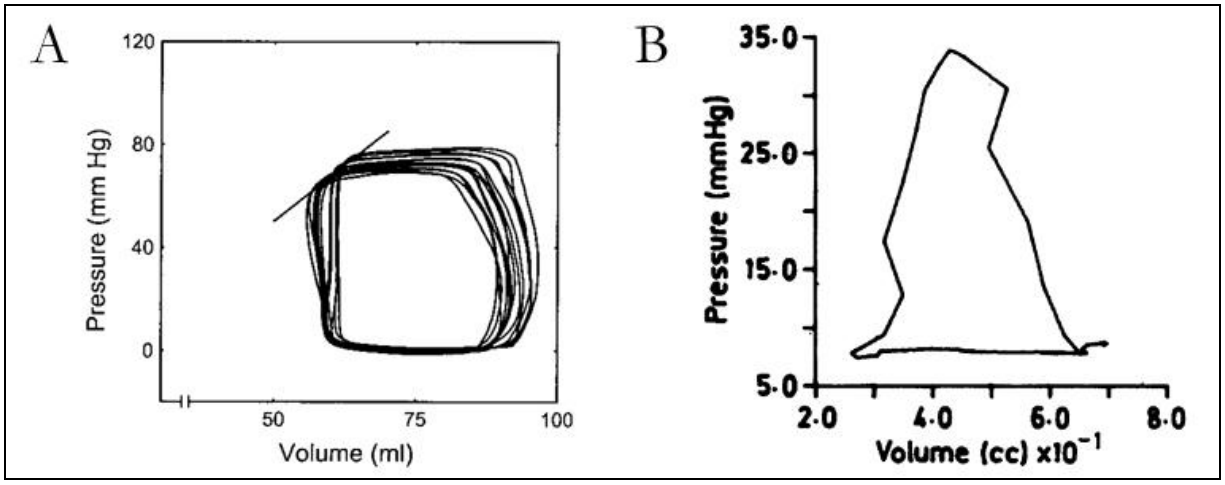

Figure 2.12 *Representative examples of right* (A) *and left* (B) *ventricular pressure-volume loop in separate patients with transposition of the great arteries following atrial switch procedure (Mustard operation). Reproduced from Derrick et al.* [66] *and Redington et al.* [67]*, respectively.*

2.5 PHYSIOLOGICAL DETERMINANTS OF VENTRICULAR FUNCTION

The cardiovascular system ordinarily operates as a closed-loop system, in which the heart and the vasculature are connected with one another to form a hydraulic loop. The performance of one part of the system depends on its interaction with the rest of the system. *In vitro* and *in vivo* studies have identified four major factors that influence cardiac performance, namely preload, afterload, heart rate and contractility [68].

In order to illustrate the effect of these factors on ventricular function, it is first necessary to define a measure of that function. The most basic index of ventricular function is the volume of blood that the heart can pump in one minute. This is known as the cardiac output (*CO*). The *CO* is the product of the stroke volume (*SV*) and heart rate (*HR*; Equation 2.8).

Equation 2.8 $$CO = SV \cdot HR \quad \text{or} \quad CO = (EDV - ESV) \cdot HR,$$

where *EDV* is end-diastolic volume and *ESV* is end-systolic volume.

2.5.1 Preload and afterload

The terms preload and afterload, used in the context of isolated papillary muscle experiments, have very precise definitions [11]. Preload refers to the resting tension within the muscle. This is

calculated as the force applied to the resting muscle (i.e. the weight attached to the isotonic lever) divided by the cross-sectional area of the muscle. This term allows for direct comparison between specimens with different thicknesses. Similarly, afterload refers to the muscle tension the shortening phase of isotonic contraction. Like preload, this is calculated as the weight lifted during contraction normalised for the cross-sectional area of the muscle.

The terms preload and afterload have also been applied to the study of ventricular function in vivo. However, their definition in the intact ventricle is less clear. As already described, the tension within the myofibres cannot be directly measured and, furthermore, varies according to the location within the ventricular mass and point in the cardiac cycle. What then is the best estimate for preload and afterload in vivo?

2.5.1*a* *Preload*

The relationship between preload and cardiac output have been described using isolated canine heart-lung preparations and chronically instrumented dogs *in vivo* [37,69,70]. These studies have demonstrated that cardiac output rises to a plateau during acute changes in preload, as indicated by the change in right atrial pressure (Figure 2.13).

In clinical practice, central venous pressure (***CVP***) and pulmonary capillary wedge pressure (***PCWP***) are often used as proxy measurements of right ventricular and left ventricular end-diastolic pressures, respectively. However, these pressures are associated with significant limitations as measures of preload, as they are altered by changes in compliance within the ventricle as well as changes in the intrathoracic pressure [71,72].

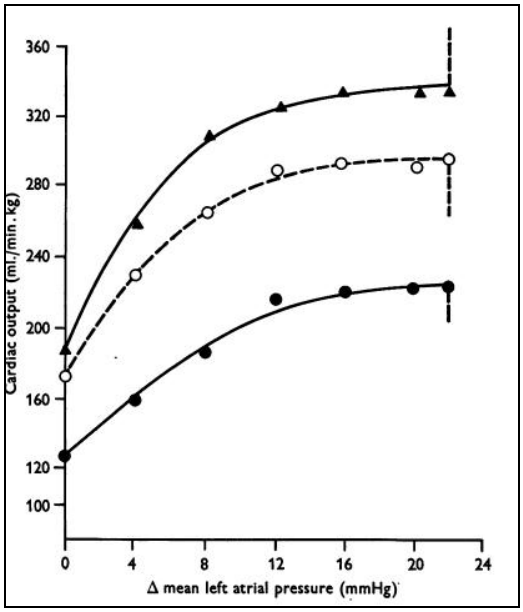

Figure 2.13 *Relationship between cardiac output and mean left atrial pressure. The relationship is illustrated during control states* (●)*, vagal blockade* (○) *and vagal blockade plus isoprenaline* (▲).
Reproduced from Bishop & Horwitz [73].

Preload in the intact circulation is probably best represented by the end-diastolic volume (***EDV***) [74]. The end-diastolic volume represents the degree of filling of the ventricle. Changes in ***EDV*** therefore reflect changes in the shape of the ventricle and, by extension, changes in the length of the myofibres within the ventricular mass [29]. For the purposes of this thesis, preload has been defined as the ventricular end-diastolic volume.

2.5.1*b* *Afterload*

In its simplest form, afterload reflects the amount of work the ventricle must perform in order to produce a given pulsatile blood flow at a fixed preload. However, as the ventricle is not called on to lift a weight but to move a viscous fluid into a viscoelastic system, it cannot be adequately described using a single, simple quantity.

Afterload has been defined based on the analysis of the properties of the arterial system, the arterial input impedance. The arterial input impedance influences but is independent of cardiac ejection into the vascular tree [75]. Systolic blood flow and pressure can be considered as coupling variables that reflect the interaction between the ventricular pump and afterload. The

arterial system load can be approximated using a three-element Windkessel model [76,77], based on analysis of aortic pressure and flow in the frequency domain [78]. Using this method, arterial impedance can be separately described according to the characteristic impedance (Z_c), arterial compliance (C), and arterial resistance (R).

The influence of acute changes in arterial impedance on left ventricular function were examined by Maughan *et al.* in an isolated canine heart preparation [79]. A four-fold increase in arterial resistance, R was associated with a substantial reduction in stroke volume, as illustrated by the pressure-volume loop becoming taller and thinner (Figure 2.14, *top panel*). By contrast, comparable changes in the arterial compliance, C and characteristic impedance, Z_c changed the shape of the systolic portion of the curve but did not alter stroke volume substantially (Figure 2.14, *middle and bottom panels*).

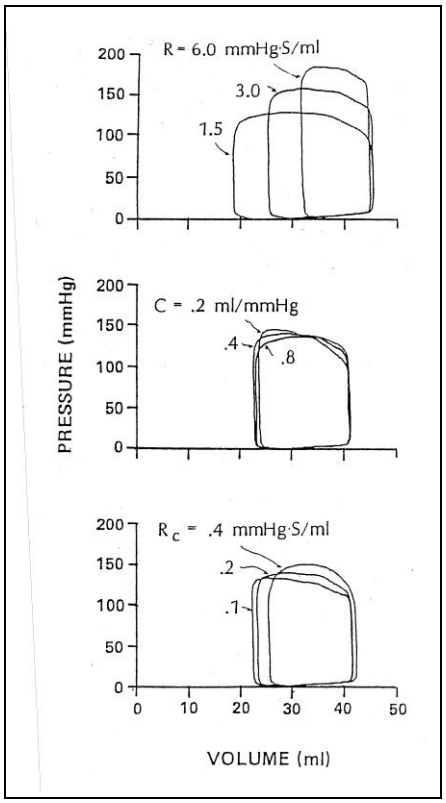

Figure 2.14 *Pressure-volume loops in a canine left ventricle with three levels of arterial resistance (top panel), three compliance (middle panel) and characteristic impedance (R_c, lower panel). Reproduced from Sagawa et al.* [35]*, pp. 116.*

Arterial input impedance is not generally used to assess afterload in clinical practice. In this context, afterload is most often approximated using the mean arterial pressure or vascular resistance. Systemic and pulmonary vascular resistance are calculated using the standard formulae [1]. However, neither of these measures reflects the dynamic nature of the resistance to blood flow during ejection [80].

An alternative approach to characterise the arterial system has been proposed by Sunagawa *et al.*, based on analysis of the pressure-volume loop [81]. Since the arterial pressure-flow relationship is linear over the physiological range [82], the total arterial resistance can be estimated as the slope of the ventricular end-systolic pressure-stroke volume relation (Equation 1.9). This slope is known as the effective arterial elastance, E_a [82].

Equation 1.9 $$E_a = \frac{P_{ES}}{SV} \approx \frac{R_T}{T_c},$$

where R_T is total mean vascular resistance and T_c is cardiac cycle length.

Under experimental conditions, Segers *et al.* demonstrated that E_a varied as a linear function of total resistance (i.e. the sum of total peripheral resistance, R and characteristic impedance, Z_c) and inversely with arterial compliance, C [83]. Effective arterial elastance has been validated as a measure of afterload under a variety of experimental and clinical conditions [84-86]. This index is particularly useful because it can be linked with indices of ventricular function to assess the mechanical efficiency of the cardiovascular system as a whole [81,87,88]. For these reasons, effective arterial elastance, E_a has been used as the principal measure of afterload in this thesis.

2.5.2 Heart rate

Changes in heart rate represent a third major determinant of cardiac function. Studies in isolated muscle preparations have demonstrated a positive relationship between the stimulation frequency and the force of contraction [11,89]. A sudden increase in the heart rate causes the amplitude of each successive contraction to increase until a new, steady-state level is reached. This is known as the positive staircase or Treppe phenomenon [90].

In the normal heart in the conscious patient, physiological tachycardia results in the reduction in length of the cardiac cycle. The duration of systole and diastole are both shortened, but the effect upon the diastolic filling time is greater. This potentially reduces the end-diastolic volume and cardiac output. Freeman *et al.* demonstrated that increments in heart rate were also associated with increased ventricular contractility [91]. As a result, the heart can deliver the same or increased stroke volume at a lower end-diastolic volume. Tachycardia represents an important mechanism for increasing cardiac output, particularly during exercise [92]. However, if the heart rate is increased excessively, diastolic filling time will decrease to such a degree that cardiac output will eventually fall, in spite of the improved ventricular contractility [93].

2.5.3 Contractility

The term contractility describes the "performance potential" of the heart independent of changes in the loading conditions [10,15]. This term represents the intrinsic property of the myocardium and predicts how cardiac function will change in response to external stimuli. It follows that if one is to make a valid comparison of ventricular function, cardiac output and its derivatives are only useful if preload, afterload and heart rate are not allowed to change. This is often not practicable, especially *in vivo* [94].

The ideal index of ventricular function would be exquisitely sensitive to changes in the inotropic state of the ventricle, insensitive to changes in the loading conditions and heart rate, reproducible and would not require excessive assumptions for its derivation. A wide variety of indices of ventricular function have been developed [95-98]. The sheer number of indices suggests that this important attribute cannot be adequately defined by a single measurement [35,99].

2.5.3*a* *Assessment of systolic function*

The assessment of ventricular function is pragmatically divided into the separate evaluation of ventricular systolic and diastolic function. Conventional measures of ventricular systolic function, like ejection fraction or the peak rate of rise of ventricular pressure during the isovolumic contraction phase (dP/dt_{max}) [100], are generally based on the assessment of changes in

ventricular volume or pressure in the time domain. However, these measurements are implicitly dependent on loading conditions as well as contractility [101-103]. For example, the stroke volume from a given end-diastolic volume (and thus ejection fraction as well) decreases linearly with increments in left ventricular end-systolic pressure [102]. Similarly, increments in end-diastolic volume are associated with a progressive rise in the measured left ventricular dP/dt_{max} [104]. This load-dependence limits the value of these measurements as indices of ventricular systolic function.

It has long been recognised that further insight into ventricular function can be obtained from an analysis of the instantaneous pressure-volume relationship [28]. Studies in the canine left ventricle *in vivo* have demonstrated that there is a linear relationship between pressure and volume over the physiological range [43,45]. In a series of reports, Suga demonstrated that the instantaneous end-systolic pressure-volume relationship was virtually independent of changes in preload and afterload [103,105]. However, this ratio did vary markedly with inotropic interventions [106] and he concluded that the slope of the end-systolic pressure-volume relationship could be used to characterise ventricular contractility [45].

Suga *et al.* used the same approach to examine the time course of the pressure-volume ratio over the entire cardiac cycle [45]. They defined the elastance at any point in the cardiac cycle, $E(t)$ as:

Equation 2.10 $$E(t) = P(t) / (V(t) - V_0)$$

where $P(t)$ and $V(t)$ are the instantaneous ventricular pressure and volume, respectively; and V_0 is the equilibrium volume, i.e. the minimum ventricular volume at which contraction generates a pressure greater than atmospheric pressure [45].

The time-varying elastance curve (Figure 2.15) is characterised by a trapezoidal curve that rises to a peak, E_{max} and then declines. The time from the start of systole to E_{max} is termed t_{max}. Suga *et al.* demonstrated that time-varying elastance was independent of end-diastolic volume and arterial pressure within their physiological ranges but was affected specifically and sensitively by inotropic

interventions. Inotropic interventions increased E_{max}, decreased t_{max} or caused a combination of the two [45,107].

Regardless of the changes in E_{max} and t_{max} that followed changes in the level of inotropy, the unique basic shape of the systolic part of the time-varying elastance curve remains unchanged [107]. Therefore, any given time-varying elastance curve can be fully represented by the parameters, E_{max} and t_{max} and the normalised $E(t)$ curve. The process of normalisation for elastance and time are described in Figure 2.15. This curve, in turn, provides a simplified, phenomenological description of contraction within the ventricular chamber [56].

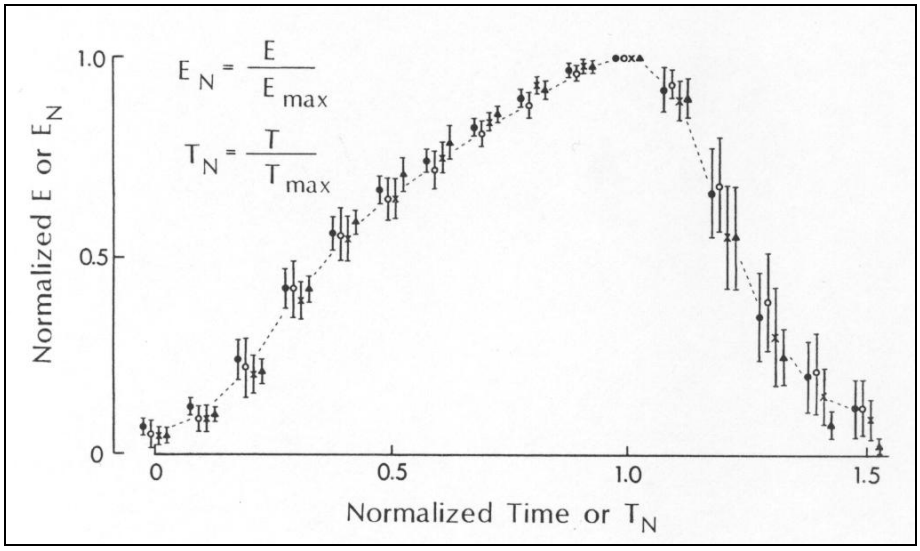

Figure 2.15 *Plot of many normalised pressure-volume ratio curves, E_N against normalised time, T_N to demonstrate their relatively constant shape. The two equations in the Figure describe the process of normalisation. Reproduced from Suga et al.*[45].

Three discrete indices of ventricular function have been derived from the time-varying elastance model of contraction. These are the end-systolic pressure-volume relation (*ESPVR*) or end-systolic elastance (E_{ES}) [45]; the dP/dt_{MAX}-*EDV* index [108]; and preload recruitable stroke work (*PRSW*) [109]. These indices represent the slope parameters of the end-systolic pressure-volume relationship; the dP/dt_{MAX}-*EDV* relationship; and the stroke work-*EDV* relationship, respectively.

The end-systolic elastance,dP/dt_{MAX}-*EDV* relation and preload recruitable stroke work are all relatively load-dependent and are therefore better indices of intrinsic systolic function. However,

each of these indices has inherent limitations. In general, the more sensitive the index is to changes in contractility, the more affected it is by changes in vascular load [110,111]. I have used all three of these indices in this thesis in order to appreciate changes in systolic function.

End-systolic elastance, E_{ES}; the dP/dt_{MAX}-*EDV* relation; and preload recruitable stroke work, *PRSW* are all calculated from pressure-volume loops that are obtained at different loading conditions (Figure 2.16). One way to alter the preload is to temporarily occlude the inferior vena cava (IVC), using either a balloon within or a tape around the IVC [112,113].

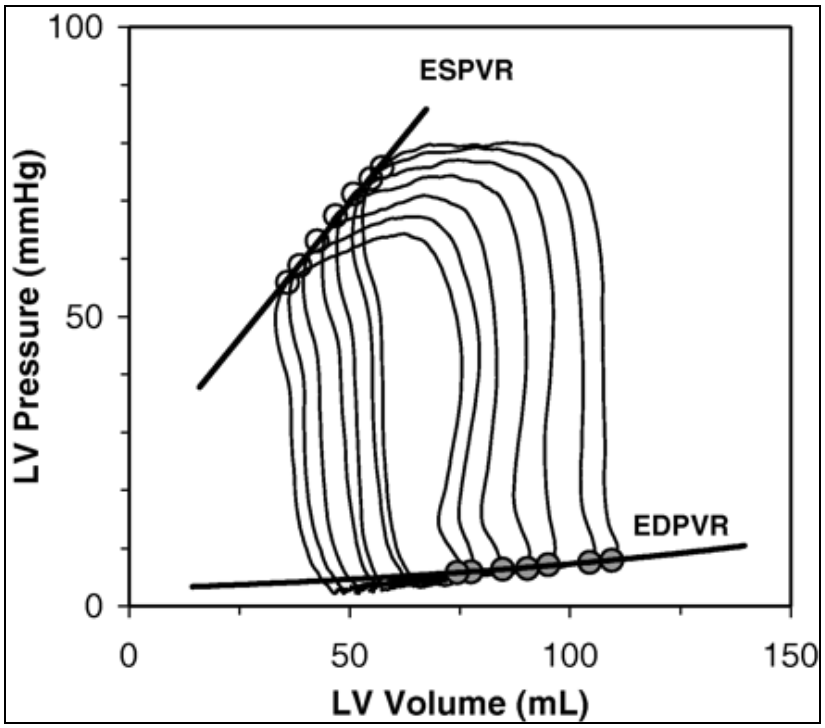

Figure 2.16 *Diagram of pressure-volume loops during IVC occlusion. The end-systolic pressure-volume relation (ESPVR) and end-diastolic pressure-volume relation (EDPVR) are derived from this "family" of pressure-volume loops. Reproduced from Steendijk et al.*[114].

2.5.3*b* *Assessment of diastolic function*

The assessment of diastolic function of the ventricle reflects the inter-relationship between a number of complex phenomena within the heart [55]. These include ventricular relaxation; elastic recoil and ventricular suction; the viscoelastic properties of the heart, as well as restraint provided by the contralateral ventricle, pericardium and lungs [95]. It is not surprising that diastolic

function cannot be quantified using any one measure [115]. However, it is possible to simplify the analysis of diastolic function by considering active ventricular relaxation and the passive properties separately. Although this separation is artificial and simplistic, it provides a practical framework for the identification of quantification of diastolic dysfunction.

Assessment of ventricular relaxation

Ventricular relaxation is an essential process by which the ventricle returns to its resting pressure and volume state after contraction. This involves an active biochemical process that result in the progressive decline of ventricular pressure during early diastole. Relaxation is a complex energy-dependent process that may use up to 15% of the total energy output of the beating heart [111].

The rate of pressure decline is influenced by a variety of physiological factors [116,117] including the magnitude of elastic recoil within the heart caused by systolic contraction [118], the arterial load [55,119] and spatial and temporal non-uniformity of the process within the ventricle as a whole [55,120]. Impaired ventricular relaxation may reflect changes in any one of these factors [55].

Ventricular relaxation may be impaired in a number of conditions including myocardial ischaemia caused by coronary artery disease [121], ventricular hypertrophy [55] and both dilated and hypertrophic cardiomyopathy [122,123]. Delay of ventricular pressure decline plays an important role in the clinical manifestations of these conditions [124]. In addition, these changes in ventricular relaxation are present before changes in systolic function become evident [55].

Assessment of ventricular relaxation is based on the analysis of pressure decline during isovolumic relaxation. A number of separate indices of ventricular relaxation have been used, including the maximal rate of pressure decline (dP/dt_{MIN}) [125] and the time required for pressure to decline by 50% of its starting value ($T_{1/2}$) [122]. Studies also identified that the fall in ventricular pressure usually followed an exponential decline. As a result, it was considered possible to describe the rate of pressure decay in terms of a time constant of relaxation or tau (τ; the time for pressure to decay to $1/e$ of any pressure) [126]. A number of mathematical models

can be used to calculate tau, which reduce the sensitivity of this index to loading conditions and pericardial constraint [123,127].

In this thesis, tau has been calculated using a monoexponential decay in which pressure decays to a non-zero asymptote (P_∞), (Equation 2.11) [128].

Equation 2.11 $$P = (P_0 - P_\infty)e^{-t/\tau} + P_\infty ,$$

where P_0 is the pressure at time, t=0 and τ is the time constant of pressure decay.

This equation can be rewritten in the form of a linear relation between pressure and its first derivative with respect to time (dP/dt; Equation 2.12).

Equation 1.12 $$dP/dt = (-1/\tau)P - P_\infty/\tau .$$

Assessment of ventricular compliance

The second major component of diastolic function is the passive chamber stiffness or its inverse, compliance. Ventricular compliance can only be derived from the analysis of the pressure-volume relationship during the diastolic filling period [129,130]. However, as the normal pressure-volume relation during this period is curvilinear, chamber compliance is not constant but varies as a function of ventricular volume; compliance is high at low ventricular volumes but decreases as the ventricle is filled. This can be compared to inflating a football with a hand-pump. As the ball fills, more effort is required in order to fill the ball further.

The ventricular compliance is equivalent to the passive length-tension relation *in vitro*. It reflects the passive elastic properties of the ventricular chamber as a whole. Compliance is reduced in patients with ventricular hypertrophy, ventricular fibrosis and in patients where the ventricle is dilated [96,129,131,132]. However, it should be noted that diastolic pressure-volume relations do not only relate to the properties of the ventricular chamber per se. Other factors, including volume loading in the contra-lateral ventricle through so-called "ventriculo-ventricular

interactions" [133]; pericardial constraint [134]; and extrinsic compression of the heart can all affect the measured diastolic pressure-volume relation and parameters derived from these data.

The period of diastasis is arguably the best portion of the cardiac cycle from which to derive indices about the passive properties of the heart. This is because there will be little influence from either ventricular relaxation or atrial systole. However, only limited data are obtained from a single cardiac cycle if this is the only part of the filling curve analysed. An alternative approach is to measure pressure-volume relations from several cardiac cycles at varying levels of volume loading and then combining the data in a single relation, as illustrated in Figure 2.16 [122].

Once obtained, the data are analysed using a mathematical curve fitting to derive parameters related to ventricular compliance. In this thesis, the passive pressure-volume relationship was described by a monoexponential formula (Equation 2.13):

Equation 2.13 $$P = \alpha\left(e^{\beta(V-V_0)}-1\right)$$

where V_0 is the volume of the heart at zero end-diastolic pressure, β is the chamber stiffness coefficient and α is a stiffness and a scaling coefficient.

This equation can be rewritten in the form of a linear relation between chamber stiffness (dP/dV) and pressure (Equation 2.14).

Equation 2.14 $$dP/dV = \beta P + \alpha$$

2.5.4 Extrinsic control of cardiac function

In addition to the four major factors that influence cardiac function described, ventricular function is also influenced by the autonomic nerves supplying the heart and a number of cardio-active substances in the blood supply.

2.5.4*a* *Cardiac autonomic nerves*

The heart is supplied by two sets of nerves, one emanating from the nuclei in the lower brainstem (parasympathetic vagal nerves) and the other from the upper thoracic segments of the spinal cord (T1 – T8; cardiac sympathetic nerves). Cardiac vagal nerves terminate in a ganglia lying in the fat pads in various regions of the heart whereas cardiac sympathetic nerves terminate in the stellate inferior cervical and associated ganglia. Post-ganglionic sympathetic and parasympathetic fibres project to the atria, conducting tissues and the ventricular myocardium [135]. The parasympathetic vagal supply decreases heart rate by direct actions on the pacemaker tissue and decreases atrial and ventricular contractility, probably mainly through an interaction with the sympathetic supply. The sympathetic supply has the opposite actions.

2.5.4*b* *Hypoxia and Hypercapnia*

The partial pressure of oxygen (P_aO_2) and carbon dioxide (P_aCO_2) in the in the arterial blood may also affect ventricular function [48]. Chronic hypoxia, in particular, is associated with a depletion of the main energy source for the heart (adenosine triphosphate, ATP) and a decrease in baseline ventricular function [136,137]. This, in turn renders the heart more susceptible to ischaemic injury during cardiac surgery, which may result in less favourable early post-operative recovery [137,138].

2.6 NORMAL DEVELOPMENT OF THE HEART

The earliest functioning embryonic heart is a single, straight tubular pump. During the early phases of development, this primary heart tube undergoes a process called cardiac looping (Figure 2.17), which transforms the primary heart tube into the normal four chambered heart [139]. Cardiac looping is the key process in cardiac morphogenesis and any disturbances in this process can lead to the development of several congenital cardiac malformations [140].

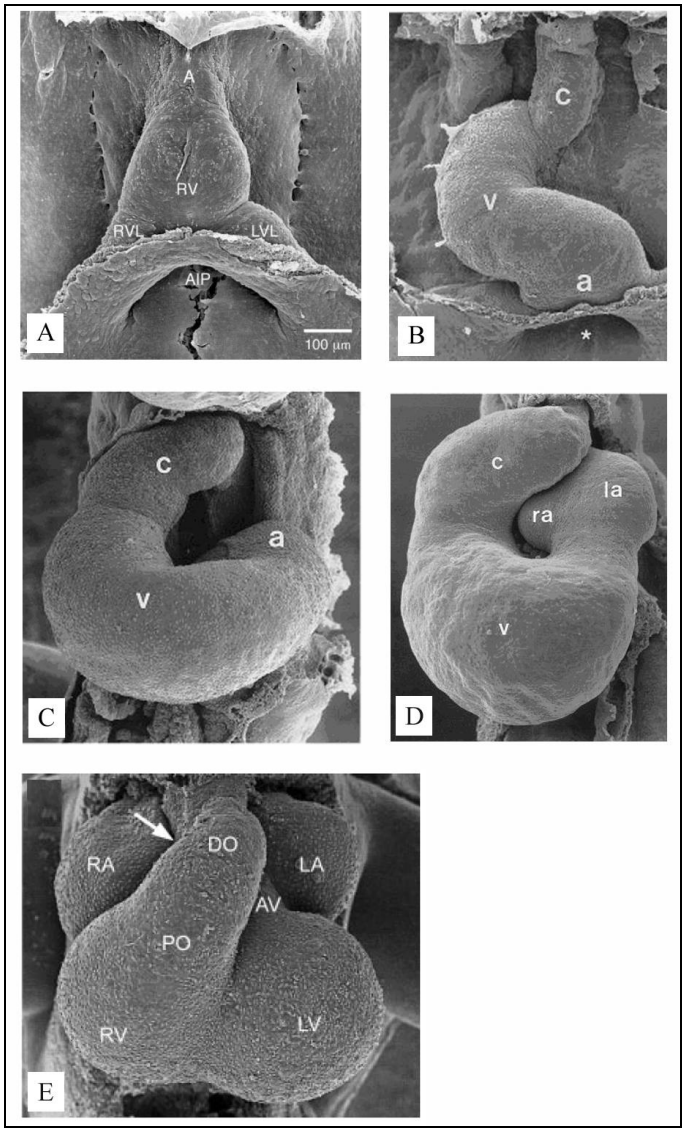

Figure 2.17 *Electron micrograph of ventral views of the chick embryo during the various stages of cardiac looping. This involves the formation of the straight and almost symmetric heart tube (*A*); followed by dextral-looping (*B*) and then the formation of the S-shaped loop (*C*). Subsequent ballooning of secondary myocardium results in the formation of separate left and right atria (*D*) and left and right ventricles (*E*). Reproduced from Manner [139,140].*

In the human, the primary heart tube develops during the third week of gestation by the fusion of bilateral cardiogenic cells in the anterior lateral plate mesoderm at the cranial border of the embryonic disc [141]. This creates a single undivided lumen lined by endothelial cells and enveloped in contractile myocardial cells[142].

The primary heart tube is aligned along the ventral midline of the embryo. It is bilaterally symmetrical with a shape like an inverted Y, Figure 2.17A. The two caudal arms are continuous with the developing venous tributaries and the short cranial stem is connected to the aortic sac and pharyngeal arch arteries [139]. Although there is minimal variation in the structure at this stage, the heart tube can be subdivided along the antero-posterior axis into a number of separate modules [143]. Each module has a distinct pattern of gene expression that regulates subsequent segmentation, differentiation and expansion into the various cardiac components of the normal four-chambered heart [143,144]. Cells at the caudal pole sequentially give rise to the myocardium of the inflow tract, atria and atrio-ventricular canal [142] whereas the short cranial stem forms the left ventricle [145]. The cranial pole of the primary heart tube is elongated by the addition of cells from a second cardiogenic centre. The cells from this secondary or anterior heart field are primarily associated with the development of the right ventricle and the primitive outflow tract [146].

The primary heart tube undergoes cardiac looping during the fourth to seventh weeks of human gestation. During this process, the heart tube undergoes a sequential change in shape with the initial formation of a C-shaped loop convex to the right (Figure 2.17B) and the subsequent transformation into an S-shaped loop (Figure 2.17C). Dextral looping (*D*-loop) establishes the left-right asymmetry of the embryonic heart whereas the formation of the S-shaped loop brings the segments of the heart tube and the great vessels into effectively their final topographical relationships [140].

At the start of cardiac looping, the primary heart tube can be divided into atrial and ventricular segments together with a single outflow tract. The atrial and ventricular segments are separated by the atrio-ventricular canal and the outflow tract is supported by the distal part of the

ventricular segment. The three segments are connected in series, so that blood flowing through the primary atrium must pass through the entire ventricular segment in order to reach the outflow tract.

The major step in the formation of the separate atrial and ventricular chambers involves ballooning of secondary myocardium from the outer curvature of the primary heart tube (Figure 2.17D). In the primary atrium, this gives rise to the separate left and right atrial appendages. The formation of the atrial appendages, together with a change in the orientation of the atrial segment, is a prerequisite for normal atrial septation [142,147]. At the same time, the atrio-ventricular canal undergoes complex growth, rightward expansion and remodelling. As a result, the atrio-ventricular canal is incorporated into both atria and eventually leads to the establishment of separate left and right atrio-ventricular connections [148].

Sequential balloon dilatation of the proximal and distal parts of the ventricular segment is also responsible for the formation of the left and right ventricles, respectively (Figure 2.17E) [142]. As these outpouchings develop, they develop characteristic trabeculations that differentiate the two ventricles from each other [149]. Remodelling of the primary interventricular foramen and the inner curve of the ventricular segment is ultimately responsible for the formation of the inlet portions of both ventricles, the outlet portion of the left ventricle and ventricular septation [142,147,150].

The outlet portion of the primary heart tube develops as a myocardial structure that extends from the outlet portion of the ventricular loop to the aortic sac. During subsequent development, the walls of the outflow tract change from a myocardial to an arterial phenotype. The distal portion divides to form the intrapericardial portions of the aorta and pulmonary trunk while the proximal portion forms the semilunar valves, arterial sinuses and sub-pulmonary infundibulum. Septation of the outflow tract establishes direct and separate connections between the left ventricle and aorta; and the right ventricle and pulmonary trunk [151].

2.7 THE FOETAL CIRCULATION

Almost all of our current understanding of the foetal circulation has been acquired largely from angiographic investigations in the foetal lamb [152-154] together with a limited number of studies in exteriorised human foetuses [152].

Foetal blood rich in oxygen (oxygen saturation, 80%) and nutrients returns to the foetus from the placenta in the umbilical veins. On approaching the liver, the majority of blood in the umbilical vein flows directly into the IVC through the ductus venosus. A smaller proportion passes through the liver parenchyma and mixes with deoxygenated blood from the portal circulation. In the IVC, blood from the ductus venosus mixes with deoxygenated blood from the hepatic veins as well as blood return from the lower trunk and extremities.

Inferior vena cava blood represents approximately 70% of the systemic venous return to the heart. Within the right atrium, inferior vena caval return is divided into two streams by a fold in the endocardium (crista dividens). The larger stream is deflected through the foramen ovale into the left atrium, where it mixes with the deoxygenated pulmonary venous return. The blood in the left atrium (oxygen saturation, 62%) then flows into the left ventricle, where it is pumped into ascending aorta to supply the coronary arteries, head and upper extremities, and the remainder passes into the descending thoracic aorta [152,153].

The SVC brings deoxygenated venous blood (oxygen saturation, 40%) from the upper portion of the body. The blood in the SVC flows into the right atrium where it mixes with the smaller stream of blood from the IVC. The blood in the right atrium then passes into the right ventricle and is pumped into the pulmonary trunk [152,153]. The pulmonary vascular resistance (*PVR*) in the foetus is high, primarily due to pulmonary arterial hypoxia-mediated increased vasomotor tone [154,155]. As a result, only a small proportion of blood passes through the pulmonary vasculature; the major part of the right ventricular output flows through the ductus arteriosus into the descending thoracic aorta[156]. The blood in the descending thoracic aorta supplies the lower part of the body and the placenta, via two umbilical arteries [153]. The organs distal to the ductus arteriosus are supplied with blood that has a lower oxygen saturation (oxygen saturation,

58%) than blood supplying the brain and upper extremities. This arrangement ensures the placenta receives blood with a lower oxygen saturation, maximising the efficiency of placental gas exchange.

The left and the right sides of the foetal circulation function effectively in parallel. Both sides of the heart contribute to blood flow in the systemic circulation of the foetus [152,157]. This parallel configuration is associated with pressure and volume loading conditions of the foetal heart that are markedly different from the adult circulation. In the foetal circulation, the right ventricle ejects approximately 65% of the combined ventricular output, whereas the left ventricle ejects only 35% [157]. The large ductus arteriosus allows equalisation of the pressure between the aorta and the pulmonary trunk. Left and right ventricular afterload are therefore equivalent. Direct measurements of the ventricular pressure in the foetus have shown that pressure generated in the left and right ventricles are equal (systolic blood pressure, 60 mmHg) [158,159]. As a result of these loading conditions in utero, the left and right ventricles have a similar size and wall thickness at birth [152]. The parallel arrangement of blood flow in the foetus and the normal physiological adaptation may explain why most complex congenital heart defects are well tolerated in utero.

2.8 THE TRANSITION FROM FOETAL TO NEONATAL CIRCULATION

The transition from foetal to neonatal extrauterine circulation is associated with sudden and dramatic changes in the circulation as gas exchange is transferred from the placenta to the neonatal lungs [159]. This is accompanied by substantial changes in the pressure and volume loading conditions of the two ventricles, as the circulation changes from a parallel arrangement to an in-series arrangement, in which the left ventricle is connected exclusively to the aorta and the right ventricle is connected exclusively to the main pulmonary artery (MPA) [160-162].

At birth, smooth muscle contraction within the umbilical arteries, vein and ductus venosus result in the functional closure of these vessels within a few minutes [152]. The interruption of the umbilical vessels causes a substantial increase in systemic vascular resistance (*SVR*). Concurrently,

the onset of respiration is associated with a rapid decrease in the *PVR* and a five-fold increase in pulmonary blood flow [163].

The increase in pulmonary blood flow and pulmonary venous return results in a rise in left atrial pressure. There is a corresponding reduction in right atrial pressure following the cessation of placental flow. The changes in atrial pressure result in the reversal of the foetal right-to-left atrial pressure gradient, which in turn cause the septum primum to become apposed to the septum secundum, functionally closing the foramen ovale [164]. The two septa subsequently fuse, although there is considerable variation in the age at which fusion occurs [165].

The decrease in *PVR* coupled with the rise in *SVR* results in a reversal of the flow through the patent ductus arteriosus from the foetal right-to-left direction to provide a left-to-right shunt [166]. However, within a few minutes following birth, the large ductus arteriosus begins to constrict primarily in response to the rise in arterial oxygen saturation. Constriction of the ductus arteriosus is progressive and usually results in the functional closure within 12 to 24 hours following birth in the mature infant [152]. There is subsequent anatomical obliteration of the ductus arteriosus that is usually complete by about 2 months of age [165].

The fall in *PVR* is accompanied by an exponential decline in pulmonary arterial and right ventricular pressure [167] such that the pulmonary artery pressure achieves an adult level within two weeks following birth (systolic pulmonary artery pressure, < 25 mmHg; *PVR*, 1 – 3 Woods units·m^{-2}) [168]. In the systemic circulation, cessation of placental blood flow is associated with an abrupt rise in the systemic blood pressure [159] and there is a further, more gradual rise in the blood pressure during the first 6 weeks of life [167,169]. The blood pressure then remains relatively constant until about 6 years (systolic blood pressure, 100 mmHg; *SVR*, 15 – 20 Woods units·m^{-2})[169].

At the time of birth, the left and right ventricles have a similar size and wall thickness. The changes in pressure and volume loading after birth result in a marked physiological adaptation in both ventricles. The left ventricle undergoes a rapid increase in left ventricular mass, such that

the left ventricular mass indexed to body surface area increases by almost 20% within the first 2 weeks after birth [170]. The increase in ventricular mass is much slower in the absence of systemic pressure loading [171,172]. Consequently, there is a gradual involution of the right ventricular mass index. This progressive right ventricular "deconditioning" means that the right ventricle is no longer able to maintain adequate cardiac output against a systemic afterload beyond about 1 month of age [173].

2.10 OVERVIEW OF CONGENITAL HEART DISEASE

In approximately 1% of births, the development to the heart does not follow this normal pattern. This results in the development of a number of congenital cardiac malformations [140].

Congenital heart disease (CHD) is defined, "as a gross structural abnormality of the heart or intrathoracic great vessels that is actually or potentially of functional significance" and is present at birth [174].The definition proposed by Mitchell *et al.* excludes functionless abnormalities of the great veins and the branches of the aortic arch [174].

Congenital heart disease is the single most common form of birth defect, which affects 4 – 14 per 1000 live births [174,175]. Congenital heart disease occurs with a similar frequency in all ethnics groups and in all regions of the world [176]. Hoffman *et al.* identified that there had been a progressive increase in the published incidence of CHD, which was mainly attributed to an improved ability to identify patients with clinically less important lesions [176]. If children with a small patent ducts arteriosus, small ventricular septal defect or the potentially important bicuspid aortic valve were also included, CHD may affect as many as 75 per 1000 live births [176].

Congenital heart disease encompasses a wide spectrum of heart defects with varying levels of severity, which can be classified according to the type and severity of the lesion [176-178] or the functional impact on the patient [179].

Hoffman *et al.* defined three grades of CHD (mild, moderate and severe) according to the severity of the lesion [176]. The incidence of CHD varies according to the severity of the lesion.

Hoffman *et al.* estimated that the incidence of moderate and severe CHD is 3 per 1,000 live births and 2.5 – 3 per 1,000 live births, respectively [176]. Based on these estimates, approximately 2000 children are born in the United Kingdom each year with severe CHD [180].

Severe CHD included all patients with cyanotic heart disease, in which relatively deoxygenated blood circulates around the systemic circulation. This occurs in patients with transposition of the great arteries, tetralogy of Fallot and functionally single ventricle anatomy, for example. Severe CHD also included patients with severe forms of acyanotic heart disease, such as patients with critical aortic or pulmonary valve stenosis, critical coarctation of the aorta or a large ventricular septal defect. The majority of children that require medical intervention, surgery or die with CHD in the neonatal period or during infancy have severe CHD [181].

Moderate CHD was defined as less severe forms of acyanotic heart disease. This included patients with moderate aortic or pulmonary valve disease, non-critical coarctation of the aorta or a large atrial septal defect. These patients will also usually require specialist treatment during their lifetime [181], although this treatment is generally less intensive than that required for patients with severe CHD [176].

Mild CHD included patients with a small atrial or ventricular septal defect or a small patent ductus arteriosus. Most of these patients are asymptomatic and many of these lesions may close spontaneously or never cause medical problems.

Over the last 30 years, advances in the diagnosis and treatment of patients with CHD together with a greater understanding of the anatomy and physiology have led to a substantial improvement in the long-term outcome for children with congenital heart disease. Currently, approximately 94% of children will survive for at least one year following paediatric cardiac surgery in the United Kingdom [182]. It is estimated that at least 85% of patients with even the most serious heart defects can now expect to reach adult life [183,184]. However, few patients with CHD are actually cured. The life expectancy for adults with severe CHD is 35 – 40 years and 55 years for adults with moderate CHD [183]. The majority of patients with CHD will

require life-long follow-up in order to manage the medical, social and psychological issues faced by children and adults with CHD [185].

2.10.1 Classification and nomenclature of congenital heart disease

The classification of CHD requires a nomenclature system that allows the abnormal anatomical features to be described accurately, succinctly and unambiguously [186]. Historically, congenital heart disease was usually defined as a series of discrete categories according to their characteristic morphology, as illustrated by the terminology agreed upon by the New York Heart Association, *NYHA* [187]. Complex and unusual malformations did not fit within these rigid classification systems and were usually assigned to a "miscellaneous" group. Several centres developed more inclusive systems for the classification of CHD. In 2002, these systems were unified in, 'The International Paediatric and Congenital Cardiac Code' (IPCCC) [188]. The IPCCC provides a comprehensive nomenclature system to describe congenital heart malformations, associated symptoms and genetic syndromes as well as surgical and interventional procedures used to palliate or correct them [189,190].

2.10.1*a* *Segmental approach to classification of congenital heart disease*

The IPCCC classification of CHD is based on the segmental approach to the description of congenital heart defects [186,191-196]. In the segmental approach, the heart is considered to have atrial, ventricular, and arterial segments. Normal and congenitally abnormal hearts are described according to how these segments are sequentially connected; what associated anomalies are present in each of the cardiac segments; and what spatial relationship the segments have with one another and the heart has within the thorax [192]. Van Praagh *et al.* advocate that this description may be summarised using a special, three-letter notation [197].

The first step in the segmental analysis requires the identification of the segments of the heart. Each segment is made up of a strictly limited number of components (Figure 2.18). In the normal heart, the atrial segment consists of the left and right atria, the ventricular segment comprises the left and right ventricles and the arterial segment consists of the aortic and

pulmonary trunks. These cardiac chambers and the arterial trunks components can be identified based on their normal, characteristic appearances [193,198].

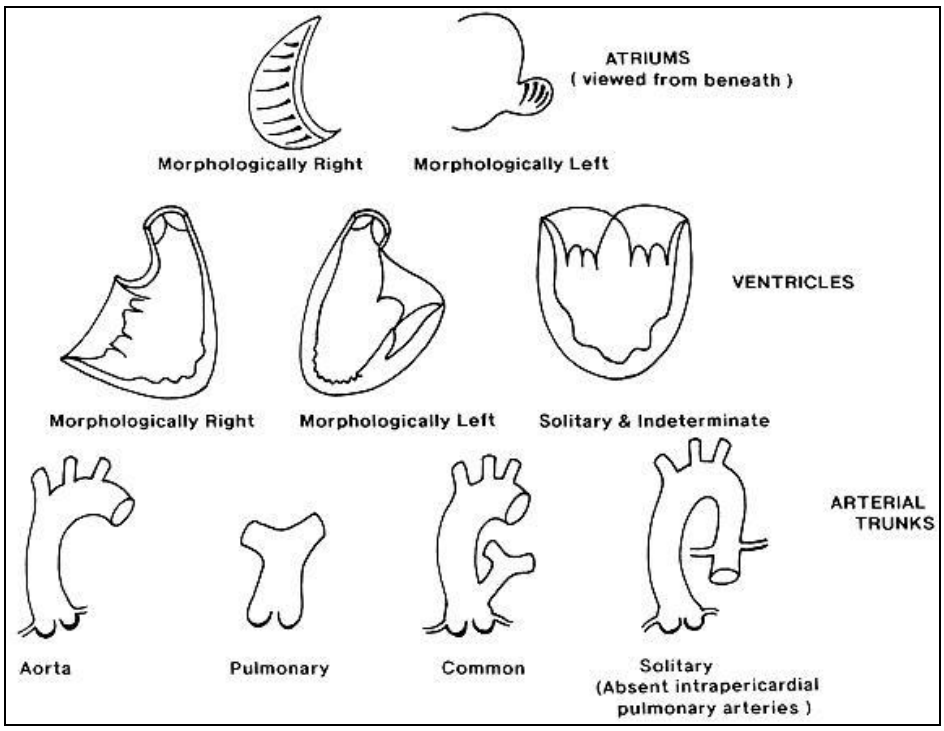

Figure 2.18 *Sequential analysis of the heart. The three segments of the heart are made up of a strictly limited components. The atria may be of left or right atrial morphology. The ventricles may be of right, left, or indeterminate morphology. Four types of arterial trunk can be recognised according to the pattern of branching. Reproduced from Anderson et al.*[192].

In congenitally malformed hearts, the most constant parts of each component are also used to identify the morphology of each component, regardless of their relative position. The shape of the atrial appendage and the nature of the junction of the atrial appendage with the remainder of the atrium determine whether the atrium is morphologically left or right (Figure 2.18). Each atrial component may be morphologically left or right allowing the possibility of one left and one right atrium, two left atria (left atrial isomerism) or two right atria (right atrial isomerism). The ventricular segment usually consists of two components, one has left ventricular morphology and the other has right ventricular morphology. Rarely, there may be only a single ventricle of indeterminate morphology. The morphology of the ventricular component is defined by the pattern of the trabeculations within the apical part of the ventricle (Figure 2.18). The arterial segment usually consists of two trunks. Occasionally, the segment may have a common or a

solitary arterial trunk. The morphology of the arterial segment is defined by the branching patterns of the arterial trunk, in particular the origin of the brachiocephalic arteries (Figure 2.18) [192,199].

The greater majority of hearts have biventricular atrioventricular connections, where each atrial component is connected to a separate ventricle. There is atrioventricular concordance if the morphological left atrium (mLA) connects with the morphological left ventricle (mLV) and the morphological right atrium (mRA) connects with the morphological right ventricle (mRV). Atrioventricular discordance occurs when the mLA connects with the mRV and the mRA connects with the mLV [200]. In hearts with atrial isomerism the atrioventricular connections are ambiguous (Figure 2.19).

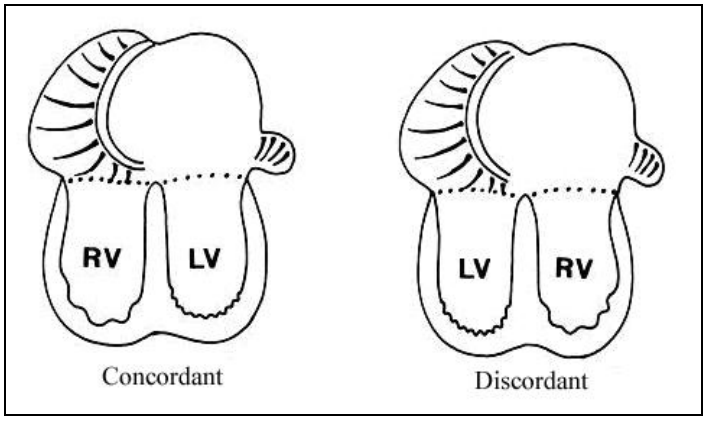

Figure 2.19 *The atria can be connected to the ventricles in either a concordant (left panel) or discordant fashion. Reproduced from Anderson et al.*[192].

The ventriculo-arterial junction is described in a similar manner to the atrioventricular connection. The ventriculo-arterial junction is concordant when the aorta arises from the mLV and the MPA arises from the mRV. The ventriculo-arterial junction is discordant when the aorta arises from the mRV and the MPA arises from the mLV. This is more commonly known as transposition of the great arteries. A double outlet ventricle occurs when both arterial components arise from a single ventricular component. When an arterial valve overrides a ventricular septal defect, the arterial trunk is considered to belong to the ventricle that supports

the greater part of its circumference. This may, therefore, result in the ventriculoarterial junction being normal, transposed or double-outlet.

In some patients, only one arterial trunk arises from the ventricular segment. This may be a common truncus; a solitary aorta when the MPA is not connected to the ventricular chambers; a solitary MPA when the aorta is not connected to the ventricular chambers [201]; or a solitary trunk, which occurs in patients with certain types of pulmonary atresia, ventricular septal defect and major aorto-pulmonary collateral arteries [202].

In addition to abnormal connections, congenital heart malformations are characterised by abnormalities of each heart segment. These may include abnormalities of the systemic and pulmonary venous return; the atria and atrial septum; the atrioventricular junction; the ventricle, ventricular septum and ventricular outflow tract; and the great arteries. In the majority of cases, these associated anomalies are the only abnormalities present [198,201].

Finally, complex congenital heart malformations are often associated with cardiac malposition. This may affect the topology or spatial arrangement of the cardiac chambers within the heart [197,198] or the position and alignment of the heart within the thorax [198,201].

2.10.1*b* *Form and function*

The accurate and appropriate classification of heart malformations is of fundamental importance to the successful management of CHD. Alterations in anatomy are associated with predictable physiological changes that determine the patient's symptoms, signs and functional well-being. These changes in cardiac form and function evolve over time. This may occur as part of the natural history of the disease or the development of pathophysiological processes such as ventricular hypertrophy, acquired obstruction of the outflow pathways or the development of atrioventricular valve regurgitation. Knowledge of predictable and possible abnormalities of cardiac form and function allow clinicians to determine what interventions will be required, when they should be performed and what effect that intervention should have on the natural history of the disease [203].

2.11 FUNCTIONALLY SINGLE VENTRICLE ANATOMY

The term *functionally single ventricle anatomy* refers to a heterogeneous group of heart malformations that are characterised by only one ventricle within the ventricular mass that can independently support blood flow in either the systemic or pulmonary circulation [204]. In fact, most of these hearts actually have two ventricles, one large and one small [204-209] although rarely the heart may contain a truly solitary ventricle [205,207,209,210]. However, none of these hearts are suitable for a biventricular repair and long-term survival is dependent on the function of the dominant or single ventricle [208].

2.11.1 Nomenclature of functionally single ventricle anatomy

Although physiologically equivalent, the term functionally single ventricle anatomy encompasses a wide spectrum of distinct anatomic abnormalities [207,209,211]. This morphological variability is reflected in the nomenclature; for example, Van Praagh *et al*. identified twenty-one different terms that had been used to describe hearts with apparently only one ventricle [205]. According to the segmental approach previously outlined, the atrial segment may consist of any one of the four atrial arrangements. The ventricular segment may consist of a dominant ventricle with left ventricular morphology and a small or rudimentary ventricle of right ventricle morphology, or vice versa; or, very rarely, a single ventricle of indeterminate morphology. The atrial and ventricular segments are joined by a univentricular or biventricular atrio-ventricular connection [208,211]. Any one of the arterial trunks and ventriculo-arterial connections may be observed along with a wide variety of associated cardiac anomalies [204,209,211].

Hearts with functionally single ventricle anatomy can be grouped into two broad categories according to the atrio-ventricular connection. In the majority of cases, there is a univentricular atrio-ventricular connection, Figure 2.20 [204,206,208]. This can occur when the left or right-sided atrioventricular connection is absent, like in tricuspid atresia or mitral atresia, for example. Alternatively, there may be double-inlet ventricle, in which both atria connect to the dominant ventricle.

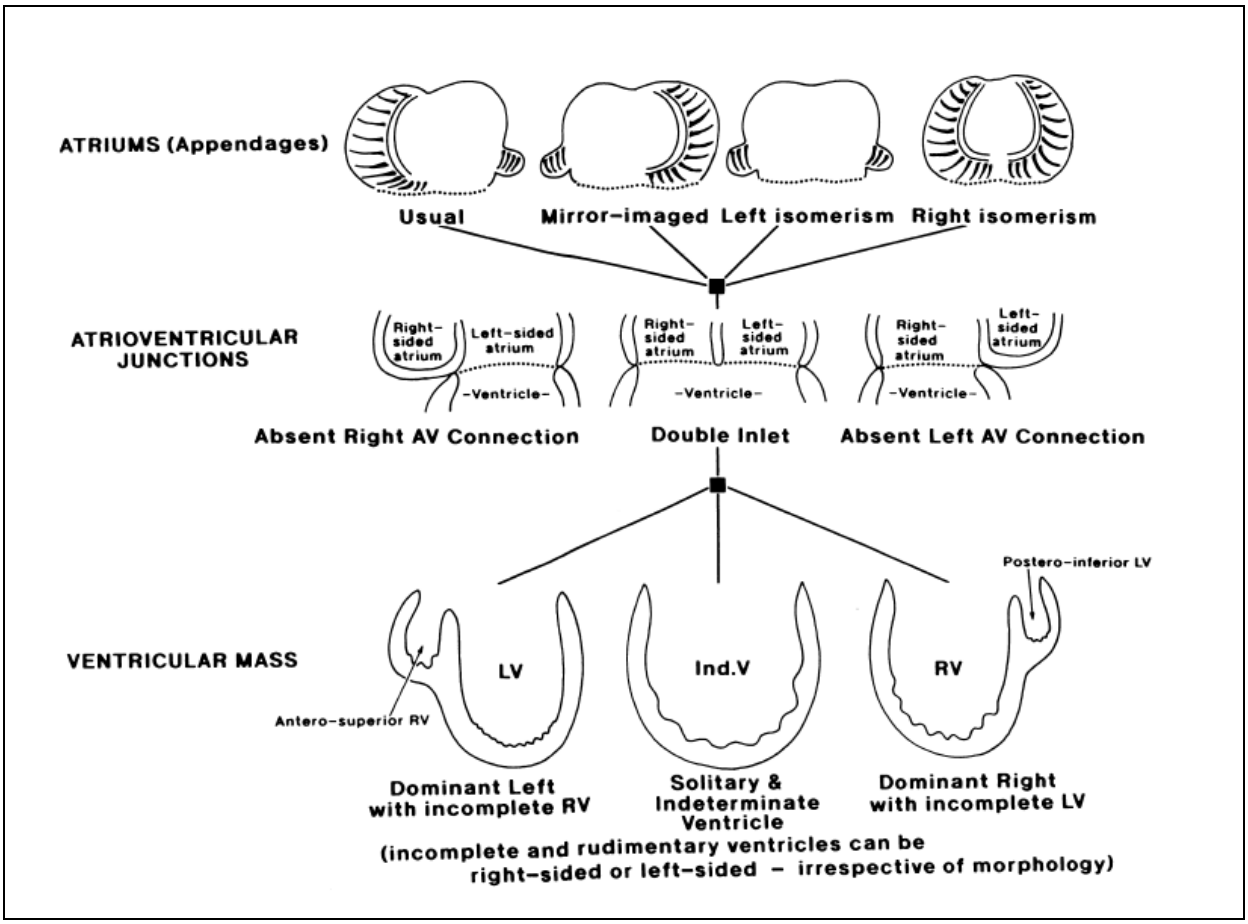

Figure 2.20 *This diagram illustrates how the atrial, atrio-ventricular junctions and ventricular segments are arranged within the ventricular mass.*
(Ind. = indeterminate; LV = left ventricle; RV = right ventricle)
Reproduced from Anderson & Ho [208].

In the series reported by Barlow *et al.*, hearts with a univentricular atrio-ventricular connection made up approximately two-thirds of hearts with functionally single ventricle anatomy [207]. In the remaining third, there was a biventricular atrio-ventricular connection [207]. In these cases, ventricular hypoplasia occurs because the atrio-ventricular valve are present but imperforate; the atrio-ventricular valves are "straddling"; or there is a double-outlet or discordant ventriculo-arterial connection. Obstruction of either outflow tract in combination with an intact ventricular septum and a biventricular atrio-ventricular connection also results in ventricular imbalance, producing the hypoplastic left or right heart syndromes [204,208,211,212].

2.11.2 Ventricular morphology and functionally single ventricle anatomy

The normal left and right ventricles can both be divided into three parts, namely the inlet, apical component and outlet [213,214] , as illustrated in Figure 2.21 and Figure 2.22.

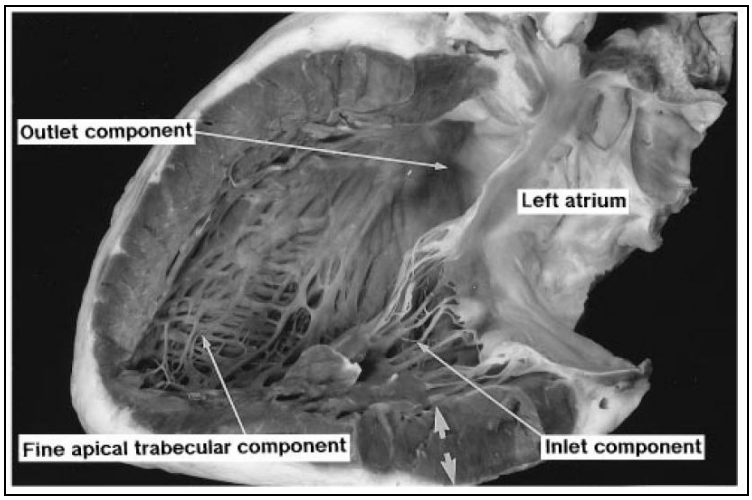

Figure 2.21 *Internal view of the human LV showing the inlet, apical and outlet components. Reproduced from Crick et al.* [214].

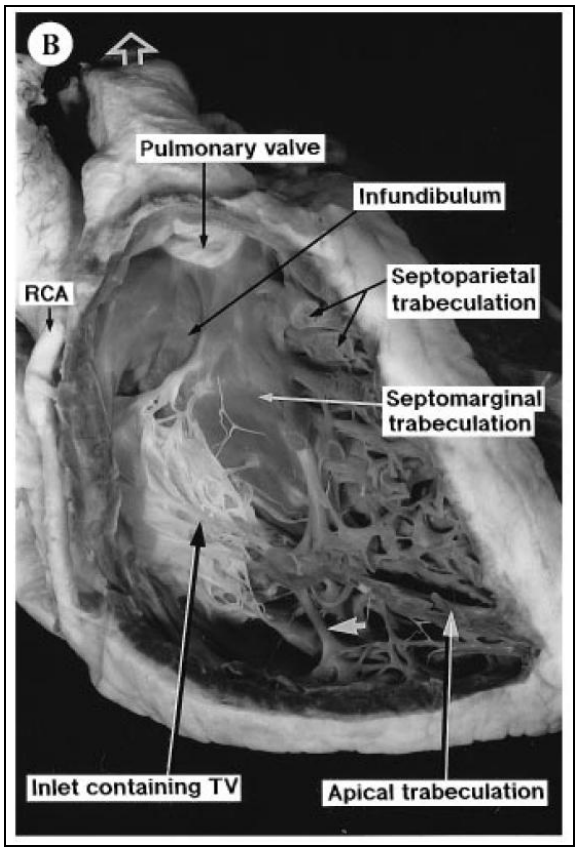

Figure 2.22 *Internal view of the human RV showing the inlet, apical and outlet components. Reproduced from Crick et al.* [214].

The *inlet* part extends from the atrioventricular junction to the distal attachments of the tension apparatus that support the corresponding atrioventricular valve. The *apical component* is heavily trabeculated. The trabeculations are coarse in the right ventricle and comparatively fine in the left ventricle. The *outlet* part is a comparatively small region of the ventricle, which lies beneath the semilunar valve. In the left ventricle, the mitral and aortic valves are in fibrous continuity with one another. By contrast, the outlet of the right ventricle is a freestanding muscular structure, the infundibulum that supports the pulmonary valve. The tricuspid and pulmonary valves are thus widely separated. In functionally single ventricle anatomy, the ventricular mass usually contains one dominant ventricle and one small or rudimentary ventricle [213,214]. The dominant ventricle is morphologically normal, possessing an inlet, an apical component together with an inlet and an outlet. The small ventricle may be either rudimentary (if it lacks one or more of its component parts) or normal in form but hypoplastic. The dominant ventricle will be of left ventricular or right ventricular morphology, as defined by the trabecular pattern within the apical component. Left and right ventricles always coexist within the same ventricular mass. Therefore, if the dominant ventricle has a left ventricular morphology then the small ventricle will have right ventricular morphology and vice versa [213,214].

Very rarely, the ventricular mass may contain a truly solitary ventricle. These hearts usually consist of a double-inlet and double-outlet from a ventricle of indeterminate ventricular morphology. The apical portion of the ventricle is coarsely trabeculated with trabeculae that are even coarser than those found in the morphologic right ventricle [204,208,211].

The morphology of the dominant ventricle is particularly important in functionally single ventricle anatomy because the dominant ventricle must support blood flow through both systemic and pulmonary circulations. The ability of the morphological right ventricle to support the entire circulation has been questioned because of anatomical, geometrical and functional differences between the morphological left and right ventricles [215].

The differences in the shape and structure of the two ventricles relate in part to their different embryological origins [146]. The normal right ventricle has a complex, truncated asymmetric

pyramidal shape, in which the septal contour is indented by the left ventricle [62,216]. The inlet is a complex ellipse; the apical portion, which triangulates at the apex, is variably flattened by the left ventricle; and the outlet is approximately cylindrical. By contrast, the normal left ventricle has a prolate spheroidal [217,218] or catenoidal shape [219,220]. This relatively simple geometry may be intrinsically better suited to sustained, high pressure contractile function.

In conjunction with the differences in ventricular shape, there are also intrinsic differences in the arrangement of myocytes within the normal left and right ventricle. Three distinct, concentric layers can be identified within the wall of the left ventricle, according to the orientation of the myofibres relative to the surface of the heart [220,221]. The myofibres in the superficial layer are orientated obliquely, circumferentially in the middle layer and the myofibres in the deep layer are aligned longitudinally. Contraction of the thick middle layer results in short-axis shortening and the clockwise "wringing" motion, which are primarily responsible for left ventricular force generation and ejection [222,223]. However, the normal right ventricle does not contain a middle layer [221]. Right ventricular contraction is therefore dependent on longitudinal shortening [62,224], which results in a sequential, peristalsis-like contraction that begins in the right ventricular inlet and extends into the outlet [225,227,228].

In addition to the anatomic and geometric considerations, there is considerable debate about whether myocytes in the left and right ventricle are intrinsically different. The current evidence suggests that the left and right ventricles are broadly similar under experimental conditions. Rouleau *et al.* examined the mechanical characteristics of isolated muscle preparations from the canine left and right ventricular free walls [225]. Peak total tension and the rate of tension development were similar. These similarities persisted during changes in loading conditions, calcium concentration and inotropic agents. However, the right ventricle had a faster rate of shortening and attained peak tension more quickly. The authors suggested that this difference may reflect physiological adaptation to the normal, low-pressure pulmonary circulation [225].

Comparable findings have also been identified in isolated, perfused hearts during isovolumic contraction. Burkhoff *et al.* reported that the force-interval relationships in the canine left and

right ventricles are virtually identical [226] and the time course for pressure generation is very similar [227]. Joyce *et al.* also identified that systolic function and active diastolic relaxation are equivalent, although the right ventricular compliance was also significantly greater [228]. The clinical implications of these similarities and subtle differences have not been fully elucidated.

In spite of this experimental research, there is a long-standing and on-going concern that the morphologic right ventricle may be intrinsically less well suited to support either the systemic circulation [229] or the entire circulation [230-233]. Patients with a systemic right ventricle have a significant risk of heart failure that is accompanied by high mortality [229]. It has a relatively low ejection fraction and reduced myocardial functional reserve [234], and it is associated with a relatively poor functional adaptation to pressure and volume overload [235,236]. In addition, the right ventricle has only a single coronary artery supply, and relative coronary insufficiency has been cited as a potential cause of progressive RV failure, particularly were RV hypertrophy co-exists [237]. At present, however, the clinical importance of these differences remains essentially speculative [238].

2.11.3 Natural history of functionally single ventricle anatomy

The natural history of various forms of functionally single ventricle anatomy has been determined based on population-based registries of children with congenital heart disease [239-242]; autopsy studies [243,244]; together with cohort and series analyses from individual institutions [245-249]. The relative merits of each these various study designs have been previously discussed [250]. Nevertheless, all of these studies confirmed that functionally single ventricle anatomy is associated with a very poor prognosis without palliative or definitive surgical treatment. There is a high early mortality rate and a subsequent, progressive attrition with time. Indeed, the survival prospects for children with functionally single ventricle are sufficiently poor that diagnosis alone strongly indicates the need to proceed along the pathway of surgical palliation. Surgical palliation culminates in the Fontan procedure, which connects the systemic and pulmonary circulations in series, powered by the single function ventricle.

2.12 PROCEDURES TO BYPASS THE RIGHT-SIDE OF THE HEART

The right or sub-pulmonary ventricle represents an integral part of the normal cardiovascular system [255-257]. Contraction of the right ventricle provides the driving force for pulmonary blood flow [251]. Right ventricular function also maintains a low pressure in the systemic venous system, which prevents systemic venous distension and the development of massive peripheral oedema [252].

Although the right ventricle is intrinsically important, it is not *essential* to maintain blood flow through the pulmonary circulation. For example, long-term survival has been reported in patients with tricuspid atresia and congenital aplasia of the right ventricular myocardium [253,254]. Experimental studies that deliberately damaged the right ventricle also confirmed that adequate pulmonary blood flow and normal venous pressure could be maintained in the absence of the pumping function of the right ventricle [252,255,256].

Studies in comparative anatomy demonstrated that the pulmonary arterial pressure in fish, amphibians, reptiles, mammals and birds were all of the order of 25/10 mmHg. Rodbard & Wagner suggested that the force for pumping systemic venous blood through the lungs could be adequately supplied by the central venous pressure [257,258].

A wide variety of surgical procedures were developed to determine the feasibility of partial or complete bypass of the right ventricle as well as provide surgical palliation for patients with various forms of cyanotic congenital heart disease (Figure 2.23). The historical developments that led to these procedures have been thoroughly reviewed in a number of separate articles [255,256,259-262].

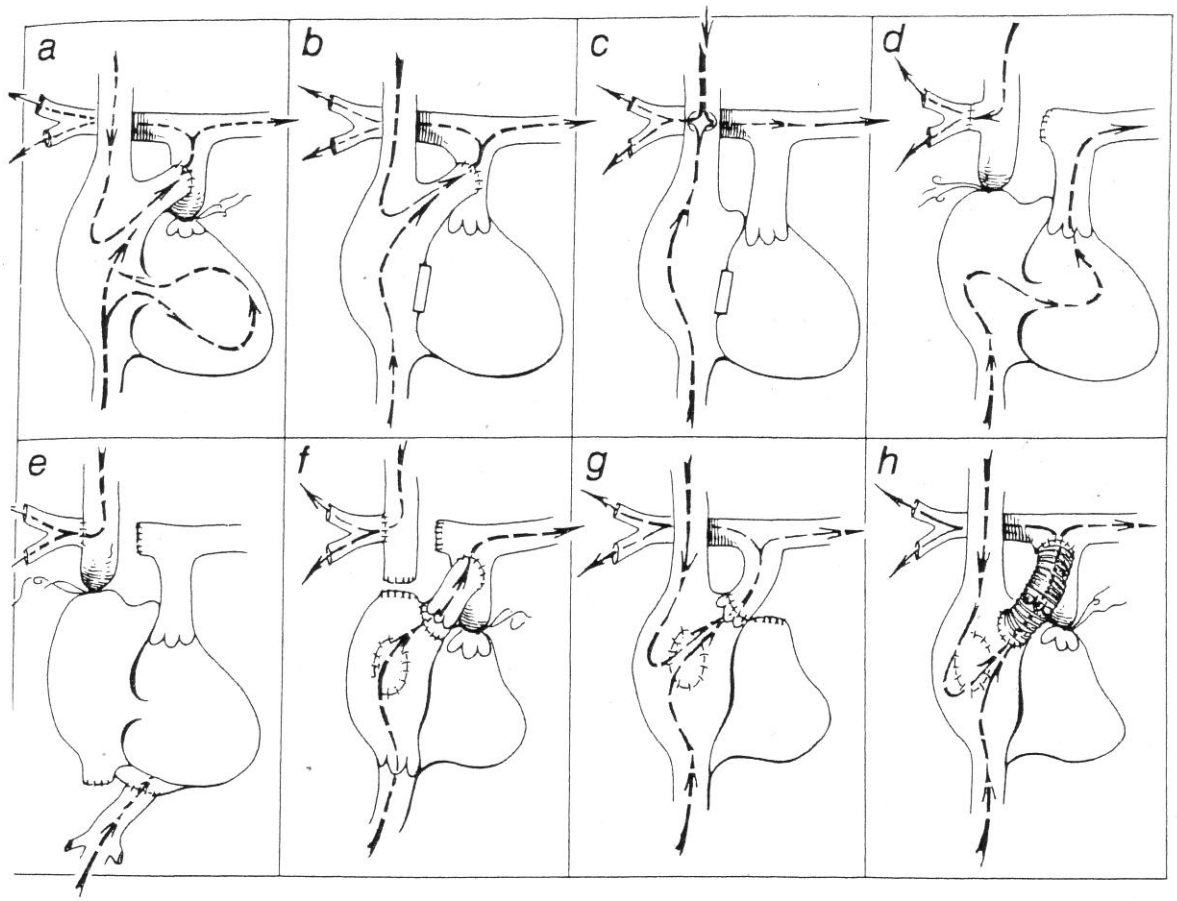

Figure 2.23 *The development of procedures to bypass the right ventricle. The figure includes the experimental procedures performed by Rodbard & Wagner (Figure 2.23a) and Haller et al. (Figure 2.23c); Carlon et al. (Figure 2.23d) and Robiscsek et al. (Figure 2.23e). The Figure also includes the clinical procedures used by Fontan & Baudet (Figure 2.23f) and Kreutzer et al. (Figure 2.23g).These procedures are discussed in more detail in the accompanying text. Reproduced from RM Sade* [255]

2.12.1 Partial bypass of the right ventricle

2.12.1a Superior cavo-pulmonary anastomosis

Several groups independently demonstrated that partial bypass of the right ventricle could be successfully achieved using a superior cavo-pulmonary anastomosis [256]. For example, Carlon *et al.* described a procedure in 1951 where the distal end of the right pulmonary artery was anastomosed to the caval origin of the azygos vein and the cavo-atrial junction was ligated (D, Figure 2.23) [263]. As a result, blood in the SVC drained directly into the right pulmonary artery with no intervening pumping chamber. These experiments formed the basis for the superior cavo-pulmonary anastomosis that Glenn used in the first successful clinical case in 1958 [264].

The original superior cavo-pulmonary anastomosis (or Glenn shunt) was used to successfully palliate a wide variety of congenital heart defects. The procedure was relatively simple to perform and had a low operative mortality in properly selected patients. It also provided effective relief of cyanosis and satisfactory, sustained long-term palliation [265-270].

The superior cavo-pulmonary anastomosis has distinct physiologic advantages compared with aorta-pulmonary shunts (e.g. Blalock-Taussig, Waterston and Potts-Smith shunts) that were traditionally used to provide long-term palliation for patients with cyanotic heart disease [271]. The superior cavo-pulmonary anastomosis is associated with more efficient gas exchange because only desaturated systemic venous blood in the SVC is directed into the pulmonary arteries rather than an arteriovenous mixture. Consequently, equivalent or improved systemic arterial oxygen saturations are achieved even though total pulmonary blood flow is reduced [271]. The superior cavo-pulmonary anastomosis is also associated with a reduced volume load of the heart compared with aorto-pulmonary shunts. This represents the principal haemodynamic advantage of the superior cavo-pulmonary anastomosis, as "volume offloading" is associated with better long-term preservation of ventricular function and improved overall outcome [269,272,273].

Despite initial enthusiasm, a number of difficulties were subsequently identified with the Glenn shunt. The procedure was associated with an increased risk in infants as a result of small pulmonary arteries and higher ***PVR*** [266,267,274]. The increased ***PVR*** was associated with decreased pulmonary blood flow and decreased arterial oxygen saturations [275]. The Glenn shunt was also associated with a late clinical deterioration with a fall in the arterial saturations. This is primarily due to the growth of the child and the change in the relative proportion of systemic venous blood that flows through the SVC, Figure 2.24 [276]. However, the development of collateral venous channels from superior to the inferior vena cava; pulmonary arteriovenous fistulas; and abnormalities in regional pulmonary perfusion also contributed [277-280]. In addition, rapid progress in surgical techniques, extracorporeal perfusion, anaesthesia and post-operative care made complete repair of congenital anomalies safer at a much earlier age [281]. This removed the need for the relatively irreversible Glenn shunt as a "first stage" palliative

procedure [282]. Finally, the successful development of the Fontan procedure for the treatment of tricuspid atresia and other forms of functionally single ventricle anatomy further decreased the need for permanent shunt palliation [283-286].

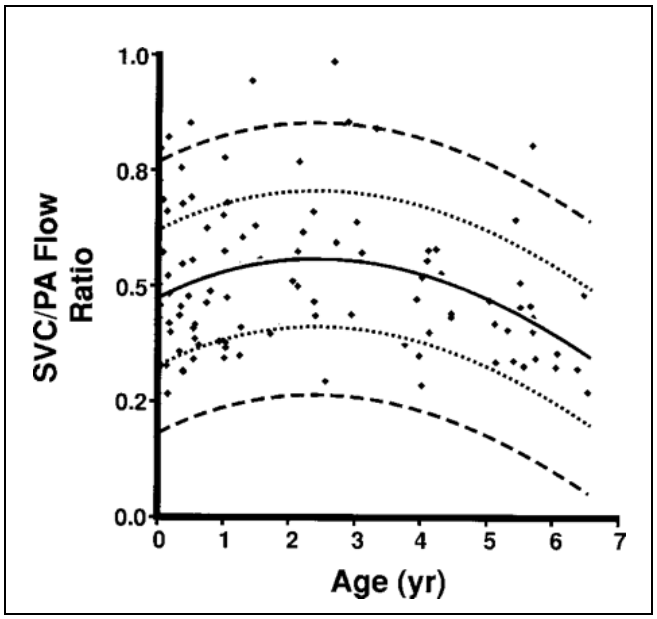

Figure 2.24 *Plot showing the relation between the ratio of superior vena caval (SVC) and pulmonary arterial (PA) flows and age in years. Solid line indicates the mean; dotted line, ±1 SD; and broken line, ±2 SD. Reproduced from Salim et al.*[276].

More recently, there has been renewed interest in using a bidirectional cavo-pulmonary anastomosis (BCPA) to provide interim palliation prior to the ultimate Fontan procedure [271,287-290]. This staging procedure was initially advocated for patients with less favourable anatomy and physiology as it may decrease the risks associated with the subsequent Fontan procedure [267,288,290,291]. Other units have applied this staged palliation more widely [292-294]. For example, at Birmingham Children's Hospital, the BCPA has been performed as an interim stage in all patients prior to completion of the Fontan procedure since 1994 [294].

Currently, the BCPA is generally performed using one of two separate operative techniques: the bidirectional Glenn procedure [268,271,295] or the hemi-Fontan procedure [296-298]. Some surgeons advocate the bidirectional Glenn procedure because it is simpler, while others advocate the hemi-Fontan procedure because it potentially simplifies the subsequent Fontan procedure

[299]. Nevertheless, both procedures leave the central pulmonary arteries in continuity. Blood flow in the SVC can therefore pass into the left or right pulmonary arteries (i.e. there is bidirectional flow). Studies based on computational fluid dynamics have also demonstrated that both procedures perform nearly identically [300,301].

2.12.1b Inferior cavo-pulmonary anastomosis

While the superior cavo-pulmonary anastomosis has proved highly successful, initial attempts to connect the IVC directly to the pulmonary artery were generally unsuccessful. The procedure was associated with a high operative mortality and almost all the animals that survived developed venous congestion in the splanchnic system and massive ascites [256,302].

More recently, Mace *et al.* established that it is possible to safely connect the inferior vena to the pulmonary arteries using a tube conduit in an *in vivo* canine model [303]. Nevertheless, the authors demonstrated that the inferior cavo-pulmonary shunt was associated with a significantly higher systemic venous pressure and lower cardiac output than the equivalent superior cavo-pulmonary shunt. These differences were felt to primarily reflect the degree of right-heart bypass rather than problems with the inferior cavo-pulmonary shunt per se [303].

In a separate article, Mace *et al.* described the use of the inferior cavo-pulmonary shunt to successfully palliate two infants with functionally single ventricle anatomy [304]. However, this procedure represented only a small fraction of their normal practice (< 1%) and the inferior cavo-pulmonary anastomosis is not widely used to provide interim palliation prior to the Fontan procedure.

2.12.2 Complete bypass of the right ventricle

The first attempt to completely bypass the right ventricle was made by Rodbard & Wagner in 1948 [257]. In these canine experiments, the right atrial appendage was anastomosed to the main pulmonary artery and the main pulmonary artery was ligated proximal to the anastomosis (A, Figure 2.23). Most of the animals survived for periods of up to 2 months after the procedure.

However, although the procedure was successful, the right ventricle still contributed to the pulmonary circulation as a result of functional tricuspid regurgitation.

Similar experiments were performed by other groups [305,306]. However, in these experiments complete right heart bypass was achieved by also occluding the tricuspid valve orifice. None of the animals survived more than a few minutes after the procedure. Rose *et al.* concluded that, "… when the right ventricle is acutely excluded from the circulation, the resulting elevated venous pressure is not capable of maintaining adequate lung perfusion" [306].

Complete right heart bypass was eventually described in 1966 [307]. In these canine experiments, Haller *et al.* performed a side-to-side superior vena cava-right pulmonary artery anastomosis. Then, at a second stage, the tricuspid valve orifice was ligated. All the vena caval blood drained via the cavo-pulmonary anastomosis (C, Figure 2.23). In three of the long-term survivors, complete obliteration of the tricuspid valve was confirmed with cineangiography. The authors postulated that the right atrium may represent an efficient power source.

This experimental research culminated in 1971, when Fontan *et al.* described the treatment of three patients with tricuspid atresia. The operation was successful in two patients, who were followed up for 10 months and 30 months respectively [283]. The surgical procedure involved a series of steps (Figure 2.25) that connected the systemic vena cava to the right pulmonary artery and the right atrium to the left pulmonary artery, thus completely bypassing the right ventricle. This procedure creates a *physiologically* normal circulation, in which the systemic and pulmonary circulations are separate and in-series, powered by the single, functional ventricle.

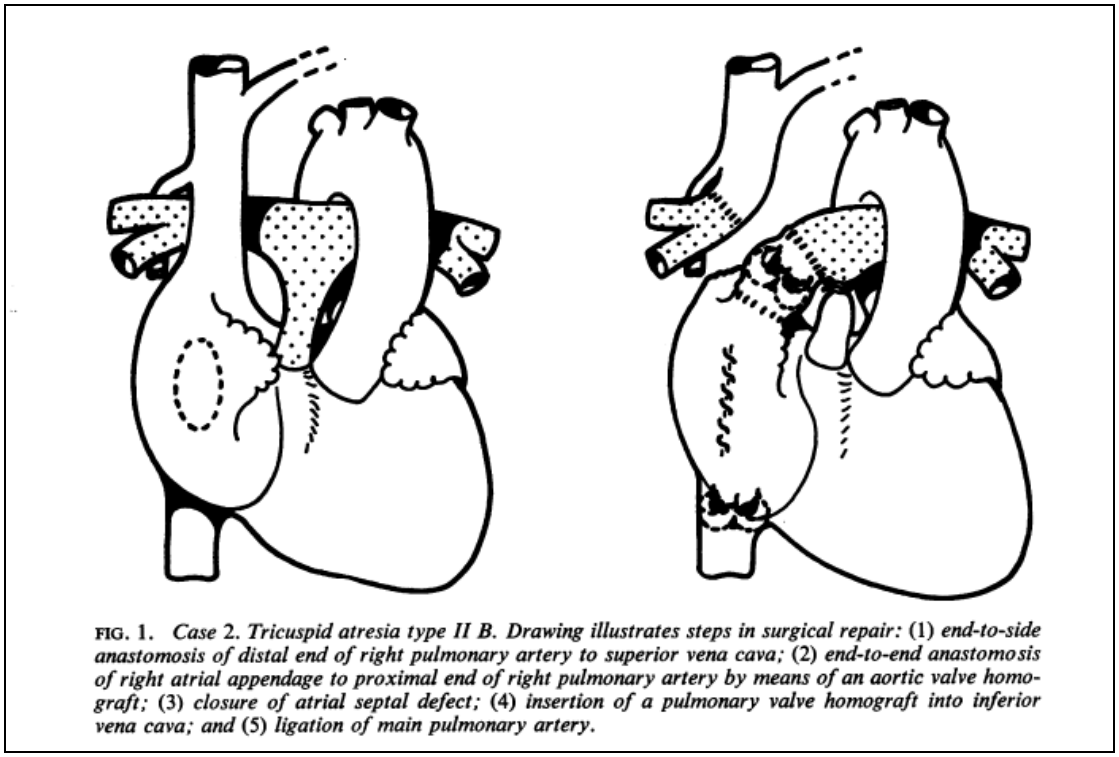

FIG. 1. *Case 2. Tricuspid atresia type II B. Drawing illustrates steps in surgical repair:* (1) *end-to-side anastomosis of distal end of right pulmonary artery to superior vena cava;* (2) *end-to-end anastomosis of right atrial appendage to proximal end of right pulmonary artery by means of an aortic valve homograft;* (3) *closure of atrial septal defect;* (4) *insertion of a pulmonary valve homograft into inferior vena cava; and* (5) *ligation of main pulmonary artery.*

Figure 2.25 *Copy of the diagrams illustrating the procedure described by Fontan & Baudet* [283].

A number of other reports confirmed the efficacy of the Fontan procedure in alleviating cyanosis and improving the clinical and functional well-being of selected patients with tricuspid atresia [284,285,308-310]. Based on this success, the principles of the Fontan procedure were subsequently applied to other more complex forms of congenital heart disease, including patients with double-inlet left ventricle, common atrio-ventricular connection, absent left atrio-ventricular connection and hypoplastic left heart syndrome [297,311-319]. At present, the Fontan procedure represents the procedure of choice for the management of all patients with functionally single ventricle anatomy as well as patients with atrio-ventricular or ventriculo-arterial valve anatomy that precludes a biventricular repair [320,321].

2.12.3 Surgical modifications of the Fontan procedure

The original operation developed by Fontan & Baudet involved a series of steps, which resulted in the separation of the systemic and pulmonary circulation (Figure 2.25). Firstly, the SVC was anastomosed to the right pulmonary artery (i.e. a Glenn shunt). The atrial appendage was then connected to the proximal stump of the right pulmonary artery using a homograft valve, thus

ensuring all the blood in the right atrium flowed into the left lung. The atrial septal defect was closed during a period of cardio-pulmonary bypass and a further homograft valve was inserted into the orifice of the IVC. Finally, the pulmonary artery was ligated.

Since the original description, the Fontan procedure has undergone a number of modifications. For example, the Glenn shunt, which Fontan included in his original procedure, was used in only 4 of the 100 patients reported in 1983 [322]. Several other reports confirmed that it was not necessary to perform the cavo-pulmonary anastomosis as a simultaneous part of the procedure[255,284,285].

Originally, Fontan & Baudet felt it was necessary to provide the right atrium with two valves to, "… prevent free flow between the inferior vena cava, right atrium and pulmonary artery ... and stasis in the lower half of the body and inadequate cardiac filling" [283]. It soon became evident that the inlet and outlet valves were dispensable [262,320]. Late follow-up studies demonstrated that the valves tended to remain open throughout the cardiac cycle [323]. The valves also represented a potential source of obstruction to the blood flow through the Fontan circulation [316,324,325]. Therefore, inlet and outlet valves are not included in the Fontan procedure used currently.

Fontan & Baudet believed that the hypertrophied right atrium present in tricuspid atresia was necessary to provide the additional work to propel the blood from the IVC into the pulmonary circulation. The application of the Fontan procedure to other forms of congenital heart disease demonstrated that a non-hypertrophied right atrium [297,311,312,316] and even atrial chambers grossly distorted by atrial septation procedures could be successfully incorporated in the Fontan circulation [314,318-320]. Although right atrium contraction contributed to forward flow through the Fontan circulation [326], this contribution was small and not clinically important [325,327]. Moreover, atrial contraction created turbulence, which actually increased the resistance to blood flow through the Fontan circulation [320].

The *in vitro* experiments conducted by de Leval *et al.* led to the development of the total cavo-pulmonary connection (TCPC) [320]. This consists of a BCPA together with the construction of a tubular connection between the IVC and the pulmonary arteries. The inferior vena caval blood travels through a cylindrical channel of uniform diameter. As a result, the blood flow pattern is laminar, which is in contrast to the turbulent blood flow pattern observed in the atrio-pulmonary connection [320,328]. The procedure is also technically simple and can be reproduced in virtually all forms of functionally single ventricle anatomy [320].

Currently, the Fontan procedure is generally constructed using the TCPC. The tubular connection between the IVC and the pulmonary arteries consists of either an intra-atrial baffle that runs along the lateral aspect of the right atrium [261,320,329] or an extracardiac tube conduit that lies adjacent to the heart [330,331]. Studies based on computational fluid dynamics have also demonstrated that both procedures perform nearly identically [300,301].

A final modification of the Fontan procedure has involved the deliberately leaving a small hole or "fenestration" between the systemic venous pathway and the pulmonary venous atrium [332]. This allows blood in the high-pressure systemic venous pathway to flow directly into the pulmonary venous atrium, particularly during transient and reversible increases in ***PVR***. This right-to-left shunt decompresses the systemic venous system, increases venous return and thus improves cardiac output, albeit at the expense of a small fall in systemic arterial oxygenation. The introduction of this modification into clinical practice has been associated with an improved outcome following the Fontan procedure, especially in high-risk patients [231,333].

Hosein *et al.* recently reviewed the surgical practice at Birmingham Children's Hospital [294]. The Fontan procedure was introduced at this hospital in 1988 and involved one of three distinct techniques, which evolved over time. Between 1988 and 1995, the Fontan procedure was generally performed using a direct, valveless atrio-pulmonary connection, in which the roof of the right atrium was anastomosed to the underside of the pulmonary artery. In 1995, the unit adopted the TCPC. This initially involved a lateral atrial tunnel, in which the atrial septum was resected and a surgical baffle was constructed to direct flow from the IVC to the superior end of

the atrio-pulmonary anastomosis. However, since 1998, the Fontan procedure has been performed using an extracardiac conduit TCPC. This involved the interposition of a polytetrafluoroethylene (PTFE) tube conduit between the IVC and the right pulmonary artery. This technique remains the current practice [294] and represents the technique that has been used in the clinical studies reported in this thesis.

2.13 Current management of functionally single ventricle anatomy

The current management of children with functionally single ventricle anatomy begins at birth and generally involves three separate, staged operations during the first few years of life. This management strategy has developed to ensure adequate interim palliation as well as optimal preparation for the eventual formation of the Fontan procedure [292,334].

Early survival and with functionally single ventricle anatomy requires a balanced circulation, in which systemic and pulmonary blood flows are approximately equal. Some children with functionally single ventricle anatomy are born with a well-balanced circulation and require no surgery at this stage. However, the majority of children have associated heart defects, which limit blood flow through either the systemic or pulmonary circulation [335]. These children require urgent surgical intervention as a neonate or young infant [334]. This initial palliation represents the first and most critical stage of the management of children with functionally single ventricle anatomy [292].

The aims of initial palliation are to create a circulation in which there is unobstructed systemic blood flow from the ventricle; unobstructed systemic and pulmonary venous return; and reliable and controlled pulmonary blood flow such that the systemic and pulmonary circulations are well-balanced [292,336]. The initial surgical palliation can be divided into three broad categories according to whether the child has inadequate pulmonary blood flow or pulmonary blood flow dependent on a patent ductus arteriosus; unobstructed systemic and pulmonary blood flow; or systemic outflow obstruction with unobstructed pulmonary blood flow. The details of the

surgical palliation for each group have been thoroughly reviewed in a number of textbooks and review articles.

The second stage in the surgical management of children with functional single ventricle anatomy involves the formation of the bidirectional cavo-pulmonary anastomosis, as previously described. This is usually performed when the child is approximately 6 months of age [294]. The third and final stage involves a modified Fontan procedure to connect the IVC to the central pulmonary arteries. This results in the completion of the Fontan circulation and the complete bypass of the right side of the heart. At Birmingham Children's Hospital, this involves a TCPC using a fenestrated extracardiac conduit, which is electively performed when the child is approximately 4 years of age [294].

2.14 Haemodynamic changes associated with staged palliation

The successful management of patients with functionally single ventricle anatomy is fundamentally dependent on the performance of the dominant ventricle, which must support blood flow through the systemic and pulmonary circulations [320]. However, functionally single ventricle anatomy is also characterised by abnormal circulatory haemodynamics, which change during the course of surgical palliation. These abnormal circulatory haemodynamics may profoundly influence the performance of the dominant ventricle and thus could potentially influence the clinical outcome of children with functionally single ventricle anatomy.

Initial surgical palliation establishes a circulation in which the systemic and pulmonary circulations are connected in parallel with one another (Figure 2.26A). Subsequent surgical management results in the progressive and ultimately complete separation of the systemic and pulmonary circulations. The BCPA results in partial separation by creating a circulation in which the pulmonary circulation is connected in series with the systemic circulation of the upper half of the body only (Figure 2.26B). Finally, the Fontan procedure creates a "physiologically normal" circulation in which the systemic and pulmonary circulations are separate and in series with one another (Figure 2.26C).

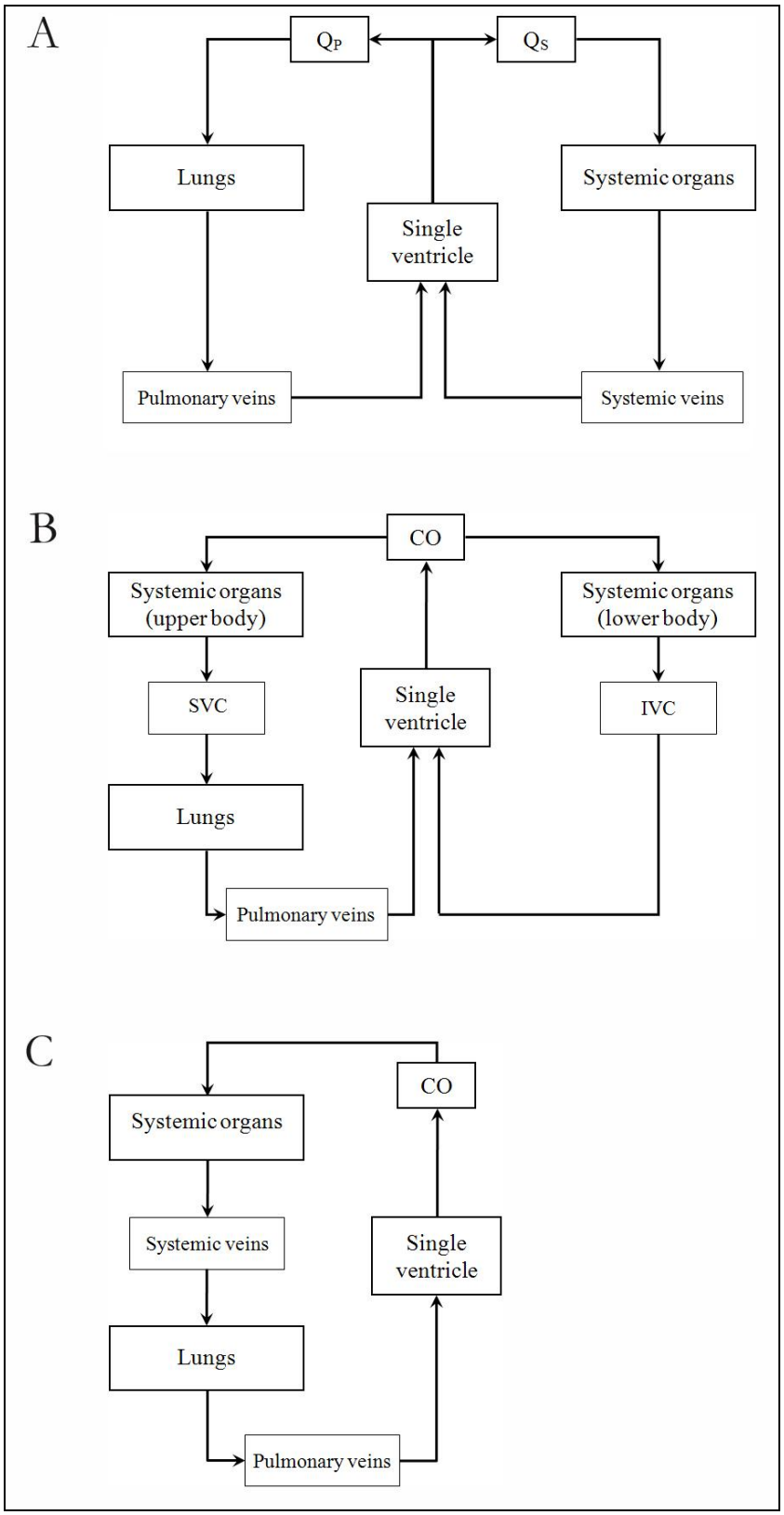

Figure 2.26 *Schematic diagram of the circulation (A) with a balanced in-parallel circulation, (B) following formation of the BCPA and (C) following the Fontan procedure.*
Q_P*, pulmonary blood flow;* Q_S*, systemic blood flow;* CO*, cardiac output.*

Barnea *et al.* demonstrated that oxygen availability in a parallel circulation varies according to cardiac output, oxygen capacity, pulmonary oxygenation and oxygen consumption of the whole body. Maximal oxygen availability occurs when the systemic-pulmonary flow ratio is equal to or slightly less than 1[337]. Therefore, the ventricle must eject between approximately 5.0 $L \cdot min^{-1} \cdot m^{-2}$ in order to maintain a systemic cardiac index of 2.5 $L \cdot min^{-1} \cdot m^{-2}$. As a result, the parallel circulation is characterised by obligate volume loading of the single functional ventricle [338].

Chronic volume loading severely affects the morphologic and functional characteristics of the ventricle. It induces a progressive dilatation and spheroid remodelling of the dominant ventricle [345-348], such that the indexed end-diastolic volume (***EDVI***) is approximately 50% higher than normal [339]. There is a corresponding increase in the ventricular mass, which helps preserve the normal ventricular mass-volume ratio [338,339]. Nevertheless, in spite of these adaptive changes, ventricular dysfunction and failure eventually develop in most children with functionally single ventricle anatomy that are palliated for a long time [340].

The subsequent surgical management of functionally single ventricle anatomy abolishes the volume overload, reduces the ***EDVI*** by approximately 50% [339] and increases the total vascular resistance (***TVR***) by more than two-fold [341]. In particular, the formation of the BCPA is associated with a 25% reduction in the ***EDVI*** within 30 days of the operation [342]. The ***TVR*** is also 40% higher in patients with a BCPA compared with patients who had undergone initial palliation only [343]. Completion of the Fontan circulation is associated with a further 20% reduction in the ***EDVI*** and 20% increase in ***TVR*** within 6 weeks of the operation [343].

The early reduction in ventricular dimensions, which accompanies the successful management of functionally single ventricle anatomy, is associated with the development of an increasingly ellipsoid shaped ventricle. This is subsequently followed by the regression of the ventricular mass, such that the ventricle ultimately develops a normal ventricular volume and wall thickness [338]. However, the rate of decrease in ventricular mass is much slower than the reduction in ventricular volume. There is, therefore, a temporary increase in the ventricular mass-volume ratio during the early post-operative period [344].

There is a complex interdependence between ventricular function, the volume and pressure loading characteristics and the ventricular shape. The changes in circulatory haemodynamics and ventricular geometry, which accompany the management of functionally single ventricle anatomy, may both influence the function of the dominant ventricle. The reduction in volume load and the development of a more ellipsoid ventricular shape provide more favourable working conditions for the ventricle, and this should be accompanied by an improvement in ventricular systolic function [338]. By contrast, the temporary increase in mass-volume ratio is generally associated with the development of diastolic dysfunction, with both impaired active ventricular relaxation and reduced ventricular compliance [345-347]. This diastolic dysfunction has been identified as a primary determinant of early outcome following the Fontan procedure [346,348,349]. The increase in ***TVR*** might also be expected to affect the performance of the dominant ventricle, with the development of systolic or diastolic dysfunction. Equally importantly, acute changes in ***TVR*** may alter the balance between ventricular systolic function and vascular load. Acute changes in this ventricular-vascular coupling ratio are generally characterised by a reduction in the mechanical efficiency of the ventricle and impaired global cardiovascular function [341,350].

A limited number of studies have been undertaken to determine the effect of surgical management on ventricular function in children with functionally single ventricle anatomy. There are no contemporary studies that have evaluated the effect of the BCPA on ventricular function. In addition, there have been only two studies to quantitatively evaluate the effect of the Fontan procedure on ventricular function in children with a pre-existing BCPA [343,351]. Tanoue *et al.* reported that the Fontan procedure was associated with an improvement in ventricular systolic function and an increase in the mechanical efficiency, despite an increase in the ***TVR*** [343]. However, this study was associated with two important limitations. Firstly, it did not evaluate changes in diastolic function, which may represent the primary determinant of outcome following the Fontan procedure. Secondly, the study involved repeat studies, which were undertaken 6 weeks post-operation. These results may, therefore, not be representative of the changes that occur during the high-risk, early post-operative period.

2.15 CONCLUSION

This chapter describes the basic anatomy and physiology of the normal human heart. The normal human heart is a complex organ that is composed of two muscular pumps, which are connected in-series with the vasculature to deliver oxygenated blood to the body. The performance of the heart as a muscular pump is controlled by intrinsic and extrinsic factors that influence the function of both individual myocytes as well as the heart as a whole.

The performance of the heart as a muscular pump is defined by changes in pressure and volume within the ventricle. A series of relatively load-independent indices of ventricular systolic and diastolic function can be calculated based on the instantaneous pressure-volume relation. This method of analysis was considered essential for this thesis, which sought to examine ventricular function and the effects of surgical palliation in children with functionally single ventricle anatomy. The advantages and disadvantages of methods available for measuring ventricular pressure and volume are discussed in Chapter 3.

CHAPTER 3

GENERAL METHODS

CHAPTER 3. GENERAL METHODS

The management of children with congenital heart disease is highly dependent on imaging. Both non-invasive and invasive diagnostic techniques are routinely used to define the intracardiac anatomy; evaluate cardiac and valvular function; and determine the most appropriate management strategy for each patient. Many patients also require serial investigations to monitor changes in haemodynamics, which generally predate changes in clinical and functional performance [352].

This Chapter will outline the various techniques that can be used to assess the ventricular volume; ventricular and intravascular pressure; and blood flow within the cardiovascular system.

3.1 VENTRICULAR VOLUME MEASUREMENTS

A variety of different imaging modalities are used to measure ventricular volume in routine clinical practice. These include echocardiography, magnetic resonance imaging (MRI), radionuclide angiography and conventional X-ray angiocardiography [353,354]. All of these techniques work well and are sufficiently accurate in most routine cases. The decision about which one to use will depend on the clinical question and information required, the need for reproducibility, the costs involved as well as the risks to the patient and clinical team. A detailed understanding of the capabilities of each method is less important than choosing an appropriate technique and using it well [355].

3.1.1 Echocardiography

Echocardiography is a specialised type of ultrasound examination, which uses high-frequency sound wave (2 – 10 MHz) to generate images using a pulse-echo technique [356]. The ultrasound transducer produces a brief pulse of high-frequency sound waves that is transmitted into the patient. The transducer then becomes a receiver to detect sound waves reflected from the tissues (i.e. echoes). The depth of the reflecting surface is determined by the time it takes for the sound wave to return to the transducer. The strength of the reflected signal is illustrated by shades of

grey. This information is used to construct one-dimensional (M-mode) or two-dimensional (B-mode) tomographic images of the heart. More advanced ultrasound transducers have now been developed, which produce three-dimensional ultrasound images in real-time [357].

Trans-thoracic echocardiography is the first-line investigation for children with congenital heart disease. It produces high quality images of the heart and great vessels, which can be used to accurately assess ventricular function. Two-dimensional and Doppler echocardiography can also be used to assess valvular, myocardial, pericardial and extra-cardiac abnormalities. Of all the non-invasive techniques currently available, echocardiography is the most versatile, provides the most additional information and has the lowest cost [358]. Nevertheless, echocardiography is associated with a number of limitations. Firstly, ultrasound does not readily cross tissue-gas or tissue-bone boundaries. As a result, the acoustic windows may be limited by the sternum, ribs or the lungs. These problems are particularly important in patients with congenital heart disease, since assessment of the right ventricle is frequently required. The right ventricle normally lies directly beneath the sternum and is, therefore, frequently inaccessible to ultrasound. In addition, patients may have undergone multiple operations that can further reduce the acoustic windows. Secondly, the endocardial surface for the greater part of the ventricular cavity lies parallel to the ultrasound beam and is, therefore, not well demonstrated. There may also be areas of signal "drop-out" where the endocardium is not demonstrated at all. As a result, a considerable subjective element is often present when the cavity is outlined on echocardiographic images [96].

At Birmingham Children's Hospital, quantitative left ventricular volume measurements are calculated using the area-length method. This method was not used in the studies reported in this thesis for the following reasons. The area-length method is based on the assumption that the shape of the left ventricle can be modelled as an ellipsoid of revolution. These assumptions may not reflect the actual changes in geometry that occur during the normal cardiac cycle [359,360]. While Mercier *et al.* demonstrated that left ventricular end-diastolic volume and ejection fraction calculated using this method were highly correlated with measurements made using X-ray angiocardiography [361], other studies have demonstrated that these volume measurements may

underestimate ventricular volume by up to 40% [218,362]. There are also reports of poor repeatability between duplicate measurements on the same patient [96]. These problems potentially limit the usefulness of echocardiography to continuously measure intraventricular volume. Consequently, two-dimensional echocardiography was not used in this thesis.

3.1.2 X-ray angiocardiography

Traditionally, more detailed anatomical and functional assessment has been acquired with X-ray angiocardiography, also known as cardiac catheterisation. At Birmingham Children's Hospital, patients considered for complete surgical repair of complex congenital heart defects will usually undergo cardiac catheterisation as part of the pre-operative investigation. This procedure is primarily used to help define the cardiac anatomy, quantify shunts between cardiac chambers, measure gradients across stenotic vessels or valves and quantify PVR. Cardiac catheterisation is not used in all patients because it is associated with an increased risk compared with non-invasive trans-thoracic echocardiography. This is as a consequence of the invasive nature of the procedure; the exposure to ionising radiation; and the use of iodinated contrast medium.

Angiocardiography images are acquired as two-dimensional planar images and are characterised by high spatial and temporal resolution. Accurate and reproducible left and right ventricular volumes can be calculated from single or biplane images [64,363]. However, like two-dimensional echocardiography, these measurements make assumptions about ventricular shape that may not reflect the actual geometry, especially in patients with congenital heart disease. In addition, there may be some uncertainty about the position of the endocardium on angiocardiographic images, which results in an underestimate of ventricular volume at end-systole [364]. Both of these factors potentially affect the absolute accuracy of volume measurements made using this technique [365-367].

At Birmingham Children's Hospital, X-ray angiocardiography is used to provide a qualitative assessment of ventricular function [368], but it is not used to quantify either left or right

ventricular function for the reasons previously outlined. Similarly, this technique was not used in this thesis.

3.1.3 Radionuclide angiography

Radionuclide imaging has been used to quantify ventricular function and intracardiac shunting as well as to assess relative pulmonary perfusion [369-371]. The production of radionuclide images involves the intravenous injection of a radioactive tracer molecule (such as ^{99m}Tc-labelled red blood cells) and mapping the distribution of the radio-labelled pharmaceutical within the body using a gamma camera. The amount of radiopharmaceutical within a particular organ is quantified by measuring the radiation emitted within a particular time.

Radionuclide angiography with ECG-gating allows the construction of time-activity curves that measure "time-averaged" left and right ventricular volumes throughout the cardiac cycle [371,372]. Quantitative measurements of ejection fraction in both the left and right ventricles are highly accurate provided that the images separate the chambers from one another [371]. However, radionuclide imaging is not suitable for beat-to-beat measurements of ventricular volume. The technique is also associated with a significant radiation exposure [373] and equivalent information can generally be obtained using other lower-risk techniques. Consequently, this technique was not used in this thesis.

3.1.4 Magnetic resonance imaging

More recently, cross-sectional cardiovascular imaging, using MRI and multi-detector computed tomography, have developed as important techniques for the diagnosis and follow-up in patients with congenital heart disease [374,375]. MRI is currently the three-dimensional imaging modality of choice, as it allows accurate assessment of intracardiac anatomy, function and flow without ionising radiation or the potential complications of iodinated contrast media [353]. Ventricular volume measurements are generally obtained using 8 to 12 contiguous time-resolved short-axis slices that extend from just above the atrio-ventricular valve to the apex of the heart. The

endocardial borders are traced on all images at the phases of interest (i.e. end-diastole and end-systole). The ventricular volume is then calculated using Simpson's rule (Equation 3.1).

Equation 3.1 $$V = \sum_{0}^{n} A \cdot d \,,$$

where V is the volume, A is the measured area, d is the slice thickness and n is the number of slices.

MRI is the most accurate method for measuring volume in the left and right ventricle, since it makes no assumptions about the shape of the ventricle [376]. Consequently, MRI is currently regarded as the clinical "gold standard" for the assessment of ventricular volume and mass [377,378]. Kuehne *et al.* have also demonstrated that MRI volume measurements can be combined with synchronous pressure measurements to analyse ventricular function using instantaneous pressure-volume relations [379].

It should be acknowledged that MRI is associated with a number of practical difficulties. For example, the complete evaluation of the heart and central vessels requires a number of separate MRI sequences. The majority of these sequences are acquired using ECG-gating while the patient holds their breath to reduce the artefacts associated with respiratory motion. As a result, cardiac MRI examinations are time consuming. The complete evaluation of complex case, for example, may take up to 1 hour. In addition, cardiovascular MR imaging in children less than 8 years of age is only performed under general anaesthesia. Because of these practical problems, this technique was not used in the studies reported in this thesis.

3.1.5 Conductance catheter technique

In addition to the conventional imaging techniques already described, ventricular volume can also be measured using the conductance catheter technique. This technique uses a multi-electrode catheter to produce continuous, real-time ventricular volume measurements based on the electrical conductance of blood within the ventricular cavity [380-382]. Although this technique is not used in routine practice, it has been used extensively in both animal experiments and clinical

studies to evaluate normal physiology and determine the effects of various pharmacological, interventional and surgical procedures on systolic and diastolic ventricular function [97,98].

3.1.5*a* *History of conductance volume measurements*

Electrical conductance or its reciprocal electrical impedance has been used to used to measure intravascular volume since the beginning of the twentieth century [97,383,384]. In 1953, Rushmer *et al.* fixed electrodes to the left and right ventricular myocardium in dogs to record electrical impedance during the cardiac cycle. The authors demonstrated that the impedance increased during ejection and decreased during filling of the ventricle [385]. In 1966, Geddes *et al.* applied this technique to measure the continuous stroke volume using two bipolar electrodes inserted into the base and apex of the canine left ventricle. These measurements were combined with simultaneous intraventricular pressure measurements to produce probably the first intraventricular pressure-impedance diagram [386].

All of the initial experimental studies used electrodes that were attached to the myocardium. In 1967, Palmer showed it was possible to measure impedance using a catheter placed inside the ventricle (Reported in White & Redington, [384]). This catheter consisted of five electrodes, two of which could be used to measure volume. However, while the catheter produced high-quality volume recordings, the measurements were characterised by a high variability [387].

In 1981, Baan *et al.* reported a new conductance catheter that could be used to accurately measure the continuous stroke volume in the dog [380]. The authors subsequently demonstrated that the same catheter could be used to measure the absolute volume in both canine and human left ventricles [381]. The current design of the conductance catheter is essentially the same as that developed by Baan *et al.* [380,381], as will be discussed in more detail in the following sections.

3.1.5*b* *Theoretical basis of conductance catheter technique*

Electrical conductance is a measure of how easily electricity flows through an electrical element. It is the reciprocal of electrical impedance, which represents the total resistance to an alternating

current. In biological materials like blood and muscle, impedance arises from both the resistive and dielectric properties (capacitance or inductance) of the material [388].

The conductance catheter technique is based on the principle that the bioelectrical properties of the ventricle vary as a function of the ventricular volume [383,389]. This principle can be illustrated using a physical model like a cylinder. The impedance of the cylinder, Z will vary according to length, L and cross-sectional area of the cylinder, A; and the resistivity, ρ of the material (Equation 3.2).

Equation 3.2 $$Z = \rho \cdot L / A$$

The volume can be affected by changes either in the length or the cross-sectional area of the cylinder. However, these two effects cause opposite changes in the measured impedance. The measured impedance will increase with increments in cylinder length while conversely the measured conductance will increase with increments in the cross-sectional area [383].

In the conductance catheter technique, the relative positions of the electrodes on the catheter are fixed, so that change in the measured conductance signal reflects a change in the cross-sectional area of the ventricle. Consequently, the conductance signal is high when the ventricle is full (i.e. end-diastole) and low when the ventricle is only partially filled (i.e. end-systole) or empty.

3.1.5*c* *Volume measurements using the conductance catheter technique*

The conductance catheter consists of a series of up to twelve electrodes that are mounted along the distal end of a standard angiographic catheter. This catheter is inserted along the long-axis of the ventricular cavity, as illustrated in Figure 3.1.

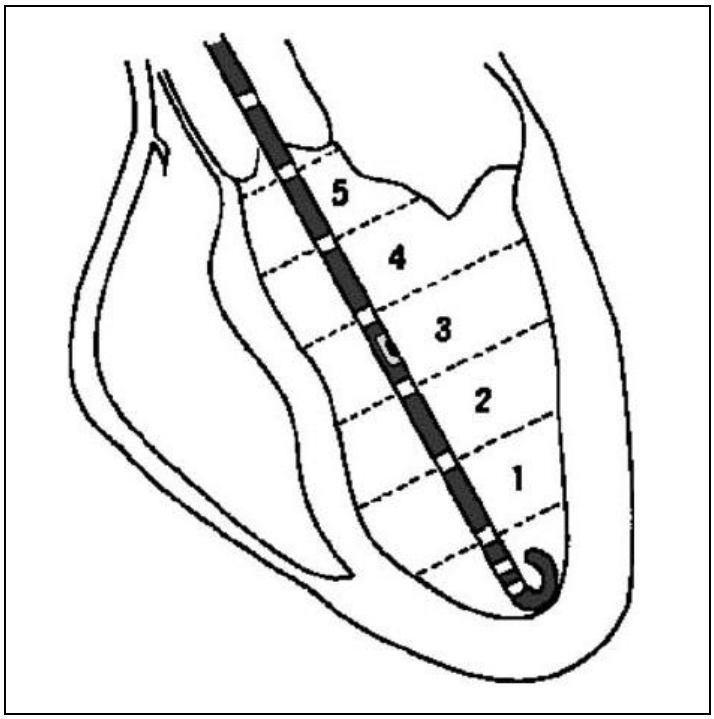

Figure 3.1 *The combined pressure-conductance catheter in the left ventricle. The electrodes are used to establish an intracavitary electric field and measure segmental conductance volumes. The pressure transducer is positioned in segment 3. Reproduced from Steendijk et al.*[114].

The most proximal and most distal electrodes are used to generate an intracavitary electric field. The intensity and frequency of the current are chosen to ensure that the electric field does not cause heating or stimulate the heart [390]. Higher frequencies allow higher currents to be used, thus improving the signal to noise ratio [387]. In practice, frequencies in the range of 1 kHz – 100 kHz can be used with a current of between 50 μA – ~5 mA, respectively.

The remaining eight electrodes are "sensing" electrodes. They measure the potential difference between consecutive electrodes to derive up to seven segmental conductance signals, $G_i(t)$. Conductance is defined as the applied current divided by the measured potential difference between adjacent electrodes. As a first approximation, the conductance signal measured between any two adjacent "sensing" electrodes can be considered as a cylinder in which the boundaries are defined by the endothelial surface of the myocardium and the equipotential surfaces of the electrodes. The total conductance signal within the ventricular cavity can then be likened to a column of cylinders stacked one on top of the other.

Absolute time-varying volume measurements, $V(t)$ are obtained from the conductance signal using a simple algorithm (Equation 3.3), which takes into account the inter-electrode distance on the catheter, L and the specific resistivity of blood, ρ [381].

Equation 3.3 $$V(t) = \frac{1}{\alpha} \cdot L^2 \cdot \rho \cdot \left[\sum_{i=1}^{7} G_i(t) - G_P \right],$$

where α is a dimensionless calibration coefficient and G_P is a volume offset called parallel conductance.

The specific resistivity of blood, ρ is approximately 150 Ω·cm at normal body temperature [391]. However, this value may vary between individuals and in the same patient under different conditions. Changes in the concentration and morphology of the red blood cells, electrolyte composition and blood temperature can all affect the measured blood resistivity [387]. Consequently, the specific blood resistivity should be measured in all patients and re-measured whenever it is likely to have changed [392].

In this thesis, the resistivity was measured before each test using a dedicated measuring cuvette (CD Leycom, Zoetermeer, The Netherlands).

3.1.5*d* *Calibration of conductance volume measurements*

The conductance catheter technique is based on the assumptions that, firstly, the electric field produced by the catheter is homogeneous and parallel to the long-axis of the ventricle; and, secondly, that the electric field is contained within the ventricular cavity. In practice, however, neither is the case. The calculation of absolute ventricular volume from conductance measurements requires the estimation of a volume offset (parallel conductance, G_P) and the dimensionless calibration coefficient, α (Equation 3.3).

Parallel conductance

When the frequency of the current is between 20 kHz and 1 MHz, the resistivity of the myocardium (400 Ω·cm) is only 2.5-times greater than the resistivity of blood [391]. As a

consequence, the electric field extends beyond the ventricular cavity into the surrounding structures (e.g. the myocardium, the contralateral ventricle, the atria and the pericardium). Therefore, the measured conductance signal tends to overestimate the actual blood volume due to this parallel conductance.

In the experimental studies included in this thesis (Chapters 4 and 5), the problems posed by parallel conductance have been avoided by using a physical model of the left ventricle, which was develop by Dr A.H. Al-Khalidi as part of his PhD thesis [98]. However, parallel conductance is a potential problem in the clinical studies (Chapters 6 and 7). Consequently, the effect of parallel conductance on the accuracy of conductance volume measurements needs to be considered in detail.

Several different methods have been described to deal with the problem of parallel conductance [381,393-395]. McKay *et al.* proposed a method that exploits the difference in resistivity between muscle and blood at different frequencies [395]. They developed a conductance catheter that used a frequency of 1.3 kHz. At this frequency, the myocardial resistivity is 1000 Ω·cm or 7-times higher than that of blood and a much smaller proportion of the current will dissipate from the ventricle [395]. However, signal loss still occurs. In addition, the catheter was associated with a poor signal-to-noise ratio, which meant they were unable to obtain accurate measurements of absolute volume.

The conductance catheter used in this thesis generates a current of 30 μA at 20 kHz, in order to ensure patient safety and good signal-to-noise ratio. These parameters mean that the method advocated by McKay *et al.* cannot be used. Instead, the contribution of parallel conductance is usually measured using the hypertonic saline injection method [381]. This involves injecting a small bolus of hypertonic saline (10%) into a central vein or the pulmonary artery [396]. The saline causes a dramatic fall in blood resistivity and an apparent increase in the measured intraventricular volume (Figure 3.2), while the parallel conductance is assumed to remain constant.

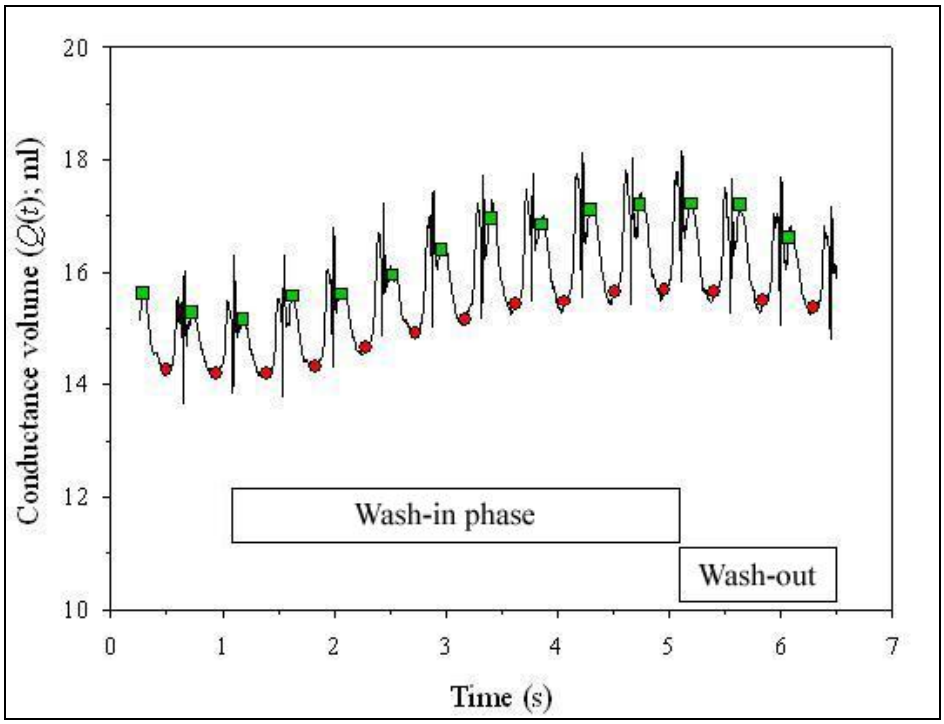

Figure 3.2 *Plot of conductance volume, $Q(t)$ versus time during the passage of a bolus of 0.25 ml·kg^{-1} 10% NaCl solution into the dominant ventricle. The conductance volumes at end-diastole (green squares) and end-systole (red circles) are identified for each beat. The "wash-in" and "wash-out" phases are also illustrated.*

The parallel conductance can be calculated using one of two linear regression analysis techniques [381,397]. In the method proposed by Baan *et al.*, the maximum conductance (Q_{ED}) is plotted against the subsequent minimum conductance (Q_{ES}) of each beat, using at least eight data points during the "wash-in" phase (Figure 3.3A) [381,398]. The theoretical relationship between Q_{ED} and Q_{ES} represents a straight line. This line is extrapolated to the line of identity (i.e. $Q_{ED} = Q_{ES}$); the conductance at this point of intersection represents parallel conductance [381]. The alternative method proposed by Steendijk *et al.* involves plotting the maximum conductance (Q_{ED}) against the stroke conductance ($Q_{SV} = Q_{ED} - Q_{ES}$) and the relation is extrapolated to the point where stroke conductance is zero (Figure 3.3B) [397]. Parallel conductance, G_P is then subtracted from the measured conductance signal, as set out in Equation 3.3.

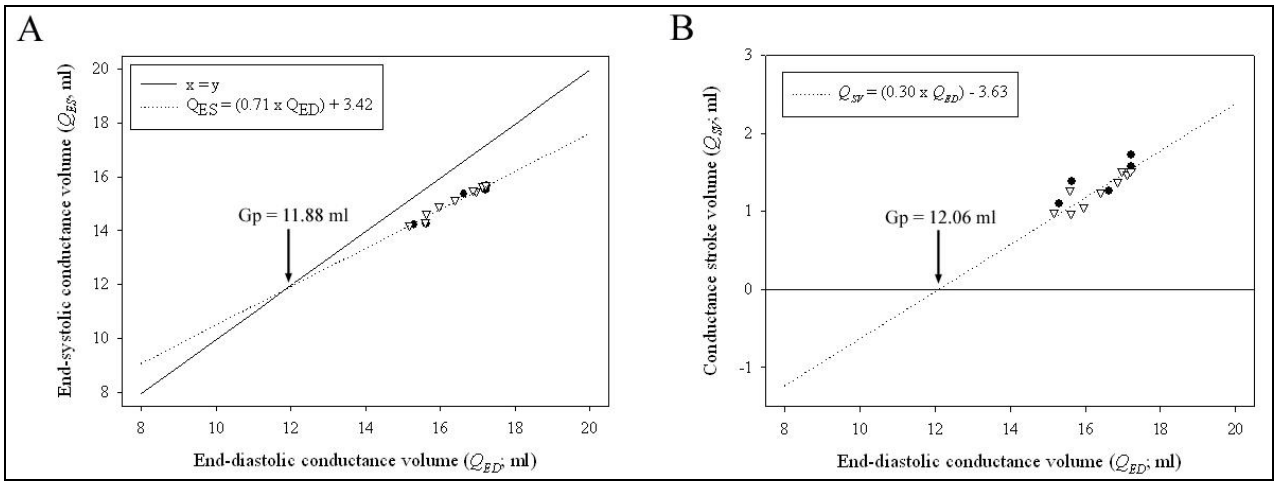

Figure 3.3 *Linear regression analyses were used to calculate parallel conductance. The data corresponds with the data presented in* Figure 3.2. *The data-points from the "wash-in" phase (white inverted triangles) and other data (black circles) are both plotted. A, The relationship between end-systolic conductance versus end-diastolic conductance. The parallel conductance is equal to the point of intersection with the line of identity (*$x = y$*). B, The relationship between end-diastolic conductance and stroke conductance. Parallel conductance is equal to the intersection with the* x*-axis (i.e. stroke conductance = 0).*

Both of these methods make a number of assumptions about parallel conductance and the effect of hypertonic saline on parallel conductance. For example, parallel conductance is assumed to remain constant throughout the cardiac cycle; it is also assumed that the injection of hypertonic saline does not alter the ventricular volume or parallel conductance or the conductivity of the surrounding structures. Subsequent studies have demonstrated that some of these assumptions may not strictly be true [399-402].

Despite these concerns, I have chosen to measure parallel conductance in the clinical studies using the method described by Baan *et al.* [381]. This choice was based on some preliminary studies in which I used both approaches. In addition, I was concerned that the method advocated by Steendijk *et al.* [397] may be more susceptible to measurement error. Specifically, the variance associated with stroke conductance (Q_{SV}) is equal to the variance associated with Q_{ED} measurements *plus* the variance associated with Q_{ES} measurements. In other words, the variance associated with Q_{SV} measurements will inevitably be greater than the variance associated with either individual conductance volume measurement.

The dimensionless slope factor, α

Conductance volume measurements are based on the assumption that the electrical field created by the catheter is homogeneously distributed within the ventricular cavity. This can only be achieved if the electrodes are large end-plate electrodes. However, if small electrodes are used (as in the conductance catheter), these electrodes act as a point source [388]. The electric field is concentrated around the outermost electrodes and attenuated in the middle of the catheter [403,404]. The density of the current also varies in the transverse plane, decreasing exponentially as the distance from the catheter increases [404-406].

A number of modifications to the conductance catheter technique have been proposed in order to address the problem of electric field non-homogeneity and improve the accuracy of conductance volume measurements. These have included the development of the dual-field excitation catheter [407]; together with mathematical techniques of field extrapolation to estimate the expected field distribution under ideal conditions [403,408-410].

The dual-field excitation catheter generates an electric field by applying an alternating current between the outermost electrodes and a second alternating current of opposite polarity between the two adjacent electrodes [411]. Dual-field excitation improves the field dispersion within the ventricular cavity by correcting the curvature of the equipotential lines close to the excitation electrodes [411,412]. This improves the accuracy of conductance volume measurements but the system is still not perfect [404,405].

Despite the problems with dual-field excitation, we have used this system throughout this thesis. One alternating current (20 kHz, 30 μA RMS) was applied between the two outermost electrodes (electrodes 1 and 12) and a second alternating current of opposite polarity (20 kHz, -10 μA RMS) was applied between the two adjacent electrodes (electrodes 2 and 11).

One consequence of electric field non-homogeneity is that the conductance catheter tends to slightly overestimate the absolute volume at low volumes and progressively underestimate the absolute volume with further increments in the ventricular volume [404,405]. In addition, the

conductance-derived stroke volume generally underestimates the actual stroke volume [381]. To address these problems, conductance volume measurements are calibrated with the dimensionless calibration coefficient in order to improve the accuracy of ventricular volume measurements [381]. This calibration coefficient represents the slope of either the conductance-absolute volume relationship [382] or the stroke conductance-stroke volume relationship [114].

In the isolated post-mortem canine heart, Mur & Baan reported that the conductance-volume relation was virtually linear over a finite volume range [382]. The authors predicted that a similar, virtually linear conductance-volume relation would be observed for the human left ventricle up to a volume of 200ml [382]. Unfortunately, *in vivo* experiments in the intact circulation have subsequently demonstrated that α is not constant but varies according to the ventricular volume [401,413,414].

The non-linearity of the conductance-absolute volume relationship potentially affects the accuracy of conductance volume measurements calibrated using this technique. This is particularly important in patients with congenital heart disease, since the changes in volume-loading conditions are generally more marked than those observed in patients undergoing diagnostic catheterisation or adult cardiac surgery. For this reason, this relationship was analysed in detail. This study is presented in Chapter 4.

Despite these concerns, conductance volume measurements in the clinical studies (Chapters 6 and 7) were calibrated using a calibration coefficient, α that represented the stroke conductance-stroke volume relationship, in which stroke volume was independently measured using an transit-time ultrasound flow meter with a probe placed around the ascending aorta (Transonic Systems Europe B.V., Maastricht, The Netherlands).

3.1.5*e* *Calibrated conductance volume measurements*

In spite of the potential limitations already described, the conductance catheter technique represents on of the most powerful tools for the assessment of cardiac function in vivo. The technique provides continuous measurements of ventricular volume in real-time. Animal

experiments and clinical studies have consistently demonstrated that, after calibration, the technique provides accurate and reproducible volume measurements that are highly correlated with volume measurements made using other techniques [413-417]. In addition, the technique does not make any specific assumptions about ventricular geometry and can therefore be used to measure left and right ventricular volume.

The particular advantage of the conductance catheter technique, however, is that it can provide continuous and accurate volume measurements during rapid changes in ventricular volume, such as inferior vena caval occlusion (IVCO). When combined with simultaneous pressure measurements, this enables the accurate assessment of ventricular systolic and diastolic function using pressure-volume analysis. In this regard, the conductance catheter technique represents probably the most powerful method for the assessment of cardiac function in vivo.

3.2 PRESSURE MEASUREMENTS

Various methods are commonly used to measure blood pressure in clinical practice. Blood pressure is routinely measured non-invasively by external compression of an artery in the arm or leg with a sphygmomanometer [418]. Blood pressure can also be measured invasively by positioning a catheter within the desired cardiac chamber or vessel. The catheter is attached to a calibrated pressure transducer or manometer, which converts the pressure into a signal output (e.g. electrical voltage or current) to provide continuous blood pressure measurements in real-time [419].

Invasive measurements of arterial or central venous pressure are routinely performed in paediatric patients undergoing cardiac surgery using a fluid-filled catheter-manometer system. This consists of a disposable manometer mounted near the patient, which is connected to the intravascular cannula by a length of stiff, non-compliant fluid-filled tubing. A pressurised, continuous flush system is also connected to the catheter-manometer system in order to maintain the patency of the invasive pressure monitoring line [420]. The fluid-filled catheter-manometer system provides reliable pressure measurements that are adequate for most clinical situations.

However, when it is important to obtain precise pressure recordings (like the transvalvular pressure gradient, for example) micromanometer catheters may be used. These catheters have the manometer mounted at the tip of the catheter, which improves the accuracy of the measurements and also reduces some of the artefacts associated with fluid-filled catheter-manometer system.

3.2.1 Accuracy of the catheter-manometer system

The quantitative analysis of pressure waves requires a system that can faithfully reproduce the intravascular or intraventricular pressure waveform. The absolute accuracy of the measurements will vary according to the dynamic response characteristics of each catheter-manometer system [421]. It is important to understand the specific characteristics of the system being used and, in particular, the amplitude linearity or sensitivity; frequency and phase response; and stability of the system [48,387].

The pressure wave can be thought of as the sum of a series of sine waves, called harmonics. The fundamental sine wave, or first harmonic, has the same frequency as the heart rate and higher harmonics are multiples of this basic frequency [422,423]. At least 5 or 6 harmonics are required to replicate the original pressure waveform [424,425]; and at least 15 harmonics are necessary for accurate reproduction of the first-derivative of ventricular pressure with respect to time (dP/dt) [426]. The average heart rate in young children is approximately 100 beat·min^{-1}. Therefore, in these patients, the catheter-manometer system needs to have a constant frequency response up to at least 25 Hz in order to faithfully reproduce the time-varying pressure and dP/dt waves.

The catheter-manometer system can be characterised as a second-order dynamic system [427]. This system is analogous to a bouncing tennis ball. When the tennis ball is dropped onto a hard, flat floor, it bounces several times before eventually coming to rest. With each bounce, the ball does not rise as high as on the previous bounce. Each bounce has a characteristic frequency and the time it takes for the ball to come to rest is related to the damping coefficient [428]. The frequency response of the catheter-manometer system can similarly be described by the natural frequency and damping coefficient of the system [429], Figure 3.4.

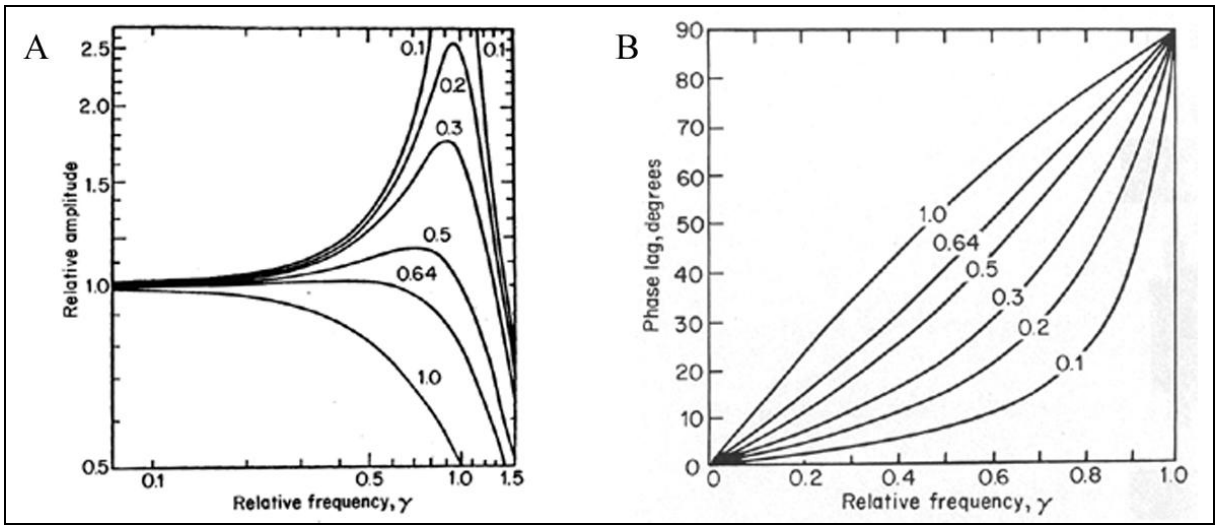

Figure 3.4 *Plots illustrating the dynamic response characteristics of the catheter-manometer system. A, the amplitude – frequency curve; B, phase lag – frequency curve. Reproduced from WW Nichols & MF O'Rourke* [430].

The catheter-manometer system is usually "under-damped" with a damping coefficient of less than 0.3 [421,428]. If the pressure wave contains harmonics with a frequency similar to the natural frequency of the catheter-manometer system, the amplitude of these harmonics will be amplified. This is important clinically, as it may lead to an artefactual increase in the systolic blood pressure and a corresponding decrease in the diastolic blood pressure measurements [431]. Amplification of the pressure pulse can be avoided by increasing the damping coefficient, such that the system becomes "optimally damped". However, increasing the damping coefficient alters the relative timing (or phase) of the separate harmonics. This phase distortion can result in a significant change to the shape of the overall pressure wave.

Ideally, one would like to have accurate pressure measurements without any phase distortion. This requires a catheter-manometer system with a very high natural frequency and a very low damping coefficient. These specifications are best achieved by micromanometer catheters, which commonly have a natural frequency in the kilohertz range and a phase lag that can hardly be discriminated from zero [430]. Sufficiently accurate blood pressure measurements can also be made using a fluid-filled catheter-manometer system provided it has a sufficiently high natural frequency and is adequately damped [428,432].

3.2.2 Other problems with the catheter-manometer system

In addition to the problems associated with the frequency and phase response of the catheter-manometer system, pressure recordings are also affected by events that occur within the vascular system. Three specific problems, namely the "end-pressure artefact", "catheter whip artefact" and the "catheter impact artefact" will be discussed.

The end-pressure artefact arises if the tip of the catheter points upstream into the blood flow. In this position, the manometer will record the kinetic energy of blood flow as well as the lateral pressure within the vessel. This may add between 2 – 10 mmHg to the actual pressure reading. Although the absolute pressure generated is small, the end-pressure artefact can also substantially alter the shape of the pressure waveform as the peak velocity of blood flow tends to occur before the peak pressure [430]. This artefact can be avoided by measuring pressure through the side of the catheter rather than at the end.

The catheter whip and catheter impact artefacts are similar. The catheter whip artefact occurs as a result of motion of the tip of the catheter in the heart or great vessels. By contrast, the catheter impact artefact occurs when the catheter is hit by the opening or closing of the valves or by the wall of the ventricular chamber. In each case, the movement results in the acceleration of the fluid within the catheter. This creates a transient pressure wave, which may add up to 10 mmHg to the actual pressure reading. Catheter whip and catheter impact artefacts are a particular problem in the fluid-filled catheter-manometer system. There effect is minimised in the micromanometer catheter primarily because of the absence of the fluid column within the catheter.

3.2.3 Dynamic response characteristics of clinical catheter-manometer system

Invasive pressure measurements at Birmingham Children's Hospital are generally performed with a fluid-filled catheter-manometer system. This consists of a disposable strain-gauge catheter-manometer system (DPT-6000; Codan Ltd, Wokingham, UK) connected to a pressure transducer (M1006B; Philips Medical Systems, Reigate, UK) that is attached to the patient monitoring

system. The manometer is normally connected to the arterial or venous cannula with a 200cm fluid-filled extension tube (Vygon UK Ltd, Cirencester, UK). Direct measurements within the heart can also be made using a green needle attached to the end of the extension tube.

I had originally planned to simultaneously measure other intracardiac and intravascular pressures using this system. However, the dynamic response characteristics of this system had not previously been determined (personal communication, Codan UK Ltd), even though this system has been used at Birmingham Children's Hospital since 1998.

The dynamic response characteristics of the fluid-filled catheter-manometer system were determined using the free vibration method based on a sudden, transient "step" change in pressure. This pressure step causes the catheter-manometer system to oscillate at its damped natural frequency. The oscillations will be sinusoidal and will decay exponentially in accordance with the damping coefficient.

3.2.3*a* *Materials and Methods*

Model ventricle

A square-wave pressure step was generated using a physical model of the left ventricle, which is described in detail in Chapter 4. For the purposes of this experiment, the solenoid valve at the top of the model ventricle (Figure 4.1) remained closed throughout the model ventricular cycle thus producing isovolumic contractions.

Pressure measurements

Instantaneous pressure within the model ventricle was measured using two separate catheter-manometer systems. The first consisted of a high-fidelity solid-state micromanometer laterally positioned between electrodes 5 and 6 within the combined pressure-conductance catheter (Millar Instruments) that was amplified using a combined amplifier-interface unit (PCU-2000; Millar Instruments). This pressure signal represented the reference pressure, based on the known dynamic response characteristics of this system [433]. The second system consisted of the pressurised flush, fluid-filled catheter-manometer system, as previously described. Both catheter-

manometer systems were zeroed according to the atmospheric pressure at the mid-ventricular level.

Experimental data

Analogue signals representing the two pressure measurements within the model ventricle and the ECG signal were digitised at 12-bit accuracy and a sample frequency of 250 Hz. End-diastole and end-systole were retrospectively identified. End-diastole was defined as the R-wave on the ECG [434] and end-systole was defined as the point immediately prior to IABP circuit deflation. The simulated cardiac cycle was defined as the period between end-diastole of one beat to end-diastole of the following beat.

A typical step response recorded with a catheter-manometer system of low frequency response and damping is illustrated in Figure 3.5.

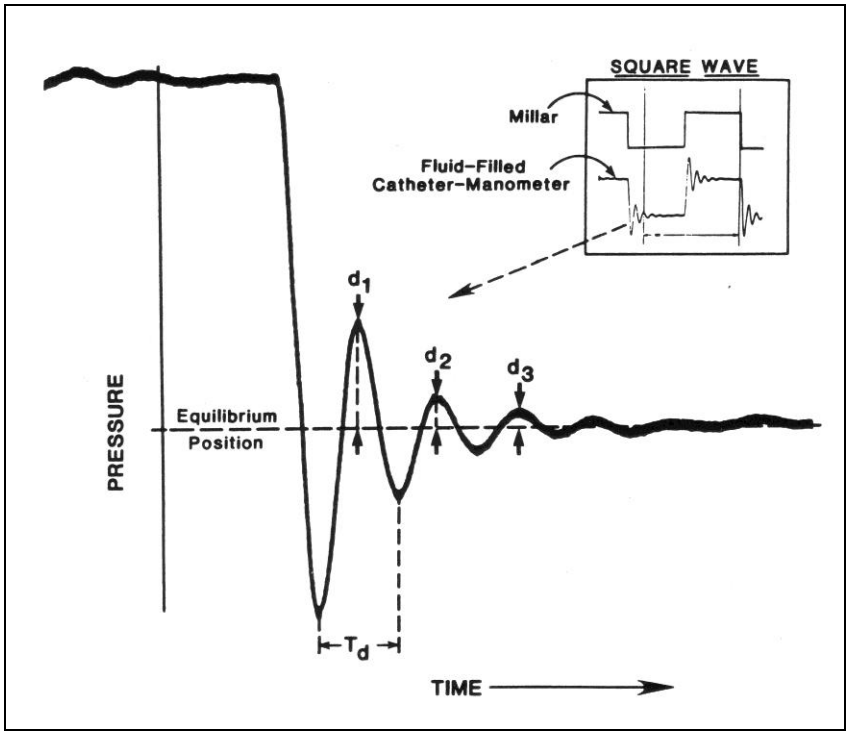

Figure 3.5 *Example of catheter-manometer response to square-wave change in pressure. Reproduced from WW Nichols & MF O'Rourke* [430], pp. 150

The damped natural frequency, f_d is derived directly from the time period, T_d of each completed cycle:

Equation 3.4 $$f_d = 1/T_d$$

The damping coefficient, β is calculated from the logarithmic decrement of pressure, Λ, from cycle to cycle:

Equation 3.5 $$\Lambda = \log_e\left(\frac{d_1}{d_2}\right) = \frac{2\pi\beta}{\sqrt{(1-\beta^2)}}$$

where d_1 and d_2 are the first and second pressure overshoot, respectively.

The damping coefficient, β is then found by solving Equation A.3:

Equation 3.6 $$\beta = \frac{\beta_0}{\omega_0} = \frac{\Lambda}{\sqrt{(4\pi^2 + \Lambda^2)}},$$

where β_0 is the damping constant and ω_0 is the angular frequency of undamped motion [430].

Finally, the undamped natural frequency, f_0 was calculated according to the damped natural frequency, f_d and the damping coefficient, β:

Equation 3.7 $$f_0 = \frac{f_d}{\sqrt{(1-\beta^2)}}$$ [424].

Statistical analysis

The experiment was repeated three times during a 1-hour period. Each experiment was conducted under steady-state conditions and data from 10 consecutive cardiac cycles was analysed. The estimated within-experiment standard deviation in the reference end-diastolic and end-systolic pressure measurements during the 30 cardiac cycles was 0.95 mmHg and 0.62 mmHg, respectively. The standard deviation was not significantly correlated with the mean pressure (Kendall's τ coefficient = 0.18). Therefore, all subsequent analyses were based on the average data for the experiment as a whole [435].

Data were analysed using SPSS for Windows (v16, SPSS Inc., Chicago, Il, USA). All values are expressed as mean ± SD and comparative analyses have been made using the paired two-tail Student *t*-test. A probability, $P<0.05$, was taken to represent statistical significance.

3.2.3*b* *Results*

Representative data illustrating the time-varying pressure signal obtained during this experiment are illustrated in Figure 3.6.

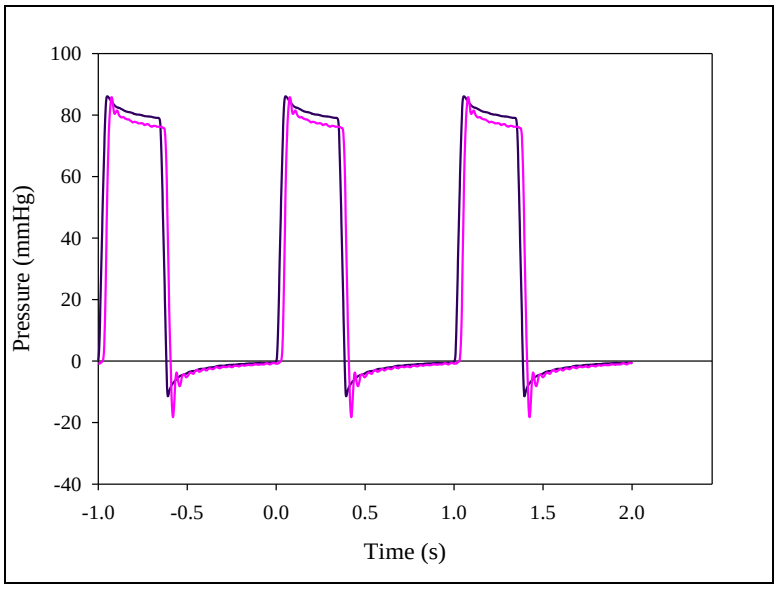

Figure 3.6 *Ventricular pressure measurements versus time. Pressure measurements were made using either the high-fidelity solid-state micromanometer (dark blue line) or the fluid-filled catheter-manometer system (purple line).*

The intraventricular pressure was characterised by a rapid increase and decrease in pressure that corresponded with inflation and deflation of the intra-aortic balloon pump (IABP). The pressure rise was associated with a pressure overshoot (point A; +7.3 mmHg), which then fell in a non-linear fashion to the end-systolic pressure (79 mmHg). Similarly, deflation was associated with a pressure undershoot (point B; -11.9 mmHg) that then returned non-linearly to the end-diastolic pressure (0 mmHg).

Pressure measurements made using the fluid-filled catheter-manometer system were characterised by a temporal delay of 28 ± 3 ms. In addition, this system slightly underestimated both the

maximal and end-systolic pressure (-3.3 mmHg and -0.5 mmHg, respectively; both $P<0.05$), although these differences are not clinically important.

The response of the catheter-manometer system following IABP deflation was used to determine the natural frequency and damping coefficient of the system (Figure 3.7). The first and second pressure overshoots were calculated as the difference from the reference pressure trace, after correction for the temporal delay.

The time between consecutive cycles, T_d, was 72 ms, which equated to a damped natural frequency of 13.9 Hz (Equation 3.4). The first (d_1) and second pressure overshoot (d_2) were 5.7 mmHg and 3.8 mmHg, respectively. This corresponds to a damping coefficient of 0.12 (Equations 3.5 and 3.6). Finally, the undamped natural frequency was estimated at 14.0 Hz.

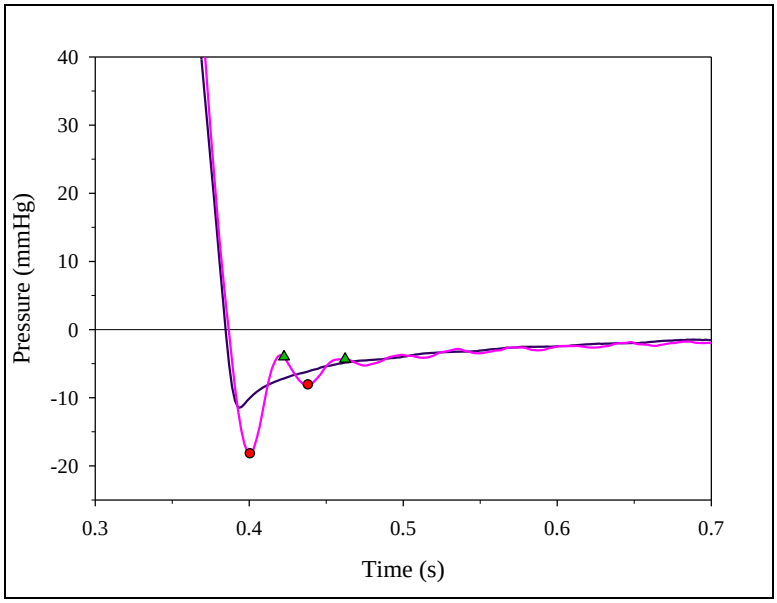

Figure 3.7 *Detail of the time-varying ventricular pressure. The pressure signal from the fluid-filled catheter-manometer system (purple line) has been adjusted to account for the temporal delay. The first and second pressure overshoot (▲) and pressure undershoot (●) are indicated.*

3.2.3*c* *Discussion and Conclusion*

The dynamic characteristics of the fluid-filled catheter-manometer system routinely used at Birmingham Children's Hospital were determined for the first time. These characteristics will allow accurate, finite pressure measurements (i.e. end-diastolic pressure or end-systolic pressure) in patients with a heart rate of up to approximately 140 bpm. By contrast, measurements of the first derivative of ventricular pressure with respect to time will only be accurate in patients with a heart rate up to 55 bpm.

The dynamic characteristics of this catheter-manometer system enabled reasonably accurate measurements of aortic pressure to be obtained. However, the measurements were not sufficiently accurate to allow more complex analyses such as wave intensity analysis [436] or analysis of vascular load based on impedance spectra [437,438], for example. is not sufficiently accurate to allow more complex analyses such as wave intensity analysis [436] or analysis of vascular load based on impedance spectra [437,438]. This system was, therefore, only used to statically calibrate pressure measurements made using the high-fidelity solid-state micromanometer only. for use in the clinical studies reported in this thesis. However, the measurements were not sufficiently accurate

3.2.4 Pressure measurements in this thesis

For this thesis, pressure measurements were primarily made using a high-fidelity miniaturised semiconductor strain gauge manometer [433], which is laterally positioned between electrodes 5 and 6 on the combine pressure-conductance catheter (Millar Instruments, Houston, TX, USA). This pressure signal was amplified using a combined amplifier-interface unit (PCU-2000; Millar Instruments). The frequency response of this micromanometer catheter is flat from 0 – 10 kHz, allowing accurate pressure measurements to be made over a wide range of pressure and temperature with high electrical safety [433,439].

Aortic pressure measurements were made using the pressurised flush, fluid-filled catheter-manometer system, as previously described. This system was also used to calibrate intraventricular pressure measurements made using the combined pressure-conductance catheter.

3.3 FLOW MEASUREMENTS

Several different techniques have been developed to directly measure cardiac output, and thus blood flow through the cardiovascular system. The principle techniques used to monitor patients in the intensive care unit involve the Fick principle; an indicator-dilution technique or Doppler ultrasound of blood flow in the thoracic aorta [440,441]. Each of these techniques is relatively invasive, requiring the insertion of a catheter into the pulmonary artery or an ultrasound probe into the oesophagus. These techniques are therefore mainly reserved for adult and paediatric patients on the intensive care unit or in the operating theatre. It is also possible to make direct, invasive measurements of cardiac output during open heart surgery, using a flow meter with a probe positioned around the ascending aorta.

3.3.1 The Fick principle

The Fick principle is based on the law of conservation of mass for an indicator and states that the amount of substance taken up by the body per unit of time is equal to the arteriovenous concentration difference of the substance (i.e. the arterial concentration minus the venous concentration) multiplied by the blood flow (Equation 3.8).

Equation 3.8
$$M(t) = \dot{Q} \cdot \left[\int_0^t (Ca - Cv)\, dt \right]$$

where $M(t)$ is the amount of indicator taken up in the period of time, t; $\dot{Q}$ is the blood flow; and Ca and Cv are the arterial and venous concentrations of the substance, respectively.

This principle can be used to determine cardiac output based on the oxygen concentration and the arteriovenous oxygen concentration difference. The oxygen consumption can be measured directly, based on the oxygen concentration in inspired and expired gases [442]. More commonly, oxygen consumption is only predicted according to the patient's gender and body surface area [443]. The arteriovenous oxygen difference is calculated using arterial and mixed venous blood samples taken from a peripheral arterial and pulmonary arterial catheter, respectively.

Measurements of cardiac output based on the Fick principle represent the "gold standard" in routine clinical practice. When performed carefully, the measurements are accurate to within approximately 5% of the actual cardiac output. However, the technique generally requires steady-state conditions. Furthermore, the technique measures the average blood flow over a given period of time; it does not provide any information about the pulsatile nature of the blood flow.

3.3.2 Indicator-dilution techniques

The indicator-dilution technique, in its simplest form, involves the rapid injection of a known amount of indicator substance in the venous system and then its concentration is measured as it passes into the arterial system. The greater the cardiac output, the more rapidly the dilution curve of the substances appears and disappears in the arterial system. The cardiac output can be calculated based on the amount of indicator injected and the area under the dilution curve (Equation 3.9).

Equation 3.9
$$\dot{Q} = \frac{m}{\int_0^{t1} C(t) \cdot dt},$$

where m is the amount of indictor injected; $C(t)$ is the time-varying concentration of the indicator; and t_1 is the time after which the indicator has completely passed.

A number of different indicators have been used, including indocyanine green and temperature. Transpulmonary thermodilution is the most commonly used indicator-dilution technique in current use. This uses a special four-lumen catheter that is positioned inserted via a central vein into the main pulmonary artery. Cold saline is rapidly injected through one lumen into the right atrium and the temperature change is detected using a thermistor on the tip of the catheter to record the dilution curve [444].

Transpulmonary thermodilution is relatively simple technique, which has been validated against cardiac output measurements based on the Fick principle [445]. However, a number of studies have identified poor repeatability, which limits the value of the technique [446,447]. In addition,

the indicator-dilution technique only measures average blood flow over a given period of time and does not provide any information about the pulsatile blood flow.

3.3.3 Oesophageal Doppler

The oesophageal Doppler technique is based on the measurement of blood flow velocity in the descending aorta using an ultrasound transducer on the end of a flexible probe. The probe may be introduced orally in anaesthetised, mechanically ventilated patients and advanced until the transducer is located approximately in the mid-thoracic level. The probe is then positioned so that the transducer faces the descending aorta and the characteristic continuous Doppler wave signal is obtained [448].

The volumetric flow in the descending aorta is calculated by measuring the area under the maximum aortic velocity profile (the velocity-time integral or stroke distance) multiplied by the cross-sectional area of the aorta. The total stroke volume can then be calculated by assuming the relative distribution of blood flow between the cephalic (i.e. the head and upper limbs) and caudal territories (i.e. the remainder of the systemic circulation). The cardiac output can then be calculated by multiplying the average stroke volume by the heart rate [448].

The oesophageal Doppler technique involves a number of assumptions about the nature of blood flow in the descending thoracic aorta, the cross-sectional area of the aorta, and the division of blood flow within the systemic circulation. These assumptions potentially limit the accuracy of absolute measurements of cardiac output [449]. Despite these assumptions and potential sources of error, the oesophageal Doppler technique provides measurements of cardiac output that are at least as accurate as those made using transpulmonary thermodilution, as previously described [447-449]. In addition, this technique measures the instantaneous pulsatile blood flow in the thoracic aorta and thus provides important information about the beat-to-beat variation in stroke volume.

3.3.4 Aortic flow probes

A number of commercially available flow meters are available, which can be used to measure blood flow in native vessels and vascular grafts during cardiovascular surgery. These flow meters measure blood flow using either electromagnetic fields or ultrasound.

3.3.4*a* *Electromagnetic flow meters*

Electromagnetic flow meters are based on Faraday's law that the motion of a conductor in a magnetic field generates an electromagnetic force (i.e. voltage) orientated at right-angles to the motion. As blood is a conductor of electricity, the velocity of blood flow can be measured by aligning the blood vessel across a magnetic field and recording the measured electromagnetic force (Equation 3.10).

Equation 3.10 $$u = \frac{e}{B \cdot L}$$

where u is blood velocity, e is the electromagnetic force; B is the magnetic field strength; and L is the distance between recording electrodes. In the case of parabolic flow profiles, the flow measured u is replaced by the cross-sectional average flow velocity, $\bar{u}$. The volumetric flow can then be calculated by multiplying the average flow velocity by the cross-sectional area.

Electromagnetic flow meters have been used to provide direct and reliable measurements of pulsatile blood flow in the ascending aorta [450]. However, the method is associated with several limitations that may affect the accuracy of the measurements [451-453]. The electromagnetic flow signal is influenced by the "fit" between the probe and the vessel, the angle of the probe relative to the vessel and the haemoglobin concentration in the blood. In addition, flow measurements need to be calibrated against an alternative measurement of cardiac output. These issues potentially limit the use of electromagnetic flow meters in clinical practice.

3.3.4*b* *Ultrasound flow meters*

The transit-time ultrasound flow meter is based on the principle that ultrasound waves travelling in the direction of blood flow travel faster than ultrasound waves travelling in the opposite direction. The perivascular flow probe contains two piezoelectric crystals that are diagonally placed on either side of the vessel (Figure 3.8).

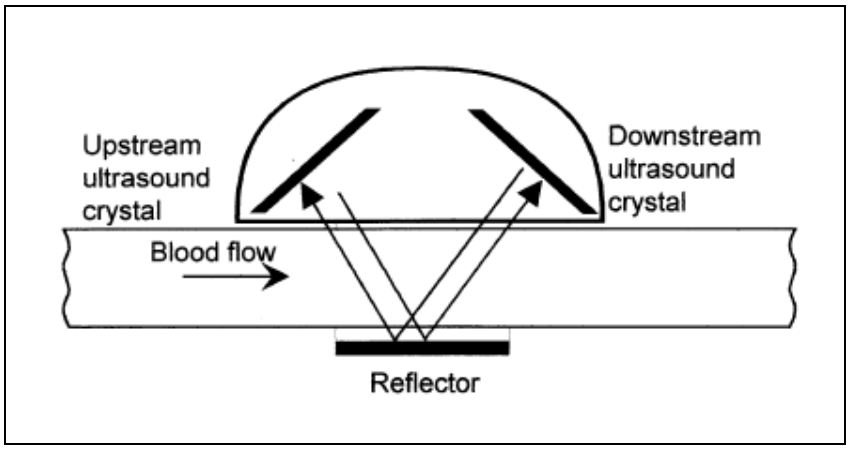

Figure 3.8 *Principles of transit-time ultrasound flow measurements. The arrows indicate the direction of travel of the ultrasound signal. Reproduced from G Beldi et al.* [454].

Both crystals can act as transmitter and receiver. Each crystal emits a brief burst of ultrasound and then waits to receive the signal from the opposite crystal. The difference in transit time between the two crystals varies as a function of blood velocity in the axial direction, $U(x)$; the distance between the two crystals, L; the angle of the ultrasound beam, ϕ; and the velocity of ultrasound in blood, C (Equation 3.11). This process is repeated at a rapid rate in order to provide effectively instantaneous measurement of the mean blood flow through the vessel.

Equation 3.11 $$\Delta t = \frac{2\cos\phi}{C^2} \cdot \int_0^L U(x) \cdot dx$$

The accuracy of the transit-time ultrasound method is approximately the same as the electromagnetic technique. However, transit-time ultrasound does not require a particularly close fit between the probe and the vessel and does not require calibration *in vivo*. As a result, the transit-time ultrasound apparatus is simple to use and provides fast and comparatively more accurate measurements of blood flow [454-456].

3.3.5 Flow measurements in this thesis

In the clinical studies described in this thesis, aortic flow measurements were made using a transit-time ultrasound flow meter (HT 323; Transonic Systems Europe B.V.) together with flow probes for vessels of 6 – 14mm in diameter (A-series flow probes; Transonic Systems Europe B.V.). These flow measurements were used primarily to calibrate conductance volume measurements made using the conductance catheter technique, as previously described.

In addition to the measurement of blood flow, we used the flow signal to independently identify the start and end of ejection. However, it became apparent during the initial studies that the time-varying aortic flow signal was delayed relative to the first-derivative of ventricular volume with respect to time (dV/dt). As a result, the onset of ejection and the end of ejection (defined using the aortic flow signal) occurred later than the equivalent points defined using the intraventricular pressure-volume measurements.

Following discussions with the manufacturer, it transpired that this was because the aortic flow signal was filtered using a 10Hz second-order Butterworth filter (personal communication, Transonics Systems Europe B.V.). The dynamic frequency and phase response of this filter are illustrated in Figure 3.9.

A transfer function was developed in Matlab® (The MathWorks) based on the dynamic frequency and phase response of the filter (Appendix A). This work was undertaken in conjunction with Dr D Ewert, North Dakota State University, ND, USA. This transfer function was applied to all aortic flow signals off-line in order to obtain a "defiltered", delay-free aortic flow signal. This "defiltered" aortic flow signal was then filtered using a 170 Hz Butterworth filter.

The effect of this process on the aortic flow signal is illustrated in Figure 3.6. Figure 3.6B illustrates the value of this technique, since the end of ejection identified using the aortic flow trace or the instantaneous change in intraventricular volume ($-dV/dt$) are comparable. All of the aortic flow data presented in the clinical studies used the 170Hz Butterworth filtered aortic flow signal.

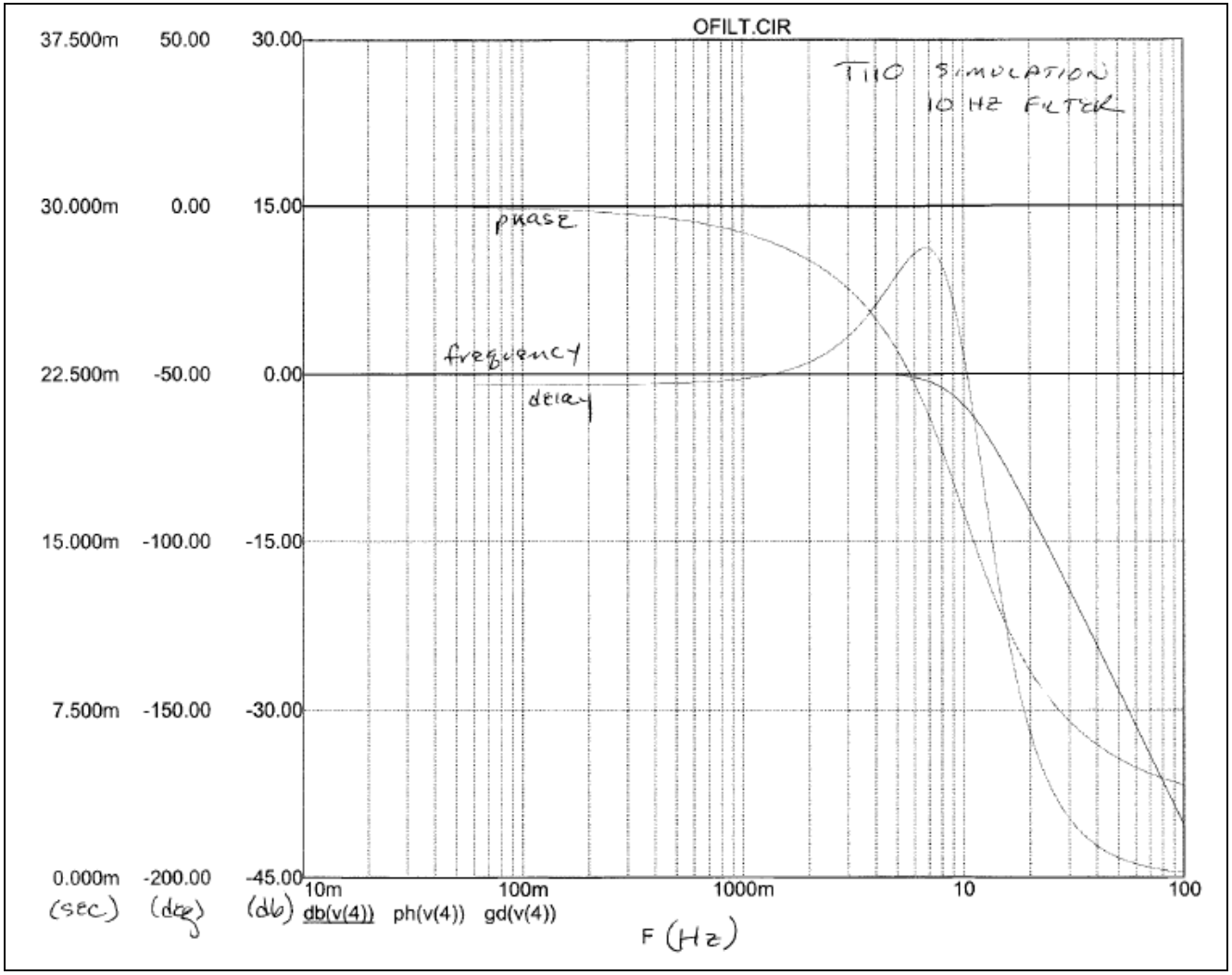

Figure 3.9 *Dynamic response characteristics of the second-order 10Hz Butterworth filter (HT-323). The phase response, frequency response and temporal delay are all illustrated as a function of frequency.*

The effect of this process on the aortic flow signal is illustrated in Figure 3.10. Figure 3.10B illustrates the value of this technique, since the end of ejection identified using the aortic flow trace or the instantaneous change in intraventricular volume ($-dV/dt$) are comparable. All aortic flow data presented in the clinical studies used the 170Hz Butterworth filtered aortic flow signal.

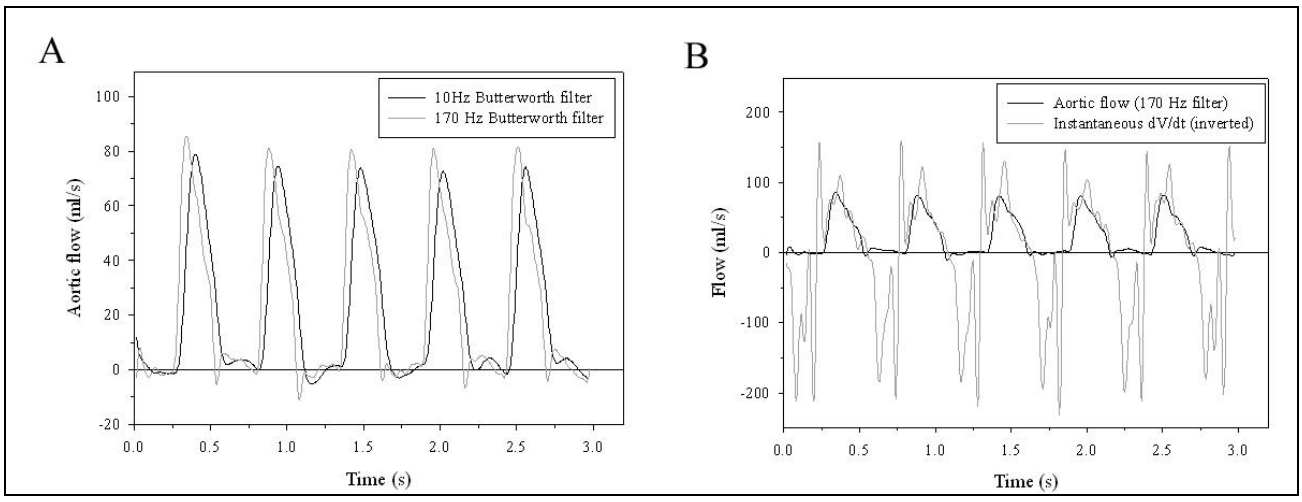

Figure 3.10 *A, Plot of aortic flow versus time. 10Hz and 170Hz Butterworth filtered data have been presented for comparison. B, Plot of aortic flow and instantaneous change in ventricular volume ($-dV/dt$) versus time.*

3.4 DATA COLLECTION

The conductance catheter lead of the pressure-conductance catheter was connected directly to the patient module of the signal-processor unit (CFL-512; CD Leycom). In addition, analogue signal outputs from the combined amplifier-interface unit (intraventricular pressure); the transit-time ultrasound flow meter (aortic flow) and the lead II surface electrocardiogram (ECG) were each connected to the CFL-512. All data were displayed and acquired simultaneously at 12-bit accuracy and a sample frequency of 250 Hz.

Data were analysed using custom-designed software developed with Professor D.E. Ewert, North Dakota State University, USA. This software program was developed using Matlab® (The MathWorks Ltd., Cambridge, UK) and was based on the previously described HEART program [457]. Subsequent analyses were performed using additional software developed in Delphi (Borland Software Corporation, Austin, TX, USA) with Mr J. Stickley, Birmingham Children's Hospital NHS Trust, UK.

3.5 CONCLUSION

In this Chapter I have extensively reviewed the techniques that are available to measure ventricular volume, intravascular pressure and cardiac output and have highlighted the advantages and disadvantages of the various techniques. In the light of this earlier discussion, I have used the following techniques for the remainder of this thesis.

Ventricular volume and pressure measurements were obtained using two commercially available pressure-conductance catheters (Millar Instruments). A 3-French catheter consisted of 10 evenly spaced platinum electrodes at the distal end of the catheter (inter-electrode spacing = 4.3 mm). A 5-French catheter consisted of 12 evenly spaced platinum electrodes with an inter-electrode spacing of 10 mm. Simultaneous pressure measurements were obtained using a high-fidelity miniaturised semiconductor strain-gauge manometer, which was laterally positioned between electrodes 5 and 6.

The 3-French pressure-conductance catheter was used in children up to 6 months of age and the 5-French catheter was used in older children. These sizes were chosen in order to minimise the haemodynamic effect of the catheter in the ventricle. These catheters have received the CE mark of approval for use in humans and can be re-used up to five times following appropriate sterilisation [458].

In the clinical studies described in this thesis, conductance volume measurements were calibrated using independent measurements of stroke volume obtained using a transit-time ultrasound flow meter (HT 323; Transonic Systems Europe B.V.) together with flow probes for vessels of 6 – 14mm in diameter (A-series flow probes; Transonic Systems Europe B.V.). Each flow probe could also be re-used following appropriate sterilisation, as provided by the manufacturer.

CHAPTER 4

CALIBRATING VOLUME MEASUREMENTS MADE USING THE DUAL-FIELD CONDUCTANCE CATHETER

CHAPTER 4. CALIBRATING VOLUME MEASUREMENTS MADE USING THE DUAL-FIELD CONDUCTANCE CATHETER

4.1 INTRODUCTION

The accurate measurement of cardiac volumes is essential to accurate diagnosis and management of patients with congenital heart disease. The conductance catheter technique represents one of the most powerful tools for the assessment of cardiac function in vivo. However, the technique is associated with certain limitations, notably parallel conductance and the non-homogeneous electric field distribution. This Chapter has been undertaken to further explore the effect of the non-homogeneous field distribution on conductance volume measurements.

As described previously, the conductance catheter technique is an established method to measure the ventricular volume in real-time, based on the electrical conductivity of blood within the ventricular cavity [380-382]. Conductance volume measurements are based on the assumption that the electric field produced by the conductance catheter is homogeneously distributed within the ventricular cavity [380]. However, theoretical and experimental studies have demonstrated that this assumption is not valid [404,405,409]. As a result, the conductance catheter tends to overestimate the volume in small ventricles and underestimate the volume in larger ventricles [381,382].

The dimensionless calibration coefficient, α, was introduced by Baan *et al.* [381] in order to account for the non-uniform conductance-absolute volume relationship [381]. This calibration coefficient represents the slope of the relationship between the conductance-derived volume and the true volume. The calibration coefficient, α may also vary with ventricular volume. It is relatively high in small animals [399], lower in humans [381] and intermediate values are found in dogs [381,400,401]. Experimental studies demonstrate that α also varies during IVCO [401] and may even fluctuate during the normal cardiac cycle [413,414].

The tissues and fluid surrounding the ventricular cavity also contribute to the measured conductance signal [381]. This creates a volume offset called parallel conductance. Parallel

conductance also varies according to the ventricular volume [399-402,405,406]. This volume-dependent parallel conductance may confound the calibration coefficient estimation.

This study was undertaken to examine the variation in the calibration coefficient, α, over a range of volumes pertaining to clinical studies, in a physical model of the left ventricle without parallel conductance.

4.2 MATERIALS AND METHODS

4.2.1 Model ventricle

This study used a physical model of the left ventricle previously described by this laboratory [392]. This model consisted of an ellipsoid latex balloon enclosed in a pressurised Perspex chamber (Figure 4.1). The chamber was filled with distilled water and hydraulically pressurised with an intra-aortic balloon pump (IABP; Datascope Medical Co. Ltd, Huntingdon, UK) with a paediatric volume-limiting chamber. The IABP console was connected to two 25ml intra-aortic balloon catheters in parallel. The IABP circuit was filled with helium gas to ensure a rapid pneumatic response.

The electrocardiogram (ECG) from a patient simulator (Bioma Research Inc, Quebec, Canada) was used to trigger the IABP console at a predetermined rate (60 beats·min^{-1}). Inflation of the IABP balloon catheters caused a rise in the ventricular pressure. This displaced saline from the latex balloon through a 2/2-way solenoid valve (Bürkert GmbH, Ingelfingen, Germany) into a calibrated measuring cylinder at the top of the model ventricle. Deflation of the IABP balloon catheters caused ventricular pressure to fall, which allowed the latex balloon to refill. Electronic circuitry was used to control the opening and closure times of the solenoid valve in order to simulate different contraction patterns.

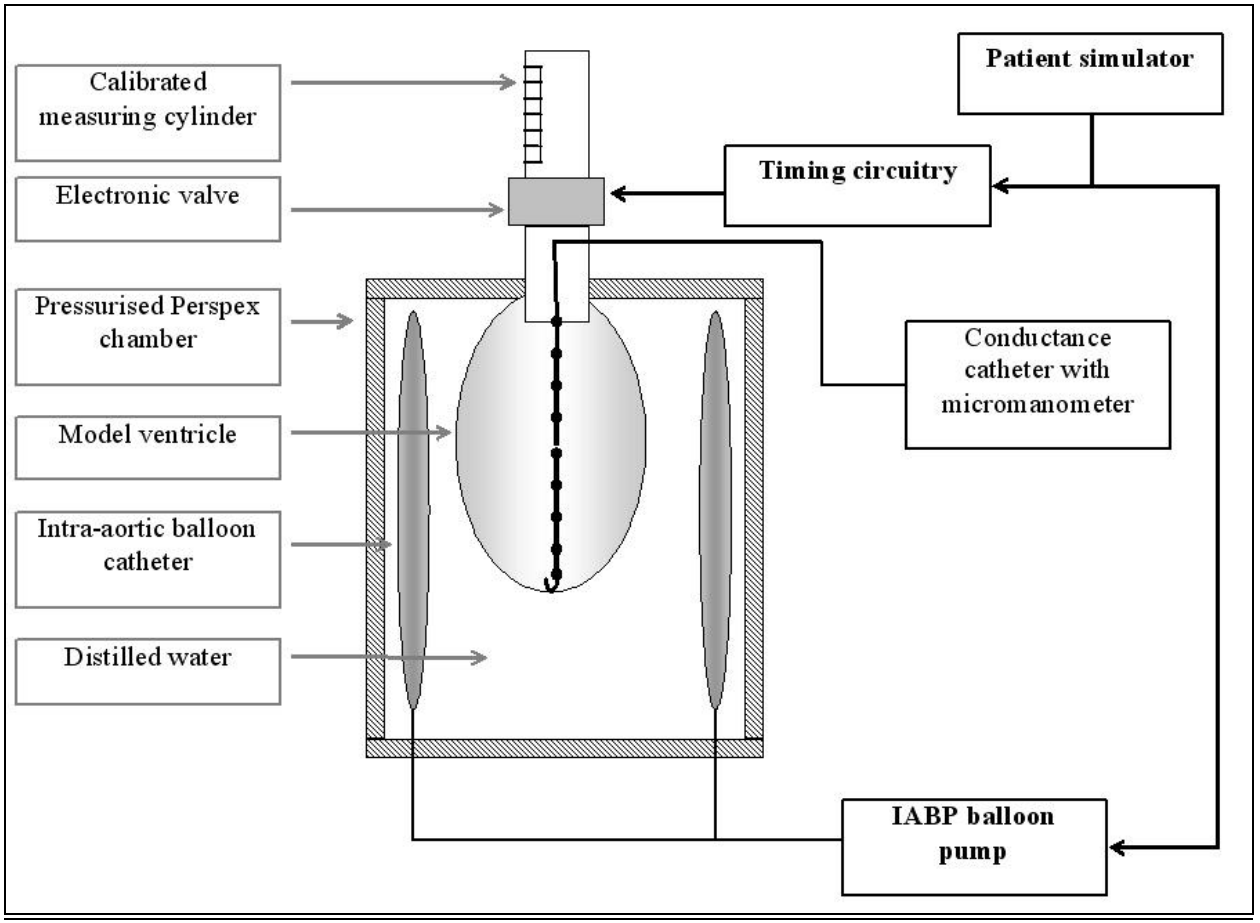

Figure 4.1 *Schematic diagram of the model heart. This consists of a model ventricle and outflow tract. The position of the conductance catheter is also illustrated.*

For the purposes of this study, the solenoid valve remained open throughout the model ventricular cycle to produce isobaric contractions. Each inflation of the IABP balloon catheters displaced a fixed stroke volume (*SV*) of 50ml. The stroke volume was independently quantified before each experiment. The IABP balloon catheters were manually inflated and the displaced volume was measured in the measuring cylinder.

Three separate latex balloons were used to simulate the change in volume that may be observed during IVCO. Each balloon was 13 cm in length and had a maximal volume at atmospheric pressure of 125ml, 215ml and 500ml, respectively. The shape of the balloons was ellipsoid at low volumes and became increasingly spheroid as the volume increased. The length-diameter ratio at maximal filling decreased from 3.03 for the smallest balloon to 1.52 for largest balloon.

During each experiment, the model ventricle was filled with a known volume of 0.9% normal saline at room temperature. The end-diastolic volume (*EDV*) was varied between 100 – 125ml for the 125ml balloon; 160 – 215ml for the 215ml balloon; and 410 – 500ml for the 500ml balloon. The resistivity (conductivity^{-1}) of this solution was measured before each test using the dedicated measuring cuvette (CD Leycom). The mean ± SD resistivity was 68.3 ± 0.5 Ω·cm.

4.2.2 Conductance catheter

The principle of the conductance catheter technique for measuring LV volume has been described elsewhere [381]. In this study, a 7-French 12-electrode high-fidelity dual pressure-volume conductance catheter (Millar Instruments) was used. The electrodes were mounted at 10 mm intervals near the tip of the catheter. One alternating current (20 kHz, 30 μA RMS) was applied between the two outermost electrodes (electrodes 1 and 12) and a second alternating current (20 kHz, -10 μA RMS) was applied between the two adjacent electrodes (electrodes 2 and 11). This dual-field configuration was used in all studies [407]. A signal processor unit (CFL-512; CD Leycom) was used to measure the potential difference between seven consecutive pairs of the remaining eight electrodes (electrodes 3 – 10). These measured voltages were converted into seven time-varying segmental conductance signals, $G_i(t)$.

The conductance volume, $Q(t)$, was measured using the following formula:

Equation 4.1 $$Q(t) = L^2 \cdot \rho \cdot \left(\left[\sum_{i=1}^{7} G_i(t) \right] - G_P \right),$$

where ρ is the blood resistivity, L is the inter-electrode distance, and G_P is parallel conductance.

By assuming that parallel conductance is negligible (i.e. $G_P = 0$), this formula can be simplified to:

Equation 4.2 $$Q(t) = L^2 \cdot \rho \cdot \left[\sum_{i=1}^{7} G_i(t) \right],$$

The volume estimated using the conductance catheter technique, $V_g(t)$ was then calculated:

Equation 4.3 $$V_g(t) = \frac{1}{\alpha} \cdot Q(t),$$

where α is the dimensionless calibration coefficient [381].

4.2.3 Experimental data

Analogue signals representing 7 segmental conductance volumes within the model ventricle and the ECG were digitised at 12-bit accuracy and a sample frequency of 250 Hz. End-diastole and end-systole were retrospectively identified. End-diastole was defined as the R-wave on the ECG and end-systole was defined as the point immediately prior to IABP circuit deflation. The simulated cardiac cycle was defined as the period between end-diastole of one beat to end-diastole of the following beat.

Two separate calibration coefficients were calculated. Firstly, the calibration coefficients, $\alpha_{V(t)}$ was calculated by dividing the conductance-derived volume measurement by the absolute ventricular volume at either end-diastole or end-systole:

Equation 4.4 $$\alpha_{V(t)} = \frac{Q_{ED}}{EDV} \text{ or } \frac{Q_{ES}}{ESV},$$

where $ESV = EDV - SV$.

Including a "phase of measurement" (i.e. *ED* or *ES*) in this equation did not improve the goodness of fit of the model. The effect of "phase of measurement" was not statistically significant and was therefore not included in the model used to predict $\alpha_{V(t)}$.

The conductance-stroke volume quotient, α_{SV}, was calculated by dividing the conductance-derived stroke volume by the absolute stroke volume:

Equation 4.5 $$\alpha_{SV} = \frac{Q_{ED} - Q_{ES}}{SV}$$

Finally, the measurement error, ζ was calculated as a percentage of the absolute ventricular volume:

Equation 4.6 $$\zeta = \frac{V_g(t)}{V(t)} \cdot 100$$

The terms $\zeta_{V(t)}$ and ζ_{SV} were used to denote the measurement error associated with $\alpha_{V(t)}$ and α_{SV}, respectively.

4.2.4 Statistical analysis

Each experiment was conducted three times and, in each, data from 10 consecutive cardiac cycles were analysed. The estimated within-experiment standard deviation in the conductance volume measurement for the 30 cardiac cycles was 0.45 ml. The standard deviation was not significantly correlated with the mean conductance volume (Kendall's τ coefficient = -0.72). Subsequent analyses were therefore based on the average data from each experiment [435].

The coefficients of the linear regression analyses, in both the overall and covariance analyses, are expressed as mean ± standard error and a probability, $P<0.05$, was taken to represent statistical significance. The "goodness of fit" of the prediction equation was assessed as the square of the correlation between dependent and significant independent variables.

Data were analysed using SPSS for Windows (v12, SPSS Inc., Chicago, IL, USA). Conductance volumes, calibration coefficients and measurement errors were in turn examined as functions of

the known volume of the model ventricle. These relationships were evaluated using a stepwise least squares linear regression analysis. This analysis was based on fractional polynomials of the ventricular volume that included $\sqrt[3]{V}$, $\sqrt{V}$, $V/3$, $V/2$, $1/V$, V, $2V$, $3V$, V^2 and V^3, where V represents the ventricular volume. The coefficients of the linear regression analyses are expressed as mean ± standard error and a probability, $P<0.05$, was taken to represent statistical significance. The "goodness of fit" of the prediction equation was assessed as the square of the correlation between dependent and significant independent variables.

4.3 RESULTS

4.3.1 Relationship between conductance and absolute volume

The simultaneous conductance volume, $Q(t)$, and absolute volume measurements, $V(t)$ for the three balloons are illustrated in Figure 4.2. There was a non-linear relationship between these two volume measurements. When analysed as a whole, the conductance-absolute volume relationship was best approximated by the following relationship (Equation 4.7).

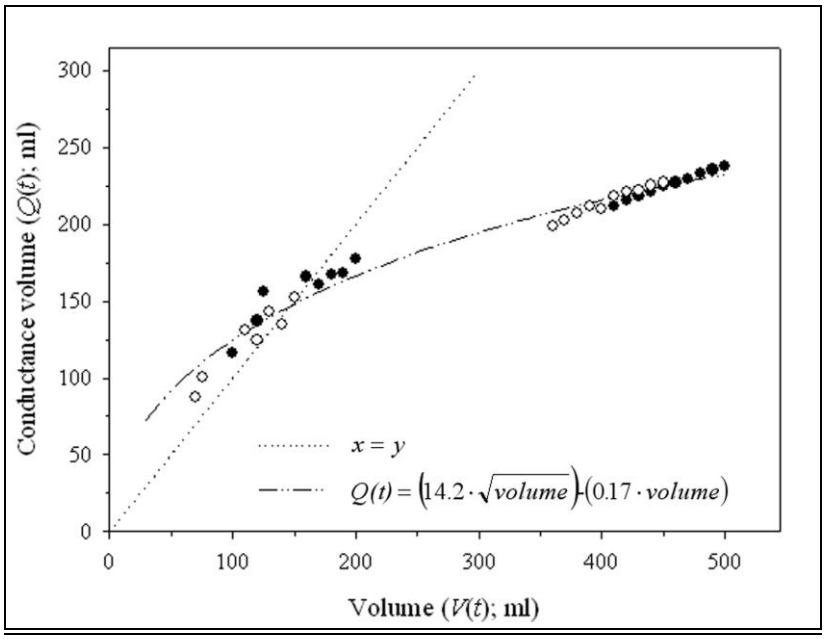

Figure 4.2 *Conductance volume measurements, $Q(t)$ versus absolute volume, $V(t)$ at end-diastole (●) and end-systole (○) for each of the three latex balloons. The curve (dashed line) represents the regression analysis of the conductance-absolute volume relationship. The curve (dotted line) representing the line of identity (x=y) is also illustrated.*

Equation 4.7 $$Q(t) = (4.2 \pm 0.39) \cdot \sqrt{volume} - (0.17 \pm 0.02) \cdot volume$$, (r^2=0.90, P<0.05)

Compared with the line of identity (i.e. $x = y$), conductance volume measurements predicted using this model were equal to ventricular volume at approximately 150 ml; slightly overestimated ventricular volume when the absolute volume was less than 150 ml; but underestimated ventricular volume at volumes over 150 ml.

The volume measurements formed two distinct subsets. Data from the small and medium balloons were clustered on the left-hand side of the plot while data from the large balloon was clustered on the right-hand side. When considered individually, the conductance-absolute volume relationship was well approximated by linear regression (Equations 4.8 and 4.9). In neither case was the quadratic term significant. For the small and medium-sized balloons, the linear regression was:

Equation 4.8 $$Q(t) = (0.63 \pm 0.06) \cdot V(t) - (65 \pm 9)$$, (r^2=0.90, P<0.05)

while for the large balloon, the corresponding equation was:

Equation 4.9 $$Q(t) = (0.27 \pm 0.01) \cdot V(t) - (104 \pm 5)$$, (r^2=0.96, P<0.05)

The slope of these two mathematical models are significantly different from one another (P<0.05), further illustrating that a single, common linear relationship does not hold over the entire range of absolute volumes. In addition, the intercepts differ significantly from one another and from zero (P<0.05). Therefore, neither of these two lines passes through the origin. This introduces a "volume offset", which in this apparatus cannot be due to parallel conductance.

4.3.2 Relationship between calibration coefficients and absolute volume

The calibration coefficients, $\alpha_{V(t)}$ and α_{SV} were calculated using equations 4.4 and 4.5, respectively. Neither calibration coefficient was constant or linearly related to the ventricular volume. Instead, both calibration coefficients decreased progressively as the ventricular volume increased (Figures 4.3A and 4.3B). The calibration coefficient, $\alpha_{V(t)}$ varied as a function of the square root of the absolute volume (r^2=0.97, P<0.05). By contrast, α_{SV} varied as a function of the

inverse absolute volume (r^2=0.98, P<0.05; and r^2=0.93, P<0.05 for end-diastolic and end-systolic measurements respectively).

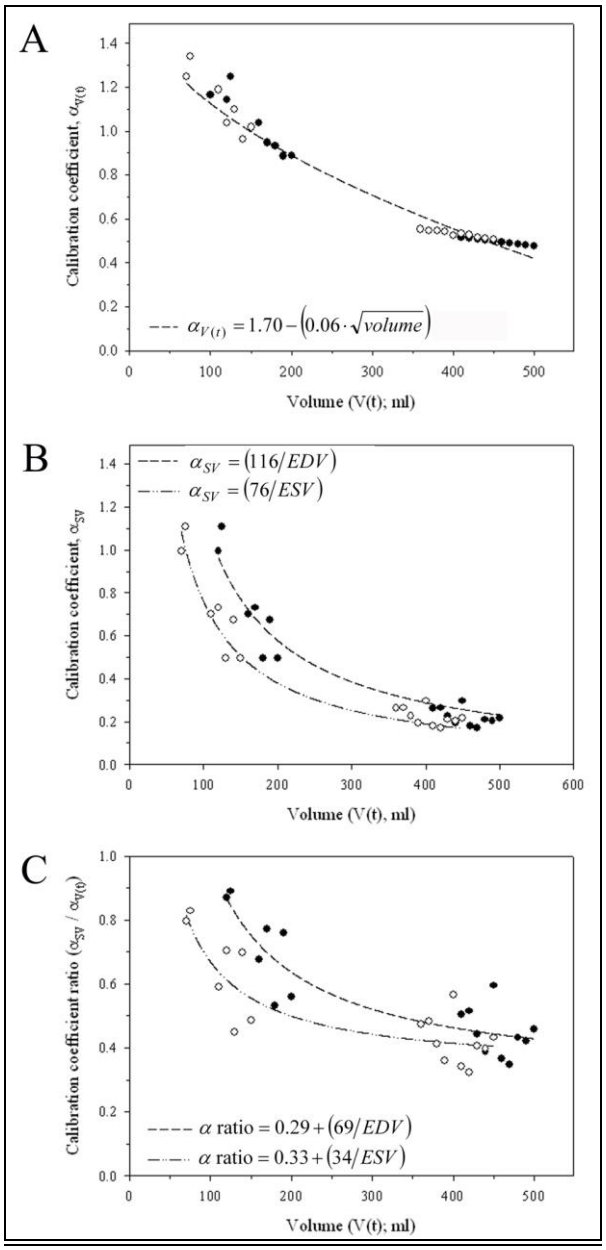

Figure 4.3 *Calibration coefficient, α versus absolute volume, V(t) at end-diastole (●) and end-systole (○) for each of the three latex balloons. The calibration coefficient was calculated as the conductance-absolute volume quotient ($\alpha_{V(t)}$, A) or the conductance-stroke volume quotient (α_{SV}, B). The calibration coefficient ratio (C) represented α_{SV} as a proportion of $\alpha_{V(t)}$. Curves (dashed lines) representing regression analyses of the calibration coefficient-conductance volume relations are also illustrated.*

The relative ratio of the two calibration coefficients (i.e. α_{SV} / $\alpha_{V(t)}$) was also examined over the volume range (Figure 4.3C). The stroke volume quotient, α_{SV} was lower than $\alpha_{V(t)}$ at each volume

measurement. However, the slope calibration coefficient ratio was not constant but became progressively smaller as the absolute volume was increased. For example, the α_{SV} / $\alpha_{V(t)}$ ratio decreased from 0.98 ± 0.52 to 0.43 ± 0.23 as the end-diastolic volume increased from 100ml to 500ml.The best approximation for this relationship was that the α_{SV} / $\alpha_{V(t)}$ ratio varied as a function of the inverse ventricular volume (r^2=0.81, P<0.05; r^2=0.75, P<0.05 for end-diastolic and end-systolic measurements, respectively).

4.3.3 Relationship between calibrated conductance and absolute volume and measurement error

Calibrated conductance volume measurements, $V_g(t)$ were calculated using Equation 4.3, in which α was either $\alpha_{V(t)}$-volume or α_{SV}-volume relationship, as previously described (Figure 4.4). Conductance volume measurements calibrated with the $\alpha_{V(t)}$-volume relation increased linearly with the absolute volume (r^2 =0.99, P<0.05). Conductance volume measurements calibrated with the α_{SV}-volume relation also increased linearly with absolute volume (r^2=0.99, P<0.05), but overestimated the absolute volume.

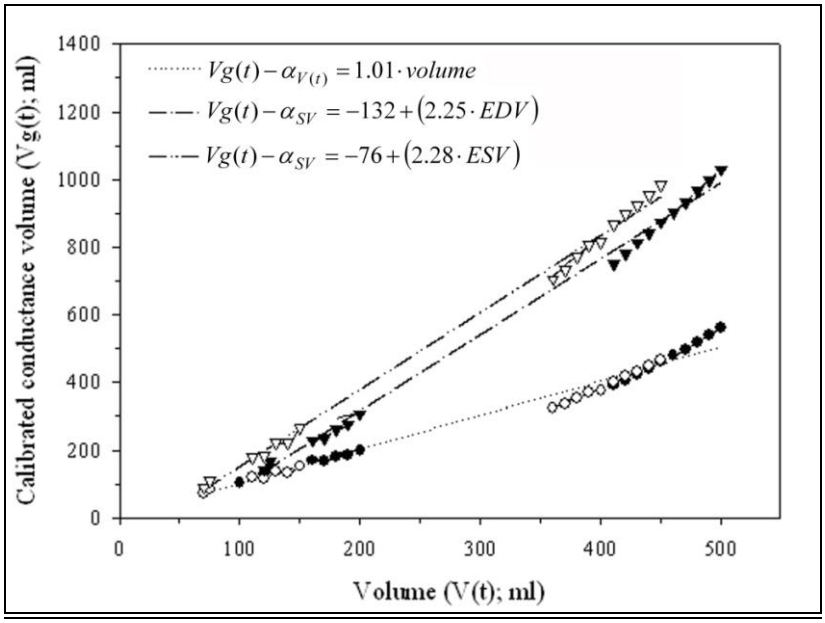

Figure 4.4 *Calibrated conductance volume measurements, $V_g(t)$ versus absolute volume, $V(t)$ at end-diastole (●) and end-systole (○) for each of the three latex balloons. Conductance volume measurements were calibrated using either $\alpha_{V(t)}$ (●, ○) or α_{SV} (▼, ▽).Curves (dashed lines) representing regression analyses of the calibrated conductance volume-absolute volume relations are also illustrated.*

The volume measurement error, expressed as a percentage of the absolute volume, was calculated for each calibration coefficient (Figure 4.5). Conductance volume measurements calibrated with the $\alpha_{V(t)}$-volume relation had a measurement error of 2.0 ± 6.9%, which was relatively constant across the span of volume measurements. On the other hand, the measurement error associated with the α_{SV}-volume relation was volume-dependent, increasing linearly from 26 ± 20% to 106 ± 36% as the end-diastolic volume increased from 100ml to 500ml (r^2=0.96, P<0.05).

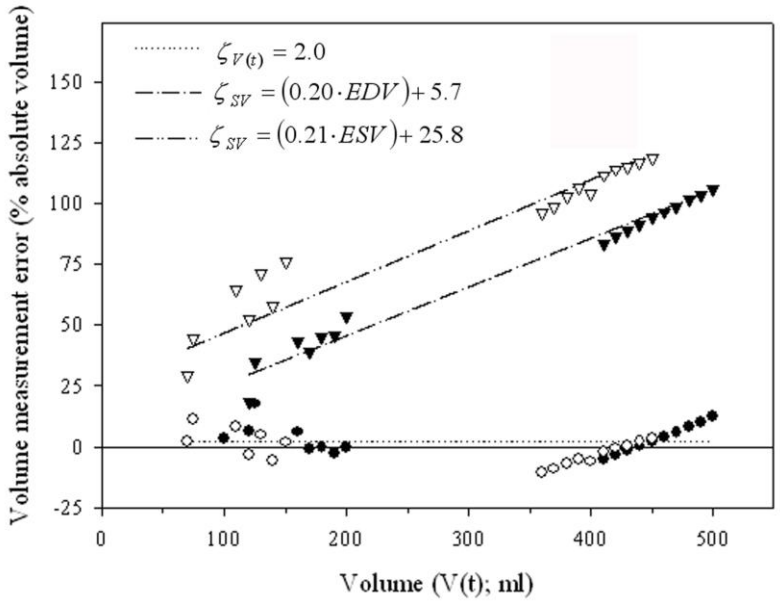

Figure 4.5 *Calibrated conductance volume measurement error, ζ versus absolute volume, V(t) at end-diastole (●) and end-systole (○).Conductance volume measurements calibrated using either* $\alpha_{V(t)}$ *(●, ○) or* α_{SV} *(▼, ▽). Volume measurement error was calculated as a percentage of the absolute volume. Curves (dotted and dashed lines) representing regression analyses of the measurement error-absolute volume relations are also illustrated.*

4.4 DISCUSSION

The non-homogeneous electric field generated by the conductance catheter results in a non-linear relationship between conductance and true ventricular volume measurements. Conductance measurements are, therefore, calibrated using the dimensionless calibration coefficient, α in order to obtain absolute volume measurements. This study investigated the accuracy of conductance volume measurements, and the effect of calibration, in a series of *in vitro* experiments that

spanned the volume range observed in clinical studies [459]. This model design also avoided the potential problems associated with parallel conductance.

This study has confirmed that there is a non-linear relationship between dual-field conductance and absolute volume measurements, such that the conductance-volume relation is concave towards the true volume. The conductance volume measurements underestimated ventricular volume as the volume was increased above 150ml. This finding is in accord with previous experimental studies [404,405].

Conductance volume measurements are generally calibrated with the dimensionless calibration coefficient in order to improve the accuracy of ventricular volume measurements made using this technique [381]. In the isolated post-mortem canine heart, Mur & Baan reported that the conductance-volume relation was virtually linear over a finite volume range [382] and the authors predicted that a similar, virtually linear conductance-volume relation would be observed for the human left ventricle up to a volume of 200ml [382].

However, this study has shown that the calibration coefficient, α is not constant, but varies as a non-linear function of the ventricular volume. Using a fixed or constant α during acute volume change will inevitably result in volume measurement errors. These measurement errors may be relatively small during the normal cardiac cycle. However, procedures that produce an acute and substantial change in volume load, like vena caval occlusion, will potentially result in significant measurement errors.

Kornet *et al.* suggested that the variation in α observed *in vivo* might reflect synchronous volume-dependent changes in parallel conductance during the cardiac cycle [402]. However, this study used a physical model of the left ventricle without parallel conductance. Our findings suggest that parallel conductance is not a comprehensive explanation for why the calibration coefficient varies as a function of the ventricular volume.

Although conductance volume measurements can be calibrated against another synchronous estimate of ventricular volume [381,413,460], they are generally calibrated with an alternate

measurement of stroke volume [399,404]. Calibration with either an alternate measurement of ventricular volume or stroke volume are generally considered equivalent. However, this study identified that the $\alpha_{V(t)}$ and α_{SV} are different. The stroke volume quotient, α_{SV} was lower than $\alpha_{V(t)}$ and the calibration coefficient ratio, α_{SV} / $\alpha_{V(t)}$ became progressively smaller as the ventricular volume increased. Calibrating conductance volume measurements with α_{SV} resulted in the significant overestimation of end-diastolic and end-systolic volume, and the degree of overestimation was even more pronounced at higher volumes. This demonstrates that conductance volume measurements should ideally be calibrating using an independent measure of ventricular volume like, for example, contrast cineangiography, echocardiography or magnetic resonance imaging.

The difference between the $\alpha_{V(t)}$-volume and α_{SV}-volume relations may be attributed to the non-homogeneous electrical field distribution established by the conductance catheter [405,406]. Conductance volume measurements are disproportionately influenced by the areas around the longitudinal axis of the ventricle where the electrical field is strongest. By contrast, changes in volume that occur during ejection or when loading conditions are varied primarily affect the myocardial boundary where the electrical field density is weakest. Consequently, α_{SV} and $\alpha_{V(t)}$ are not equivalent and cannot be used interchangeably.

4.4.1 Study Limitations

The physical model of the isolated left ventricle used in this study did not allow changes in the volume loading conditions could not be modelled continuously. Instead, a series of steady-state experiments were made at incremental end-diastolic volumes in three separate models, which carries with it the risk of repeated measurement errors. The changes in ventricular volume resulted from changes in the short-axis dimension of the model only. It was not possible to examine any effect of changing ventricular length, such as those that may occur during the cardiac cycle [223].

Ideally, the volumes within the model ventricle would have been acquired simultaneously using the conductance catheter and another independent method. In the original design, the ejected

volume was measured according to the pressure generated within the fluid column [392]. However, preliminary experiments demonstrated that the fluid-filled micromanometer was not sufficiently accurate to enable instantaneous volume measurements throughout the cardiac cycle and, therefore, measurements were made with the calibrated measuring cylinder.

4.5 CONCLUSION

The conductance catheter technique incorporates a calibration coefficient, α, in order to obtain accurate volume measurements. This study has demonstrated that this calibration coefficient varies as a function of absolute volume, independent of parallel conductance. Assuming that the calibration coefficient is fixed or constant will introduce measurement errors. The conductance-stroke volume quotient, α_{SV} is associated with particularly significant and volume-dependent measurement errors. This limits the value of volume measurements calibrated using α_{SV}.

Conductance volume measurements should ideally be calibrated with an alternative measurement of ventricular volume, using any one of the techniques that are now available. However, in some circumstances this may not be possible. This is particularly true in clinical studies where the resources may not be available and the use of another technique may compromise patient safety. In the clinical studies described in Chapters 6 and 7, for example, it was decided that there was not an alternative, safe and reproducible measurement of ventricular volume that could be performed in the operating theatre at Birmingham Children's Hospital. Therefore, the conductance volume measurements were calibrated using an alternative measurement of stroke volume even though this may adversely affect the absolute accuracy of the volume measurements.

CHAPTER 5

ELECTROCARDIOGRAPHIC INTERFERENCE AND CONDUCTANCE VOLUME MEASUREMENTS

CHAPTER 5. ELECTROCARDIOGRAPHIC INTERFERENCE AND CONDUCTANCE VOLUME MEASUREMENTS

5.1 INTRODUCTION

The assessment of ventricular function is fundamentally important for the evaluation of patients with known or suspected heart disease. Analysis of ventricular volume in the time and pressure domains allows systolic and diastolic function to be separately quantified. The conductance catheter technique was developed to continuously measure ventricular volume in real-time [380,382]. These measurements are recorded simultaneously with intraventricular pressure measurements to provide instantaneous pressure-volume data [460].

The conductance catheter technique is associated with two, well-known sources of error. Firstly, the current density generated by the conductance catheter is not uniformly distributed throughout the ventricular cavity [403-405]. This results in a non-linear conductance-absolute volume relationship [382,405,408]. Conductance volume measurements must be corrected with a calibration coefficient, α [381]. Secondly, the tissues and fluid surrounding the ventricular cavity also contribute to the conductance signal [381,382]. This results in an offset in the conductance-absolute volume relationship, called parallel conductance. In practice, conductance volume measurements are usually calibrated for parallel conductance using the hypertonic saline method in order to derive accurate ventricular volume measurements [381].

In our paediatric clinical experience, we have observed that the pattern of LV volume measurements is frequently abnormal (Figure 5.1). The conductance volume measurements are characterised by a narrow upward spike followed by a narrow downward spike during late diastole without any commensurate change in LV pressure (Figures 5.1A and 5.1B). This alters the shape of the pressure-volume loop, with the loss of the normal lower right-hand corner (Figure 5.1D). To our knowledge, this abnormal conductance volume pattern has not previously been described. However, we understand that similar findings have been observed in other patient groups, particularly in patients with a permanent pacemaker [personal communication, Professor M.P. Frenneaux, Department of Cardiovascular Sciences, University of Birmingham,

UK; Dr P. Steendijk, Department of Cardiology, Leiden University Medical Center, The Netherlands].

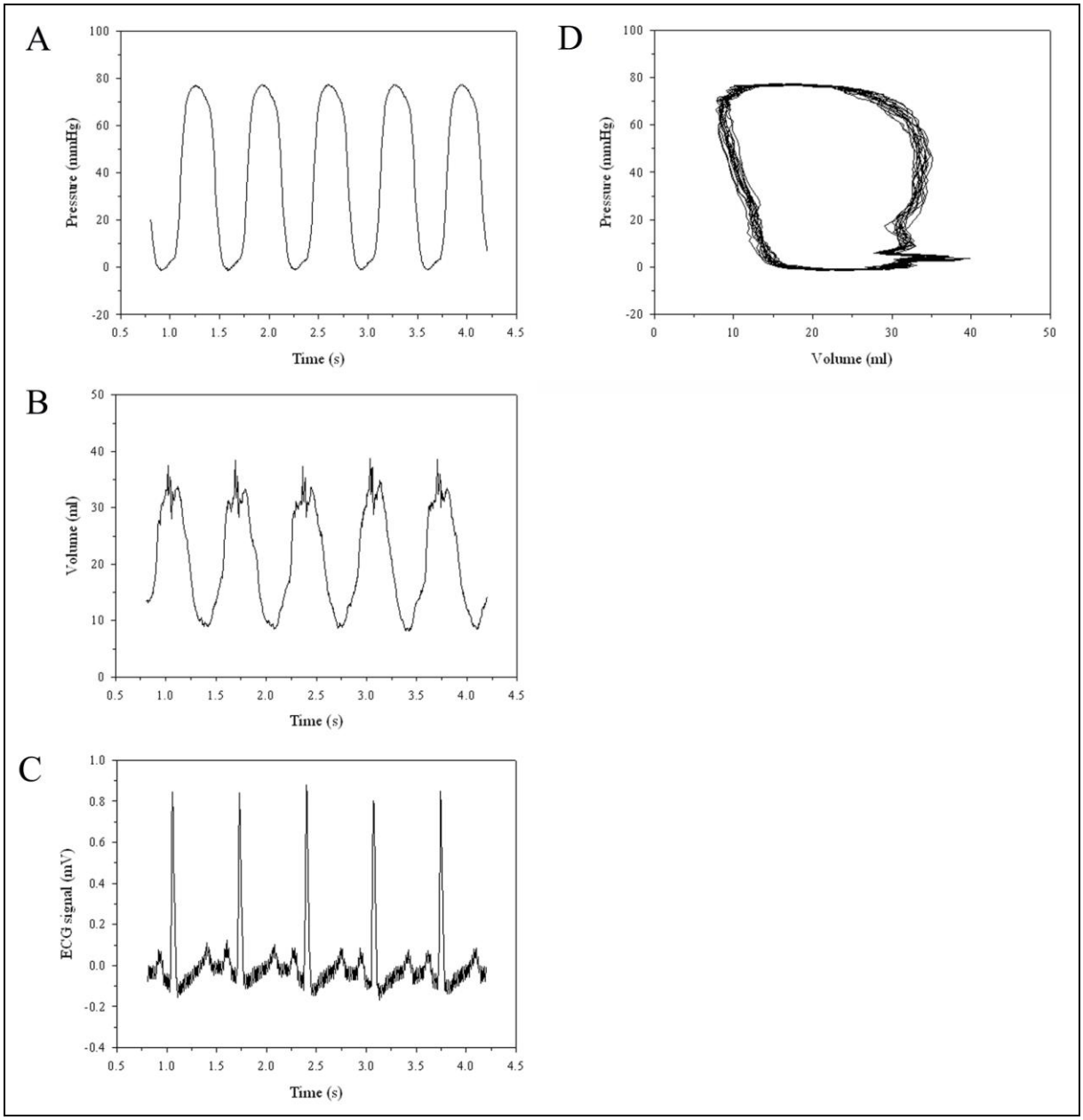

Figure 5.1 *Time-varying pressure (A), conductance volume (B) and surface electrogram (C) signals obtained in a 6 year-old child with tricuspid atresia. The corresponding pressure-conductance volume loop for the same child (D) was developed by plotting the instantaneous pressure against the corresponding conductance volume.*

We observed that the abnormal LV conductance volume measurements occurred synchronously with the QRS complex on the surface electrocardiogram (ECG; Figure 5.1C). We hypothesised that this abnormal LV conductance measurement may represent the effect of ventricular excitation on conductance volume measurements, which is superimposed on the normal ventricular volume cycle. This study was undertaken to examine the relationship between the ventricular electrogram and conductance volume measurements in a physical model of the left ventricle without parallel conductance. In addition, we sought to determine how this relationship was influenced by changes in electrical resistance across the model ventricle.

5.2 MATERIALS AND METHODS

5.2.1 Model ventricle

This study used the physical model of the left ventricle previously developed by this laboratory [392] and described in Chapter 4. In summary, this consisted of an ellipsoid latex balloon enclosed in a pressurised Perspex chamber. The chamber was filled with distilled water and hydraulically pressurised with an intra-aortic balloon pump (IABP; Datascope Medical Co. Ltd) connected to two 25ml intra-aortic balloon catheters in parallel. A patient simulator (Bioma Research Inc) was used to trigger the IABP console at a predetermined rate (60 beats·min^{-1}).

Inflation of the intra-aortic balloon catheters displaced the stroke volume (SV, 50ml) from the model ventricle through a 2/2-way solenoid valve (Bürkert GmbH) into a calibrated measuring cylinder at the top of the model ventricle. Deflation of the IABP balloon catheters caused ventricular pressure to fall, which allowed the latex balloon to refill. Electronic circuitry was used to control the opening and closure times of the solenoid valve in order to simulate different contraction patterns.

The latex balloon was 13 cm in length and had a maximal volume at atmospheric pressure of 500ml. The balloon was filled with 385 – 500ml of buffered saline solution (V) at room temperature. The saline concentration was varied between 0.18 – 1.57%. The resistivity (ρ;

conductivity^{-1}) of these solutions was measured before each test using the dedicated measuring cuvette (CD Leycom). The resistivity ranged between 37 ± 0.8 to 330 ± 0.5 Ω·cm.

Ventricular depolarisation was simulated using a fixed output ECG signal, ECG_{input}, from the patient simulator (maximum 150.4 ± 0.1 mV, minimum -35.8 ± 0.2 mV). This was connected, via a resistor (200 Ω), to a dipole within the latex balloon. This dipole consisted of two copper ring electrodes (diameter 30mm, depth 5mm and thickness 1mm) that were positioned perpendicular to the long-axis of the balloon, Figure 5.2. The in-series resistor was adjusted so that the signal range of the intracavitary electrogram (*ECGc*) in the model ventricle was equivalent to that observed in vivo (~ 1mV).

In vivo, the intracavitary electrogram primarily reflects the pattern of ventricular depolarisation and repolarisation in the endocardium of the ventricle [51]. The position of the endocardium relative to the long-axis of the ventricle will vary as the ventricular volume changes during the cardiac cycle. This effect was simulated by altering the distance between the two electrodes of the dipole. The distance between the two electrodes (D) was varied between 3 cm and 11.5 cm such that both electrodes remained equidistant from the centre of the balloon.

5.2.2 Conductance catheter

The principle of the conductance catheter technique for measuring LV volume has been described in Chapter 3. The details of the conductance catheter used in this study are described in Chapter 4. The catheter measured seven time-varying segmental conductance signals, $G_i(t)$. As parallel conductance is negligible in our model, the total conductance volume, $Q(t)$, was determined using the following formula:

Equation 5.1
$$Q(t) = L^2 \cdot \rho \cdot \left[\sum_{i=1}^{7} G_i(t) \right],$$

where ρ is the blood resistivity and L is the inter-electrode distance.

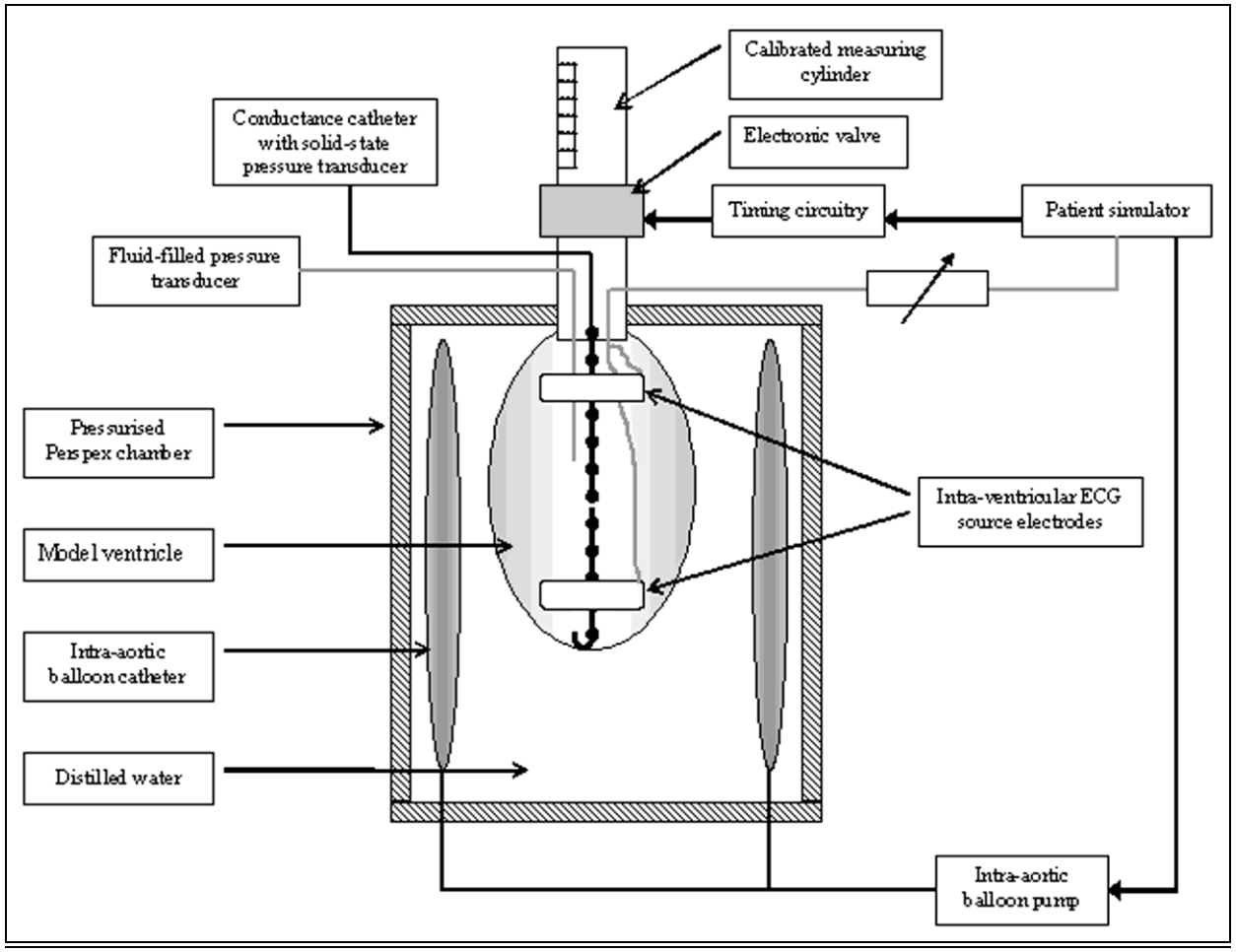

Figure 5.2 *Schematic diagram of the model heart used including the modifications for this experiment. The location of the intraventricular dipole electrodes and their position relative to the pressure-conductance catheter are illustrated.*

The dimensionless calibration coefficient, $\alpha_{V(t)}$ was calculated from conductance volume measurements without the ECG signal by dividing the conductance-derived volume measurement by the absolute volume at end-diastole or end-systole, as detailed in Chapter 4.

Equation 5.2 $$\alpha_{V(t)} = \frac{Q_{ED}}{EDV} \text{ or } \frac{Q_{ES}}{ESV}$$

The calibration coefficient, $\alpha_{V(t)}$ varies as a non-linear function of the absolute ventricular volume (Chapter 4) and we used this non-linear $\alpha_{V(t)}$-volume relation to calibrate conductance volume measurements:

Equation 5.3 $$V_g(t) = \frac{1}{\alpha_{VV}} \cdot Q(t),$$

where α_{VV} is the $\alpha_{V(t)}$-volume relation (Chapter 4).

Instantaneous pressure within the model ventricle was measured using a high-fidelity solid-state micromanometer laterally positioned between electrodes 5 and 6 within the conductance catheter. This pressure signal was amplified using a combined amplifier-interface unit (PCU-2000; Millar Instruments) and statically calibrated using a separate fluid-filled catheter-manometer system.

The cavitary electrogram, *ECGc* was measured as part of the conductance catheter technique. The conductance signal between electrodes 5 and 6 was measured, amplified and filtered using a second-order filter with a high cut-off frequency (-3dB; 125 Hz) in order to derive the *ECGc* [personal communication; CD Leycom].

5.2.3 ECG interference

The conductance signal was measured either with, $G_i^+(t)$, or without the ECG signal, $G_i^-(t)$. ECG interference, $G_{ECG}(t)$ was calculated as the difference between these two conductance signals:

Equation 5.4 $$G_{ECG}(t) = \sum_{i=1}^{7} G_i^+(t) - \sum_{i=1}^{7} G_i^-(t)$$

The difference between calibrated volume measurements made with, $V_g^+(t)$ and without the ECG signal, $V_g^-(t)$ was expressed as a percentage of the $V_g^-(t)$ signal:

Equation 5.5 $$\Delta V_{ECG} = \frac{V_g^+(t) - V_g^-(t)}{V_g^-(t)}$$

5.2.4 Experimental data

Analogue signals representing 7 segmental conductance signals, the pressure within the model ventricle, and both ECG_{input} and $ECGc$ were all digitised at 12-bit accuracy and a sample frequency of 250 Hz. End-diastole and end-systole were retrospectively identified. End-diastole was defined as the R-wave on the ECG and end-systole was defined as the point immediately prior to IABP circuit deflation.

The effect of intracavitary volume (V), resistivity of the saline solution (ρ) and inter-electrode distance (D) on the intracavitary electrogram and conductance volume measurements were examined in turn. This involved a series of experiments, in which one variable was altered incrementally while the other two variables remained unchanged. This process was repeated until the data from the entire range was obtained (see above).

5.2.5 Statistical analysis

Each experiment was conducted three times and data from 5 consecutive cardiac cycles were analysed. Only 5 cardiac cycles were included, in view of the limited variance associated with conductance volume measurements (Chapter 4). The estimated within-experiment standard deviation was 0.71 ml and, at its worst, this represented <0.5% of the total conductance volume. All subsequent analyses were therefore based on the average data from each experiment.

Data were analysed using SPSS for Windows (v12, SPSS Inc., Chicago, Il, USA). All values are expressed as mean ± SD and comparative analyses have been made using the paired two-tail Student *t*-test.

The relationship between the ECG_{input}, $ECGc$ and the ECG interference pattern was evaluated using a stepwise least squares linear regression analysis. This analysis was based on fractional polynomials of the data that included $\sqrt[3]{x}$, $\sqrt{x}$, $x/3$, $x/2$, $1/x$, x, $2x$, $3x$, x^2 and x^3, where x represented the independent variable in each analysis.

As the ECG interference pattern will vary according to the resistance of the volume conductor, the intracavitary volume, resistivity of the saline solution and the inter-electrode distance were included as covariables in the regression analyses.

Initial examination of the ECG signals demonstrated that changes in the resistance of the volume conductor were associated with a change in the scale of $ECGc$ and the ECG interference pattern but the basic shape of the signals remained the same. Therefore, separate linear regression analyses were performed to examine the relationship between between the intercept values and the linear regression coefficient (β_0 and β_1 in Equation 5.6, respectively) and each covariables. Fractional polynomials of each covariable were used, as described previously. Covariables that demonstrated a significant association ($P<0.05$) with β_0 or β_1 based on univariate analysis were combined to create a unified covariable. For example, if $\beta_1 \propto A$ and $\beta_1 \propto 1/B$, then A and B were combined to create the final covariable, A/B.

Finally, the relationship between the ECG_{input}, $ECGc$ and the ECG interference pattern was evaluated using a further stepwise least squares linear regression analysis that included significant covariables. The coefficients of the linear regression analyses, in both the overall and covariance analyses, are expressed as mean ± standard error and a probability, $P<0.05$, was taken to represent statistical significance. The "goodness of fit" of the prediction equation was assessed as the square of the correlation between dependent and significant independent variables.

5.3 RESULTS

Indices of systolic and diastolic ventricular function showed variability between repeated measurements. The coefficient of variation (SD/mean · 100) together with its standard deviation was 17 ± 10% for E_{ES}, 12 ± 9% for $PRSW$ and 13 ± 9% for dP/dt_{MAX}-EDV' [461]. The coefficient of variation for chamber stiffness was 21 ± 13%.

5.3.1 Comparison between ECG signal and cavitary electrogram

The ECG signal, ECG_{input}, consisted of P, Q, R, S and T deflections that resembled the normal lead II electrocardiogram (Figure 5.3A). The P-wave was 84 ms in duration with a peak of 6.2 mV (40 ms). The P-wave represented approximately half the PR interval (156 ms). The positive QRS complex had an overall duration of 84 ms, with a maximum at 192 ms (150.4 mV) and two minima at 164 ms (-26.4 mV) and 224 ms (-34.1 mV). The ST segment was isoelectric (-8.2 mV) and 36 ms long. The duration of the T-wave was 236 ms, with a peak of 41.4 mV (408 ms). Finally, the QT interval and TP segment were both isoelectric and 120 ms and 468 ms long, respectively.

The $ECGc$ signal resembled the ECG_{input} signal turned upside down, with an inverted P wave, an rSR' wave (i.e. an inverted qRS wave) and an inverted T wave (Figure 5.3B). The overall relationship between the two signals was best approximated by a mathematical model in which the $ECGc$ signal was inversely proportional to the ECG_{input} signal (r^2=0.74, P<0.05):

Equation 5.6 $$ECGc(t) = \beta_0 - \beta_1 \cdot ECG_{input}(t),$$

where β_0 is the intercept value and β_1 is the linear regression coefficient.

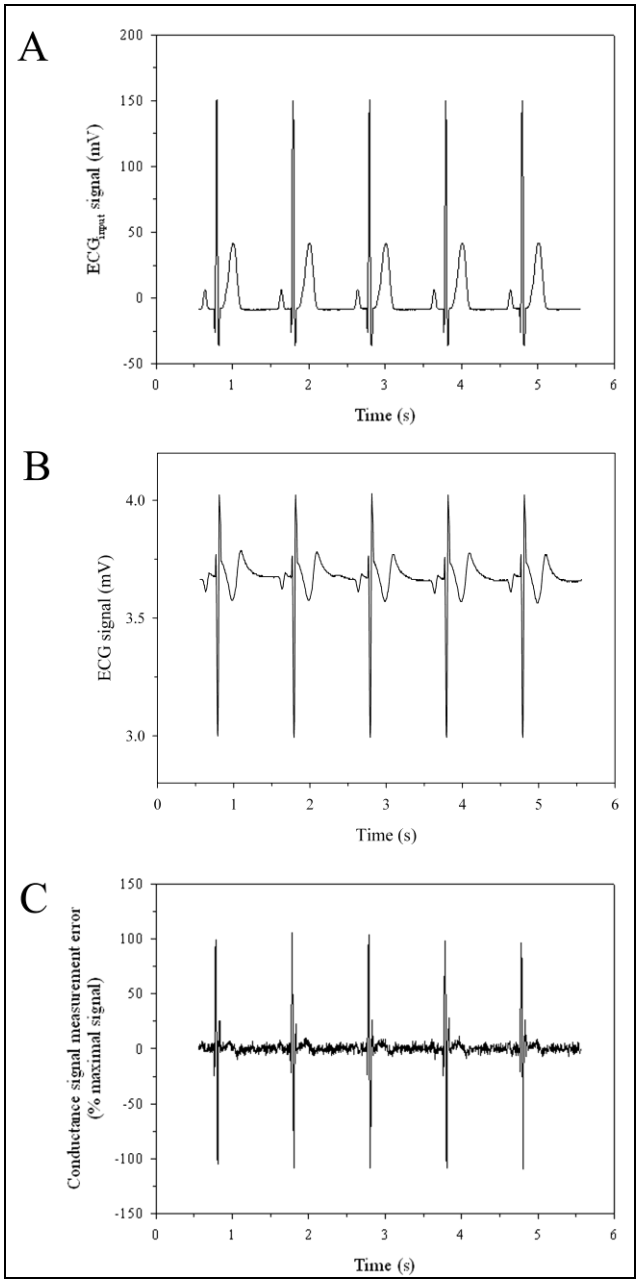

Figure 5.3 *The ECG signal (**ECG**$_{input}$; A), cavitary electrogram (**ECGc**; B) and ECG interference (**G**$_{ECG}$**(t)**; C) signals versus time.*

Although the ***ECG***$_{input}$ and ***ECGc*** signals were similar, they were not identical. There were differences in timing and amplitude of the two signals. The ***ECGc*** P and S-wave minima and the R-wave peak occurred either synchronously or within one data point (i.e. 4 ms) of the corresponding points on the ***ECG***$_{input}$ signal. By contrast, the ***ECGc*** R'-wave peak and the T-wave minimum were 12 ms and 32 ms earlier than the corresponding points on the ***ECG***$_{input}$ signal. The ***ECGc*** R'-wave peak was also disproportionately pronounced compared to the

corresponding S-wave of the ECG_{input} signal. The $ECGc$ R'-S wave ratio was -0.51 ± 0.03 whereas the ECG_{input} S-R wave ratio was -0.17 ± 0.02 (P<0.05). In addition, the $ECGc$ did not accurately reproduce the isoelectric phases of the ECG_{input} signal. During the PR, R'T and TP segments, the $ECGc$ signal was initially elevated and decreased progressively towards the baseline signal.

In the covariance analyses, the intercept value (β_0) varied as a linear function of inter-electrode distance (P<0.05), but was not affected by variation in the other two factors. By contrast, the linear regression coefficient (β_1) varied as the inverse function of intracavitary volume and as a direct function of inter-electrode distance and resistivity of the solution (all P<0.05).

When these effects are combined, the relationship between $ECGc$ and ECG_{input} was influenced by the inter-electrode distance (intercept value) and by the total resistance of the volume conductor (Equation 5.7; r^2=0.65):

Equation 5.7
$$ECGc(t) = \beta_2 + \left(\beta_3 \cdot D\right) + \left[\beta_4 \cdot \left(\frac{D \cdot \rho}{V}\right) \cdot ECG_{input}(t)\right],$$

where β_2 = 3.66 ± 0.01; β_3 = 7.29·10^{-3} ± 1.53·10^{-3} and β_4 = -7.00·10^{-3} ± 0.06·10^{-3} (P<0.05 for each coefficient).

5.3.2 Comparison between ECG interference and ECG input signals

The ECG interference signal, $G_{ECG}(t)$ was characterised by a low amplitude biphasic P-wave; a high amplitude equiphasic qRSr' complex; and a low-amplitude biphasic T-wave (Figure 5.3C). Each phase of the $G_{ECG}(t)$ signal was synchronous with the P-wave, QRS complex and T-wave of the ECG signal, respectively.

The amplitude of the $G_{ECG}(t)$ has been described as a percentage of the maximum $G_{ECG}(t)$ signal from the isoelectric line. The $G_{ECG}(t)$ P wave had a sine wave-like appearance with an initial upward deflection immediately followed by a downward deflection of comparable duration and amplitude. The maximum and minimum $G_{ECG}(t)$ P wave signals were 4.0 ± 2.6% (28 ms) above

and 4.4 ± 2.6% (64 ms) below the isoelectric line. The spiked wave $G_{ECG}(t)$ qRSr' complex had two maxima at 180 ms (R-wave; 100 ± 3%) and 232 ms (r'-wave; 22 ± 3%) and two minima at 160 ms (q-wave; -24 ± 3%) and 204 ms (S-wave; -107 ± 3%). The $G_{ECG}(t)$ q and R-waves occurred 32 ms and 12 ms before the ECG_{input} R-wave whereas the $G_{ECG}(t)$ S and r'-waves occurred 12 ms and 40 ms after the ECG_{input} R-wave. The $G_{ECG}(t)$ T wave had a similar overall appearance to the $G_{ECG}(t)$ P-wave with an initial upward deflection immediately followed by an equivalent downward deflection. The maximum and minimum $G_{ECG}(t)$ T wave signals were 4.4 ± 2.6% (352 ms) and 4.8 ± 2.6% (452 ms) below the isoelectric line and occurred 80 ms and 180 ms after the start of the ECG_{input} T wave, respectively.

The relationship between $G_{ECG}(t)$ and ECG_{input} was well approximated (r^2=0.92, P<0.05) by a regression equation in which the interference signal varied proportionally to the first-derivative of ECG_{input} with respect to time:

Equation 5.8 $$G_{ECG}(t) = \beta_0 - \beta_1 \cdot dECG_{input}(t),$$

where β_0 is the intercept value and β_1 is the linear regression coefficient.

In the covariance analyses, the intercept (β_0) values varied as a linear function of the inter-electrode distance (P<0.05), but was not affected by variation in the other two factors. By contrast, the linear regression coefficient (β_1), varied as a function of the intracavitary volume; and as the inverse function of both the inter-electrode distance and the resistivity of the solution (all P<0.05).

Overall, the relationship between $G_{ECG}(t)$ and the first derivative of ECG_{input} varied as a function of the inter-electrode distance and the conductivity of the volume conductor (Equation 9; r^2=0.88):

Equation 5.9 $$G_{ECG}(t) = \beta_0 \cdot D + \left[\beta_1 \cdot \left(\frac{V}{D \cdot \rho} \right) \cdot dECG_{input}(t) \right]$$

where $\beta_0 = 1.49 \cdot 10^{-3} \pm 0.39 \cdot 10^{-3}$ and $\beta_1 = 6.07 \cdot 10^{-3} \pm 0.38 \cdot 10^{-3}$ (P<0.05 for both coefficients).

5.3.3 ECG interference and calibrated conductance volume measurements

For the purposes of this simulation, the inter-electrode distance was assumed to change in accordance with the instantaneous volume within the latex balloon. The inter-electrode distance was estimated as the maximal short-axis diameter of the spheroid, which varied from 7.0 cm (V_{ES} = 335 ml) to 8.6 cm (V_{ED} = 500 ml). Calibrated conductance volume measurements with the ECG signal, $V_g^+(t)$ were compared against synchronous calibrated conductance volume measurements without the ECG signal, $V_g^-(t)$.

A representative example of calibrated conductance volume measurements with and without the ECG signal is illustrated in Figure 5.4. The $V_g^-(t)$ signal had a smooth, sinusoidal pattern that varied throughout the model heart cycle. The $V_g^+(t)$ signal was broadly similar, but had an additional spiked-wave pattern that coincided with the simulated ventricular depolarisation. The difference between the two ventricular volumes measurements, ΔV_{ECG} during this phase of the cardiac cycle varied between -12% (i.e. an underestimation) and +9%. By contrast, the difference during the remainder of the cardiac cycle varied only slightly from -0.3 to +0.9%.

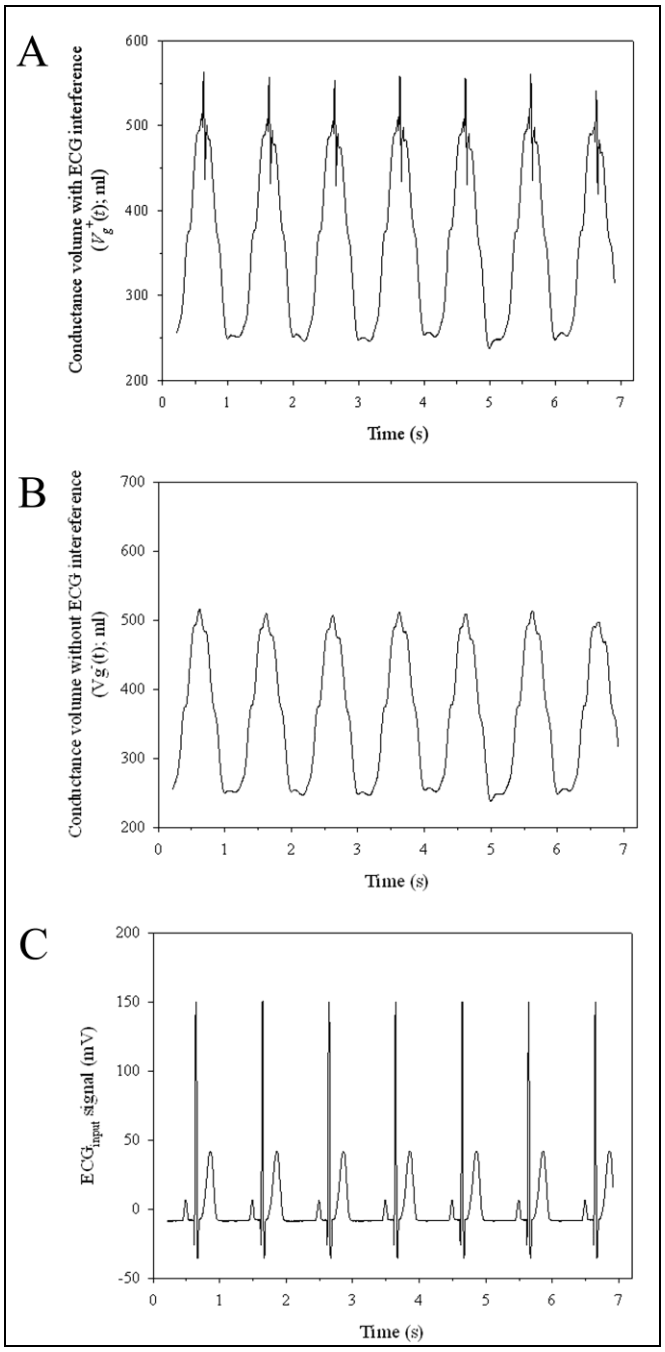

Figure 5.4 *Calibrated conductance volume measurements versus time. Conductance volume measurements were made with ($V_g^+(t)$; A) and without ECG interference ($V_g^-(t)$; B). The ECG signal (ECG_{input}) has been plotted (C) for comparison.*

The pressure-volume loop obtained with the $V_g^-(t)$ signal had a quadrilateral shape with four distinct phases (Figure 5.5). End-diastole and end-systole were each identifiable as the single pressure-volume point at the lower right-hand and upper left-hand corners, respectively. The ECG interference pattern altered the shape of the pressure-volume loop, primarily affecting the

late filling and early isovolumic contraction phases. As a result, end-diastole could not be reliably identified (Figure 5.5).

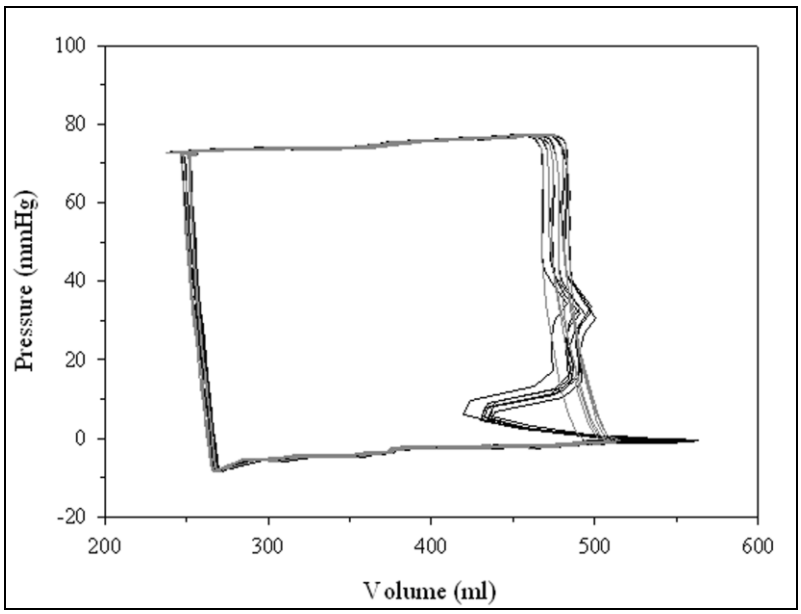

Figure 5.5 *Pressure-conductance volume loop from the model ventricle. Conductance volume measurements were made with ($V_g^+(t)$; black line) or without ECG interference ($V_g^-(t)$; grey dashed line).*

Comparable results were obtained under all experimental conditions. Increasing the end-diastolic volume from 385 ml to 500 ml did not significantly change the discrepancy between the two ventricular volume measurements. While increasing the resistivity from 37 Ω·cm to 330 Ω·cm increased the median measurement discrepancy slightly, from +0.2% to +1.8%, it did not significantly alter the maximal range of the discrepancy.

5.4 DISCUSSION

The conductance catheter technique is an established method that enables continuous volume measurements based on the electrical conductance of the intraventricular blood pool. This study has demonstrated that other electrical signals within the ventricular cavity alter the measured conductance. This produces a conductance signal "artefact", which varies as a function of the first-derivative of the additional electrical signal. This artefact represents a novel and additional source of error that potentially affects the accuracy of ventricular volume measurements made using the conductance catheter technique.

Ventricular depolarisation and repolarisation cause a measurable electrical signal within the ventricular cavity [462]. In the present study, a simulated ventricular electrogram produced a biphasic signal with a high-amplitude spiked wave pattern that coincided with the QRS complex and a comparatively low-amplitude sine wave-like pattern during the T wave. This signal was associated with a conductance volume measurement error that ranged between a 12% volume underestimation to a 9% volume overestimation. The entire range of this measurement discrepancy occurred within a 24 ms period during simulated ventricular depolarisation. By contrast, simulated repolarisation was associated with a small, clinically unimportant measurement error. The precise ECG interference pattern, $G_{ECG}(t)$ will vary with the morphology of ventricular electrogram [462-464]. Nevertheless, these in vitro findings are consistent with our previously unreported clinical findings.

The haemodynamic events during the cardiac cycle are best displayed by plotting the instantaneous left ventricular pressure versus volume [465]. Under steady-state conditions, this pressure-volume loop has a quadrilateral shape where each side represents one of four functional distinct phases: filling, isovolumic contraction, ejection and isovolumic relaxation. End-diastole and end-systole are identifiable as the single pressure-volume points in the lower right-hand and upper left-hand corners, respectively. However, ventricular depolarisation overlaps the rapid rise in intraventricular pressure that marks the onset of ventricular systole. The conductance signal artefact identified in this study meant that end-diastole could no longer be reliably identified on the pressure-conductance volume loop alone.

End-diastole may alternatively be defined using the surface electrocardiogram as the onset of the QRS complex [466]; the R-wave peak [434]; or up to 40 ms after the R wave peak [467]. End-diastole may also be defined as the R-wave peak on the ventricular electrogram. In our experience, this time-point occurs synchronously with the onset of ventricular systole [468]. However, conductance volume measurements at all of these time-points will be variably affected by the conductance signal artefact such that end-diastolic volume cannot be accurately measured using the conductance catheter technique. This in turn means that indices of ventricular function

that are based on EDV, such as cardiac output, ejection fraction together with the quantitative assessment of ventricular compliance, will be adversely affected as a consequence of the conductance signal artefact.

5.4.1 Study Limitations

The limitations of the physical model have been described in Chapter 4. Electrical activity within the ventricle was represented using a fixed dipole within the ventricular cavity. This comparatively simple model enabled characterisation and quantification of a new conductance measurement error. However, the model did not include any representation of the ventricular wall and the effect of parallel conductance was not examined. A moving dipole or multiple dipoles within an artificial ventricular wall would also have provided a more physiological model.

5.5 CONCLUSION

This study has demonstrated that the accuracy of these conductance volume measurements is adversely affected by other electrical signals, such as the ventricular electrogram. The ventricular electrogram produced a clinically important volume measurement that meant end-diastole could neither be precisely identified nor accurately measured. These original findings have potentially important implications for the quantitative assessment of ventricular function and, in particular the assessment of chamber compliance made using the conductance catheter.

Despite this problem, the combined pressure-conductance catheter represents the only technique that is approved for clinical research that allows simultaneous, real-time measurements of ventricular pressure and volume and so remains one of the most powerful tools for the quantitative assessment of ventricular function. For this reason, the pressure-conductance catheter were used to evaluate changes in ventricular function and vascular load in the clinical studies described in Chapters 6 and 7.

CHAPTER 6

ACUTE CHANGES IN VENTRICULAR PERFORMANCE FOLLOWING BIDIRECTIONAL CAVO-PULMONARY ANASTOMOSIS

CHAPTER 6. ACUTE CHANGES IN VENTRICULAR PERFORMANCE FOLLOWING BIDIRECTIONAL CAVO-PULMONARY ANASTOMOSIS

6.1 INTRODUCTION

The bidirectional cavo-pulmonary anastomosis (BCPA) represents the second stage in the three-stage management plan for children with functionally single ventricle anatomy [292]. The BCPA can be constructed as either a bidirectional Glenn or hemi-Fontan procedure [296,297], as described in Chapter 2. Both of these procedures establish a circulation in which the pulmonary circulation is connected in-series with the systemic circulation of the upper half of the body, as illustrated in Figure 6.1.

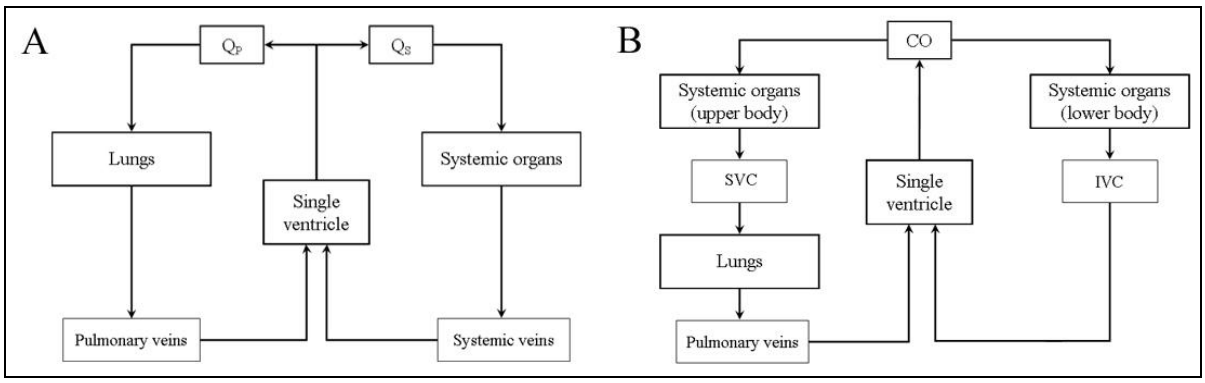

Figure 6.1 *Schematic diagram of the circulation (A) with a balanced in-parallel circulation and (B) following the formation of the BCPA.*
Q_P*, pulmonary blood flow;* Q_S*, systemic blood flow;* CO*, cardiac output.*

The circulation established following the BCPA is associated with a number of theoretical and clinical advantages when compared with a balanced in-parallel circulation. The formation of the BCPA improves the efficiency of gas exchange, by directing desaturated blood in the superior vena cava (SVC) exclusively through the pulmonary circulation. The relative contribution of the SVC to systemic venous return [276] means that the "effective" pulmonary blood flow is generally increased, with a corresponding rise in the systemic arterial oxygen saturation [271,469-471].

The formation of the BCPA is also accompanied by an immediate and persistent reduction in the volume load of the dominant ventricle [342,472-477]. This, in turn, is associated with a change in the geometry of the ventricle and a temporary increase in the ventricular mass-volume ratio [342,474,475].

The changes in circulatory haemodynamics and ventricular geometry may both influence the function of the dominant ventricle. For example, it has been suggested that the reduction in volume load and the development of a more ellipsoid ventricular shape may provide more favourable working conditions for the ventricle, and this should be accompanied by an improvement in ventricular systolic function [338]. By contrast, an increase in the mass-volume ratio may result in the development of diastolic dysfunction, with impaired active ventricular relaxation and reduced ventricular compliance [345-347].

To date, only a limited number of studies have been undertaken to assess how the changes in circulatory haemodynamics affect either ventricular function or the performance of the cardiovascular system as a whole [351,478,479]. The most important of these studies reported longitudinal changes in ventricular function and vascular load in patients with hypoplastic left heart syndrome and the effects of surgical palliation [351]. Ventricular function and vascular load were analysed using pressure-volume data acquired during routine pre-operative and post-operative cardiac catheterisation. Tanoue *et al.* identified that the BCPA was associated with a significant improvement in ventricular systolic function those patients that underwent initial palliation with a Norwood procedure and systemic-pulmonary arterial shunt (Figure 6.2)[351]. The data presented also suggested that there may be an improvement in ventricular efficiency in these patients, although this change was not statistically significant.

The study reported by Tanoue *et al.* is associated with certain important limitations. Firstly, the measurements were made during routine pre-operative cardiac catheterisation before the bidirectional Glenn and Fontan procedures, respectively. The mean time period between these two procedures was 22.4 months. It is unclear whether the haemodynamic changes reflect the effect of the surgical procedure; adaptation to the altered circulatory haemodynamics; age or a

combination of all three effects. Secondly, the study used an approximation of end-systolic elastance and arterial elastance that has only been validated in an animal model. The more general relevance of these techniques, particularly in the assessment of children with severe forms of congenital heart disease, has not been proven. Thirdly and finally, Tanoue *et al.* could not evaluate changes in diastolic function, which may be abnormal especially during the early post-operative period [478].

The present study was undertaken to quantitatively determine the effect of the formation of the BCPA on changes in volume and pressure loading characteristics and ventricular systolic and diastolic function during the immediate post-operative period. In addition, this study aimed to investigate whether the relative changes in ventricular function were influenced by the morphology of the dominant ventricle.

6.2 MATERIALS AND METHODS

Sixteen patients undergoing elective BCPA at the Diana Princess of Wales Children's Hospital, Birmingham between May 2003 and April 2005 were recruited to this study. All patients had functionally single ventricle anatomy with a dominant ventricle of left or right ventricular morphology. Children with a single ventricle of indeterminate ventricular morphology were not considered for this study. Children with clinically significant (i.e. ≥ moderate) systemic atrio-ventricular valve regurgitation, as determined by preoperative echocardiography, were also not considered for this study. A summary of the children involved in this study is provided in Table 6.1.

Written informed consent was obtained from the parents of each child and the study protocol was approved by the Local Research Ethics Committee (LREC 2002/0808).

Patient	Anatomy	Ventricular morphology	Gender	Initial palliation	Age at BCPA (m)	BCPA procedure	Concurrent procedures
1	uAVSD, sub-AS	mRV	Female	Norwood procedure (RMBTS)	5.6	Bilateral BDG	CPA patch augmentation
2	HLHS	mRV	Male	Norwood procedure (RV-PA)	5.1	Bilateral BDG	
3	TA, TGA, restrictive VSD, arch hypoplasia	mLV	Male	Norwood procedure (RMBTS)	5.7	BDG	
4	PAt- IVS	mLV	Female	RMBTS	18.1	BDG	Relief of RVOTO
5	HLHS	mRV	Female	Norwood procedure (RV-PA)	4.0	BDG	
6	HLHS	mRV	Female	Norwood procedure (RV-PA)	4.0	BDG	CPA patch augmentation
7	HLHS	mRV	Male	Norwood procedure (RV-PA)	4.1	BDG	CPA patch augmentation
8	HLHS	mRV	Male	Norwood procedure (RV-PA)	3.7	BDG	CPA patch augmentation
9	TA, PAt	mLV	Female	RMBTS	7.4	BDG	Atrial septectomy
10	HLHS	mRV	Female	Norwood procedure (RV-PA)	6.5	BDG	CPA patch augmentation
11	HLHS	mRV	Male	Norwood procedure (RV-PA)	4.3	BDG	CPA patch augmentation
12	HLHS	mRV	Male	Norwood procedure (RV-PA)	5.2	BDG	CPA patch augmentation
13	TA, VSD, PS	mLV	Male	N/A	20.2	BDG	Atrial septectomy
14	HLHS	mRV	Female	Norwood procedure (RV-PA)	6.5	BDG	CPA patch augmentation
15	PAt-IVS	mLV	Male	RMBTS	21.0	BDG	
16	DILV, TGA, arch hypoplasia	mLV	Male	Norwood procedure (RMBTS)	5.2	BDG	CPA patch augmentation

Table 6.1 *Summary of patients undergoing BCPA.*

AS, aortic stenosis; BDG, bidirectional Glenn; CPA; central pulmonary arteries; DILV, double inlet left ventricle; HLHS, hypoplastic left heart syndrome; mLV, morphologic left ventricle; mRV, morphologic right ventricle; PA, pulmonary atresia; PAt-IVS, pulmonary atresia with intact ventricular septum; PS, pulmonary stenosis; RMBTS, right modified Blalock-Taussig shunt; RVOTO, right ventricular outflow tract obstruction; RV-PA, right ventricle to pulmonary artery conduit; TA, tricuspid atresia; TGA, transposition of the great arteries; uAVSD, unbalanced atrio-ventricular septal defect; VSD, ventricular septal defect

6.2.1 Pre-operative diagnosis

The study included nine male and seven female children. All of the children had functionally single ventricle anatomy with a dominant ventricle of either left (n=6) or right ventricular morphology (n=10). The single most common primary cardiac malformation was hypoplastic left heart syndrome (HLHS; n=9). Amongst the other children, the primary cardiac malformation was tricuspid atresia (n=3); pulmonary atresia with intact ventricular septum (n=2); double-inlet left ventricle (n=1); or an unbalanced atrioventricular septal defect (uAVSD) with a dominant ventricle of right ventricular morphology (n=1). Two children had bilateral superior vena cavae, in which the left-sided SVC opened into the roof of the left atrium. In addition, one child had a known chromosomal abnormality with 45, XO / 47, XXX mosaicism.

6.2.2 Initial surgical palliation

Fifteen of the sixteen children had previously undergone surgical palliation to establish a balanced circulation with the systemic and pulmonary circulations in parallel with one another (Table 6.1). Initial surgical palliation consisted of either a Norwood stage I procedure (n=12) or a modified Blalock-Taussig (BT) shunt (n=3). Pulmonary blood flow in the Norwood procedure was established using either a modified BT shunt (n=3) or a right ventricle-pulmonary artery (RV-PA) shunt (n=9), as illustrated in Figure 6.2 [480,481]. Initial surgical palliation was performed at a median age of 4 days (range, 2 – 17 days).

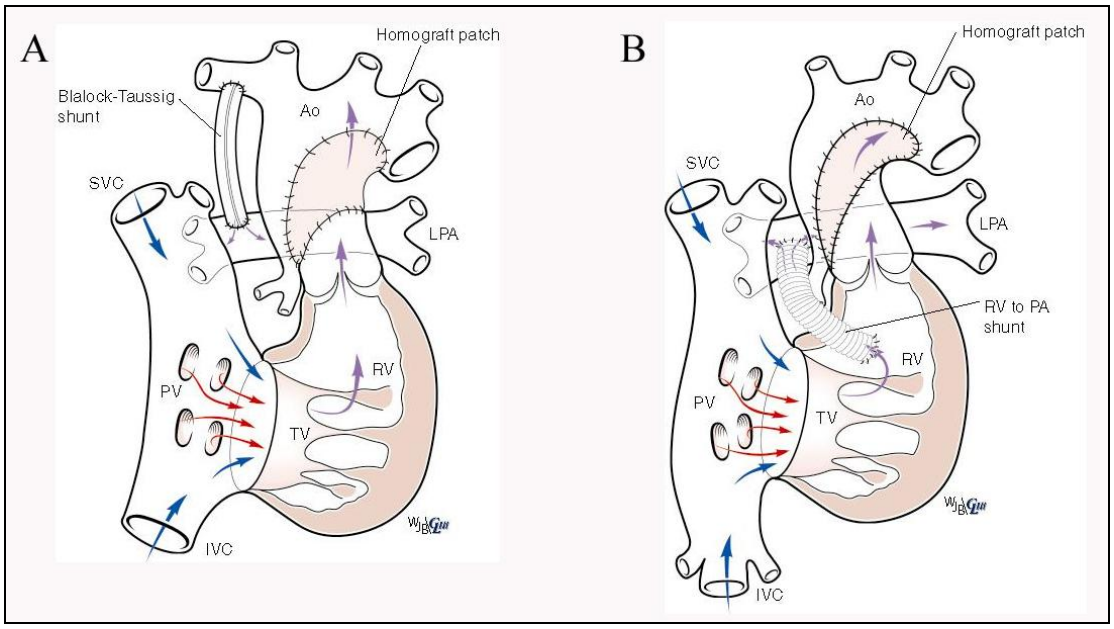

Figure 6.2 *Diagrammatic illustration of the Norwood procedure with a right-sided modified BT shunt* (A) *or RV-PA conduit* (B)*. These procedures represent the usual first-stage palliation for children with HLHS. Reproduced from Brawn & Barron* [482].

6.2.3 Assessment prior to bidirectional cavo-pulmonary anastomosis

Cardiovascular function was routinely assessed using trans-thoracic echocardiography and elective cardiac catheterisation prior to the BCPA [480,483]. Ventricular and valvular function was qualitatively assessed using echocardiography, as previously described [368]. All the children in the present study had good ventricular function. Twelve children had none or trivial atrio-ventricular valve (AVV) regurgitation while the remaining three children had mild AVV regurgitation. None of the children had aortic or neo-aortic valve regurgitation.

Cardiac catheterisation was electively performed under general anaesthesia at a median age of 4.1 months (range, 2.8 – 12.1 months). Haemodynamic and angiographic studies were performed in all children [480]. The pulmonary-systemic flow ratio ($\dot{Q}p/\dot{Q}s$) was retrospectively calculated using the modified Fick principle (Equation 6.1). The pulmonary arterial saturation ($SpaO_2$) was assumed to be identical to the systemic arterial saturation (SaO_2; i.e. complete mixing occurred within the ventricle) and the pulmonary venous saturation ($SpvO_2$) was assumed to be 98% [341].

Equation 6.1 $$\dot{Q}p/\dot{Q}s = (SaO_2 - SsvO_2)/(SpvO_2 - SpaO_2),$$

where $SsvO_2$ is systemic venous saturation, as measured in the superior or inferior vena cava.

Under general anaesthesia, the median ventricular end-diastolic pressure was 9 mmHg (range, 0 – 13 mmHg). The median $\dot{Q}p/\dot{Q}s$ was 1.0 (range, 0.4 – 2.1). Preoperative cardiac catheterisation identified nine children (56%) that had clinically important abnormalities of the central pulmonary arteries. This included seven patients with discrete central pulmonary arterial stenoses and two patients with relatively small branch pulmonary arteries.

Five patients required cardiological intervention at the time of the cardiac catheterisation. This involved an atrial balloon septostomy (n=2), balloon dilatation of neo-aortic arch obstruction (n=2) or coil embolisation of a systemic – pulmonary arterial collateral vessel (n=1).

6.2.4 Formation of bidirectional cavo-pulmonary anastomosis

The surgical procedures described in this study were all performed by one of two paediatric cardiac surgeons (Mr WJ Brawn and Mr DJ Barron).

6.2.4*a* *Intraoperative anaesthesia*

The anaesthetic technique was tailored according to the pre-procedure evaluation of cardiovascular function and the individual preference of the paediatric cardiac anaesthetist. In general, patients were pre-medicated with oral midazolam (0.5 $mg \cdot kg^{-1}$) approximately 30 minutes prior to surgery. Baseline monitoring was instituted following arrival in the anaesthetic room. This included peripheral pulse oximetry, non-invasive blood pressure measurement and a 3-lead electrocardiogram.

Anaesthesia was induced using either inhalational or intravenous techniques. In patients with stable ventricular function, inhaled sevoflurane (0 - 6%) in an air and oxygen carrier was used. In patients with limited haemodynamic reserve, intravenous ketamine (1 – 2 $mg \cdot kg^{-1}$) and fentanyl were given. A bolus of intravenous rocuronium (0.75 – 1.0 $mg \cdot kg^{-1}$) was given to facilitate orotracheal intubation. The tracheal tube was sized to minimise gas leak at an inflation pressure of 20 cmH_2O. Anaesthesia was maintained with inhaled

isoflurane (exhaled concentration 0 – 0.2%), intravenous fentanyl during the pre-cardiopulmonary bypass phase (up to a total dose of 50 $\mu g \cdot kg^{-1}$) and intravenous morphine (20 – 40 $\mu g \cdot kg^{-1}$) during the re-warming and post-bypass phases. Neuromuscular blockade was maintained with an infusion of rocuronium
(0.75 - 1 $mg \cdot kg^{-1} \cdot hr^{-1}$).

Following intubation, the patient was mechanically ventilated using a ventilator (Datex Ohmeda 7900; GE Healthcare Worldwide, Chalfont St Giles, UK) in pressure-control mode to achieve an expired tidal volume of 10 $ml \cdot kg^{-1}$, as measured by the ventilator. This was connected to the endotracheal tube via a heat and moisture exchanger. The inspired oxygen concentration (FiO_2 = 0.35 – 0.60) and ventilatory settings were adjusted to maintain acceptable peripheral oxygen saturations (SaO_2, 75 – 90%) and $PaCO_2$ between 4 - 5.5 kPa (i.e. normocarbia). Positive end expiratory pressure was used to a maximum of 5 cmH_2O, if required.

After anaesthesia was established, a 22 – 24G arterial cannula was inserted, ideally in the radial artery. A 4.5-French triple-lumen central venous catheter was inserted into the common femoral vein. An additional, 20 – 22G single-lumen central venous catheter was also inserted into the internal jugular vein. Nasopharyngeal and oesophageal temperature probes were inserted, a skin temperature probe was attached and the urinary bladder was catheterised. The ECG, peripheral oxygen saturations, arterial and central venous pressures, core and skin temperature, end-tidal CO_2 and isoflurane concentrations and inspired oxygen tension were monitored continuously. Urine output and arterial blood gases were also measured intermittently.

6.2.4*b* *Cardiopulmonary bypass management*

Cardiopulmonary bypass (CPB) is a technique that provides partial or complete circulatory and respiratory support. During cardiopulmonary bypass, the circulation bypasses the heart and lungs allowing the surgeon to operate in a bloodless surgical field. The patient's systemic venous return is diverted into the venous reservoir of the heart-lung machine via cannulae placed in the superior and inferior vena cavae or a single cannula placed in the right atrium. Blood from the venous reservoir is then mechanically pumped through a membrane oxygenator into the systemic arterial system, usually through a cannula in the ascending aorta (Figure 5.3).

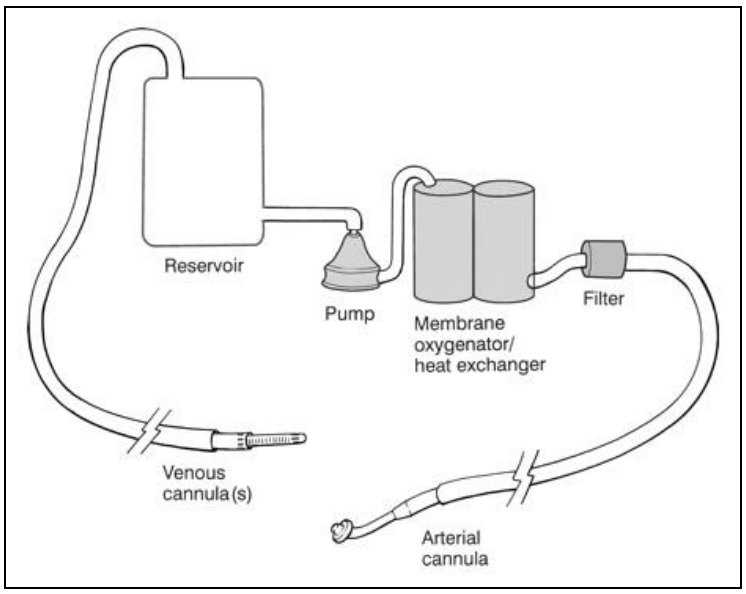

Figure 6.3 *Basic cardiopulmonary bypass circuit with membrane oxygenator and centrifugal pump. Reproduced from Cohn, pp. 350.*[484].

The BCPA was performed using deep hypothermic CPB with periods of circulatory arrest. The heart-lung machine (Sarns 8000; Terumo Europe NV, Leuven, Belgium) incorporates an occlusive roller pump, which was used to generate non-pulsatile blood flow at 2.4 $L \cdot min^{-1} \cdot m^{-2}$ [485].

The CPB circuit was primed with fluid before surgery. A 'blood prime' was used for all the children involved in this study. This consisted of isotonic electrolyte solution to which allogeneic red blood cells and fresh frozen plasma were added`[486].

Patients were fully heparinised prior to start of CPB. Patients received an initial loading dose of 300 IU·kg^{-1} heparin sodium and cardio-pulmonary bypass was started when the activated clotting time (ACT) was >300 seconds. The ACT was regularly measured during cardio-pulmonary bypass and additional heparin was administered to maintain adequate anticoagulation.

Cardio-pulmonary bypass was performed by one of two clinical perfusion scientists (Mr RG Willetts or Mrs A Horsburgh). Following the start of CPB, the patient was actively cooled to a core temperature of 18°C using an alpha-stat (temperature-uncorrected) acid-base management strategy. The mean arterial pressure was maintained between 30 – 50 mmHg by adjusting the pump flow and the administration of boluses of metaraminol or a phenylephrine infusion as required. The PaO_2, $PaCO_2$ and acid-base balance were maintained within the normal physiological range [Department of Clinical Chemistry, Birmingham Children's Hospital]. The PaO_2 and $PaCO_2$ were controlled by altering the oxygen concentration and flow rate of the ventilating gases in the oxygenator, respectively. Metabolic acidosis was corrected with boluses of sodium bicarbonate. Boluses of calcium chloride and potassium chloride were also given, as clinically indicated. The haematocrit was ideally maintained at greater than 21%. Allogeneic red blood cells were added to the perfusion circuit if the haemoglobin concentration fell below 6 g·dl^{-1}.

Short periods of reduced flow or circulatory arrest were used in order to facilitate surgical exposure. The procedure was generally performed without cross-clamping the aorta. However, the aorta was cross-clamped in patients that required concomitant intracardiac procedures. During which time myocardial protection was afforded by intermittent cold crystalloid cardioplegia (30 ml·kg^{-1}) administered into the aortic root.

At the end of the procedure, the patient was actively re-warmed to achieve normothermia (37°C, measured using the core temperature probes). Modified ultrafiltration is not standard practice at Birmingham Children's Hospital and was not used in any of the study patients. After successful separation from cardio-pulmonary bypass, protamine sulphate was administered in an adequate dose to return both the ACT to its baseline value (or less). Remaining blood in the perfusion

circuit was processed using a cell saver machine (Dideco Electa; Sorin Group, Milan, Italy) and re-transfused during the early post-operative period.

In this study, the median CPB time was 53 minutes (range, 40 – 73 minutes). All patients except one required a period of deep hypothermic circulatory arrest with a median duration of 24 minutes (range, 3 – 47 minutes). Three patients underwent concomitant intracardiac procedures. The aortic cross clamp time for these cases was 6, 23 and 43 minutes, respectively.

6.2.4*c* *Operative technique*

The BCPA was performed at a median age of 5.3 months (range, 3.7 - 21 months) and a median weight of 6.5 kg (range, 4.9 – 13.2 kg). At Birmingham Children's Hospital, the BCPA was constructed using a bidirectional Glenn procedure. This involved the formation of an end-to-side anastomosis between the right-sided SVC and the upper border of the right pulmonary artery (Figure 6.4). As a result, systemic venous blood in the SVC can flow freely into both the left and the right pulmonary arteries.

The BCPA was performed via a redo median sternotomy. Following take down of adhesions and mobilisation of the great vessels, the child was placed on CPB. The pulmonary blood flow was then controlled. In patients with a modified BT or RV-PA shunt, the shunt was ligated between two ties and divided. The distal end of the shunt was disconnected from the pulmonary artery. In patients with antegrade pulmonary blood flow through the native pulmonary artery, the main pulmonary artery was temporarily occluded using a vascular clamp. The azygos vein was then ligated.

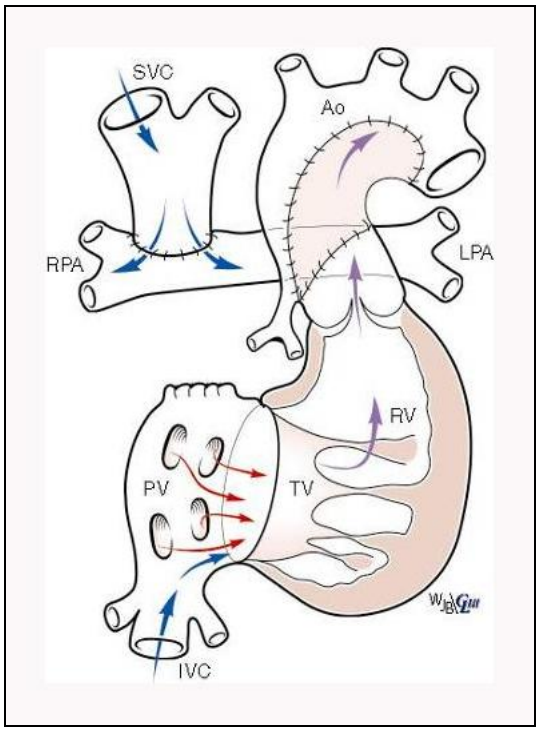

Figure 6.4 *Diagram illustrating the bidirectional Glenn procedure. This involves a superior cavo-pulmonary anastomosis so that blood in the SVC flows directly into the pulmonary arteries. Deoxygenated blood in the IVC continues to flow into the right atrium. Reproduced from Brawn & Barron* [482].

The SVC was divided immediately proximal to SVC-right atrial junction. The distal end of the SVC was oversewn. During a period of circulatory arrest, the distal end of the previous shunt was excised and the proximal end of the SVC was then anastomosed to a longitudinal incision in the superior margin on the right pulmonary artery. In patients with bilateral superior vena cavae (n=2), bilateral bidirectional Glenn procedures were constructed. The left-sided SVC was divided immediately proximal to SVC-left atrial junction and the distal end of the left SVC was oversewn. This proximal end of the left SVC was anastomosed to a longitudinal incision in the upper border of the left pulmonary artery.

Concomitant surgical procedures were performed in 12 patients (Table 5.1). This primarily involved pulmonary artery patch augmentation of the central pulmonary arteries (n=9) with a pulmonary artery patch. Two patients had a potentially restrictive atrial septal defect and underwent atrial septectomy and one other patient required relief of right ventricular outflow tract obstruction (Table 6.1).

Cardiopulmonary bypass was reinstituted and the heart de-aired once the BCPA was constructed. When the patient was warm and haemodynamically stable, CPB was weaned and discontinued.

In patients with antegrade pulmonary blood flow through the native pulmonary artery, the effect of this additional pulmonary blood flow was estimated at the end of the procedure. Haemodynamic measurements were made with the main pulmonary artery clamped and unclamped. The additional source of pulmonary blood flow might be left in place if it did not cause a significant fall in the systemic blood pressure (<10 mmHg fall in systolic arterial blood pressure), a high pulmonary artery pressure (CVP ≥15mmHg) or excessive peripheral arterial saturations (SaO_2 ≥90%). In this study, two patients had antegrade pulmonary blood flow through the native pulmonary valve. In both cases, the surgeon chose to allow continued antegrade blood flow at the end of the procedure.

An mediastinal drain was placed beneath the sternum and a GORE-TEX® membrane (W.L. Gore & Associates (UK) Ltd., Livingston, Scotland) was attached to the pericardial edges. The sternotomy was formally closed in all patients prior to transfer to the intensive care unit. Patients were routinely transferred on a dobutamine infusion (5 - 10 $\mu g \cdot kg^{-1} \cdot min^{-1}$). Additional inotropic and vasodilator therapy was administered as clinically indicated.

6.2.4*d* *Post-operative care*

Following the BCPA, all patients were recommenced on oral diuretic therapy. Patients with impaired ventricular function or clinically important systemic AVV regurgitation also received an angiotensin converting enzyme inhibitor (Captopril). Patients that underwent either a bilateral bidirectional Glenn procedure or pulmonary artery patch augmentation were also discharged from hospital on aspirin (5 $mg \cdot kg^{-1} \cdot day^{-1}$).

6.2.5 Experimental protocol

This study was designed in conjunction with normal clinical practice, as described in the preceding section. Following median sternotomy and systemic heparinisation, a nylon tape was placed around the IVC. This tape could be used to temporarily reduce ventricular preload as part of the study protocol.

6.2.5*a* *Instrumentation*

Simultaneous intraventricular pressure and volume measurements were made using a custom-made 3F integrated pressure-conductance catheter (SCD-484; Millar Instruments, Houston, TX, USA). The catheter, together with the details of the pressure-conductance measurements have been described in Chapter 3.

A purse-string suture was placed in the right atrium. The conductance catheter was inserted into the right atrium through this suture via a 4F sheath (Cordis, Roden, The Netherlands). The catheter was then passed across the atrio-ventricular valve into the dominant ventricle. The position of the catheter in the ventricle was confirmed by visual inspection of the segmental conductance volume signals. Atrial volume signals are easy to distinguish from a ventricular signals because they have a low amplitude and are out-of-phase with the ventricular volume signals. Measurements were only acquired if 4 or more segmental ventricular volume signals were obtained (Figure 6.5).

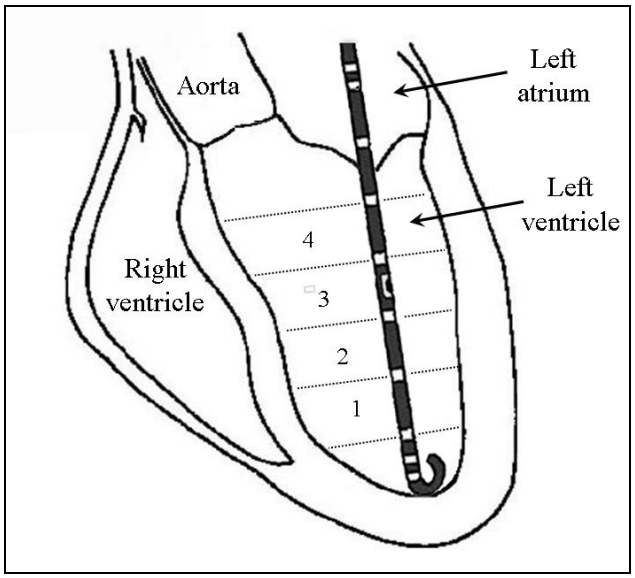

Figure 6.5 *Diagram illustrating the position of the pressure-conductance catheter when inserted into the left ventricle via the left atrio-ventricular valve. Four intra-ventricular segments are illustrated. Adapted from Steendijk et al.* [114].

The pressure signal from the pressure-conductance catheter was amplified using a combined amplifier-interface unit (PCU-2000; Millar Instruments) connected to the signal processor unit (CFL-512; CD Leycom). Micromanometer pressure measurements were statically zeroed in a bath of normal saline at the level of the mid-axillary line.

Aortic flow was measured continuously with a transit-time ultrasound flow meter (HT 323; Transonic Systems Europe B.V.) connected to a perivascular flow probe (A-series flow probes; Transonic Systems Europe B.V.) that was positioned around the ascending aorta. Stroke volume was calculated from the integrated aortic flow signal.

The signal outputs from the combined amplifier-interface unit (intraventricular pressure), the transit-time ultrasound flow meter (aortic flow) and the lead II surface ECG were each connected to the CFL-512 to allow simultaneous recordings.

6.2.5*b* *Data acquisition*

The study protocol included three separate sets of measurements. Measurements were made:

- Prior to the institution of CPB without inotropic support ("*Baseline*");
- Prior to the institution of CPB following the administration of dobutamine (10 $\mu g \cdot kg^{-1} \cdot min^{-1}$) for 10 minutes ("*Baseline + dobutamine*");
- Following completion of the surgical procedure, complete re-warming and weaning from cardio-pulmonary bypass support on 10 $\mu g \cdot kg^{-1} \cdot min^{-1}$ dobutamine ("*BCPA*").

This protocol allowed the effects of dobutamine on the in-parallel circulation and the formation of the BCPA to be separately quantified.

Intraventricular pressure and volume; aortic pressure and flow; and ECG measurements were made under both steady-state conditions and during transient (5 – 10s) inferior vena caval occlusion (IVCO). All measurements were made with the chest open at end-expiration.

Absolute time-varying ventricular volume measurements, $V(t)$ were obtained from the segmental conductance signals using Equation 6.2. This equation takes into account the inter-electrode distance on the catheter, L and the specific resistivity of blood, ρ [381].

Equation 6.2
$$V(t) = \frac{1}{\alpha} \cdot L^2 \cdot \left(\sum_{i=1}^{5} G_i \right) - G_P ,$$

where α is the dimensionless calibration coefficient and G_P is parallel conductance.

The specific resistivity of 5ml of blood, ρ was measured immediately before and after CPB using a special 4-electrode cuvette connected to the CFL-512 (CD Leycom).

The changes in the specific resistivity of blood are summarised in Table 5.2. The statistical analyses used in such comparisons are described more fully later (Section 6.2.6). Nevertheless, it is sufficient to note that the specific resistivity of blood, ρ decreased significantly after CPB. This primarily reflects the haemodilution that occurred during CPB, with a fall in the haemoglobin concentration and haematocrit (Table 6.2).

Variable	Baseline	BCPA
Specific blood resistivity, ρ	178 ± 24	128 ± 11 *
Parallel conductance, G_P (ml)	8.8 ± 2.9	7.5 ± 2.5
Calibration coefficient, α	0.37 ± 0.33	0.47 ± 0.39
Haemoglobin ($g \cdot dl^{-1}$)	13.8 ± 1.3	11.6 ± 1.6 *
Haematocrit (%)	41 ± 4	34± 5 *

Table 6.2. *Conductance catheter calibration factors, haemoglobin and haematocrit at Baseline and following BCPA. Data expressed as mean ± SD.*

* *$P<0.05$ versus Baseline as assessed by a paired two-tail Student t-test.*

Conductance volume measurements were retrospectively calibrated for the dimensionless calibration coefficient, α and parallel conductance, G_P. The dimensionless calibration coefficient, α was calculated by dividing the average conductance-derived stroke volume ($\overline{Q}_{SV}$) by the average stroke volume ($\overline{SV}_{AoF}$) calculated from the integrated aortic flow measurements under steady-state conditions.

In patients with antegrade pulmonary blood flow through the native pulmonary valve (n=2) or a RV-PA shunt (n=9), the measured aortic blood flow represents blood flow into the systemic circulation only. In these cases, the combined ventricular output (i.e. $\dot{Q}p + \dot{Q}s$) [487] was estimated using Equation 6.3.

Equation 6.3 $$\dot{Q}s + \dot{Q}p = Qs + \left(\dot{Q}p/\dot{Q}s\right)\overline{Qs},$$

where $\dot{Q}s$ is the measured aortic blood flow and $\dot{Q}p/\dot{Q}s$ is the pulmonary-systemic flow ratio measured during the preoperative cardiac catheterisation.

It was assumed that $\dot{Q}p/\dot{Q}s$ did not alter substantially in the interval between the cardiac catheterisation and surgery and was not changed by the administration of dobutamine. Postoperative measurements were all made without any antegrade pulmonary blood flow. In the two patients with persistent antegrade pulmonary blood flow, the native pulmonary artery was occluded during the period when study measurements were made.

Parallel conductance, G_P was calculated using the hypertonic saline method originally described by Baan *et al.* [381], which is discussed in detail in Chapter 3. In this study, parallel conductance was separately calculated following the injection of 0.25 $ml \cdot kg^{-1}$ and 0.5 $ml \cdot kg^{-1}$ 10% hypertonic saline into the SVC. Parallel conductance was measured before CPB and following CPB. These measurements were also made during end-expiration. It was assumed that parallel conductance was not altered by the administration of dobutamine.

6.2.5*c* *Technical considerations*

Complete pressure-volume measurements were acquired at all three time-points in 15 patients. These patients represent the study group. No data was obtained in the other patient (Patient number 5) because the pressure-conductance catheter fractured following insertion into the ventricle. The fracture occurred immediately distal to the micromanometer, although the distal end was still connected to the remainder of the catheter by one of the wires within the catheter. The catheter was removed intact and returned to the manufacturer, who notified the US Food and Drug Administration. This malfunction appeared to have occurred because of a manufacturing error.

Application of the caval tourniquet and introduction of the vascular sheath were uncomplicated. We had originally intended to introduce the pressure-conductance catheter into the dominant ventricle through the aortic valve. However, this could not be accomplished safely. Therefore, the conductance catheter was introduced into the dominant ventricle via the right atrium even though this may potentially reduce the proportion of the ventricular cavity that was investigated [488]. Insertion of the pressure-conductance catheter was safely performed in all patients using this approach. Occasionally, placement of the catheter caused ventricular extrasystolic beats, but a stable catheter position without arrhythmias could always be obtained.

After the second set of measurements (i.e. Baseline + dobutamine), the conductance catheter was withdrawn, rinsed with normal saline and left in a bowl of normal saline to be re-used after completion of the BCPA. The introducer sheath in the right atrium was removed during surgery and the incision temporarily closed with the purse-string suture. Catheter placement and all measurements were completed within approximately 30 minutes.

5.2.5*d* *Data analysis*

Baseline haemodynamic data were calculated from steady-state intraventricular pressure-volume measurements. These included: heart rate (***HR***), end-systolic volume (***ESV***), end-diastolic volume (***EDV***), end-systolic pressure (P_{ES}), end-diastolic pressure (P_{ED}), cardiac output (***CO***), stroke volume (***SV***), stroke work (***SW***), maximal and minimal rate of ventricular pressure change (dP/dt_{MAX}, dP/dt_{MIN}), ejection fraction (***EF***) and the relaxation time constant (tau). Volume measurements have been normalised to the body surface area (BSA) using the method proposed by DuBois & DuBois [485]. The volume measurements are expressed as indexed volumes.

End-systole was defined as the period during ejection where time-varying elastance was maximal [45]. This corresponds with the upper left-hand corner of the pressure volume loop (Figure 6.6). End-diastole was defined as the peak R-wave of the surface ECG [434]. However, all of the ventricular volumes in this study were characterised by an interference pattern that related to the intraventricular ECG signal, as discussed in Chapter 5. In the patients included in this study, the ECG interference pattern was associated with an end-diastolic volume overestimate of 11 ± 31%.

For the purposes of this study, end-diastolic volume was approximated as the ventricular volume at dP/dt_{MAX} (*EDV'*). *EDV'* always occurred before the onset of ejection (defined as the start of antegrade blood in the ascending aorta). In the absence of any AVV regurgitation, *EDV'* was assumed equivalent to the true ***EDV***.

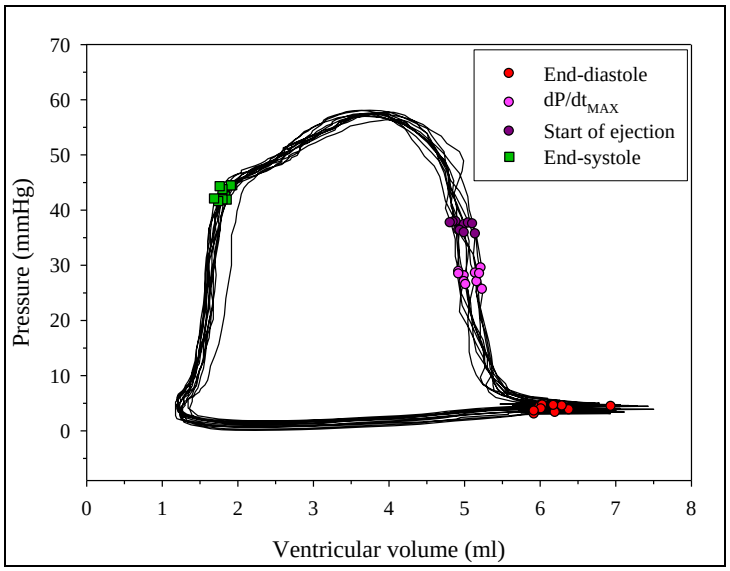

Figure 6.6 *Representative example of the intraventricular pressure-volume loop from a Baseline study. Points corresponding to end-diastole (red circles), dP/dt_{MAX} (pink circles); the start of ejection (purple circles) and end-systole (green squares) for each beat are illustrated.*

End-diastolic volume was also calculated as a percentage of the normal left ventricular or right ventricular volume (*%N-EDV*). Normal values for EDV were derived from the normal right ventricular and left ventricular EDV expressed as a function of body surface area in children with normal hearts, as reported by Nakazawa *et al.* [489] (Equations 6.4 and 6.5).

Equation 6.4 $$LVEDV = 72.5 \cdot BSA^{1.43},$$

where *LVEDV* = left ventricular end-diastolic volume.

Equation 6.5 $$RVEDV = 75.1 \cdot BSA^{1.43},$$

where *RVEDV* = right ventricular end-diastolic volume.

The ejection fraction was similarly calculated as a percentage of the normal left ventricular ejection fraction (*%N-EF*). Normal values for EF were derived from the normal left ventricular EF expressed as a function of body surface area in children with normal hearts, as described by Graham *et al.* [490] (Equation 6.6).

Equation 6.6 $$LVEF = 0.70 - (0.08 \cdot BSA),$$

where $RVEDV$ = right ventricular end-diastolic volume.

Indices of ventricular systolic and diastolic function were derived from pressure-indexed volume measurements made during temporary occlusion of the IVC. The systolic indices included the end-systolic pressure-volume relation ($ESPVR$, E_{es}) [45]; the dP/dt_{MAX}-EDV' relation [108]; and preload-recruitable stroke work relation ($PRSW$) [109]. Each relationship was characterised by the slope and volume intercept. Diastolic chamber stiffness was calculated based on the end-diastolic pressure-volume relationship ($EDPVR$).

Vascular load was estimated using the effective arterial elastance, Ea. The Ea/Ees and SW/PVA ratios were calculated as indices of ventricular efficiency [81]. The Ea/Ees ratio reflects the ventriculo-vascular coupling efficiency whereas the SW/PVA ratio reflects the mechanical efficiency of the ventricle [81]. The SW/PVA ratio was calculated using the method described by Nozawa *et al.* [491], Equation 6.7.

Equation 6.7 $$SW/PVA = 1/[+(0.5 \cdot Ea) \quad Ees] \cdot 100.$$

6.2.6 Statistical analysis

Steady-state measurements were repeated two or three times. Extrasystolic and post extrasystolic beats were retrospectively identified and excluded from analysis. In each steady-state measurement, data from 10 consecutive cardiac cycles were then analysed. The estimated within-experiment standard deviation for volume measurements (EDV' and ESV) was 0.9 ml. The estimated within-experiment standard deviation for pressure measurements (P_{ED} and P_{ES}) was 1.9 mmHg. As these represented <5% of the absolute volume or pressure measurement, all subsequent analyses were based on the average data from each measurement.

Measurements made during IVCO were also repeated two or three times. Extrasystolic and post extrasystolic beats were again retrospectively identified and excluded from analysis. Heart rate did not generally change during preload reduction. However, in order to eliminate potential heart rate effects, only beats for which heart rate varied by less than 5% of baseline were used for analysis. Indices of systolic and diastolic function were calculated using the first 9 heart beats following transient IVCO that met the inclusion criteria using least square linear regression [110,112]. For each index, the slope of the relationship was identified. In addition, the *x*-axis (i.e. volume) intercept for E_{ES} was also calculated [492].

The haemodynamic parameters, indices of ventricular function and indices of vascular load and ventriculo-vascular coupling were obtained at Baseline; Baseline + dobutamine; and following BCPA. The effect of dobutamine on the in-parallel circulation was determined by comparing data at Baseline with data at Baseline + dobutamine. Similarly, the effect of the formation of BCPA was separately established by comparing data at Baseline + dobutamine with data at BCPA. Data at Baseline and following BCPA were not compared directly, as this does not address a relevant clinical question.

Data were analysed using SPSS for Windows (v16, SPSS Inc., Chicago, Il, USA). All values were expressed as mean ± SD. A probability $P<0.05$ was considered statistically significant in all comparisons.

The effects of dobutamine and the formation of the BCPA on the steady-state haemodynamic data were analysed using the paired two-tail Student *t*-test. The influence of ventricular morphology was then analysed using a two-way analysis of variance (ANOVA) followed by Bonferroni correction. The Bonferroni test was used for post hoc analyses.

The effects of dobutamine, the formation of the BCPA and ventricular morphology on indices of ventricular function calculated during IVCO were separately analysed using a two-way analysis of variance (ANOVA) followed by Bonferroni correction. All replicate measurements were included in these analyses, which fully accounted for the expected correlation between repeated observations. Again, the Bonferroni test was used for post hoc analyses.

6.3 RESULTS

Details of the fifteen patients together with the patient who was not subsequently included in the study are summarised in Table 5.1 and described in Materials and Methods.

6.3.1 Clinical outcome

There were no deaths during the early (30-day) post-operative period. None of the children had evidence of impaired ventricular function or clinically significant AVV regurgitation. One child sustained right phrenic nerve injury and required a reoperation to plicate the right hemi-diaphragm. One other child had a prolonged hospital stay (≥21 days) due to the difficulty in re-establishing enteral feeding. The median length of in-patient hospital stay was 7 days (range, 5 – 31 days).

6.3.2 Parallel conductance and dimensionless calibration coefficient

The changes in parallel conductance, G_P and the dimensionless calibration coefficient, α are summarised in Table 6.2. Overall, there was no significant change in either parallel conductance, G_P or the dimensionless calibration coefficient, α. There was similarly no significant change in the dimensionless calibration coefficient following the administration of dobutamine (0.37 ± 0.33 versus 0.34 ± 0.26; P=NS). However, there was a substantial variation between patients. For example, pre-CPB parallel conductance measurements varied between 7.2 – 213 ml. This finding reaffirms the need to calibrate all conductance volume measurements on an individual basis.

6.3.3 Coefficient of variation for indices of ventricular function

Indices of systolic and diastolic ventricular function showed variability between repeated measurements. The coefficient of variation (SD/mean · 100) together with its standard deviation was 17 ± 10% for E_{ES}, 12 ± 9% for $PRSW$ and 13 ± 9% for $dP/dt_{MAX}\text{-}EDV'$ [461]. The coefficient of variation for chamber stiffness was 21 ± 13%.

6.3.4 Haemodynamic data

The haemodynamic parameters; indices of ventricular function; and indices of vascular load and ventriculo-vascular coupling at the three separate time-points are summarised in Tables 6.3 – 6.5, respectively.

Overall, patients were characterised by only mild dilatation of the single functional ventricle. The indexed EDV' at Baseline was 57 ± 32, which is within the limits found by Graham *et al.* for normal left and right ventricles [490,493]. Nevertheless, in this study there was mild impairment of global ventricular function. The normalised ejection fraction ($\%N\text{-}EF$) was 71 ± 22%, which is outside the range of left ventricular ejection fraction in normal patients found by Graham *et al.* [490].

Haemodynamic parameter	Baseline	Baseline + dobutamine	BCPA
Heart rate (bpm)	129 ± 13	141 ± 22 *	160 ± 12 †
Cardiac index ($L \cdot min^{-1} \cdot m^{-2}$)	3.5 ± 1.7	3.7 ± 2.1	2.1 ± 1.0 †
Indexed stroke volume ($ml \cdot m^{-2}$)	26 ± 12	26 ± 14	13 ± 7 †
Ejection fraction (%)	52 ± 16	50 ± 14	53 ± 18
Normalised ejection fraction (%)	77 ± 22	68 ± 19	71 ± 23
Indexed *EDV'* ($ml \cdot m^{-2}$)	57 ± 32	54 ± 22	26 ± 10 †
Normalised *EDV'* (%)	120 ± 66	111 ± 39	54 ± 20 †
P_{ED} (mmHg)	4.0 ± 4.4	3.5 ± 4.3	2.2 ± 6.4
Indexed *ESV* ($ml \cdot m^{-2}$)	34 ± 29	30 ± 19	13 ± 7 †
P_{ES} (mmHg)	53 ± 17	58 ± 14	68 ± 20
Stroke work ($mmHg \cdot ml^{-1} \cdot m^{-2}$)	1555 ± 811	1733 ± 1112	1060 ± 630 †
dP/dt_{MAX} ($mmHg \cdot s^{-1}$)	994 ± 343	1516 ± 740 *	1950 ± 803
dP/dt_{MIN} ($mmHg \cdot s^{-1}$)	-938 ± 279	-1066 ± 388 *	-1398 ± 522
Tau (s)	$1.44 \cdot 10^{-4}$ ± $0.43 \cdot 10^{-4}$	$1.44 \cdot 10^{-4}$ ± $0.60 \cdot 10^{-4}$	$1.14 \cdot 10^{-4}$ ± $0.33 \cdot 10^{-4}$

Table 6.3 *Haemodynamic parameters at three intra-operative time-points.*

* *$P<0.05$ versus Baseline;*

† *$P<0.05$ versus Baseline + dobutamine.*

	Baseline		Baseline + dobutamine		BCPA	
Index of ventricular function	Slope	Intercept (ml)	Slope	Intercept (ml)	Slope	Intercept (ml)
E_{ES} (mmHg·ml^{-1}·m^{-2})	1.8 ± 1.5	-21 ± 97	3.5 ± 1.7	3.7 ± 2.1	6.7 ± 5.6 †	-39 ± 84
dP/dt_{MAX}-EDV' (mmHg·s^{-1}·ml^{-1}·m^{-2})	16 ± 11	-	51 ± 43 *	-	116 ± 94 †	-
PRSW (mmHg)	14 ± 8	-	21 ± 10 *	-	28 ± 14	-
Chamber stiffness (ml^{-1}·m^{-2})	0.06 ± 0.04	-	0.06 ± 0.04	-	0.18 ± 0.12 †	-

Table 6.4 *Indices of ventricular function at three intra-operative time-points.*

* *P<0.05 versus Baseline*

† *P<0.05 versus Baseline + dobutamine.*

Parameter	Baseline	Baseline + dobutamine	BCPA
Ea (mmHg·ml^{-1}·m^{-2})	2.8 ± 1.5	3.2 ± 1.6	7.8 ± 5.0 †
Ea / E_{ES}	2.1 ± 1.3	1.7 ± 1.0	1.6 ± 0.8
SW / PVA (%)	47 ± 12	54 ± 9	54 ± 10

Table 6.5 *Indices of vascular load and ventriculo-vascular coupling efficiency at three intra-operative time-points.*

* *P<0.05 versus Baseline;*

† *P<0.05 versus Baseline + dobutamine.*

6.3.5 Influence of dobutamine infusion

Figure 6.7 illustrates typical steady-state pressure, dP/dt and volume signals and the corresponding pressure-volume loop measured prior to cardiopulmonary bypass with and without dobutamine (Baseline and Baseline + dobutamine).

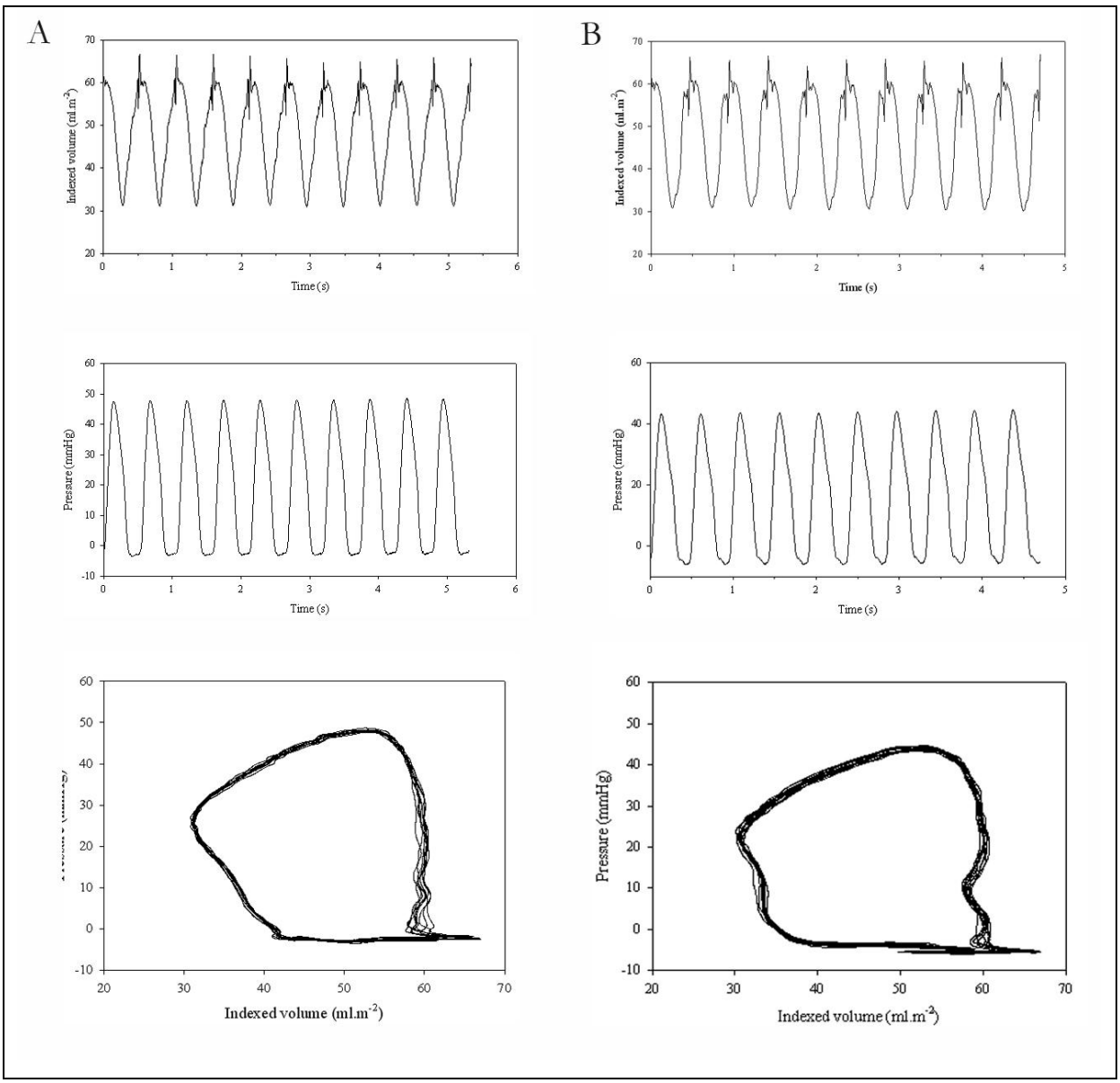

Figure 6.7 *Typical steady-state volume (upper panel) and pressure signals (middle panel) together with the corresponding pressure-volume loop (lower panel) at Baseline* (A) *and Baseline + dobutamine* (B).

Figure 6.8 illustrates the corresponding pressure-volume loop during IVCO together with the various systolic and diastolic pressure-volume relations (E_{ES}, *PRSW*, dP/dt_{MAX}-*EDV'* and *EDPVR*).

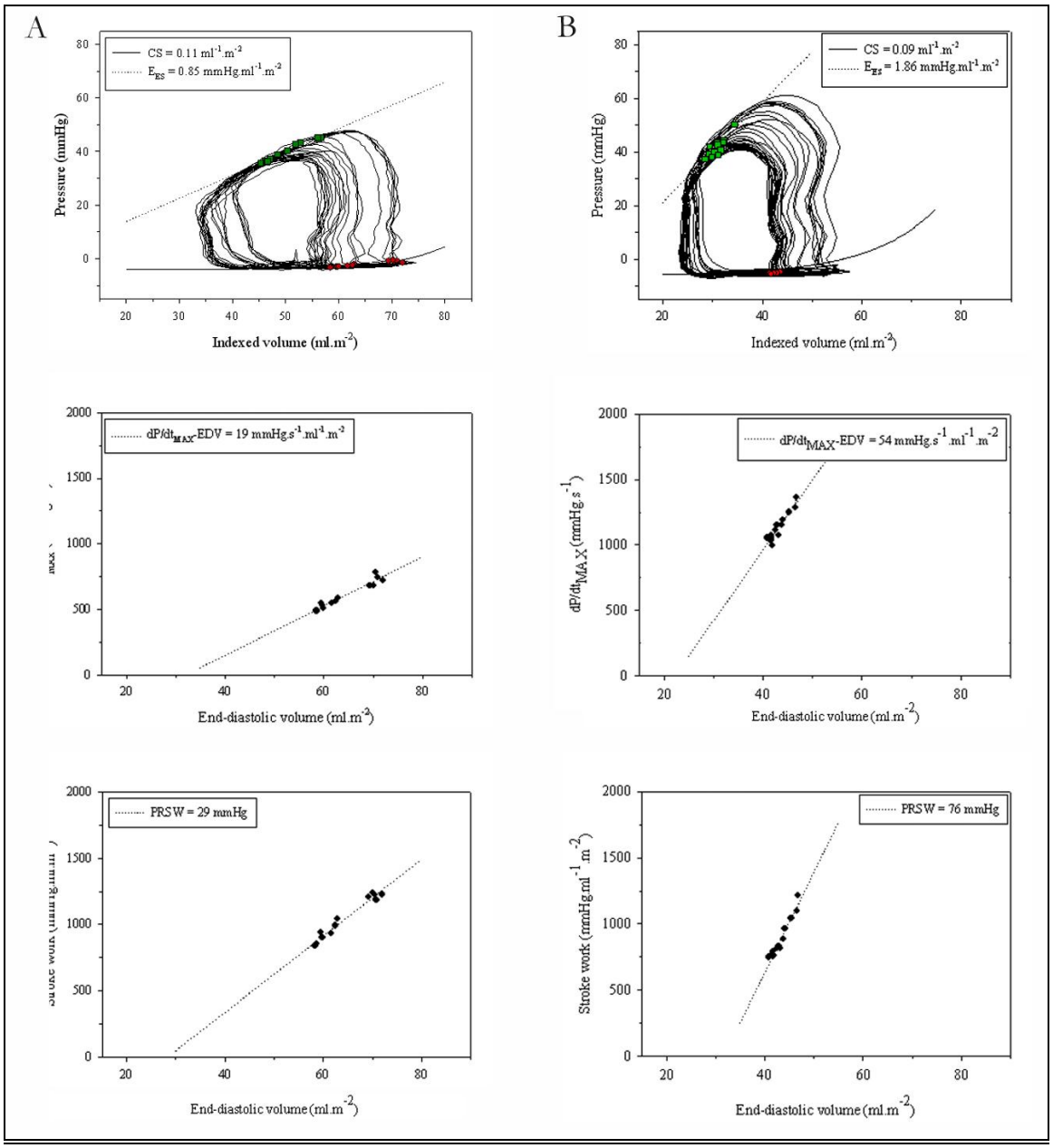

Figure 6.8 *Typical example of pressure-volume relations derived during IVC occlusion at Baseline* (A) *and Baseline + dobutamine* (B). *In this patient, the* E_{ES} *(upper panel) showed an increased in slope (i.e. contractile performance) with dobutamine. The* dP/dt_{MAX}-*EDV' relation (middle panel) and* PRSW *relation (lower panel) also demonstrated an increased slope with dobutamine. The* EDPVR *(upper panel) demonstrate no significant change in chamber stiffness following dobutamine infusion.*
The selected end-diastolic (red circles) and end-systolic points (green squares) are identified.

Dobutamine was associated with an increase in the heart rate (P<0.05) and a corresponding increase in the maximal and minimal rate of pressure change (P<0.05, respectively). However, there was no change in the end-diastolic or end-systolic pressure.

Dobutamine was not associated with a change in the indexed end-diastolic or end-systolic volumes, indexed stroke volume or ejection fraction. In spite of the change in heart rate, there was no change in the cardiac index. There was no difference in the relaxation time constant (tau).

Dobutamine was associated with a significant increase in ventricular systolic function. The $PRSW$ increased from 14 ± 8 mmHg·m^{-2} to 21 ± 10 mmHg·m^{-2} (P<0.05) and dP/dt_{MAX}-EDV' increased from 16 ± 11 mmHg·s^{-1}·ml^{-1}·m^{-2} to 51 ± 43 mmHg·s^{-1}·ml^{-1}·m^{-2} (P<0.05). There was also an overall increase in E_{ES} (1.8 ± 1.5 mmHg·ml^{-1}·m^{-2} versus 3.5 ± 1.7 mmHg·ml^{-1}·m^{-2}), although this change was not statistically significant. There was no change in chamber stiffness.

Dobutamine was not associated with a change in the effective arterial elastance, Ea. Overall, there was no change in the ventriculo-vascular coupling ratio (Ea/E_{ES}) or mechanical efficiency of the ventricle (SW/PVA) with the administration of dobutamine.

6.3.6 Effect of formation of bidirectional cavo-pulmonary anastomosis

Figure 6.9 illustrates typical steady-state pressure, dP/dt and volume signals and the corresponding pressure-volume loop measured at Baseline + dobutamine and following the formation of the BCPA.

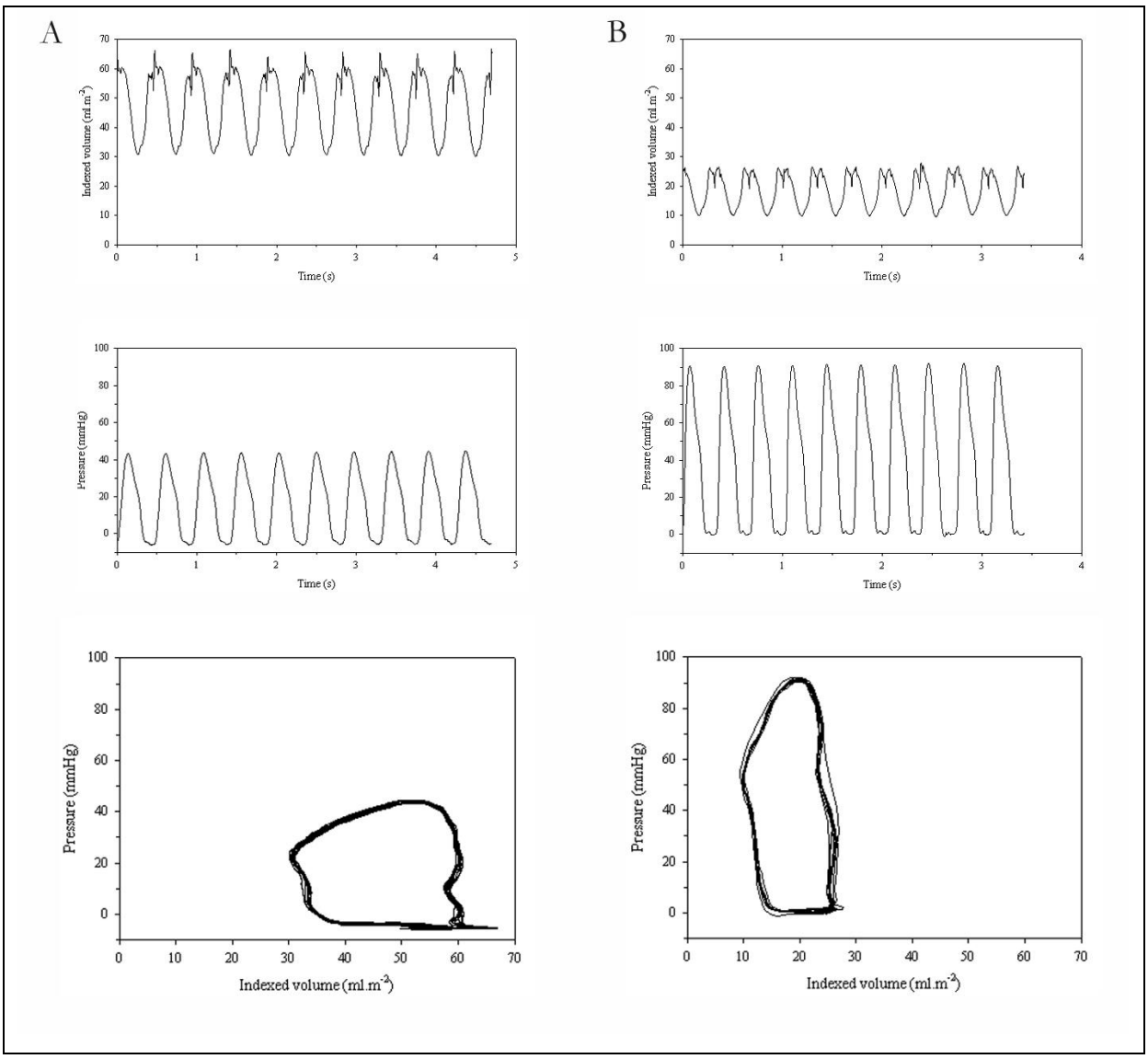

Figure 6.9 *Typical steady-state volume (upper panel) and pressure signals (middle panel) together with the corresponding pressure-volume loop (lower panel) at Baseline + dobutamine* (A) *and following BCPA* (B).

Figure 6.10 illustrates the corresponding pressure-volume loop during IVCO together with the various systolic and diastolic pressure-volume relations (*E_{ES}*, *EDPVR*, *PRSW* and *dP/dt_{MAX}-EDV'*).

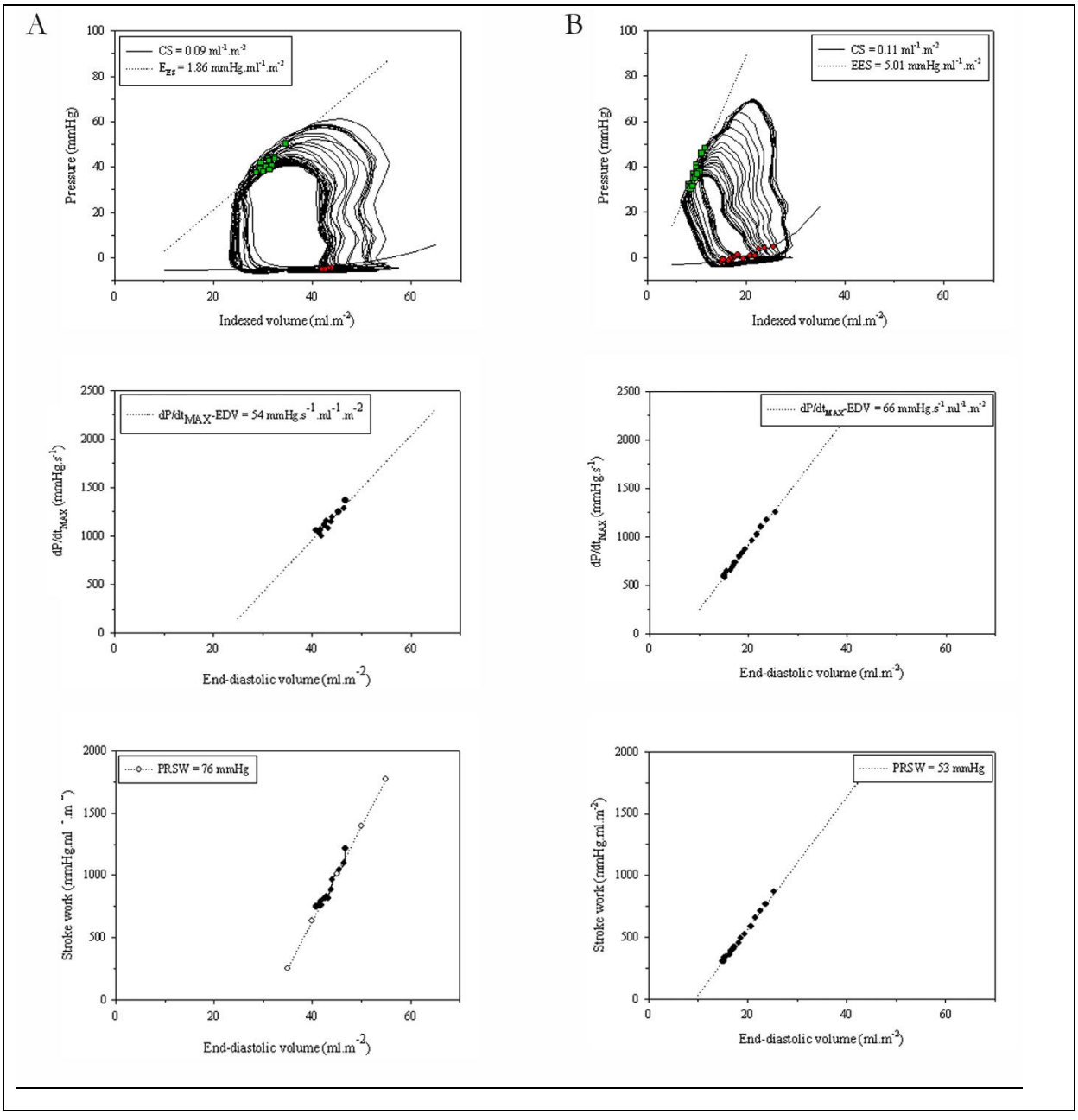

Figure 6.10 *Typical example of pressure-volume relations derived during IVC occlusion at Baseline + dobutamine* (A) *and following BCPA* (B). *In this patient, the* E_{ES} *(upper panel) and* dP/dt_{MAX}*-EDV' relation (middle panel) showed an increased in slope (i.e. contractile performance) following BCPA. There was a reduction in the* PRSW *relation (lower panel). The chamber stiffness, calculated form the* EDPVR *(upper panel) did not change in this patient, in contrast to the overall study group.*
The selected end-diastolic (red circles) and end-systolic points (green squares) are identified.

The formation of the BCPA was associated with a further increase in the heart rate (P<0.05). There was an overall increase in the maximal and minimal rate of pressure change, although these changes were not statistically significant. There was no change in the end-diastolic or end-systolic pressure.

The formation of the BCPA was associated with a reduction in the indexed end-diastolic and end-systolic volumes (P<0.05), stroke volume (P<0.05) and stroke work (P<0.05). These changes are illustrated on the pressure-volume loop (Figure 6.9). The pressure-volume loop following BCPA is narrower and shifted to the left of the plot when compared with the corresponding Baseline + dobutamine curve. There formation of the BCPA was also associated with a decrease in the cardiac index, which decreased from 3.7 ± 2.1 $L \cdot min^{-1} \cdot m^{-2}$ to 2.1 ± 1.0 $L \cdot min^{-1} \cdot m^{-2}$ (P<0.05). There was a slight reduction in the relaxation time constant (tau) from 1.44 $\cdot 10^{-4}$ ± 0.60 $\cdot 10^{-4}$ s to 1.14 $\cdot 10^{-4}$ ± 0.33 $\cdot 10^{-4}$ s, although this change was not statistically significant.

The formation of the BCPA was associated with a significant increase in ventricular systolic function. The E_{ES} increased from 3.5 ± 1.7 $mmHg \cdot ml^{-1} \cdot m^{-2}$ to 6.7 ± 5.6 $mmHg \cdot ml^{-1} \cdot m^{-2}$ (P<0.05) and dP/dt_{MAX}-EDV' increased from 51 ± 43 $mmHg \cdot s^{-1} \cdot ml^{-1} \cdot m^{-2}$ to 116 ± 94 $mmHg \cdot s^{-1} \cdot ml^{-1} \cdot m^{-2}$ (P<0.05). However, there was no significant change in the $PRSW$ (21 ± 10 $mmHg \cdot m^{-2}$ versus 28 ± 14 $mmHg \cdot m^{-2}$). In addition, there was a three-fold increase in the chamber stiffness, which increased from 0.06 ± 0.04 $ml^{-1} \cdot m^{-2}$ to 0.18 ± 0.12 $ml^{-1} \cdot m^{-2}$ (P<0.05).

The BCPA was also associated with a significant increase in the effective arterial elastance, Ea, which increased from 3.2 ± 1.6 $mmHg \cdot ml^{-1} \cdot m^{-2}$ to 7.8 ± 5.0 $mmHg \cdot ml^{-1} \cdot m^{-2}$ (P<0.05). However, there was no change in the ventriculo-vascular coupling ratio (Ea/E_{ES}) or mechanical efficiency of the ventricle (SW/PVA) following the BCPA.

6.3.7 Influence of ventricular morphology

Figure 6.11 illustrates typical steady-state pressure-volume loops that were obtained in patients under equivalent loading conditions. One patient (patient 13) had a dominant ventricle of left ventricular morphology (mLV) while the other patient (patient 8) had a dominant ventricle of right ventricular morphology. The overall shape of the pressure-volume loops were broadly similar. Both groups demonstrated a well-defined end-systolic "shoulder" (i.e. upper left hand corner) and both groups had a clearly identifiable isovolumic relaxation phase.

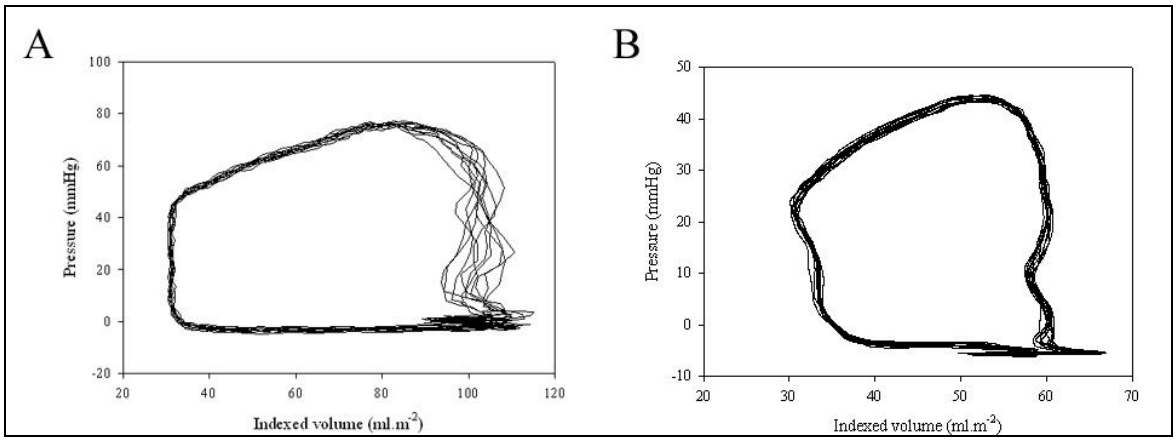

Figure 6.11 *Typical ventricular pressure-volume loops in (*A*) a patient with a morphologic left ventricle and (*B*) a patient with a morphologic right ventricle. Measurements were obtained at Baseline + dobutamine.*

Intraventricular pressure-volume measurements in patients with a mLV and mRV were comparable at all three time-points. There was no difference in the steady-state haemodynamic parameters; indices of ventricular function; or indices of vascular load and ventriculo-vascular coupling between the two groups. In addition, ventricular morphology did not influence the relative change in any of the parameters following either dobutamine infusion or the formation of the BCPA.

6.4 DISCUSSION

The management of children with functionally single ventricle generally involves three staged operations that culminate in the Fontan procedure. This management strategy has evolved to ensure adequate interim palliation as well as ensure optimal preparation for the eventual formation of the Fontan circulation [292,334].

The majority of children with functionally single ventricle anatomy require initial surgical palliation as neonates or during early infancy [292]. Initial palliative surgery establishes a balanced circulation in which the systemic and pulmonary circulations are in parallel. The systemic and pulmonary venous pathways are both connected to the dominant ventricle, which acts as a ventricular pump for antegrade blood flow through both the systemic and pulmonary circulations.

The circulation established following initial palliation is primarily characterised by obligate volume loading of the dominant ventricle [336,338]. Marc Gewillig estimated that this volume load might be almost three-times higher than the volume load in the normal left ventricle [336]. Chronic volume loading of the dominant ventricle is associated with progressive dilatation and spheroid remodelling of the ventricle [338,339,475,494], such that the indexed end-diastolic volume (*EDVI*) is approximately 150% of normal [339]. The ventricular mass also increases incrementally with the increased ventricular volume, thus preserving a normal ventricular mass-volume ratio [338,339]. However, despite these adaptive changes, ventricular dysfunction and failure eventually develop in most children with functionally single ventricle anatomy who have been palliated for a long time [340].

The bidirectional cavo-pulmonary anastomosis (BCPA) represents the second stage in the three-stage management plan for children with functionally single ventricle anatomy [292]. This procedure relieves the chronic volume overload while maintaining adequate systemic arterial oxygenation [292,342,472-474,476,477,495]. Early relief of the chronic volume load is expected to help preserve the long-term function of the ventricle [271,292,496].

The BCPA is a safe procedure with a low in-patient mortality [497]. At Birmingham Children's Hospital, for example, 380 patients underwent a BCPA between January 2000 and August 2009. The in-patient mortality was 1.3% (n=5).

Previous studies have demonstrated that the BCPA is associated with an immediate and persistent reduction in the volume load of the dominant ventricle [342,472-477] together with a change in the geometry of the ventricle [342,474,475]. However, only a limited number of studies have been undertaken to assess how these changes affect ventricular function or the performance of the cardiovascular system as a whole [351,478,479].

The current study has confirmed that the formation of the BCPA is associated with a substantial reduction in the volume load of the dominant ventricle. The indexed end-diastolic and end-systolic volumes were reduced by 52% and 56%, respectively. This was associated with a corresponding reduction in the stroke volume and stroke work. Overall, there was a reduction in the cardiac index in spite of a significant increase in the resting heart rate. These finding are consistent with the previous studies [342,472,473,475].

This study has identified a number of novel and clinically important findings. It has demonstrated that the formation of the BCPA is associated with an immediate improvement in systolic function, with a significant increase in both end-systolic elastance, E_{ES} and the dP/dt_{MAX}-EDV relation.

Tanoue *et al.* have previously demonstrated that the BCPA was associated with an improvement in end-systolic elastance [351]. However, that study measured end-systolic elastance during cardiac catheterisation prior to either the BCPA or the Fontan procedure. These measurements were separated by almost 2 years and it was not clear whether the change reflects the effect of the procedure or age. Taken in conjunction with the current study, the study of Tanoue *et al.* would indicate that the immediate improvement in ventricular systolic function is still evident up to the time of the Fontan procedure.

This study has also demonstrated that the BCPA is associated with a significant decrease in the compliance of the ventricle, with a three-fold increase in the ventricular "stiffness". This is likely to be an underestimate of the true clinical effect [498], as all measurements in this study were made with the chest and pericardium open. It is unclear what has caused the change in ventricular compliance. This may simply reflect the change in ventricular geometry [342,474,475]. However, it may also reflect the adverse effects of deep hypothermic cardiopulmonary bypass, which is also associated with ventricular diastolic dysfunction [499]. Nevertheless, this finding has important implications for the post-operative management of these children. At present, patients at Birmingham Children's Hospital are not routinely prescribed agents that improve diastolic relaxation (lusitropy) unless there is evidence of global ventricular dysfunction or significant AVV regurgitation.

While this study identified abnormal ventricular compliance following the BCPA, abnormal ventricular relaxation was not demonstrated. By contrast, the maximum rate of pressure decline (dP/dt_{MIN}) and the time constant of pressure decline (tau) both increased following the BCPA, although neither of these changes were statistically significant. The findings of the current study contrast with the previous study by Selamet Tierney *et al.*, [478] who identified abnormal ventricular relaxation, assessed using a number of echocardiographic indices. The reason for this difference is not clear but may reflect differences between the techniques used.

The BCPA is theoretically associated with a significant increase in vascular load as the circulation is transformed from an in-parallel circulation to one in which the pulmonary circuit is in-series with the systemic circulation of the upper half of the body [470]. In the current study, there was a 145% increase in the effective arterial elastance following the BCPA. The magnitude of the change is greater than one might reasonably expect, and may reflect the additional effects of deep hypothermic cardiopulmonary bypass on the vascular system. Nevertheless, the change in vascular load was not associated with a change in the performance of the cardiovascular system (measured using the Ea/E_{ES} ratio and ejection fraction, EF) or the efficiency of the heart (as

measured using the *SW/PVA* ratio). These findings are in agreement with the study by Tanoue *et al.* [351].

In addition to describing the effects of the BCPA as a whole, this study was designed to determine the influence of dominant ventricular morphology on the changes in ventricular function. As discussed in Chapter 2, there is a long-standing concern that the mRV may be intrinsically less well suited to support either the systemic circulation or the entire circulation. In a recent study, Kogon *et al.* identified that patients with a single ventricle of right ventricular morphology (mRV) were associated with an increased risk of morbidity and mortality following the BCPA [233]. This may have been associated with the duration of cardiopulmonary bypass, which was an independent risk factor for outcome in the same study. Patients with HLHS, for example, frequently require extensive pulmonary artery patch reconstruction at the time of the BCPA [480,483,500]. However, it is clear from the present study that the BCPA results in significant improvements in systolic function.

This is the first study to evaluate quantitatively the influence of ventricular morphology on ventricular function in children with functionally single ventricle anatomy. This study has demonstrated that ventricular performance is significantly improved following BCPA, at least acutely, and there is no significant difference in the steady-state haemodynamic parameters; indices of ventricular function; or indices of vascular load and ventriculo-vascular coupling between patients with a mLV or mRV. This represents an important clinical finding that may provide some reassurance about the long-term outlook for these children.

6.4.1 Study Limitations

The conductance catheter technique is associated with two well-known sources of error that are described in detail in Chapter 3. As a result, conductance volume measurements must be calibrated in order to obtain absolute volume measurements. The process of calibration is itself associated with errors that potentially affect the accuracy of the volume measurements.

In this study, parallel conductance was calculated using the hypertonic saline technique devised by Baan *et al.* [381]. One of the limitations of this technique is that the point where the regression line intersects with the line of identity (i.e. G_P) is distant from the data points used for the regression analysis. As a result, small measurement errors can result in big variations in the estimated G_P and ventricular volume. This issue is particularly important in studies involving children, because the absolute ventricular volume is much smaller. However, it is unlikely to have changed the conclusions of the present study. Errors in the estimate of parallel conductance, G_P would not have changed the slope of the relationship for indices of ventricular function. Furthermore, this study is based on a within-subject comparison and there was no substantial change in parallel conductance, G_P between pre-CPB and post-CPB measurements.

In this study, the dimensionless calibration coefficient, α was estimated by comparing the stroke conductance with the stroke volume calculated from the integrated aortic flow measurements. Conductance volume measurements are generally calibrated using an alternative measure of stroke volume. However, as we have demonstrated in Chapter 4, assuming that the calibration coefficient is fixed or constant will introduce measurement errors. Nonetheless, this study is based on a within-subject comparison and there was no substantial change in the calibration coefficient, α at any of the three time-points.

6.5 CONCLUSION

The formation of the BCPA is associated with an immediate reduction in ventricular volume. This is associated with an improvement in systolic function but interestingly a decrease in the diastolic compliance. The formation is also associated with an increase in vascular load, although there is no change in the ventriculo-vascular coupling or mechanical efficiency of the ventricle. Importantly, similar changes were observed in patients with either a mLV or a mRV. Long-term follow-up studies are necessary to determine whether these changes persist beyond the immediate post-operative period.

CHAPTER 7

ACUTE CHANGES IN VENTRICULAR PERFORMANCE FOLLOWING TOTAL CAVO-PULMONARY CONNECTION

CHAPTER 7. ACUTE CHANGES IN VENTRICULAR PERFORMANCE FOLLOWING TOTAL CAVO-PULMONARY CONNECTION

7.1 INTRODUCTION

The Fontan procedure represents the third and final stage in the management of children with functionally single ventricle anatomy [292]. Currently, this generally involves a completion total cavo-pulmonary connection (TCPC) procedure, which establishes a direct connection between the inferior vena cava (IVC) and the central pulmonary artery. All of the systemic venous return passes directly into the pulmonary circulation, completely bypassing the right side of the heart. As a result, the Fontan procedure creates a "physiologically normal" circulation in which the systemic and pulmonary circulations are separate and in-series, but powered by a single ventricle only [501] (Figure 7.1).

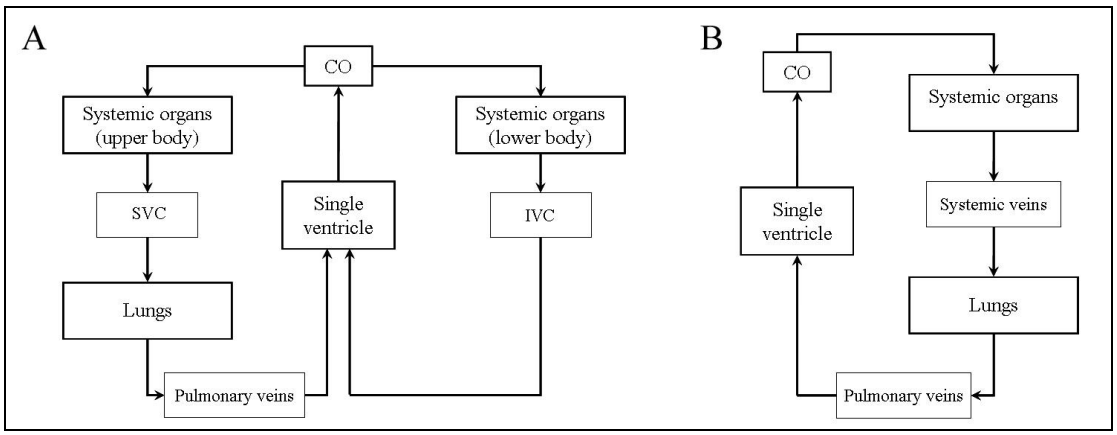

Figure 7.1 *Schematic diagram of the circulation (A) with BCPA and (B) following the Fontan procedure. (CO = Cardiac Output).*

The Fontan procedure is now amongst the most common procedures performed to treat complex congenital cardiac defects not amenable to biventricular repair [502]. In appropriately selected patients, it is associated with significant functional and clinical improvement and long-term survival [231,294,348,503-505]. For example, in a recent study from Birmingham Children's Hospital, Hosein *et al.* reported that the 15-year survival following the Fontan procedure was 82%. The majority of these patients were in NYHA functional class I and II (94%) and over half

were attending some form of schooling from primary school up to university. More than a quarter of the adult patients were working and two women had had successful pregnancies [294].

Despite this undoubted success, there are on-going concerns about the long-term outcome for children following the Fontan procedure. These concerns primarily relate to the abnormal arrangement of the circulation and the ability of the single functional ventricle to support blood flow through the systemic and pulmonary circulations in series [293,502].

To date, only two clinical studies have been undertaken to assess how the changes in load affect ventricular function or the performance of the cardiovascular system in the era of staged surgical palliation [343,351]. In 2001, Tanoue *et al.* reported the changes in ventricular function and vascular load in a series of patients following TCPC. Ventricular function and vascular load were analyses using pressure-volume data acquired during cardiac catheterisation performed before and 6 weeks after surgery. The authors identified that the TCPC was associated with a significant improvement in ventricular systolic function and mechanical efficiency [343].

In a separate study, Tanoue *et al.* reported longitudinal changes in ventricular function and vascular load in patients with hypoplastic left heart syndrome and the effects of surgical palliation [351]. That study also demonstrated an early improvement in ventricular systolic function following TCPC. In addition, the authors identified that ventricular systolic function and mechanical efficiency was even better 1-year following surgery.

Both of these two studies by Tanoue *et al.* are associated with important limitations. Firstly, post-operative cardiac catheterisation was performed approximately 6 weeks after surgery. Their results may, therefore, not be representative of the changes that occur during the high-risk, early post-operative period. Secondly, their studies used an approximation of end-systolic elastance and arterial elastance that has only been validated in an animal model. The validity of these assumptions, particularly in the assessment of children with severe forms of congenital heart disease, has not been proven. Thirdly and perhaps most importantly, their studies did not

evaluate changes in diastolic function, which may represent the primary determinant of outcome following the Fontan procedure [506].

The present study was undertaken to determine the effect of the TCPC on changes in volume and pressure loading characteristics and ventricular systolic and diastolic function during the immediate post-operative. In addition, this study aimed to investigate whether the relative changes in ventricular function were influenced by the morphology of the dominant ventricle.

7.2 MATERIALS AND METHODS

Twenty-six children undergoing elective TCPC at the Diana Princess of Wales Children's Hospital, Birmingham between May 2003 and April 2005 were recruited to this study (Table 7.1). All patients had functionally single ventricle anatomy with a dominant ventricle of left or right ventricular morphology. As in the previous clinical study (Chapter 6), children with either a single ventricle of indeterminate ventricular morphology or clinically significant (i.e. ≥ moderate) systemic atrio-ventricular valve regurgitation were not considered for this study.

Written informed consent was obtained from the parents of each child and the study protocol was approved by the Local Research Ethics Committee (LREC 2002/0809).

Patient	Anatomy	Ventricular morphology	Gender	Initial palliation	Stage II procedure	Age at TCPC (y)	TCPC procedure	Fenestration	Concurrent procedures
1	HLHS	mRV	Male	Norwood procedure	BDG	4.0	Extracardiac conduit	5.0 mm	
2	DILV, TGA	mLV	Male	MPA band, atrial septectomy	BDG, DKS, CPA patch augmentation	4.0	Extracardiac conduit	5.5 mm	
3	PAt- IVS	mLV	Male	RMBTS	BDG, atrial septectomy	3.8	Extracardiac conduit	5.0 mm	
4	HLHS	mRV	Female	Norwood procedure	BDG	4.9	Extracardiac conduit	5.0 mm	
5	HLHS	mRV	Male	Norwood procedure	BDG	6.1	Extracardiac conduit	5.0 mm	
6	TA, VSD	mLV	Male	MPA band	BDG, atrial septectomy, MPA ligation and CPA patch augmentation	6.5	Extracardiac conduit	5.0 mm	
7	DILV, MA, TGA, aortic arch hypoplasia	mLV	Male	Norwood procedure	BDG	6.1	Extracardiac conduit	5.0 mm	
8	TA, PAt	mLV	Female	RMBTS	BDG, atrial septectomy, CPA patch augmentation	4.5	Extracardiac conduit	5.0 mm	
9	DILV, DOLV, PS	mLV	Female	N/A	BDG, PA band	9.1	Extracardiac conduit	5.0 mm	MPA ligation
10	HLHS	mRV	Female	Norwood procedure	BDG	4.2	Extracardiac conduit	5.0 mm	
11	TA, VSD, sub-PS	mLV	Male	RMBTS	Bilateral BDG	6.9	Extracardiac conduit	5.5 mm	CPA patch augmentation
12	TS, hypoplastic RV, DORV, aortic arch hypoplasia	mLV	Female	DKS procedure, CoA repair, 5mm central shunt	BDG, atrial septectomy	3.9	Extracardiac conduit	5.0 mm	
13	HLHS	mRV	Male	Norwood procedure	BDG	4.2	Extracardiac conduit	5.0 mm	
14	MS, TGA, PAt, hypoplastic mLV	mRV	Male	Central shunt, atrial septectomy	BDG	4.9	Extracardiac conduit	5.0 mm	MPA ligation

Table 7.1 *Summary of patients undergoing completion TCPC.*

Patient (cont.)	Anatomy	Ventricular morphology	Gender	Initial palliation	Stage II procedure	Age at TCPC (y)	TCPC procedure	Fenestration	Concurrent procedures
15	DILV, TGA, VSD	mLV	Female	PA band	BDG, DKS	6.3	Extracardiac conduit	5.0 mm	
16	HLHS	mRV	Male	Norwood procedure	BDG	6.6	Extracardiac conduit	5.0 mm	
17	uAVSD, TGA	mLV	Female	RMBTS	BDG, left SVC ligation	5.0	Extracardiac conduit	5.0 mm	
18	HLHS	mRV	Male	Norwood procedure	BDG	4.7	Extracardiac conduit	5.0 mm	
19	HLHS	mRV	Male	Norwood procedure	BDG	5.3	Extracardiac conduit	5.0 mm	
20	TA, VSD	mLV	Female	N/A	BDG, atrial septectomy	4.2	Extracardiac conduit	5.0 mm	Repair of diaphragmatic hernia
21	TA, VSD, sub-PS	mLV	Female	RMBTS	BDG, atrial septectomy	6.4	Extracardiac conduit	5.0 mm	MPA ligation
22	DILV, TGA, restrictive VSD	mLV	Male	MPA band	BDG, MPA ligation	6.5	Extracardiac conduit	5.0 mm	
23	HLHS	mRV	Male	Norwood procedure	BDG	4.6	Extracardiac conduit	5.0 mm	
24	TA, sub-PS	mLV	Female	RMBTS	BDG	5.5	Extracardiac conduit	N/A	
25	Ebstein's anomaly, sub-PS, small CPA, hypoplastic mRV	mLV	Female	Potts shunt, atrial septectomy, patch closure of tricuspid valve	BDG, atrial septectomy	6.1	Extracardiac conduit	5.0 mm	MPA ligation
26	HLHS	mRV	Male	Norwood procedure	BDG	4.9	Extracardiac conduit	5.0 mm	

Table 7.1 *Summary of patients undergoing completion TCPC* (continued)

*BDG, bidirectional Glenn; CPA; central pulmonary arteries; DILV, double inlet left ventricle; DKS, Damus-Kaye-Stansel procedure; DOLV, double outlet left ventricle; HLHS, hypoplastic left heart syndrome; mLV, morphologic left ventricle; MA, mitral atresia; MPA, main pulmonary artery; MS, mitral stenosis; m*RV*, morphologic right ventricle; PAt, pulmonary atresia; PA-IVS, pulmonary atresia with intact ventricular septum; PS, pulmonary stenosis; RMBTS, right modified Blalock-Taussig shunt; RVOTO, right ventricular outflow tract obstruction; RV-PA, right ventricle to pulmonary artery conduit; TA, tricuspid atresia; TGA, transposition of the great arteries; TS, tricuspid stenosis; uAVSD, unbalanced atrio-ventricular septal defect; VSD, ventricular septal defect*

7.2.1 Pre-operative diagnosis

All of the children had functionally single ventricle anatomy with a dominant ventricle of either left (n=15) or right ventricular morphology (n=11). The single most common primary cardiac malformation was hypoplastic left heart syndrome (HLHS; n=10). Amongst the other children, the primary cardiac malformation was tricuspid atresia (n=6); double-inlet left ventricle (n=5); pulmonary atresia with intact ventricular septum (n=1); an unbalanced atrioventricular septal defect (AVSD) with a dominant ventricle of left ventricular morphology (n=1); and Ebstein's anomaly (n=1).

Two children had bilateral superior vena cavae, in which the left superior vena cava (SVC) opened into the roof of the left atrium. One child was originally diagnosed with abnormal pulmonary venous drainage, in which the pulmonary veins drained to the coronary sinus. In addition, one child had oculo-auriculo-vertebral spectrum.

7.2.2 Initial surgical palliation

The majority of the children (n=24) required initial surgical palliation either as neonates or young infants in order to establish a balanced circulation with the systemic and pulmonary circulations in parallel with one another (Table 7.1).

Initial surgical surgery was performed at a median age of 8 days (range, 1 – 90 days). This involved a Norwood stage I procedure (n=12); a modified Blalock-Taussig (BT) shunt (n=5); formation a central shunt (n=2) between the ascending aorta and either the main pulmonary artery or right pulmonary artery; or pulmonary artery banding to limit pulmonary blood flow (n=4). Initial surgical palliation in the child with Ebstein's anomaly involved patch closure of the tricuspid valve, atrial septectomy and a modified BT shunt. This resulted in the creation of "functional" tricuspid atresia with pulmonary blood flow supplied via the modified BT shunt.

7.2.2 Formation of bidirectional cavo-pulmonary anastomosis

An interim bidirectional cavo-pulmonary anastomosis (BCPA) similar to that describe din Chapter 5 was created in all patients, at a median age of 8.5 months (range, 44 days – 2.7 years). Universally, this involved a bidirectional Glenn procedure. One patient with bilateral superior vena cavae underwent a bilateral BDG procedure. In the other patient, the left-sided SVC was small and there was an innominate vein. In this case, the left-sided SVC was simply ligated.

7.2.3 Assessment prior to total cavo-pulmonary connection

The TCPC was indicated in patients with progressive cyanosis or increasing dyspnoea on exertion [368]. The median preoperative oxygen saturations in air were 90% (range, 81 – 94%).

Cardiovascular function was routinely assessed using trans-thoracic echocardiography and elective cardiac catheterisation prior to the TCPC [294,368]. Ventricular and valvular function was qualitatively assessed using echocardiography [368]. Based on these measurements, the majority of children in this study (n=24) had good ventricular function. The remaining two children had moderate ventricular function. Fourteen children had no or trivial atrio-ventricular valve (AVV) regurgitation while the remaining twelve children had mild AVV regurgitation. None of the children had aortic or neo-aortic valve regurgitation.

Cardiac catheterisation was electively performed under general anaesthesia at a median age of 4.3 years (range, 2.5 – 8.0 years). Haemodynamic and angiographic studies were performed in all children [368]. Cardiac catheterisation demonstrated seven patients who had relatively small central pulmonary arteries. One of these children also had an isolated left pulmonary artery stenosis. In addition, cardiac catheterisation identified one patient who had evidence of re-coarctation of the aorta.

Under general anaesthesia, the median PA pressure was 12 mmHg (range, 7 – 20 mmHg); the median atrial pressure was 7 mmHg (range, 1 – 14 mmHg); and the median transpulmonary gradient was 4 mmHg (range, 2 – 8 mmHg). Five patients (19%) had elevated PA pressures

(≥15mmHg) and 3 patients (12%) had elevated atrial pressures (≥12mmHg). The ***PVR*** was not routinely calculated.

Nine patients required cardiological intervention prior to the formation of TCPC. This involved coil embolisation of systemic – pulmonary arterial collateral vessels (n=6), left pulmonary artery balloon angioplasty and stent insertion (n=4) and balloon dilatation of re-coarctation (n=1).

7.2.4 The total cavo-pulmonary connection

The surgical procedures described in this study were all performed by one of two paediatric cardiac surgeons (Mr WJ Brawn and Mr DJ Barron).

7.2.4*a* *Intraoperative anaesthesia*

The anaesthetic technique was tailored according to the pre-procedure evaluation of cardiovascular function and the individual preference of the paediatric cardiac anaesthetist. However, the intraoperative anaesthesia used during the TCPC was essentially the same as that used during the formation of the BCPA (Chapter 6). The differences between the two techniques are highlighted in the following section.

Anaesthesia was induced using either inhalational or intravenous techniques, as previously described (Chapter 6). In some older children, anaesthesia was induced using intravenous propofol (3 – 5 $mg \cdot kg^{-1}$). However, total intravenous anaesthesia was not used in any of the children [507]. Maintenance anaesthesia invovled the same techniques described in Chapter 6.

Following intubation, the patient was mechanically ventilated using a ventilator in pressure-control mode. The ventilator circuit and ventilatory settings were identical to those used during the formation of the BCPA (Chapter 6).

After anaesthesia was established, an arterial cannula was inserted, ideally in the radial artery. A 4.5-French triple-lumen central venous catheter was inserted into the internal jugular vein. Nasopharyngeal and oesophageal temperature probes were inserted, a skin temperature probe

was attached and the urinary bladder was catheterised. The ECG, peripheral oxygen saturations, arterial and central venous pressures, core and skin temperature, end-tidal CO_2 and isoflurane concentrations and inspired oxygen tension were monitored continuously. Urine output and arterial blood gases were measured intermittently.

7.2.4*b* *Cardiopulmonary bypass management*

The TCPC was performed using bicaval cardiopulmonary bypass (CPB) with the heart beating [294]. The aorta was cross-clamped in those cases in which concomitant intracardiac procedures were performed, during which time myocardial protection was afforded by intermittent cold crystalloid cardioplegia [294,368]. None of the patients involved in the current study required concomitant intracardiac procedures.

Cardiopulmonary bypass was performed by one of two clinical perfusion scientists (Mr RG Willetts or Mrs A Horsburgh). The heart-lung machine and CPB management used during the procedure were generally the same as those described in Chapter 6. The only difference related to the type of fluid used to fill the CPB circuit before surgery. A 'clear prime' was used for all the children involved in this study. This consists of 500ml isotonic electrolyte solution (Plasmalyte 148; Baxter Healthcare, Norfolk, United Kingdom) and 100 – 500ml of colloidal plasma volume substitute (Gelofusine; Braun Medical Ltd, Sheffield, United Kingdom), supplemented with 3000 IU heparin sodium, 20 $mg \cdot kg^{-1}$ methylprednisolone and 0.5 $g \cdot kg^{-1}$mannitol.

Patients were fully heparinised prior to start of CPB and adequate anticoagulation was maintained throughout the procedure (Chapter 6). After successful separation from CPB at the end of the procedure, protamine sulphate was administered to correct the anticoagulation. Remaining blood in the perfusion circuit was processed and re-transfused during the early post-operative period as described in Chapter 6.

In this study, the median CPB time was 62 minutes (range, 45 – 101 minutes).

7.2.4*c* *Operative technique*

The TCPC was performed at a median age of 4.9 years (range, 3.8 – 9.1 years) and a median weight of 18.3 kg (range, 13.3 – 24.6 kg). The procedure was performed via a redo median sternotomy. Following take down of adhesions and mobilisation of the great vessels, the child was placed on CPB. In patients with antegrade pulmonary blood flow through the native pulmonary artery (n=4), this blood flow was then controlled using a vascular clamp applied to the main pulmonary artery. The TCPC involved the interposition of a 20 mm GORE-TEX® tube conduit (W. L. Gore & Associates (UK) Ltd.) between the IVC and the right pulmonary artery with extension to the central pulmonary artery (Figure 7.2) [294,368]. As a result, systemic venous blood in the SVC and IVC can flow freely into both the left and the right pulmonary arteries. A 5 mm or 5.5 mm fenestration was intentionally created in the Fontan circuit in all except one patient (n=25). This involved a side-to-side anastomosis between the extracardiac conduit and the lateral wall of the right atrium.

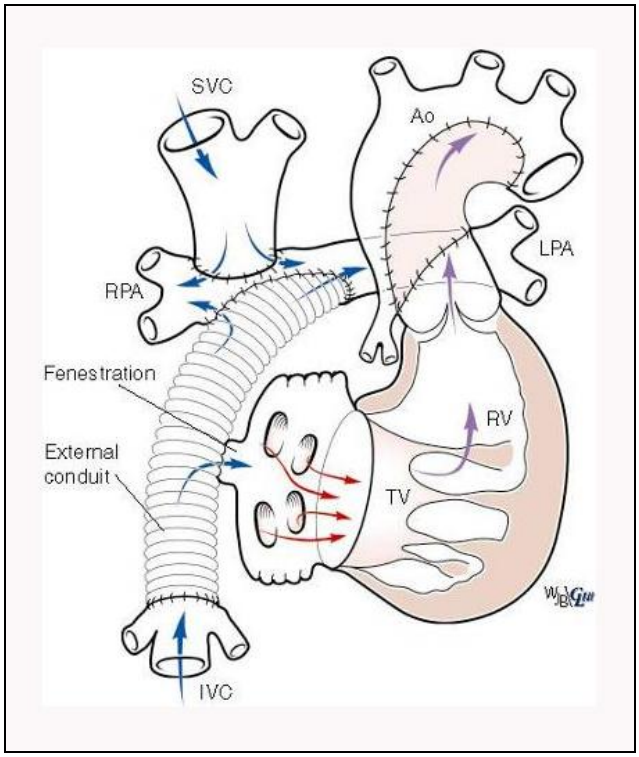

Figure 7.2 *Diagram illustrating the completion TCPC. This procedure connects the IVC to the pulmonary arteries using a tube conduit. A small fenestration is usually created between the systemic venous pathway and the pulmonary venous atrium (illustrated). Reproduced from Brawn & Barron* [482].

Concomitant surgical procedures were performed in six patients. This involved ligation of the main pulmonary artery (n=4), pulmonary artery patch augmentation of the central pulmonary arteries (n=1) and repair of an incidental right-sided diaphragmatic hernia (n=1).

Cardiopulmonary bypass was weaned and discontinued when the patient was warm and haemodynamically stable. A right atrial pressure monitoring line was inserted into the right atrium. A mediastinal drain and bilateral pleural drains were inserted at the end of the procedure. A GORE-TEX® membrane (W.L. Gore & Associates (UK) Ltd.) was attached to the pericardial edges. The sternotomy was formally closed in all patients prior to transfer to the intensive care unit. Patients were routinely transferred on a dobutamine infusion (5 - 10 $\mu g \cdot kg^{-1} \cdot min^{-1}$). Additional inotropic and vasodilator therapy was administered as clinically indicated.

7.2.4*d* *Post-operative care*

Following completion TCPC, all patients were recommenced on oral diuretic therapy. Patients with impaired ventricular function or clinically important systemic AVV regurgitation usually also received an angiotensin converting enzyme inhibitor [294,368]. All of the patients were anticoagulated with a lifelong warfarin regimen. The warfarin dose was adjusted to maintain an international normalized ratio of 2.0 – 3.0 [368].

7.2.5 Experimental protocol

This study was performed in conjunction with normal clinical practice, as described in the preceding section. Following median sternotomy and systemic heparinisation, a nylon tape was placed around the IVC. This tape could be used to temporarily reduce ventricular preload as part of the study protocol.

7.2.5*a* *Instrumentation*

Simultaneous intraventricular pressure and volume measurements were made using a 5F integrated pressure-conductance catheter (SCD-550; Millar Instruments). The catheter, together with the details of the pressure-conductance measurements have been described in Chapter 2.

A purse-string suture was placed in the right atrium. The conductance catheter was inserted into the right atrium through this suture via a 6F sheath (Cordis). The catheter was then passed across the atrio-ventricular valve into the dominant ventricle. The position of the catheter in the ventricle was confirmed by visual inspection of the segmental conductance volume signals. Measurements were only acquired if 5 or more segmental ventricular volume signals were obtained.

The pressure signal from the pressure-conductance catheter was amplified using a combined amplifier-interface unit (PCU-2000; Millar Instruments) connected to the signal processor unit (CFL-512, CD Leycom). Micromanometer pressure measurements were statically zeroed in a bath of normal saline at the level of the mid-axillary line.

Aortic flow was measured continuously with a perivascular transit-time ultrasound flow meter (HT 323; Transonic Systems Europe B.V.) connected to a flow probe (A-series flow probes; Transonic Systems Europe B.V.) that was positioned around the ascending aorta. Stroke volume was calculated from the integrated aortic flow signal.

The signal outputs from the combined amplifier-interface unit (intraventricular pressure), the transit-time ultrasound flow meter (aortic flow) and the lead II surface ECG were each connected to the CFL-512 to allow simultaneous recordings.

7.2.5*b* *Data acquisition*

The study protocol included three separate sets of measurements. Measurements were made:

- Prior to the institution of CPB without inotropic support ("*Baseline*");
- Prior to the institution of CPB following the administration of dobutamine (10 $\mu g \cdot kg^{-1} \cdot min^{-1}$) for 10 minutes ("*Baseline* + *dobutamine*");
- Following completion of the surgical procedure, complete rewarming and weaning from cardio-pulmonary bypass support on 10 $\mu g \cdot kg^{-1} \cdot min^{-1}$ dobutamine ("*TCPC*").

This protocol allowed the effects of dobutamine in patients with a BCPA and the TCPC to be separately quantified.

Intraventricular pressure and volume; aortic pressure and flow; and ECG measurements were made under both steady-state conditions and during transient (5 – 10s) inferior vena caval occlusion (IVCO). All measurements were made with the chest open at end-expiration.

Absolute time-varying ventricular volume measurements, $V(t)$ were obtained from the segmental conductance signals using Equation 7.2. This equation takes into account the inter-electrode distance on the catheter, L and the specific resistivity of blood, ρ [381].

Equation 7.2 $$V(t) = \frac{1}{\alpha} \cdot L^2 \cdot \left(\sum_{i=1}^{5} G_i - G_P \right),$$

where α is the dimensionless calibration coefficient and G_P is parallel conductance.

The specific resistivity of 5ml of blood, ρ was measured immediately before and after CPB using the 4-electrode cuvette connected to the CFL-512 (CD Leycom).

The changes in the specific resistivity of blood are summarised in Table 6.2. The statistical analyses used in such comparisons are described more fully later (Section 6.2.6). Nevertheless, it is sufficient to note that the specific resistivity of blood, ρ decreased significantly after CPB. This primarily reflects the haemodilution that occurred during CPB, with a fall in the haemoglobin concentration and haematocrit (Table 7.2).

Variable	Baseline	TCPC
Specific blood resistivity, ρ	185 ± 21	119 ± 9*
Parallel conductance, G_P (ml)	127 ± 81	94 ± 87
Calibration coefficient, α	2.13 ± 1.42	2.10 ± 1.52
Haemoglobin ($g \cdot dl^{-1}$)	14.3 ± 1.2	10.3 ± 1.1*
Haematocrit (%)	42 ± 3	30± 3*

Table 7.2 *Conductance catheter calibration factors, haemoglobin and haematocrit at Baseline and following TCPC. Data expressed as mean ± SD.*

* *$P<0.05$ versus Baseline as assessed by a paired two-tail Student t-test.*

Conductance volume measurements were retrospectively calibrated for the dimensionless calibration coefficient, α and parallel conductance, G_P. The dimensionless calibration coefficient, α was calculated by dividing the average conductance-derived stroke volume ($\overline{Q}_{SV}$) by the average stroke volume ($\overline{SV}_{AoF}$) calculated from the integrated aortic flow measurements under steady-state conditions. In patients with antegrade blood flow through the native pulmonary artery, the main pulmonary artery was occluded during the period when study measurements were made.

Parallel conductance, G_P was calculated using the hypertonic saline method originally described by Baan *et al.* [381], which is discussed in detail in Chapter 3. In this study, parallel conductance was separately calculated following the injection of 0.25 ml·kg^{-1} and 0.5 ml·kg^{-1} 10% hypertonic saline into the SVC. Parallel conductance was measured before CPB and following CPB. These measurements were also made during end-expiration. It was assumed that parallel conductance was not altered by the administration of dobutamine.

7.2.5*c* *Technical considerations*

Complete pressure-volume measurements were acquired in all patients.

Adverse events occurred in two patients included in the study. One patient (Patient number 4) developed a marked bradycardia associated with profound hypotension following the first hypertonic saline injection post-CPB. This lasted for approximately 45 seconds and necessitated the administration of a bolus of adrenaline (0.9 μg·kg^{-1}) with subsequent normalisation of the haemodynamics. This event occurred after complete data acquisition and these data have been included in the Results.

One other patient (Patient number 10) developed a significant unexpected ischaemic brain injury that resulted in brain death. Treatment was withdrawn and the patient died 2 days following surgery. An internal investigation was undertaken to investigate the cause of death, which concluded that the study was not implicated in this adverse event. Data from this patient have also been included in the Results.

As with the previous clinical study (Chapter 6), application of the caval tourniquet and introduction of the vascular sheath were uncomplicated. The conductance catheter was introduced into the dominant ventricle via the right atrium. Insertion of the pressure-conductance catheter was safely performed in all patients. Occasionally, placement of the catheter caused ventricular extrasystolic beats, but a stable catheter position without arrhythmias could always be obtained.

The management of the conductance catheter during cardiopulmonary bypass was identical to that described in Chapter 6. After the second set of measurements (i.e. Baseline + dobutamine), the conductance catheter was withdrawn, rinsed with normal saline and left in a bowl of normal saline to be re-used after the TCPC. The introducer sheath in the right atrium was removed during surgery and the incision temporarily closed with the purse-string suture. Catheter placement and all measurements were completed within approximately 30 minutes.

7.2.5*d* *Data analysis*

Data have been analysed in exactly the same manner as in Chapter 6.

Baseline haemodynamic data were calculated from steady-state intraventricular pressure-volume measurements. These included: heart rate (***HR***), end-systolic volume (***ESV***), end-diastolic volume (***EDV***), end-systolic pressure (P_{ES}), end-diastolic pressure (P_{ED}), cardiac output (***CO***), stroke volume (***SV***), stroke work (***SW***), maximal and minimal rate of ventricular pressure change (dP/dt_{MAX}, dP/dt_{MIN}), ejection fraction (***EF***) and the relaxation time constant (tau). Volume measurements have been normalised to the body surface area (BSA) using the method proposed by DuBois & DuBois [485]. The volume measurements are expressed as indexed volumes.

End-systole was defined as the period during ejection where time-varying elastance was maximal [45]. This corresponds with the upper left-hand corner of the pressure volume loop (Figure 7.3). End-diastole was defined as the peak R-wave of the surface ECG [434]. However, all of the ventricular volumes in this study were characterised by an interference pattern that related to the intraventricular ECG signal (***ECGc***). This was essentially the same phenomenon observed during

the other clinical study (Chapter 6). The ECG interference pattern was associated with an end-diastolic volume measurement overestimate of 9 ± 23% [see Chapter 5].

Therefore, for the purposes of this study, end-diastolic volume was approximated as the ventricular volume at dP/dt_{MAX} (*EDV'*). *EDV'* always occurred before the onset of ejection (defined as the start of antegrade blood in the ascending aorta). In the absence of any AVV regurgitation, *EDV'* was assumed equivalent to the true *EDV*.

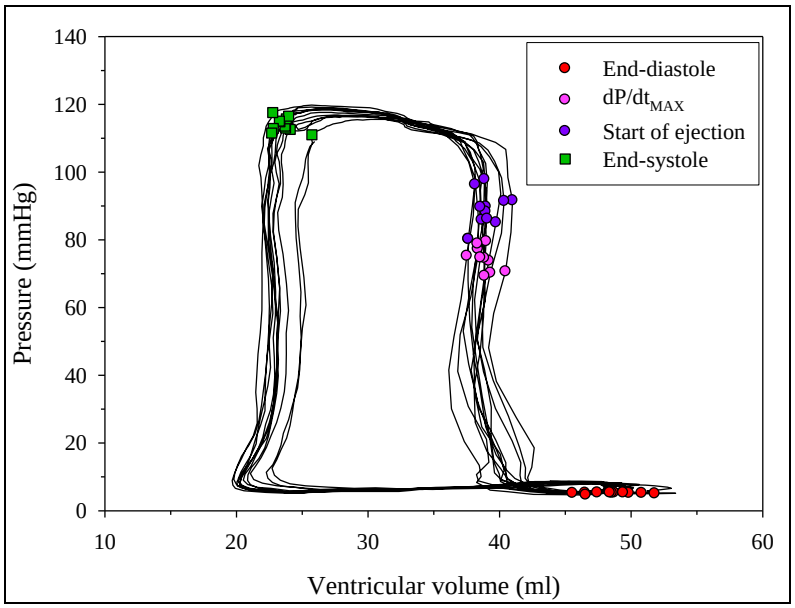

Figure 7.3 *Representative example of the intraventricular pressure-volume loop from a Baseline study. Points corresponding to end-diastole (red circles),* dP/dt_{MAX} *(pink circles); the start of ejection (purple circles) and end-systole (green squares) for each beat are illustrated.*

The end-diastolic volume was also calculated as a percentage of the normal left ventricular or right ventricular volume (*%N-EDV'*) and the ejection fraction was calculated as a percentage of the normal left ventricular ejection fraction (*%N-EF*), as previously described (Chapter 6).

Indices of ventricular systolic and diastolic function were derived from pressure-indexed volume measurements made during temporary occlusion of the IVC. The systolic indices included the end-systolic pressure-volume relation (*ESPVR*, E_{es}) [45]; the dP/dt_{MAX}-*EDV'* relation [108]; and preload-recruitable stroke work relation (*PRSW*) [109]. Each relationship was characterised by the

slope and volume intercept. Diastolic chamber stiffness was calculated based on the end-diastolic pressure-volume relationship.

Vascular load was estimated using the effective arterial elastance, Ea. The Ea/Ees and SW/PVA ratios were calculated as indices of ventricular efficiency [81]. The Ea/Ees ratio reflects the ventriculo-vascular coupling efficiency whereas the SW/PVA ratio reflects the mechanical efficiency of the ventricle [81]. The SW/PVA ratio was calculated using the method described by Nozawa *et al.* [491], Equation 7.4.

Equation 7.4 $$SW/PVA = 1/\left(+0.5\cdot Ea\right)\ Ees\cdot 100 .$$

7.2.6 Statistical analysis

The statistical procedures used in this Chapter as exactly the same as those used in Chapter 5.

Steady-state measurements were repeated two or three times. Extrasystolic and post extrasystolic beats were retrospectively identified and excluded from analysis. In each steady-state measurement, data from 10 consecutive cardiac cycles were then analysed. The estimated within-experiment standard deviation for volume measurements (EDV' and ESV) was 2.2 ml. The estimated within-experiment standard deviation for pressure measurements (P_{ED} and P_{ES}) was 1.0 mmHg. As these represented <5% of the absolute volume or pressure measurement, all subsequent analyses were based on the average data from each measurement.

Measurements made during IVCO were also repeated two or three times. Extrasystolic and post extrasystolic beats were retrospectively identified and excluded from analysis. Heart rate did not generally change during preload reduction. However, in order to eliminate potential heart rate effects, only beats for which heart rate varied by less than 5% of baseline were used for analysis. Indices of systolic and diastolic function were calculated using the first 9 heart beats following transient IVCO that met the inclusion criteria using least square linear regression [110,112]. For each index, the slope of the relationship was identified. In addition, the x-axis (i.e. volume) intercept for E_{ES} was also calculated [492].

The haemodynamic parameters, indices of ventricular function and indices of vascular load and ventriculo-vascular coupling were obtained at Baseline; Baseline + dobutamine; and following TCPC. The effect of dobutamine was determined by comparing data at Baseline with data at Baseline + dobutamine. Similarly, the effect of the formation of TCPC was separately established by comparing data at Baseline + dobutamine with data at TCPC. Data at Baseline and following TCPC were not compared directly, as this does not address a relevant clinical question.

Data were analysed using SPSS for Windows (v16, SPSS Inc., Chicago, Il, USA). All values were expressed as mean ± SD. A probability $P<0.05$ was considered statistically significant in all comparisons.

The effects of dobutamine and the formation of the superior CP shunt on the steady-state haemodynamic data were analysed using the paired two-tail Student's *t*-test. The influence of ventricular morphology was then analysed using a two-way analysis of variance (ANOVA) followed by Bonferroni correction. The Bonferroni test was used for post hoc analyses.

The effects of dobutamine, the formation of the superior CP shunt and ventricular morphology on indices of ventricular function calculated during IVCO were separately analysed using a two-way analysis of variance (ANOVA) followed by Bonferroni correction. All replicate measurements were included in these analyses, which fully accounted for the expected correlation between repeated observations. Again, the Bonferroni test was used for post hoc analyses.

7.3 RESULTS

7.3.1 Clinical outcomes

In the present study, there was one early death. The patient developed an ischaemic cerebral injury that resulted in brain death, This death was unexplained, occurring after an apparently uneventful operation and intensive care course [294]. None of the patients required acute takedown of the Fontan circulation for Fontan failure.

One patient required early reoperation for continued early post-operative bleeding from the sternotomy. The median duration of pleural drainage was 11 days (range, 5 – 30 days). Six patients had prolonged pleural drainage with persistent drainage for 14 days or more. Three of these patients had chylothoraces, with chylomicrons in the pleural fluid. The median length of in-patient hospital stay was 14 days (range, 8 – 32 days). Four patients had a prolonged hospital stay (≥21 days). This included the three patients with chylothoraces and one other patient with a prolonged non-chylous pleural effusion.

7.3.2 Parallel conductance and dimensionless calibration coefficient

The changes in parallel conductance, G_P and the dimensionless calibration coefficient, α are summarised in Table 6.2. Parallel conductance, G_P, decreased from 127 ± 81 ml to 94 ± 87 ml after the TCPC. However, this change was not statistically significant (P=0.07). There was no significant change in the dimensionless calibration coefficient, α. There was similarly no significant change in the dimensionless calibration coefficient following the administration of dobutamine (2.13 ± 1.42 versus 2.04 ± 1.28; P=NS). However, there was a substantial variation between patients. For example, pre-CPB parallel conductance measurements varied between 5.5 – 263 ml. This finding reaffirms the need to calibrate all conductance volume measurements on an individual basis.

7.3.3 Coefficient of variation for indices of ventricular function

Indices of systolic and diastolic ventricular function showed variability between repeated measurements. The coefficient of variation (SD/mean · 100) together with its standard deviation was 18 ± 12% for E_{ES}, 16 ± 14% for $PRSW$ and 18 ± 11% for dP/dt_{MAX}-EDV' [461]. The coefficient of variation for chamber stiffness was 20 ± 16%.

7.3.4 Haemodynamic data

The haemodynamic parameters for the twenty-six patients with complete data and at the three time-points are summarised in Table 7.3 – 7.5.

Overall, patients were characterised by only mild dilatation of the single functional ventricle. The indexed EDV' at Baseline was 57 ± 35, which is within the limits found by Graham *et al.* for normal left and right ventricles [490,493]. Nevertheless, in this study there was mild impairment of global ventricular function. The normalised ejection fraction ($\%N$-EF) was 66 ± 24%, which is outside the range of left ventricular ejection fraction in normal patients found by Graham *et al.* [490].

Haemodynamic parameter	Baseline	Baseline + dobutamine	TCPC
Heart rate (bpm)	101 ± 14	118 ± 23 *	140 ± 20 †
Cardiac index ($L \cdot min^{-1} \cdot m^{-2}$)	2.5 ± 0.7	3.1 ± 1.0 *	2.5 ± 0.8 †
Indexed stroke volume ($ml \cdot m^{-2}$)	24 ± 8	26 ± 10	18 ± 7 †
Ejection fraction (%)	50 ± 18	49 ± 19	53 ± 15
Normalised ejection fraction (%)	66 ± 24	64 ± 26	70 ± 20
Indexed *EDV'* ($ml \cdot m^{-2}$)	57 ± 35	61 ± 26	39 ± 25 †
Normalised *EDV'* (%)	87 ± 50	93 ± 38	60 ± 38 †
P_{ED} (mmHg)	5.9 ± 4.3	7.3 ± 5.5	6.7 ± 4.4
Indexed *ESV* ($ml \cdot m^{-2}$)	33 ± 34	35 ± 25	22 ± 12 †
P_{ES} (mmHg)	66 ± 18	83 ± 25 *	77 ± 18
Stroke work ($mmHg \cdot ml^{-1} \cdot m^{-2}$)	1771 ± 731	2350 ± 918 *	1465 ± 557 †
dP/dt_{MAX} ($mmHg \cdot s^{-1}$)	1070 ± 363	2345 ± 1300 *	2360 ± 962
dP/dt_{MIN} ($mmHg \cdot s^{-1}$)	-1068 ± 317	-1598 ± 621 *	-1518 ± 499
Tau (s)	$1.50 \cdot 10^{-4}$ ± $0.38 \cdot 10^{-4}$	$1.21 \cdot 10^{-4}$ ± $0.27 \cdot 10^{-4}$ *	$1.61 \cdot 10^{-4}$ ± $0.48 \cdot 10^{-4}$

Table 7.3 *Haemodynamic parameters at three intra-operative time-points.*

* *P<0.05 versus Baseline;*

† *P<0.05 versus Baseline + dobutamine.*

	Baseline		Baseline + dobutamine		TCPC	
Index of ventricular function	Slope	Intercept (ml)	Slope	Intercept (ml)	Slope	Intercept (ml)
E_{ES} (mmHg·ml^{-1}·m^{-2})	3.1 ± 1.8	-16 ± 75	4.6 ± 2.3 *	3.7 ± 2.1	6.6 ± 4.2	-0.7 ± 91
dP/dt_{MAX}-EDV' (mmHg·s^{-1}·ml^{-1}·m^{-2})	41 ± 18	-	141 ± 96 *	-	160 ± 96	-
PRSW (mmHg·m^{-2})	56 ± 29	-	80 ± 29	-	85 ± 43	-
Chamber stiffness (ml^{-1})	0.06 ± 0.03	-	0.07 ± 0.07	-	0.06 ± 0.05	-

Table 7.4 *Indices of ventricular function at three intra-operative time-points.*

* *P<0.05 versus Baseline;*

† *P<0.05 versus Baseline + dobutamine.*

Parameter	Baseline	Baseline + dobutamine	TCPC
Ea (mmHg·ml^{-1}·m^{-2})	3.3 ± 0.7	3.5 ± 1.6 *	5.7 ± 2.6 †
Ea / E_{ES}	1.9 ± 0.7	1.5 ± 0.7 *	1.8 ± 0.9
SW / PVA (%)	56 ± 12	61 ± 14 *	58 ± 16

Table 7.5 *Indices of vascular load and ventriculo-vascular coupling efficiency at three intra-operative time-points.*

* *P<0.05 versus Baseline;*

† *P<0.05 versus Baseline + dobutamine.*

7.3.5 Influence of dobutamine infusion

Figure 7.4 illustrates typical steady-state pressure, dP/dt and volume signals and the corresponding pressure-volume loop measured prior to cardiopulmonary bypass with and without dobutamine (Baseline and Baseline + dobutamine).

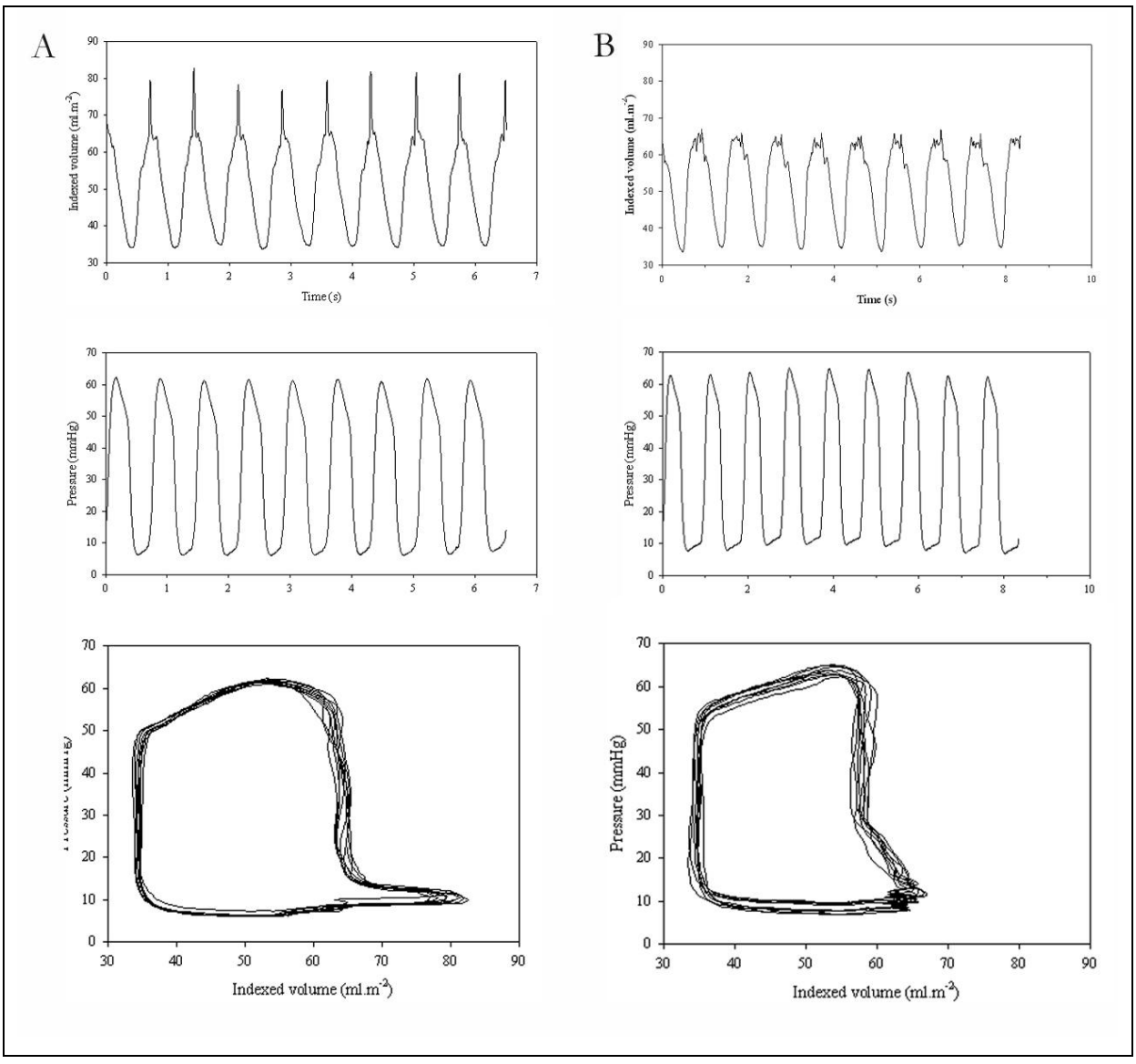

Figure 7.4 *Typical steady-state volume (upper panel) and pressure signals (middle panel) together with the corresponding pressure-volume loop (lower panel) at Baseline* (A) *and Baseline + dobutamine* (B).

Figure 7.5 illustrates the corresponding pressure-volume loop during IVCO together with various systolic and diastolic pressure-volume relations (*E_{ES}*, *EDPVR*, *PRSW* and *dP/dt_{MAX}-EDV*).

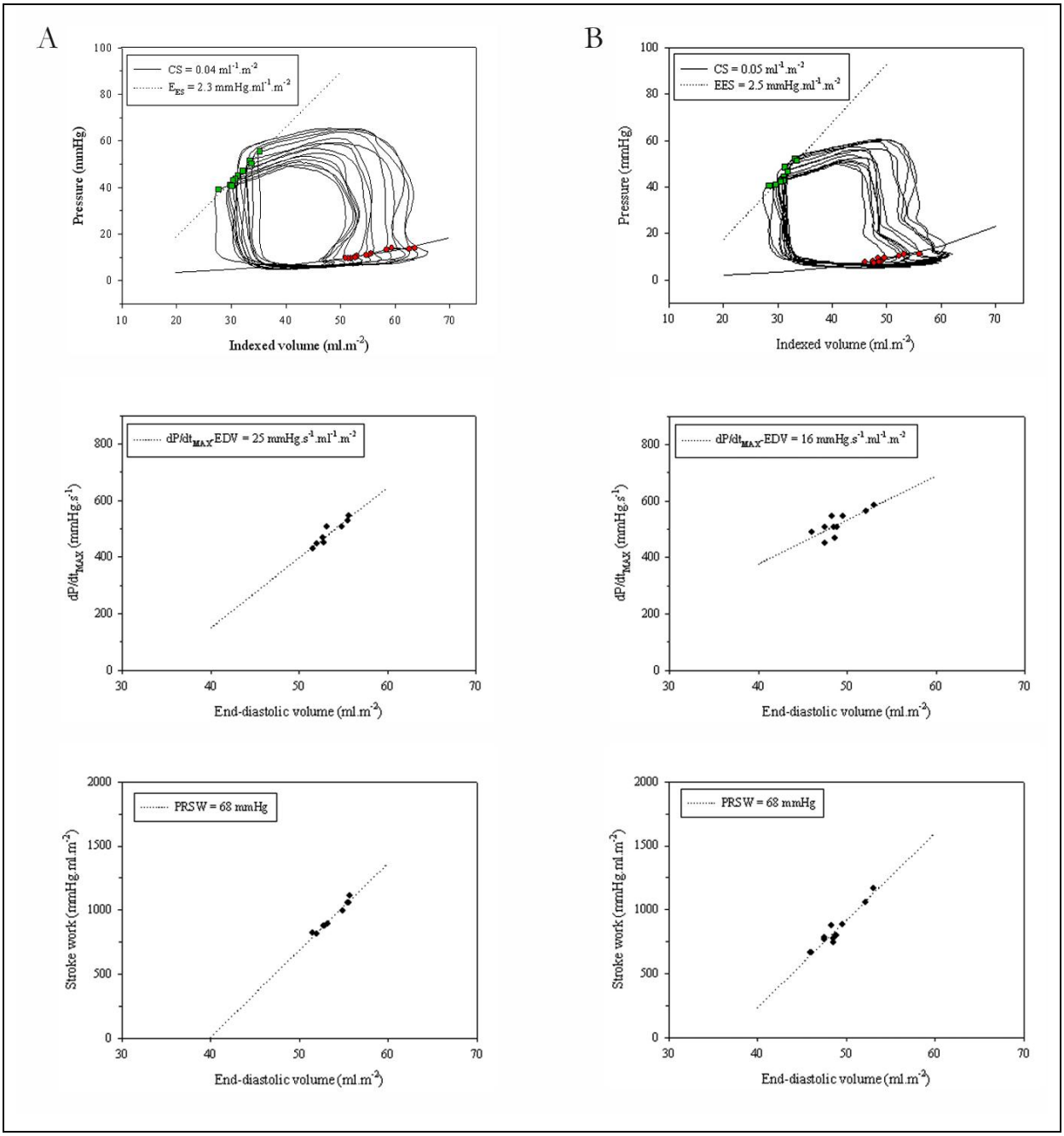

Figure 7.5 *Typical example of pressure-volume relations derived during IVC occlusion at Baseline and Baseline + dobutamine. In this patient, there was no significant change in systolic function with dobutamine. The slope of the E_{ES} (upper panel), dP/dt_{MAX}-EDV (middle panel) and PRSW relations (lower panel) were similar at the two time-points. This was in contrast with the group as a whole. There was no change in EDPVR or chamber stiffness (upper panel). The selected end-diastolic (red circles) and end-systolic points (green squares) are identified.*

Dobutamine was associated with an increase in the heart rate (P<0.05). Dobutamine was also associated with an increase in the end-systolic pressure and a corresponding increase in the maximal and minimal rate of pressure change (P<0.05, respectively). There was no change in the end-diastolic pressure.

There was no change in the indexed end-diastolic or end-systolic volumes, indexed stroke volume or ejection fraction following dobutamine infusion. Nevertheless, dobutamine was associated with an increase in the indexed stroke work and cardiac index, and also associated with a significant shortening of the relaxation time constant (tau).

Dobutamine was associated with an overall improvement in ventricular systolic function. For example, the E_{ES} increased from 3.1 ± 1.8 mmHg·ml^{-1}·m^{-2} to 4.6 ± 2.3 mmHg·ml^{-1}·m^{-2} (P<0.05) and dP/dt_{MAX}-EDV' increased from 41 ± 18 mmHg·s^{-1}·ml^{-1}·m^{-2} to 141 ± 96 mmHg·s^{-1}·ml^{-1}·m^{-2} (P<0.05). There was also an overall increase in $PRSW$ (56 ± 29 mmHg·m^{-2} versus 80 ± 29 mmHg·m^{-2}), although this change was not statistically significant (P<0.06). However, there was no change in the diastolic compliance of the ventricle (chamber stiffness).

There was a significant increase in vascular load (effective arterial elastance) following dobutamine infusion. In spite of this increased vascular load, there was a significant reduction in the ventriculo-vascular coupling ratio (Ea/E_{ES}) and also a significant increase in the SW/PVA ratio.

7.3.6 Effect of completion total cavo-pulmonary connection

Figure 7.6 illustrates typical steady-state pressure, dP/dt and volume signals and the corresponding pressure-volume loop measured at Baseline + dobutamine and following the TCPC.

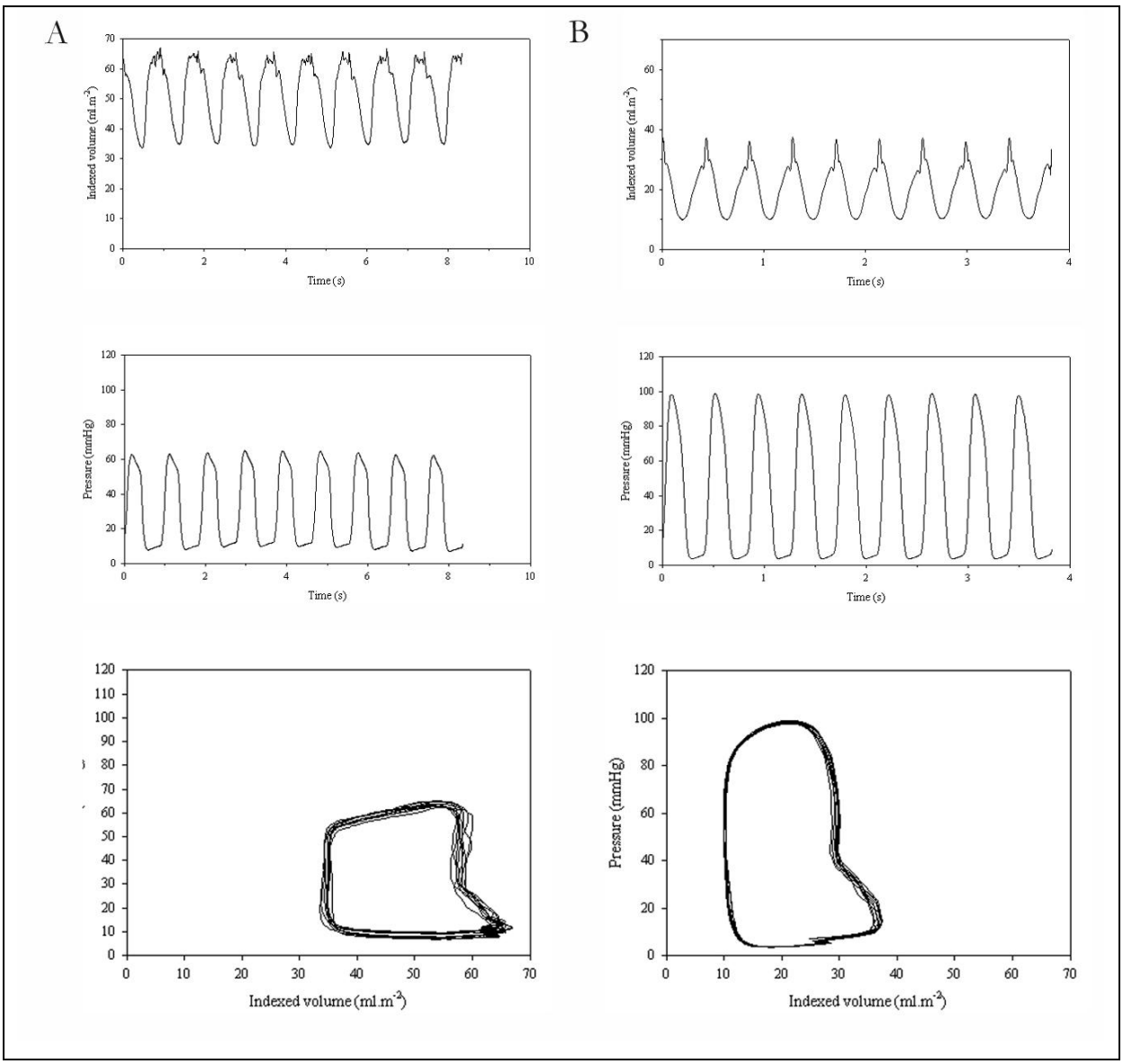

Figure 7.6 *Typical steady-state volume (upper panel) and pressure signals (middle panel) together with the corresponding pressure-volume loop (lower panel) at Baseline + dobutamine* (A) *and following TCPC* (B)*. The steady-state pressure-volume loops show a significant reduction in end-diastolic and end-systolic volumes with a reduction in the stroke work following TCPC.*

Figure 7.7 illustrates the corresponding pressure-volume loop during IVCO together with various systolic and diastolic pressure-volume relations (E_{ES}, *EDPVR*, *PRSW* and dP/dt_{MAX}-*EDV'*).

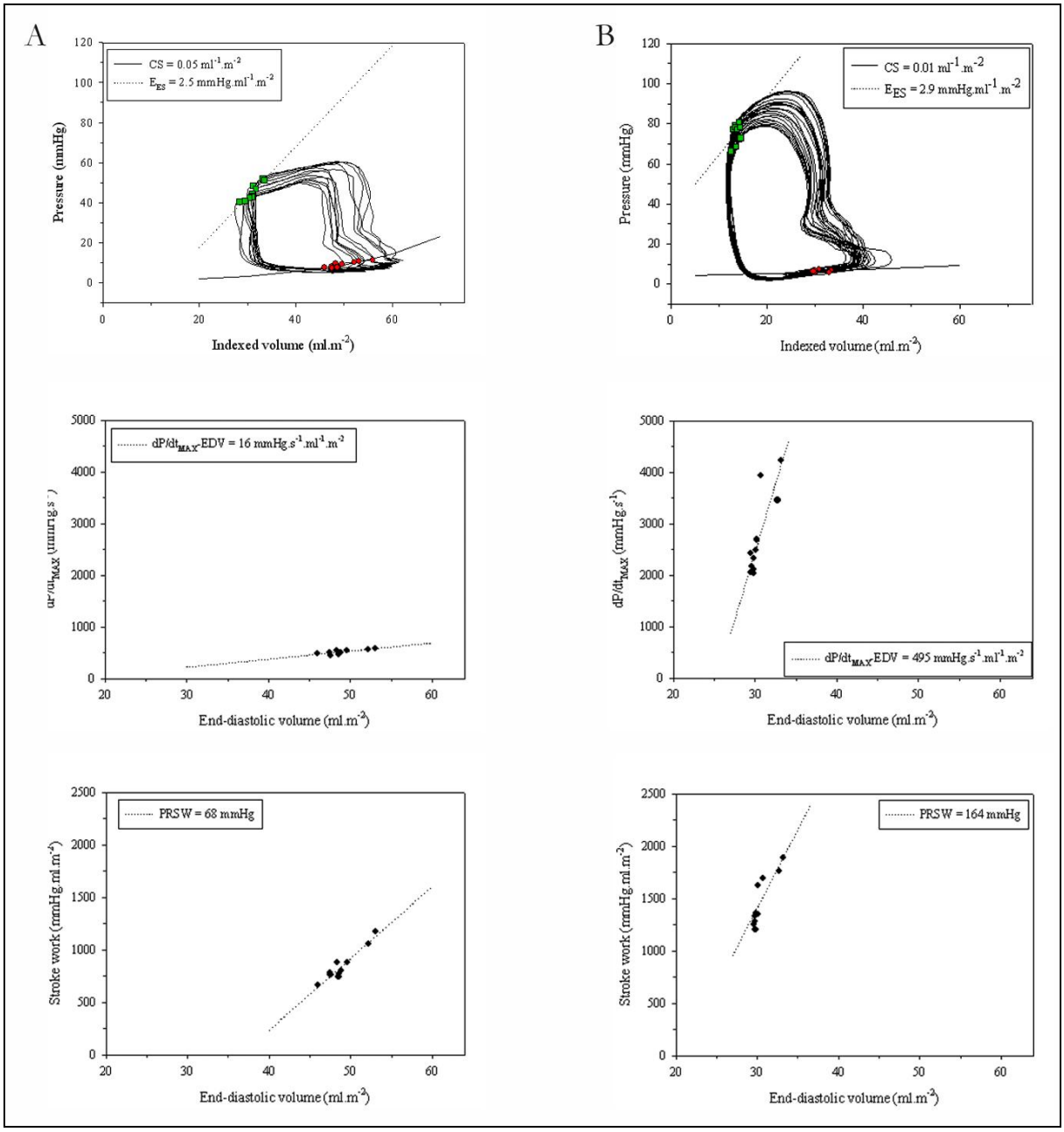

Figure 7.7 *Typical example of pressure-volume relations derived during IVC occlusion at Baseline + dobutamine (A) and TCPC (B). In this patient, there was an increase in systolic function following the TCPC, with an increase in the slope of the* E_{ES} *(upper panel),* dP/dt_{MAX}-*EDV' (middle panel) and* *PRSW* *relation (lower panel). There was no change in the* *EDPVR* *following TCPC. The selected end-diastolic (red circles) and end-systolic points (green squares) are identified.*

The TCPC was associated with a further increase in the heart rate ($P<0.05$). In spite of this change, there was no change in maximal and minimal rate of pressure change nor was there a change in the end-diastolic or end-systolic pressure.

The TCPC was associated with a reduction in the indexed end-diastolic and end-systolic volumes ($P<0.05$), stroke volume ($P<0.05$) and stroke work ($P<0.05$). These changes are illustrated on the pressure-volume loop (Figure 6.6). The pressure-volume loop following TCPC is narrower and shifted to the left of the plot when compared with the corresponding Baseline + dobutamine curve. There was also a decrease in the cardiac index, which declined from 3.5 ± 1.0 $L \cdot min^{-1} \cdot m^{-2}$ to 2.5 ± 0.8 $L \cdot min^{-1} \cdot m^{-2}$ ($P<0.05$).

The TCPC was not associated with significant changes in ventricular systolic function or chamber stiffness.

The TCPC was also associated with a significant increase in the effective arterial elastance, Ea, which increased from 3.5 ± 1.6 $mmHg \cdot ml^{-1} \cdot m^{-2}$ to 5.7 ± 2.6 $mmHg \cdot ml^{-1} \cdot m^{-2}$ ($P<0.05$). However, there was no change in the ventriculo-vascular coupling ratio (Ea/E_{ES}) or mechanical efficiency of the ventricle (SW/PVA) following completion TCPC.

7.3.7 Influence of ventricular morphology

Figure 7.8 illustrates typical steady-state pressure-volume loops that were obtained in two patients under equivalent loading conditions. One patient (patient number 21) had a dominant ventricle of left ventricular morphology (mLV) while the other patient (patient number 23) had a dominant ventricle of right ventricular morphology. The overall shape of the pressure-volume loops were broadly similar. Both groups demonstrated a well-defined end-systolic "shoulder" (i.e. upper left hand corner) and both groups had a clearly identifiable isovolumic relaxation phase.

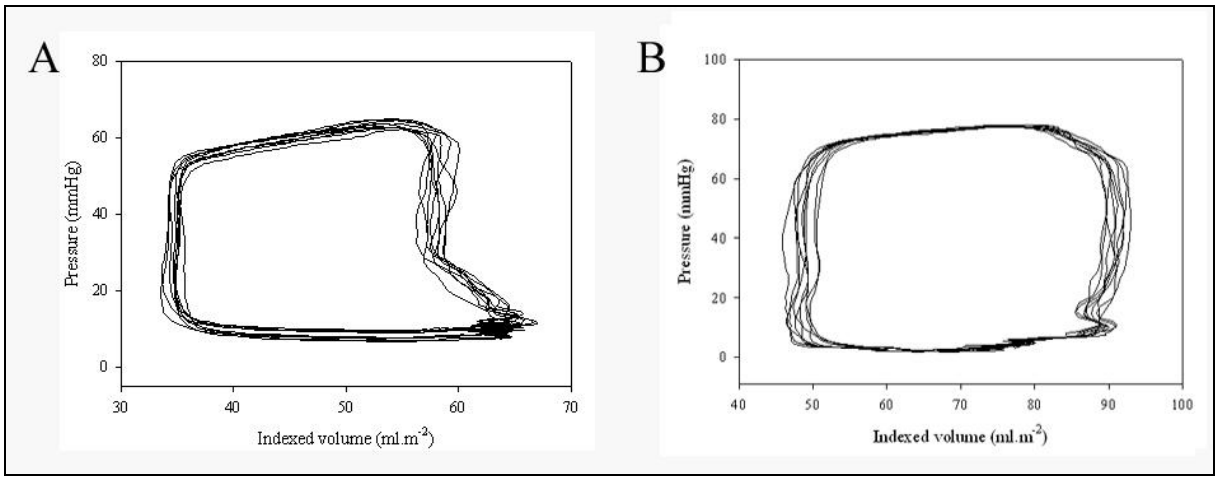

Figure 7.8 *Typical ventricular pressure-volume loops in patients with either (A) a morphologic left ventricle or (B) a morphologic right ventricle. Measurements were obtained at Baseline + dobutamine.*

Intraventricular pressure-volume measurements in patients with a mLV and mRV were comparable at all three time-points. There was no difference in the steady-state haemodynamic parameters; indices of ventricular function; or indices of vascular load and ventriculo-vascular coupling between the two groups. In addition, ventricular morphology did not influence the relative change in any of the parameters following either dobutamine infusion or the TCPC.

7.4 DISCUSSION

The management of children with functionally single ventricle generally involves three staged operations that culminate in the Fontan procedure. The Fontan procedure results in the complete bypass of the right side of the heart, by connecting the systemic venous return directly to the pulmonary arteries. This procedure establishes a circulatory pattern that is as normal as possible in patients with functionally single ventricle anatomy [292].

The circulation established following the Fontan procedure is not normal. The Fontan circulation is characterised by a high afterload [341,343,350,508], which primarily relates to the in-series arrangement of the systemic and pulmonary circulations [328]. The lack of pulsatile blood flow within the pulmonary circulations also contributes to increase the effective ***PVR*** [326,350,509-512]. The additional resistance imposed by the pulmonary vasculature in-series with the systemic

venous return explains the propensity of these patients to develop effusions and protein-losing enteropathy [509].

Completion of the Fontan circulation is also associated with an acute reduction in the volume load of the single functional ventricle [343]. The ventricular volume is reduced to approximately 70% of the normal indexed left ventricular volume [513,514]. Marc Gewillig proposed that this chronic reduction in the volume load may result in the development of a "disuse hypofunction", with a progressive decline in ventricular systolic function [336]. In addition, the chronic reduction in volume load may also be responsible for the development of diastolic dysfunction, which is observed in these patients [346,515].

The abnormal pressure and volume loading conditions limit the ability of the Fontan circulation to adapt to higher ventricular energy requirements [502]. As a result, the Fontan circulation is generally characterised by a decreased cardiac output at rest and during exercise [339,340,516]. However, only a limited number of clinical studies have been undertaken to assess how the changes in load affect ventricular function or the performance of the cardiovascular system in the era of staged surgical palliation [343,351].

The current study has confirmed that the completion TCPC is associated with an increase in the total vascular load, as measured using the effective arterial elastance, Ea [85]. There was a 63% increase in the overall effective arterial elastance following the TCPC. The magnitude of this change is greater than that observed by Tanoue *et al.* (20% change) [343]. This may reflect differences in the method used to calculate effective arterial elastance or the additional effects of cardiopulmonary bypass on the vascular system [517].

The TCPC is also associated with a reduction in the volume load of the dominant ventricle. The indexed end-diastolic and end-systolic volumes were reduced by 56% and 59%, respectively. This was associated with a corresponding reduction in the stroke volume and stroke work. Overall, there was a reduction in the cardiac index in spite of a significant increase in the resting heart rate. These finding are consistent with the previous studies [339,343,351].

In addition, this study has identified a number of clinically important findings. It has demonstrated that the TCPC is not associated with any significant change in the systolic or diastolic function, in spite of the substantial reduction in volume loading. Indeed, there was a small increase in all of the indices of ventricular systolic function, although these changes were not statistically significant. Furthermore, this study showed that there is no acute change in the performance of the cardiovascular system (measured using the Ea/E_{ES} ratio and ejection fraction, EF) or the efficiency of the heart (as measured using the SW/PVA ratio). These findings are in agreement with the study by Tanoue *et al.* [351].

In addition to describing the effects of the completion TCPC as a whole, this study was designed to determine the influence of dominant ventricular morphology on the changes in ventricular function. As discussed in Chapter 1, there is a long-standing concern that the mRV may be intrinsically less well suited to support either the systemic circulation or the entire circulation. In two separate studies, Julsrud *et al.* and Gentles *et al.* each identified a mRV as an independent risk factor for early failure following a modified Fontan procedure [231,232]. However, in a more recent study, McGuirk *et al.* reported that the morphology of the dominant ventricle did not influence early mortality, 5-year actuarial survival or functional capacity following the Fontan procedure [368].

The present study has demonstrated that ventricular performance is maintained following the TCPC, at least acutely, and there is no significant difference in the steady-state haemodynamic parameters; indices of ventricular function; or indices of vascular load and ventriculo-vascular coupling between patients with a mLV or mRV. This represents an important clinical finding that may provide some reassurance about the long-term outlook for these children. These findings support our clinical data that demonstrated that ventricular morphology did not influence the early or actuarial survival following the Fontan procedure [368].

7.4.1 Study Limitations

The conductance catheter technique is associated with two well-known sources of error, which are described in detail in Chapter 2 and Chapter 5. Conductance volume measurements must therefore be calibrated in order to obtain absolute volume measurements. Calibration is itself associated with errors that potentially affect the accuracy of the volume measurements. However, as was discussed in Chapter 5, it is felt that the errors associated with calibration do not materially alter the conclusions of the present study.

7.5 CONCLUSION

The completion TCPC is associated with an immediate reduction in ventricular volume and an increase in vascular load. These changes in loading conditions are not associated with any significant change in ventricular systolic or diastolic function; ventriculo-vascular coupling or mechanical efficiency of the ventricle. This indicates that the procedure does not have any adverse effects on cardiac function. The changes in end-systolic elastance indicate that systolic function may have improved, although this did not reach statistical significance. Importantly, similar changes were observed in patients with either a morphologic left or morphologic right ventricle. Long-term follow-up studies are necessary to determine whether these changes persist beyond the immediate post-operative period.

CHAPTER 8

GENERAL DISCUSSION AND CONCLUSIONS

CHAPTER 8. GENERAL DISCUSSION AND CONCLUSIONS

The studies described in this thesis were designed to investigate ventricular function in children with various forms of congenital heart disease that are characterised by functionally single ventricle anatomy. The management of these children generally involves three separate operations that are performed during the first few years of life [292]. This thesis focussed on the acute, intra-operative changes that occurred following the bidirectional cavo-pulmonary anastomosis (BCPA; Stage II) and the modified Fontan procedure (Stage III).

Ventricular function has been assessed, in both the preliminary studies using a model ventricle and in the subsequent clinical studies, with invasive pressure and volume measurements made using a pressure-conductance catheter. In the clinical studies, this catheter was inserted directly into the cavity of the single functional ventricle and measurements were made before and immediately after surgical intervention. The pressure-conductance catheter provides simultaneous, real-time measurements of pressure and volume. In addition, it allows construction of dynamic pressure-volume loops and calculation of the instantaneous pressure-volume relation. Analysis of the ventricular pressure-volume relation has evolved as the dominant approach to the assessment of global ventricular function [95,384,465]. It provides a number of relatively load-independent indices of ventricular systolic and diastolic function [95,96,460,518] that enable a more sophisticated and precise measurement of global ventricular performance than examination of cardiac function based on changes in volume or pressure alone [95]}[96].

There is a substantial body of evidence to support the value of the conductance catheter in the assessment of ventricular function in paediatric patients [66,519,520] and during cardiac surgery [521-526]. In particular, it provides the most accurate method of determining myocardial contractility in vivo. However, this technique has not previously been used to examine ventricular function in children with functionally single ventricle anatomy. This poses a number of problems that relate, in particular, to the size, shape and morphology of the ventricle in these patients. Parallel conductance may also be different. All of these factors could influence quality and accuracy of pressure-volume measurements obtained. Therefore, initial studies were undertaken

to assess the accuracy of the conductance volume measurements in a model that more accurately reflected the clinical conditions that occur in functional single ventricle anatomy.

Initial studies described in Chapters 4 and 5 were performed using a physical model of the left ventricle that had previously been developed in this laboratory [98]. The experiments described in Chapter 4 confirmed that there was a non-linear relationship between conductance and absolute volume measurements. As a result, ideally conductance volume measurements should be calibrated using an alternative volume measurement. However, this study also demonstrated that the dimensionless calibration coefficient, α varied as a function of both the absolute volume and the type of calibration coefficient used. Using a fixed or constant calibration coefficient, particularly one derived from an alternate stroke volume measurement, would introduce measurement errors. These measurement errors were potentially significant during acute changes in loading conditions, like those seen during surgical palliation in children with functionally single ventricle anatomy.

In an ideal world, I would have liked to calibrate the conductance volume measurements made in this thesis using an independent method of volume measurement. In principle, one might envisage simultaneous volume measurements using echocardiography or magnetic resonance imaging, for example. However, it would not have been practicable or clinically appropriate to perform magnetic resonance imaging during the surgical procedures described in this thesis. Two-dimensional echocardiography is often used in the operating theatre, using either a trans-oesophageal probe or a probe placed on the epicardium [294,368]. However, two-dimensional echocardiography is associated with limited accuracy [527,528] and is subject to substantial inter-observer measurement error [529,530], particularly when used to measure right ventricular volume [384]. At Birmingham Children's Hospital, two-dimensional echocardiography is not used to routinely measure ventricular volume, especially in children with functionally single ventricle anatomy.

For these reasons, conductance volume measurements made in the clinical studies (Chapters 5 and 6) were calibrated using an alternative measurement of stroke volume. These measurements

were calculated from integrated aortic flow measurements made using a transit-time ultrasound flowmeter with a perivascular flowprobe around the ascending aorta. The results presented in Chapter 4 indicated that the conductance-stroke volume quotient, α_{SV} was associated with significant volume measurement error. However, the extent to which this influenced the results presented in the clinical studies may have been lessened by within-subject comparison.

Chapter 5 described a further series of experiments that investigated the effects of additional electrical signals on the accuracy of conductance volume measurements. This study identified for the first time that the accuracy of conductance volume measurements can be adversely affected by the other electrical signals, including a simulated ventricular electrogram. The ventricular electrogram produced a clinically important volume measurement error that meant end-diastole could neither be precisely identified nor accurately measured, as illustrated in Figure 5.1, 6.6 and Figure 7.3. As a result, end-diastolic volume was approximated as the ventricular volume at dP/dt_{MAX}, which occurred during the isovolumic contraction phase. Nonetheless, measurement error associated with ventricular depolarisation has important implications for the quantitative assessment of chamber stiffness made using the conductance catheter technique.

While this study (Chapter 5) has identified that electrical signals within the ventricular cavity can alter the measured conductance, it was first thought that this problem should be easy to resolve. In principle, it would appear possible to limit the frequency bandwidth of the recording system to filter the intracavitary electrogram. It was suggested that this could be achieved with a 10 Hz filter. Unfortunately, this also would have removed potentially important data form the conductance volume signal.

Of course, the physical model provided only a limited simulation of the single functional ventricle. The model assumed that parallel conductance was zero. This was important so that a true measure of the dimensionless calibration coefficient factor, α was obtained. Further work is still required to define how increments in ventricular volume and changes in ventricular shape affect parallel conductance; and to define the relationship between parallel conductance and the dimensionless calibration coefficient factor, α. Are changes in one the dimensionless calibration

coefficient, α always accompanied by changes in the parallel conductance and vice versa, as some investigators have suggested [402]? These are questions that remain to be answered but which were outside the scope of the present thesis.

Nevertheless, the initial studies on three different sized model ventricles provided a clear indication of the performance characteristics of the pressure-conductance catheter under standardised controlled conditions. It was then possible to have greater confidence in the interpretation of the data subsequently obtained in the real-life clinical studies and to understand better the limitations.

Thus on the completion of the preliminary studies, two clinical studies were undertaken to investigate the separate effects of the BCPA (Chapter 6) and the completion total cavo-pulmonary connection (TCPC; Chapter 7) on ventricular function. To characterise pump function of the single ventricle, pressure-volume loops were constructed. These gave an indication of stroke volume, ejection fraction, cardiac output and stroke work. An important limitation of these indices is that they are all load-dependent. A series of relatively load-independent indices of systolic and diastolic function were also derived [112-114], by measuring the instantaneous pressure-volume relations over a series of beats during preload reduction (e.g. IVCO).

The first clinical study (Chapter 6) demonstrated that the BCPA was associated with an immediate and substantial reduction in ventricular volume. This, in turn, was associated with a substantial improvement in systolic function but also a decrease in the diastolic compliance. The formation of the BCPA was also accompanied by an increase in vascular load, although this did not alter the ventriculo-vascular coupling or mechanical efficiency of the ventricle. The procedure resulted in the ventricle become less spheroid and more ellipsoid in shape. Theoretically, this should improve pump performance, just as this study observed. These findings provide further support to the concept that the BCPA should be performed as early as possible in order to help preserve the myocardium and ventricular function [531,532].

The second clinical study demonstrated that the completion TCPC (and the formation of the Fontan circulation) was associated with an immediate reduction in ventricular volume and an increase in vascular load. However, these changes in loading conditions did not adversely affect ventricular systolic or diastolic function; ventriculo-vascular coupling or mechanical efficiency of the ventricle. Systolic function may even have improved, although this change was not statistically significant.

In both clinical studies, ventricular function was measured immediately following the surgical procedure. Ventricular function at this stage is likely to be modified by the effects of anaesthesia [533], cardiopulmonary bypass [534,535] as well as the surgical procedure itself. The true benefits of the procedure may only become apparent once the heart has fully recovered. The early changes in post-operative ventricular function [536] could not be investigated as part of this study because it would not be safe or practicable to leave the conductance catheter in situ for that time.

In addition to describing the effects of the two procedures, this thesis also sought to determine whether the morphology of the dominant ventricle influenced the change in ventricular function. Both studies demonstrated that similar changes were evident in patients with a single functional ventricle of left or right ventricular morphology. Further studies will be required to ascertain whether this similarity persists, but it is encouraging to note that the midterm survival and functional status of these two groups are also comparable [294,368].

Finally, it would be extremely valuable to determine how the ventricular function in this group of patients' changes with time. Unfortunately, the data presented in this thesis does not answer this question. There is currently no information to determine how ventricular function (based on the pressure-volume relations) changes with time in either normal children or children with congenital heart disease. In my opinion, one of the most important areas of future research should be the characterisation of normal pressure-volume relations and the changes with age. Obviously, it would not be appropriate to use invasive intraventricular pressure-volume

measurements. However, a less invasive approach, incorporating cardiac MRI and invasive arterial pressure measurements may be feasible.

Pressure-volume analysis using the conductance catheter is a powerful technique for the assessment of ventricular performance. The studies in this thesis have confirmed and extended our current knowledge. They have shown that the technique has some limitations and hence the data have to be interpreted with caution. However, the technique is the best available for the assessing changes in the function of the heart. The use of this technique for the first time in children with a functionally single ventricle anatomy, as described in this thesis, has enabled direct and more precise measurements of the physiological changes that accompany surgical palliation. These findings confirm the validity of current clinical practice in the management of children with a functionally single ventricle anatomy.

APPENDIX A

TRANSFER FUNCTION TO DEFILTER FLOW MEASUREMENTS MADE USING A TRANSIT-TIME ULTRASOUND FLOWMETER

APPENDIX A. TRANSFER FUNCTION TO DEFILTER MEASUREMENTS MADE USING A TRANSIT-TIME ULTRASOUND FLOWMETER

A.1 MATLAB CODE FOR TRANSFER FUNCTION (UNFILTEREDFLOW.M)

```
colheaderss=[colheaders {'none'}];
[x,v] = listdlg ('PromptString', 'Select AoF signal to defilter:', 'SelectionMode', 'single', 'ListString',
colheaderss, 'InitialValue', 13);
if v == 0
errordlg ('No AoF signal selected' , 'AoF Selection Error');
end
lgnd = colheaderss(x);
if x ~= length (colheaderss)
        y1 = data;
        y = y1 (: , x);
        for ii=1:length(x)
                dFdt(:,ii) = fiveptder (y (:, ii), 250);
                dF2dt (:,ii) = fiveptder (dFdt (:, ii), 250);
                b = 2*pi*5.2;
                num = [1,sqrt(2)*b,b*b] / b / b;
                AoFnew (:, ii) = dF2dt (:, ii) * num (1) + num (2) *dFdt (:, ii) + num (3) * y (:, ii);
                [B,A] = butter (2,85 / 125);
                AoFnewfilt (:, ii) = filterfilter (B, A, AoFnew (:, ii));
        end
        newvarcol = length(colheaders) + 1;
        colheaders{newvarcol}=[lgnd{1} '_defiltered'];
        data(:, newvarcol) = AoFnewfilt;
        t = 1:length(y);
plot (t/fs, y, '.', t/fs, AoFnewfilt)
title ('Plot of UnFiltered Data before Butterworth Filter');
xlabel('Time (seconds)');
ylabel('Units depend on signal');
legend('Filtered Data', 'Unfilered Data');
end
```

APPENDIX B

STERILISATION PROTOCOL FOR MILLAR PRESSURE-CONDUCTANCE CATHETER

APPENDIX B. STERILISATION PROTOCOL FOR MILLAR DUAL PRESSURE-CONDUCTANCE CATHETER

B.1 INTRODUCTION

Each Millar dual pressure-conductance catheters is licensed for re-use up to 5 times. After each application, the catheter was thoroughly cleaned and sterilised using ethylene oxide gas according to the manufacturer's guidelines. Ethylene oxide sterilisation was performed at the Hospital Sterile Supply Unit (HSSU); Sandwell & West Birmingham NHS Trust. The manufacturer's guidelines are reproduced in the following sub-sections.

B.1.1 Initial cleaning protocol

1. Immediately following removal from the patient, immerse the catheter in cold water;
2. Wipe the catheter with wet swab to remove all blood products;
3. Soak in detergent solution for 20 minutes, e.g. Alconox® (10 $g \cdot l^{-1}$);
4. Wipe the catheter again and rinse in fresh, pyrogen-free water three times;
5. Carefully dry the catheter;
6. Re-pack catheter in tray supplied by manufacturer and send to sterilisation unit.

A plastic ring was attached to the catheter following each use. Catheters were withdrawn from clinical use when they had been re-used five times.

B.1.2 Ethylene oxide sterilisation cycle parameters used at HSSU

- Concentration: 1100 $mg \cdot l^{-1}$
- Pressure: 15 – 20 Atm
- Time: 1 hour 40 minutes
- Temperature: 55º C
- Humidity: 50%

The catheter was stored for two weeks after sterilisation, in order to allow the complete evaporation of any residual Ethylene Oxide.

APPENDIX C

STERILISATION PROTOCOL FOR TRANSONIC A-SERIES FLOW PROBES

APPENDIX C. STERILISATION PROTOCOL FOR TRANSONIC A-SERIES FLOW PROBES

C.1 INTRODUCTION

Transonic A-series flow probe can be re-used after appropriate cleaning and ethylene oxide gas sterilisation. Ethylene oxide sterilisation was performed at the Hospital Sterile Supply Unit (HSSU); Sandwell & West Birmingham NHS Trust. The manufacturer's guidelines are reproduced in the following sub-sections.

C.1.1 Initial cleaning protocol

7. Following removal from the patient, remove all excess soil from the instrument;
8. Clean the probe for 3-5 minutes with a soft brush and either detergent or alcohol;
9. Rinse in clean water;
10. Carefully dry the instrument;
11. Send for ethylene oxide sterilisation.

C.1.2 Ethylene oxide sterilisation cycle parameters used at HSSU

- Concentration: 1100 $mg \cdot l^{-1}$
- Pressure: 15 – 20 Atm
- Time: 1 hour 40 minutes
- Temperature: 55º C
- Humidity: 50%

The catheter was stored for two weeks after sterilisation, in order to allow the complete evaporation of any residual Ethylene Oxide.

REFERENCES

REFERENCES

1. Best, C.H., Taylor, N.B. and West, J.B. *Best and Taylor's physiological basis of medical practice* 12th ed. Baltimore: Williams & Wilkins; 1991.

2. Ho, S.Y., Anderson, R.H. and Sanchez-Quintana, D. Atrial structure and fibres: morphologic bases of atrial conduction. *Cardiovascular Research*. 2002;54:325-36.

3. Anderson, R.H., Ho, S.Y., Redmann, K., Sanchez-Quintana, D. and Lunkenheimer, P.P. The anatomical arrangement of the myocardial cells making up the ventricular mass. *European Journal of Cardio-thoracic Surgery*. 2005;28:517-525.

4. Forbes, M.S. and Sperelakis, N. Intercalated discs of mammalian heart: A review of structure and function. *Tissue and Cell*. 1985;17:605-768.

5. Huxley, A.F. and Niedergerke, R. Structural changes in muscle during contraction; interference microscopy of living muscle fibres. *Nature*. 1954;173:971-3.

6. Huxley, H. and Hanson, J. Changes in the cross-striations of muscle during contraction and stretch and their structural interpretation. *Nature*. 1954;173:973-6.

7. Sonnenblick, E.H. and Skelton, C.L. Reconsideration of the ultrastructural basis of cardiac length-tension relations. *Circulation Research*. 1974;35:517-526.

8. Downing, S.E. and Sonnenblick, E.H. Cardiac Muscle Mechanics and Ventricular Performance: Force and Time Parameters. *American Journal of Physiology*. 1964;207:705-15.

9. Sonnenblick, E.H. Correlation of myocardial ultrastructure and function. *Circulation*. 1968;38:29-44.

10. Braunwald, E., Ross Jr., J. and Sonnenblick, E.H. *Mechanisms of contraction of the normal and failing heart*. 2nd ed. Boston: Little, Brown and Co.; 1976.

11. Sonnenblick, E.H. Force-velocity relations in mammalian heart muscle. *American Journal of Physiology*. 1962;202:931-939.

12. Sonnenblick, E.H., Spiro, D. and Cottrell, T.S. Fine structural changes in heart muscle in relation of the lengthtension curve. *Proceedings of the National Academy of Sciences of the United States of America*. 1963;49:193-200.

13. Spiro, D. and Sonnenblick, E.H. Comparison of the ultrastructural basis of the contractile process in heart and skeletal muscle. *Circulation Research*. 1964;15, Suppl. 2:14-37.

14. Sonnenblick, E.H., Spotnitz, H.M. and Spiro, D. Role of the sarcomere in ventricular function and the mechanism of heart failure. *Circulation Research*. 1964;15, Suppl. 2:70-81.

15. Frank, O. Zur dynamik des herzmuskels. *Zeitschrift fur Biologie*. 1895;32:370-437.

16. Starling, E.H. and Visscher, M.B. The regulation of the energy output of the heart. *Journal of Physiology*. 1926;62:243-261.

17. Mirsky, I. and Parmley, W.W. Assessment of passive elastic stiffness for isolated heart muscle and the intact heart. *Circulation Research*. 1973;33:233-43.

18. Gay Jr., W.A. and Johnson, E.A. An anatomical evaluation of the myocardial length-tension diagram. *Circulation Research*. 1967;21:33-43.

19. Tarr, M., Trank, J.W., Leiffer, P. and Shepherd, N. Sarcomere length-resting tension relation in single frog atrial cardiac cells. *Circulation Research*. 1979;45:554-9.

20. Winegrad, S. Resting sarcomere length-tension relation in living frog heart. *Journal of General Physiology*. 1974;64:343-55.

21. Fish, D., Orenstein, J. and Bloom, S. Passive stiffness of isolated cardiac and skeletal myocytes in the hamster. *Circulation Research*. 1984;54:267-76.

22. Katz, A.M. The descending limb of the Starling curve and the failing heart. *Circulation*. 1965;32:871-5.

23. Brutsaert, D.L. and Sonnenblick, E.H. Cardiac muscle mechanics in the evaluation of myocardial contractility and pump function: problems, concepts, and directions. *Progress in Cardiovascular Diseases*. 1973;16:337-61.

24. Parmley, W.W., Chuck, L. and Sonnenblick, E.H. Relation of Vmax to Different Models of Cardiac Muscle. *Circulation Research*. 1972;30:34-43.

25. Pollack, G.H. Maximum Velocity as an Index of Contractility in Cardiac Muscle: A critical evaluation. *Circulation Research*. 1970;26:111-127.

26. Sonnenblick, E.H., Spiro, D. and Spotnitz, H.M. The Ultrastructural Basis of Starling's Law of the Heart. The Role of the Sarcomere in Determining Ventricular Size and Stroke Volume. *American Heart Journal*. 1964;68:336-46.

27. Ross, J., Jr., Covell, J.W., Sonnenblick, E.H. and Braunwald, E. Contractile State of the Heart Characterized by Force-Velocity Relations in Variably Afterloaded and Isovolumic Beats. *Circulation Research*. 1966;18:149-163.

28. Frank, O. Isometrie und isotonie des herzmuskels. *Zeitschrift fur Biologie*. 1901;412:13-34.

29. Spotnitz, H.M., Sonnenblick, E.H. and Spiro, D. Relation of ultrastructure to function in the intact heart: sarcomere structure relative to pressure volume curves of intact left ventricles of dog and cat. *Circulation Research*. 1966;18:49-66.

30. Lorenz, C.H., Pastorek, J.S. and Bundy, J.M. Delineation of normal human left ventricular twist throughout systole by tagged cine magnetic resonance imaging. *Journal of Cardiovascular Magnetic Resonance*. 2000;2:97-108.

31. Frank, O. Die Grundform des arteriellen Pulses. Erste Abhandlung. Mathematische Analyse. *Zeitschrift fur Biologie*. 1898;37:483-526.

32. Sonnenblick, E.H., Ross, J., Jr., Covell, J.W., Spotnitz, H.M. and Spiro, D. The ultrastructure of the heart in systole and diastole. Chantes in sarcomere length. *Circulation Research*. 1967;21:423-31.

33. Zimmer, H.-G. Who discovered the Frank-Starling mechanism? *News in Physiological Sciences*. 2002;17:181-4.

34. Suga, H. and Sagawa, K. Assessment of absolute volume from diameter of the intact canine left ventricular cavity. *Journal of Applied Physiology*. 1974;36:496-9.

35. Sagawa, K., Maughan, L., Suga, H. and Sunagawa, K. *Cardiac contraction and the pressure-volume relationship*. New York: Oxford University Press, Inc.; 1988.

36. Katz, L.N. Analysis of several factors regulating the performance of the heart. *Physiological Reviews*. 1955;35:90-106.

37. Patterson, S.W., Piper, H. and Starling, E.H. The regulation of the heartbeat. *Journal of Physiology*. 1914;48:465-613.

38. Kozawa, S. The mechanical regulation of the heart beat in the tortoise. *Journal of Physiology*. 1915;49:233-245.

39. Sulzer, R. Die mechanischen Eigenschaften der Herzmuskels. *Zeitschrift fur Biologie*. 1932;92:545-554.

40. Reichel, H. and Kapel, E. Die Mechanik des Herzens bei Aenderung des arteriellen Drucks. *Zeitschrift fur Biologie*. 1939;99:63-79.

41. Ullrich, K.J., Riecker, G. and Kramer, K. Das Druckvolumdiagramm des Warmbluterherzens. Isometriche Gleichgewichtskurven. *Pflügers Archiv - European Journal of Physiology*. 1954;259:481-498.

42. Monroe, R.G., French, G. and Whittenberger, J.L. Effects of hypocapnia and hypercapnia on myocardial contractility. *American Journal of Physiology*. 1960;199:1121-4.

43. Monroe, R.G. and French, G.N. Left ventricular pressure-volume relationships and myocardial oxygen consumption in the isolated heart. *Circulation Research*. 1961;9:362-74.

44. Jacob, R. and Weigand, K.H. Die endsystolischen Druck-Volumenbeziehungen als Grundlage einer Beurteilung der Kontraktilitaet des linken Ventrikels in situ. *Pflügers Archiv - European Journal of Physiology*. 1966;289:37-49.

45. Suga, H., Sagawa, K. and Shoukas, A.A. Load independence of the instantaneous pressure-volume ratio of the canine left ventricle and effects of epinephrine and heart rate on the ratio. *Circulation Research*. 1973;32:314-22.

46. Sagawa, K. The ventricular pressure-volume diagram revisited. *Circulation Research*. 1978;43:677-87.

47. Wiggers, C.J. Dynamics of ventricular contraction under abnormal conditions. *Circulation*. 1952;5:321-348.

48. Milnor, W.R. *Cardiovascular physiology*. Oxford: Oxford University Press; 1990.

49. Anderson, R.H., Ho, S.Y. and Becker, A.E. The surgical anatomy of the conduction tissues. *Thorax*. 1983;38:408-20.

50. Noble, D. *The initiation of the heartbeat*. 2nd ed. Oxford: Clarendon Press; 1979.

51. Durrer, D., van Dam, R.T., Freud, G.E., Janse, M.J., Meijler, F.L. and Arzbaecher, R.C. Total excitation of the isolated human heart. *Circulation*. 1970;41:899-912.

52. Spach, M.S. and Barr, R.C. Ventricular intramural and epicardial potential distributions during ventricular activation and repolarization in the intact dog. *Circulation Research*. 1975;37:243-57.

53. Anderson, R.H. and Ho, S.Y. The morphologic substrates for pediatric arrhythmias. *Cardiology in the Young*. 1991;1:159-176.

54. Wiggers, C.J. Studies in the consecutive phases of the cardiac cycle. *American Journal of Physiology*. 1921;56:415-459.

55. Brutsaert, D.L., Rademakers, F.E. and Sys, S.U. Triple control of relaxation: implications in cardiac disease. *Circulation*. 1984;69:190-6.

56. Sagawa, K. The end-systolic pressure-volume relation of the ventricle: definition, modifications and clinical use. *Circulation*. 1981;63:1223-7.

57. Maughan, W.L., Shoukas, A.A., Sagawa, K. and Weisfeldt, M.L. Instantaneous pressure-volume relationship of the canine right ventricle. *Circulation Research*. 1979;44:309-15.

58. Suga, H. End-systolic pressure-volume relations. *Circulation*. 1979;59:419-420.

59. Hori, M., Yeliin, E.L. and Sonnenblick, E.H. Left ventricular diastolic suction as a mechanism of ventricular filling. *Japanese Circulation Journal*. 1982;46:124-9.

60. Suga, H., Goto, Y., Igarashi, Y., Yamada, O., Nozawa, T. and Yasumura, Y. Ventricular suction under zero source pressure for filling. *American Journal of Physiology*. 1986;251:H47-55.

61. Ohno, M., Cheng, C.P. and Little, W.C. Mechanism of altered patterns of left ventricular filling during the development of congestive heart failure. *Circulation*. 1994;89:2241-50.

62. Sheehan, F. and Redington, A.N. The right ventricle: Anatomy, physiology and clinical imaging. *Heart*. 2008;94:1510-1515.

63. Shaver, J.A., Nadolny, R.A., O'Toole, J.D., Thompson, M.E., Reddy, P.S., Leon, D.F. and Curtiss, E.I. Sound pressure correlates of the second heart sound. An intracardiac sound study. *Circulation*. 1974;49:316-25.

64. Redington, A.N., Gray, H.H., Hodson, M.E., Rigby, M.L. and Oldershaw, P.J. Characterisation of the normal right ventricular pressure-volume relation by biplane angiography and simultaneous micromanometer pressure measurements. *British Heart Journal*. 1988;59:23-30.

65. Topham, W.S. Comparison of methods for calculation of left ventricular stroke work *Journal of Applied Physiology*. 1969;27:767-769.

66. Derrick, G.P., Narang, I., White, P.A., Kelleher, A., Bush, A., Penny, D.J. and Redington, A.N. Failure of stroke volume augmentation during exercise and dobutamine stress is unrelated to load-independent indexes of right ventricular performance after the Mustard operation. *Circulation*. 2000;102:III154-9.

67. Redington, A.N., Rigby, M.L., Shinebourne, E.A. and Oldershaw, P.J. Changes in the pressure-volume relation of the right ventricle when its loading conditions are modified. *British Heart Journal*. 1990;63:45-9.

68. von Spiegel, T., Wietasch, G. and Hoeft, A. Basics of myocardial pump function. *Thoracic & Cardiovascular Surgeon*. 1998;46 Suppl 2:237-41.

69. Guyton, A.C. Determination of cardiac output by equating venous return curves with cardiac response curves. *Physiological Reviews*. 1955;35:123-9.

70. Bishop, V.S. and Horwitz, L.D. Left ventricular transverse internal diameter: Value in studying left ventricular function. *American Heart Journal*. 1970;80:507-14.

71. Hansen, R.M., Viquerat, C.E., Matthay, M.A., Wiener-Kronish, J.P., DeMarco, T., Bahtia, S., Marks, J.D., Botvinick, E.H. and Chatterjee, K. Poor correlation between pulmonary arterial wedge pressure and left ventricular end-diastolic volume after coronary artery bypass graft surgery. *Anesthesiology*. 1986;64:764-70.

72. Lichtwarck-Aschoff, M., Zeravik, J. and Pfeiffer, U.J. Intrathoracic blood volume accurately reflects circulatory volume status in critically ill patients with mechanical ventilation. *Intensive Care Medicine*. 1992;18:142-7.

73. Bishop, V.S. and Horwitz, L.D. Quantitative assessment of cardiac pump performance. *Journal of Physiology*. 1977;269:355-70.

74. Weber, K.T. and Hawthorne, E.W. Descriptors and determinants of cardiac shape: an overview. *Federation Proceedings*. 1981;40:2005-10.

75. Milnor, W.R. Arterial impedance as ventricular afterload. *Circulation Research*. 1975;36:565-70.

76. Westerhof, N., Elzinga, G. and Sipkema, P. An artificial arterial system for pumping hearts. *Journal of Applied Physiology*. 1971;31:776-81.

77. Westerhof, N., Lankhaar, J.-W. and Westerhof, B.E. The arterial Windkessel. *Medical & Biological Engineering & Computing*. 2009;47:131-141.

78. Avolio, A., Westerhof, B.E., Siebes, M. and Tyberg, J.V. Arterial hemodynamics and wave analysis in the frequency and time domains: an evaluation of the paradigms. *Medical & Biological Engineering & Computing*. 2009;47:107-10.

79. Maughan, W.L., Sunagawa, K., Burkhoff, D. and Sagawa, K. Effect of arterial impedance changes on the end-systolic pressure-volume relation. *Circulation Research*. 1984;54:595-602.

80. Nichols, W.W. and Pepine, C.J. Left ventricular afterload and aortic input impedance: implications of pulsatile blood flow. *Progress in Cardiovascular Diseases*. 1982;24:293-306.

81. Sunagawa, K., Maughan, W.L., Burkhoff, D. and Sagawa, K. Left ventricular interaction with arterial load studied in isolated canine ventricle. *American Journal of Physiology*. 1983;245:H773-80.

82. Sagawa, K. and Eisner, A. Static pressure-flow relation in the total systemic vascular bed of the dog and its modification by the baroreceptor reflex. *Circulation Research*. 1975;36:406-13.

83. Segers, P., Stergiopulos, N. and Westerhof, N. Relation of effective arterial elastance to arterial system properties. *American Journal of Physiology - Heart & Circulatory Physiology*. 2002;282:H1041-6.

84. Sunagawa, K., Sagawa, K. and Maughan, W.L. Ventricular interaction with the loading system. *Annals of Biomedical Engineering*. 1984;12:163-89.

85. Kelly, R.P., Ting, C.T., Yang, T.M., Liu, C.P., Maughan, W.L., Chang, M.S. and Kass, D.A. Effective arterial elastance as index of arterial vascular load in humans. *Circulation*. 1992;86:513-21.

86. Asanoi, H., Sasayama, S. and Kameyama, T. Ventriculoarterial coupling in normal and failing heart in humans. *Circulation Research*. 1989;65:483-93.

87. Burkhoff, D. and Sagawa, K. Ventricular efficiency predicted by an analytical model. *American Journal of Physiology*. 1986;250:R1021-7.

88. Takaoka, H., Takeuchi, M., Odake, M. and Yokoyama, M. Assessment of myocardial oxygen consumption (Vo2) and systolic pressure-volume area (PVA) in human hearts. *European Heart Journal*. 1992;13 Suppl E:85-90.

89. Buckley, N.M., Penefsky, Z.J. and Litwak, R.S. Comparative force-frequency relationships in human and other mammalian ventricular myocardium. *Pflügers Archiv - European Journal of Physiology*. 1972;332:259-270.

90. Bowditch, H.P. Uber die eigenthumlichkeiten der reizbarkeit, welche die muskalfasern des herzens zeigen. *Arbeiten Aus Der Physiologischen Anstalt Zu Leipzig*. 1871;6:139-176.

91. Freeman, G.L., Little, W.C. and O'Rourke, R.A. Influence of heart rate on left ventricular performance in conscious dogs. *Circulation Research*. 1987;61:455-64.

92. Higginbotham, M.B., Morris, K.G., Williams, R.S., McHale, P.A., Coleman, R.E. and Cobb, F.R. Regulation of stroke volume during submaximal and maximal upright exercise in normal man. *Circulation Research*. 1986;58:281-291.

93. Mitchell, J.H., Wallace, A.G. and Skinner Jr., N.S. Intrinsic effects of heart rate on left ventricular performance. *American Journal of Physiology*. 1963;205:41-48.

94. Noble, M.I. Problems concerning the application of concepts of muscle mechanics to the determination of the contractile state of the heart. *Circulation*. 1972;45:252-5.

95. Schertel, E.R. Assessment of left-ventricular function. *Thoracic & Cardiovascular Surgeon*. 1998;46 Suppl 2:248-54.

96. Penny, D.J. The basics of ventricular function. *Cardiology in the Young*. 1999;9:210-223.

97. Lewis, M.E. The use of the conductance catheter in cardiac surgery. In: *Department of Physiology*. Birmingham: University of Birmingham; 2002.

98. Al-Khalidi, A.H.Q. The conductance catheter as a method for studying factors influencing pressure-volume relationships in the left ventricle in the heart. In: *Department of Physiology*. Birmingham: University of Birmingham; 1999.

99. Mason, D.T., Spann, J.F., Jr., Zelis, R. and Amsterdam, E.A. Alterations of hemodynamics and myocardial mechanics in patients with congestive heart failure: pathophysiologic mechanisms and assessment of cardiac function and ventricular contractility. *Progress in Cardiovascular Diseases*. 1970;12:507-57.

100. Gleason, W.L. and Braunwald, E. Studies on the first derivative of the ventricular pressure pulse in man. *Journal of Clinical Investigation*. 1962;41:80-91.

101. Mahler, F., Ross, J., Jr., O'Rourke, R.A. and Covell, J.W. Effects of changes in preload, afterload and inotropic state on ejection and isovolumic phase measures of contractility in the conscious dog. *American Journal of Cardiology*. 1975;35:626-34.

102. Elzinga, G. and Westerhof, N. The pumping ability of the left heart and the effect of coronary occlusion. *Circulation Research*. 1976;38:297-302.

103. Suga, H. Time course of left ventricular pressure-volume relationship under various end-diastolic volume. *Japanese Heart Journal*. 1969;10:509-515.

104. Mason, D.T. Usefulness and limitations of the rate of rise of intraventricular pressure (dp-dt) in the evaluation of myocardial contractility in man. *American Journal of Cardiology*. 1969;23:516-27.

105. Suga, H. time course of left ventricular presure-volume relationship under various extents of aortic occlusion. *Japanese Heart Journal*. 1970;11:373-378.

106. Suga, H. Left ventricular pressure-volume ratio in systole as an index of myocardial inotropism. *Japanese Heart Journal*. 1971;12:153-160.

107. Suga, H. and Sagawa, K. Instantaneous pressure-volume relationships and their ratio in the excised, supported canine left ventricle. *Circulation Research*. 1974;35:117-26.

108. Little, W.C. The left ventricular dP/dtmax-end-diastolic volume relation in closed-chest dogs. *Circulation Research*. 1985;56:808-15.

109. Glower, D.D., Spratt, J.A., Snow, N.D., Kabas, J.S., Davis, J.W., Olsen, C.O., Tyson, G.S., Sabiston Jr., D.C. and Rankin, J.S. Linearity of the Frank-Starling relationship in the intact heart: the concept of preload recruitable stroke work. *Circulation*. 1985;71:994-1009.

110. Kass, D.A., Maughan, W.L., Guo, Z.M., Kono, A., Sunagawa, K. and Sagawa, K. Comparative influence of load versus inotropic states on indexes of ventricular contractility: experimental and theoretical analysis based on pressure-volume relationships. *Circulation*. 1987;76:1422-36.

111. Langer, G.A. Ion fluxes in cardiac excitation and contraction and their relation to myocardial contractility. *Physiological Reviews*. 1968;48:708-57.

112. Kass, D.A., Midei, M., Graves, W., Brinker, J.A. and Maughan, W.L. Use of a conductance (volume) catheter and transient inferior vena caval occlusion for rapid determination of pressure-volume relationships in man. *Catheterization & Cardiovascular Diagnosis*. 1988;15:192-202.

113. Tulner, S.A.F., Klautz, R.J.M., van Rijk-Zwikker, G.L., Engbers, F.H.M., Bax, J.J., Baan, J., van der Wall, E.E., Dion, R.A. and Steendijk, P. Perioperative assessment of left ventricular function by pressure-volume loops using the conductance catheter method.[see comment]. *Anesthesia & Analgesia*. 2003;97:950-7.

114. Steendijk, P., Tulner, S.A.F., Wiemer, M., Bleasdale, R.A., Bax, J.J., van der Wall, E.E., Vogt, J. and Schalij, M.J. Pressure-volume measurements by conductance catheter during cardiac resynchronization therapy. *European Heart Journal Supplement*. 2004;6:D35-42.

115. Ormerod, O.J., Barber, R.W., Stone, D.L. and Wraight, E.P. Radionuclide assessment of diastolic function in aortic regurgitation: a critical study of its measurement. *Cardiovascular Research*. 1987;21:835-40.

116. Zile, M.R. and Gaasch, W.H. Mechanical loads and the isovolumic and filling indices of left ventricular relaxation. *Progress in Cardiovascular Diseases*. 1990;32:333-46.

117. Brutsaert, D.L. and Sys, S.U. Relaxation and diastole of the heart. *Physiological Reviews*. 1989;69:1228-315.

118. Nikolic, S., Yellin, E.L., Tamura, K., Vetter, H., Tamura, T., Meisner, J.S. and Frater, R.W. Passive properties of canine left ventricle: diastolic stiffness and restoring forces. *Circulation Research*. 1988;62:1210-22.

119. Leite-Moreira, A.F., Correia-Pinto, J. and Gillebert, T.C. Afterload induced changes in myocardial relaxation: a mechanism for diastolic dysfunction. *Cardiovascular Research*. 1999;43:344-53.

120. Heyndrickx, G.R., Vantrimpont, P.J., Rousseau, M.F. and Pouleur, H. Effects of asynchrony on myocardial relaxation at rest and during exercise in conscious dogs. *American Journal of Physiology*. 1988;254:H817-22.

121. McLaurin, L.P., Grossman, W. and Herndon, W. Defective left ventricular relaxation during experimental myocardial ischemia. *Clinical Research*. 1975;23:196A.

122. Kass, D.A. Assessment of diastolic dysfunction. Invasive modalities. *Cardiology Clinics*. 2000;18:571-86.

123. Senzaki, H., Fetics, B., Chen, C.H. and Kass, D.A. Comparison of Ventricular Pressure Relaxation Assessments in Human Heart Failure. Quantitative Influence on Load and Drug Sensitivity Analysis. *Journal of the American College of Cardiology*. 1999;34:1529-1536.

124. Grossman, W. Diastolic dysfunction in congestive heart failure. *New England Journal of Medicine*. 1991;325:1557-1564.

125. Brutsaert, D.L., Rademakers, F.E., Sys, S.U., Gillebert, T.C. and Housmans, P.R. Analysis of relaxation in the evaluation of ventricular function of the heart. *Progress in Cardiovascular Diseases*. 1985;28:143-63.

126. Weiss, J.L., Frederiksen, J.W. and Weisfeldt, M.L. Hemodynamic determinants of the time-course of fall in canine left ventricular pressure. *Journal of Clinical Investigation*. 1976;58:751-60.

127. Matsubara, H., Takaki, M., Yasuhara, S., Araki, J. and Suga, H. Logistic Time Constant of Isovolumic Relaxation Pressure–Time Curve in the Canine Left Ventricle : Better Alternative to Exponential Time Constant. *Circulation*. 1995;92:2318-2326.

128. Raff, G.L. and Glantz, S.A. Volume loading slows left ventricular isovolumic relaxation rate. Evidence of load-dependent relaxation in the intact dog heart. *Circulation Research*. 1981;48:813-824.

129. Gaasch, W.H., Bing, O.H. and Mirsky, I. Chamber compliance and myocardial stiffness in left ventricular hypertrophy. *European Heart Journal*. 1982;3 Suppl A:139-45.

130. Kass, D.A., Wolff, M.R., Ting, C.T., Liu, C.P., Chang, M.S., Lawrence, W. and Maughan, W.L. Diastolic compliance of hypertrophied ventricle is not acutely altered by pharmacologic agents influencing active processes. *Annals of Internal Medicine*. 1993;119:466-73.

131. Aroney, C.N., Ruddy, T.D., Dighero, H., Fifer, M.A., Boucher, C.A. and Palacios, I.F. Differentiation of restrictive cardiomyopathy from pericardial constriction: assessment of diastolic function by radionuclide angiography. *Journal of the American College of Cardiology*. 1989;13:1007-14.

132. Fester, A. and Samet, P. Passive elasticity of the human left ventricle: The "parallel elastic element". *Circulation*. 1974;50:609-618.

133. Bove, A.A. and Santamore, W.P. Ventricular interdependence. *Progress in Cardiovascular Diseases*. 1981;23:365-88.

134. Holt, J.P. The normal pericardium. *American Journal of Cardiology*. 1970;26:455-65.

135. Armour, J.A. Cardiac neuronal hierarchy in health and disease. *American Journal of Physiology - Regulatory, Integrative & Comparative Physiology*. 2004;287:R262-271.

136. Silverman, N.A., Kohler, J., Levitsky, S., Pavel, D.G., Fang, R.B. and Feinberg, H. Chronic hypoxemia depresses global ventricular function and predisposes to the

depletion of high-energy phosphates during cardioplegic arrest: implications for surgical repair of cyanotic congenital heart defects. *Annals of Thoracic Surgery*. 1984;37:304-308.

137. Najm, H.K., Wallen, W.J., Belanger, M.P., Williams, W.G., Coles, J.G., Van Arsdell, G.S., Black, M.D., Boutin, C. and Wittnich, C. Does the degree of cyanosis affect myocardial adenosine triphosphate levels and function in children undergoing surgical procedures for congenital heart disease? *Journal of Thoracic & Cardiovascular Surgery*. 2000;119:515-524.

138. Modi, P., Suleiman, M.S., Reeves, B., Pawade, A., Parry, A.J., Angelini, G.D. and Caputo, M. Myocardial metabolic changes during pediatric cardiac surgery: a randomized study of 3 cardioplegic techniques.[see comment]. *Journal of Thoracic & Cardiovascular Surgery*. 2004;128:67-75.

139. Manner, J. Cardiac looping in the chick embryo: a morphological review with special reference to terminological and biomechanical aspects of the looping process. *Anatomical Record*. 2000;259:248-62.

140. Manner, J. The anatomy of cardiac looping: A step towards the understanding of the morphogenesis of several forms of congenital cardiac malformations. *Clinical Anatomy*. 2009;22:21-35.

141. Harvey, R.P. Patterning the vertebrate heart. *Nature Reviews Genetics*. 2002;3:544-56.

142. Moorman, A., Webb, S., Brown, N.A., Lamers, W. and Anderson, R.H. Development of the heart: (1) Formation of the cardiac chambers and arterial trunks. *Heart*. 2003;89:806-14.

143. Fishman, M.C. and Olson, E.N. Parsing the heart: genetic modules for organ assembly. *Cell*. 1997;91:153-6.

144. Srivastava, D. and Olson, E.N. A genetic blueprint for cardiac development. *Nature*. 2000;407:221-6.

145. de la Cruz, M.V., Gomez, C.S. and Cayre, R. The developmental components of the ventricles: their significance in congenital cardiac malformations. *Cardiology in the Young*. 1991;1:123-128.

146. Kelly, R.G. and Buckingham, M.E. The anterior heart-forming field: voyage to the arterial pole of the heart. *Trends in Genetics*. 2002;18:210-216.

147. Anderson, R.H., Webb, S., Brown, N.A., Lamers, W. and Moorman, A. Development of the heart: (2) septation of the atriums and ventricles. *Heart*. 2003;89:949-58.

148. Kim, J.S., Viragh, S., Moorman, A.F., Anderson, R.H. and Lamers, W.H. Development of the myocardium of the atrioventricular canal and the vestibular spine in the human heart. *Circulation Research*. 2001;88:395-402.

149. Sedmera, D., Pexieder, T., Vuillemin, M., Thompson, R.P. and Anderson, R.H. Developmental patterning of the myocardium. *Anatomical Record*. 2000;258:319-37.

150. Lamers, W.H., Wessels, A., Verbeek, F.J., Moorman, A.F., Viragh, S., Wenink, A.C., Gittenberger-de Groot, A.C. and Anderson, R.H. New findings concerning ventricular septation in the human heart. Implications for maldevelopment. *Circulation*. 1992;86:1194-205.

151. Anderson, R.H., Webb, S., Brown, N.A., Lamers, W. and Moorman, A. Development of the heart: (3) formation of the ventricular outflow tracts, arterial valves, and intrapericardial arterial trunks. *Heart*. 2003;89:1110-8.

152. Lind, J. and Wegelius, C. Human fetal circulation: changes in the cardiovascular system at birth and disturbances in the post-natal closure of the foramen ovale and ductus arteriosus. *Cold Spring Harbor Symposia on Quantitative Biology*. 1954;19:109-25.

153. Barclay, A.E., Franklin, K.J. and Pritchard, M.M.L. *The foetal circulation*. Oxford: Blackwell Scietific Publications; 1944.

154. Cassin, S., Dawes, G.S., Mott, J.C., Ross, B.B. and Strang, L.B. The vascular resistance of the foetal and newly ventilated lung of the lamb. *Journal of Physiology*. 1964;171:61-79.

155. Cook, C.D., Drinker, P.A., Jacobson, H.N., Levison, H. and Strang, L.B. Control of pulmonary blood flow in the foetal and newly born lamb. *Journal of Physiology*. 1963;169:10-29.

156. Rudolph, A.M. and Heymann, M.A. The circulation of the fetus in utero. Methods for studying distribution of blood flow, cardiac output and organ blood flow. *Circulation Research*. 1967;21:163-84.

157. Rudolph, A.M. Fetal and neonatal pulmonary circulation. *Annual Review of Physiology*. 1979;41:383-95.

158. Hamilton, W.F., Woodbury, R.A. and Woods, E.B. The relation between systemic and pulmonary blood pressure in the fetus. *American Journal of Physiology*. 1937;119:206-212.

159. Rudolph, A.M. The changes in the circulation after birth. Their importance in congenital heart disease. *Circulation*. 1970;41:343-59.

160. Agata, Y., Hiraishi, S., Oguchi, K., Misawa, H., Horiguchi, Y., Fujino, N., Yashiro, K. and Shimada, N. Changes in left ventricular output from fetal to early neonatal life. *Journal of Pediatrics*. 1991;119:441-5.

161. Veille, J.C., Hanson, R., Steele, L. and Tatum, K. M-mode echocardiographic evaluation of fetal and infant hearts: Longitudinal follow-up study from intrauterine life to year one. *American Journal of Obstetrics & Gynecology*. 1996;175:922-8.

162. Clark, S.J., Yoxall, C.W. and Subhedar, N.V. Measurement of right ventricular volume in healthy term and preterm neonates. *Archives of Disease in Childhood Fetal & Neonatal Edition*. 2002;87:F89-93; discussion F93-4.

163. Dawes, G.S., Mott, J.C., Widdicombe, J.G. and Wyatt, D.G. Changes in the lungs of the new-born lamb. *Journal of Physiology*. 1953;121:141-62.

164. Dawes, G.S., Milne, E.D., Mott, J.C. and Widdicombe, J.G. The closure of the foramen ovale after birth. *Journal of Physiology*. 1953;122:38P.

165. Scammon, E. and Norris, E.H. On the time of the post-natal obliteration of the fetal blood passages (foramen ovale, ductus arteriosus, ductus venosus). *Anatomical Record*. 1918;15:165-180.

166. Dawes, G.S., Milne, E.D., Mott, J.C. and Widdicombe, J.G. The patency of the ductus arteriosus after birth. *Journal of Physiology*. 1953;122:37-8P.

167. Rudolph, A.M., Auld, P.A., Golinko, R.J. and Paul, M.H. Pulmonary vascular adjustments in the neonatal period. *Pediatrics*. 1961;28:28-34.

168. Rowe, R.D. and James, L.S. The normal pulmonary arterial pressure during the first year of life. *Journal of Pediatrics*. 1957;51:1-4.

169. Earley, A., Fayers, P., Ng, S., Shinebourne, E.A. and de Swiet, M. Blood pressure in the first 6 weeks of life. *Archives of Disease in Childhood*. 1980;55:755-7.

170. Joyce, J.J., Dickson, P.I., Qi, N., Noble, J.E., Raj, J.U. and Baylen, B.G. Normal right and left ventricular mass development during early infancy. *American Journal of Cardiology*. 2004;93:797-801.

171. Danford, D., Huhta, J. and Gutgesell, H. Left ventricular wall stress and thickness in complete transposition of the great arteries. Implications for surgical intervention. *Journal of Thoracic & Cardiovascular Surgery*. 1985;89:610-615.

172. Bano-Rodrigo, A., Quero-Jimenez, M., Moreno-Granado, F. and Gamallo-Amat, C. Wall thickness of ventricular chambers in transposition of the great arteries: surgical implications. *Journal of Thoracic & Cardiovascular Surgery*. 1980;79:592-597.

173. Poirier, N.C. and Mee, R.B.B. Left ventricular reconditioning and anatomical correction for systemic right ventricular dysfunction. *Seminars in Thoracic & Cardiovascular Surgery. Pediatric Cardiac Surgery Annual*. 2000;3:198-215.

174. Mitchell, S.C., Korones, S.B. and Berendes, H.W. Congenital heart disease in 56,109 births. Incidence and natural history. *Circulation*. 1971;43:323-32.

175. Bruneau, B.G. The developmental genetics of congenital heart disease. *Nature*. 2008;451:943-948.

176. Hoffman, J.I.E. and Kaplan, S. The incidence of congenital heart disease. *Journal of the American College of Cardiology*. 2002;39:1890-900.

177. Connelly, M.S., Webb, G.D., Somerville, J., Warnes, C.A., Perloff, J.K., Liberthson, R.R., Puga, F.J., Collins-Nakai, R.L., Williams, W.G., Mercier, L.A., Huckell, V.F., Finley, J.P. and McKay, R. Canadian consensus conference on adult congenital heart disease 1996. *Canadian Journal of Cardiology*. 1998;14:395-452.

178. Warnes, C.A., Liberthson, R., Danielson, G.K., Dore, A., Harris, L., Hoffman, J.I., Somerville, J., Williams, R.G. and Webb, G.D. Task force 1: the changing profile of congenital heart disease in adult life. *Journal of the American College of Cardiology*. 2001;37:1170-5.

179. Moons, P., Van Deyk, K., De Geest, S., Gewillig, M. and Budts, W. Is the severity of congenital heart disease associated with the quality of life and perceived health of adult patients? *Heart*. 2005;91:1193-1198.

180. Office for National Statistics. *Series FM1 Number 36. Birth Statistics. Review of the National Statistician on births and patterns of family building in England and Wales, 2007*. London: The Stationery Office; 2008.

181. Fyler, D.C., Buckley, L.P., Hellenbrand, W.E. and Cohn, H.E. Report of the New England regional infant cardiac care program. *Pediatrics*. 1980;65:376-446.

182. The Information Centre. National Statistics 2005-2006. *Unpublished data, Congenital Heart Disease Website*.

183. Reid, G.J., Webb, G.D., Barzel, M., McCrindle, B.W., Irvine, M.J. and Siu, S.C. Estimates of life expectancy by adolescents and young adults with congenital heart disease. *Journal of the American College of Cardiology*. 2006;48:349-355.

184. British Cardiac Society. Grown-up congenital heart (GUCH) disease: current needs and provision of service for adolescents and adults with congenital heart disease in the UK. *Heart*. 2002;88:i1-14.

185. Curtis, S.L. and Stuart, A.G. Outcome in congenital heart disease. *Current Paediatrics*. 2005;15:549-556.

186. Wilkinson, J.L. and Acerete, F. Terminological pitfalls in congenital heart disease. Reappraisal of some confusing terms, with an account of a simplified systemof basic nomenclature. *British Heart Journal*. 1973;35:1166-1177.

187. New York Heart Association Criteria Committee and Dolgin, M. *Nomenclature and criteria for diagnosis of diseases of the heart and great vessels*. Philadelphia: Lippincott, Williams and Wilkins; 1994.

188. Franklin, R.C.G., Jacobs, J.P., Krogmann, O.N., Beland, M.J., Aiello, V.D., Colan, S.D., Elliott, M.J., Gaynor, J.W., Kurosawa, H., Maruszewski, B., Stellin, G., Tchervenkov, C.I., Walters III, H.L., Weinberg, P. and Anderson, R.H. Nomenclature for congenital and paediatric cardiac disease: Historical perspectives and The International Pediatric and Congenital Cardiac Code. *Cardiology in the Young*. 2008;18:70-80.

189. Beland, M., Jacobs, J.P., Tchervenkov, C.I. and Franklin, R.C.G. The international nomenclature project for paediatric and congenital heart disease: Report from the executive of the international working group for mapping and coding of nomenclatures for paediatric and congenital heart disease. *Cardiology in the Young*. 2002;12:425-430.

190. Franklin, R.C.G., Jacobs, J.P., Tchervenkov, C.I. and Beland, M.J. The international nomenclature project for congenital heart disease: Bidirectional crossmap of the short lists of the european paediatric cardiac code and the international congenital heart surgery nomenclature database project. *Cardiology in the Young*. 2002;12:431-435.

191. Anderson, R.H. and Wilcox, B.R. Understanding cardiac anatomy: the prerequisite for optimal cardiac surgery. *Annals of Thoracic Surgery*. 1995;59:1366-75.

192. Anderson, R.H. How should we optimally describe complex congenitally malformed hearts? *Annals of Thoracic Surgery*. 1996;62:710-6.

193. Van Praagh, R. *The segmental approach to diagnosis in congenital heart disease*. Baltimore: Williams and Wilkins; 1972.

194. Van Praagh, R. The segmental approach clarified. *Cardiovascular & Interventional Radiology*. 1984;7:320-5.

195. de la Cruz, M.V. and Nadal-Ginard, B. Rules for the diagnosis of visceral situs, truncoconal morphologies, and ventricular inversions. *American Heart Journal*. 1972;84:19-32.

196. de la Cruz, M.V., Amoedo, M., Rivera, F. and Attie, F. Arterioventricular relations and their classification. Two specimens of arterioventricular discordance and review of published reports. *British Heart Journal*. 1974;36:539-53.

197. Van Praagh, R. Terminology of congenital heart disease. Glossary and commentary. *Circulation*. 1977;56:139-143.

198. Shinebourne, E.A., Macartney, F.J. and Anderson, R.H. Sequential chamber localisation - logical approach to diagnosis in congenital heart disease. *British Heart Journal*. 1976;38:327-340.

199. Van Praagh, R., David, I., Wright, G.B. and Van Praagh, S. Large RV plus small LV is not single RV. *Circulation*. 1980;61:1057-1059.

200. Kirklin, J.W., Pacifico, A.D., Bargeron Jr, L.M. and Soto, B. Cardiac repair in anatomically corrected malposition of the great arteries. *Circulation*. 1973;48:153-159.

201. Tynan, M.J., Becker, A.E., Macartney, F.J., Quero Jimenez, M., Shinebourne, E.A. and Anderson, R.H. Nomenclature and classification of congenital heart disease. *British Heart Journal*. 1979;41:544-553.

202. Griselli, M., McGuirk, S.P., Winlaw, D.S., Stumper, O., de Giovanni, J.V., Miller, P., Dhillon, R., Wright, J.G., Barron, D.J. and Brawn, W.J. The influence of pulmonary artery morphology on the results of operations for major aortopulmonary collateral arteries and complex congenital heart defects. *Journal of Thoracic and Cardiovascular Surgery*. 2004;127:251-8.

203. Somerville, J. Changing form and function in one ventricle hearts. *Herz*. 1979;4:206-12.

204. Cook, A.C. and Anderson, R.H. The functionally univentricular circulation: anatomic substrates as related to function. *Cardiology in the Young*. 2005;15:7-16.

205. van Praagh, R., Plett, J.A. and van Praagh, S. Single ventricle. Pathology, embryology, terminology and classification. *Herz*. 1979;4:113-50.

206. Anderson, R.H., Becker, A.E., Freedom, R.M., Quero-Jimenez, M., Macartney, F.J., Shinebourne, E.A., Wilkinson, J.L. and Tynan, M. Problems in the nomenclature of the univentricular heart. *Herz*. 1979;4:97-106.

207. Barlow, A., Pawade, A., Wilkinson, J.L. and Anderson, R.H. Cardiac anatomy in patients undergoing the Fontan procedure. *Annals of Thoracic Surgery*. 1995;60:1324-30.

208. Anderson, R.H. and Ho, S.Y. Which hearts are unsuitable for biventricular correction? *Annals of Thoracic Surgery*. 1998;66:621-6.

209. Thies, W.R., Bargeron Jr., L.M., Bini, R.M., Colvin, E.V. and Soto, B. Spectrum of hearts with one underdeveloped and one dominant ventricle. *Pediatric Cardiology*. 1986;7:129-39.

210. Wilkinson, J.L., Becker, A.E., Tynan, M., Freedom, R., Macartney, F.J., Shinebourne, E.A., Quero-Jimenez, M. and Anderson, R.H. Nomenclature of the univentricular heart. *Herz*. 1979;4:107-12.

211. Anderson, R.H. and Ho, S.Y. Pathologic substrates for 1 1/2 ventricular repair. *Annals of Thoracic Surgery*. 1998;66:673-7.

212. Freedom, R.M. and Van Arsdell, G.S. Biventricular hearts not amenable to biventricular repair. *Annals of Thoracic Surgery*. 1998;66:641-3.

213. Anderson, R.H. and Ho, S.Y. What is a ventricle? *Annals of Thoracic Surgery*. 1998;66:616-20.

214. Crick, S.J., Sheppard, M.N., Ho, S.Y., Gebstein, L. and Anderson, R.H. Anatomy of the pig heart: comparisons with normal human cardiac structure. *Journal of Anatomy*. 1998;193:105-19.

215. Graham Jr., T.P. and Johns, J.A. Pre-operative assessment of ventricular function in patients considered for Fontan procedure. *Herz*. 1992;17:213-9.

216. Boxt, L.M. Radiology of the right ventricle. *Radiologic Clinics of North America*. 1999;37:379-400.

217. Kendall, S.W.H., Biitner, H.B., Peterseim, D.S., Cambell, K.A. and Van Trigt, P. Right ventricular function in the donor heart. *European Journal of Cardio-thoracic Surgery*. 1997; 11 609-615.

218. Rankin, J.S., McHale, P.A., Arentzen, C.E., Ling, D., Greenfield, J.C., Jr. and Anderson, R.W. The three-dimensional dynamic geometry of the left ventricle in the conscious dog. *Circulation Research*. 1976;39:304-13.

219. Hutchins, G.M., Bulkley, B.H., Moore, G.W., Piasio, M.A. and Lohr, F.T. Shape of the human cardiac ventricles. *American Journal of Cardiology*. 1978;41:646-54.

220. Greenbaum, R.A., Ho, S.Y., Gibson, D.G., Becker, A.E. and Anderson, R.H. Left ventricular fibre architecture in man. *British Heart Journal*. 1981;45:248-263.

221. Sanchez-Quintana, D., Garcia-Martinez, V., Climent, V. and Hurle, J.M. Morphological changes in the normal pattern of ventricular myoarchitecture in the developing human heart. *Anatomical Record*. 1995;243:483-95.

222. Buckberg, G.D. Basic science review: The helix and the heart. *Journal of Thoracic & Cardiovascular Surgery*. 2002;124:863-883.

223. Rushmer, R.F., Crystal, D.K. and Wagner, C. The functional anatomy of ventricular contraction. *Circulation Research*. 1953;1:162-70.

224. Armour, J.A., Pace, J.B. and Randall, W.C. Interrelationship of architecture and function of the right ventricle. *American Journal of Physiology*. 1970;218:174-9.

225. Rouleau, J.L., Paradis, P., Shenasa, H. and Juneau, C. Faster time to peak tension and velocity of shortening in right versus left ventricular trabeculae and papillary muscles of dogs. *Circulation Research*. 1986;59:556-61.

226. Burkhoff, D., Yue, D.T., Franz, M.R., Hunter, W.C., Sunagawa, K., Maughan, W.L. and Sagawa, K. Quantitative comparison of the force-interval relationships of the canine right and left ventricles. *Circulation Research*. 1984;54:468-73.

227. Burkhoff, D., Kronenberg, M.W., Yue, D.T., Maughan, W.L., Hunter, W.C. and Sagawa, K. Quantitative comparison of canine right and left ventricular isovolumic pressure waves. *American Journal of Physiology*. 1987;253:H475-9.

228. Joyce, J.J., Ross-Ascuitto, N.T. and Ascuitto, R.J. A direct comparison of right and left ventricular performance in the isolated neonatal pig heart. *Pediatric Cardiology*. 2000;21:216-22.

229. Piran, S., Veldtman, G., Siu, S., Webb, G.D. and Liu, P.P. Heart failure and ventricular dysfunction in patients with single or systemic right ventricles. *Circulation*. 2002;105:1189-94.

230. Alejos, J.C., Williams, R.G., Jarmakani, J.M., Galindo, A.J., Isabel-Jones, J.B., Drinkwater, D., Laks, H. and Kaplan, S. Factors influencing survival in patients undergoing the bidirectional Glenn anastomosis. *American Journal of Cardiology*. 1995;75:1048-50.

231. Gentles, T.L., Mayer Jr., J.E., Gauvreau, K., Newburger, J.W., Lock, J.E., Kupferschmid, J.P., Burnett, J., Jonas, R.A., Castaneda, A.R. and Wernovsky, G. Fontan operation in five hundred consecutive patients: Factors influencuing early and late outcome. *Journal of Thoracic & Cardiovascular Surgery*. 1997;114:376-391.

232. Julsrud, P.R., Weigel, T.J., Van Son, J.A., Edwards, W.D., Mair, D.D., Driscoll, D.J., Danielson, G.K., Puga, F.J. and Offord, K.P. Influence of ventricular morphology on outcome after the Fontan procedure. *American Journal of Cardiology*. 2000;86:319-323.

233. Kogon, B.E., Plattner, C., Leong, T., Simsic, J., Kirshbom, P.M. and Kanter, K.R. The bidirectional Glenn operation: A risk factor analysis for morbidity and mortality. *Journal of Thoracic and Cardiovascular Surgery*. 2008;136:1237-1242.

234. Uemura, H., Yagihara, T., Kawashima, Y., Yamamoto, F., Nishigaki, K., Matsuki, O., Okada, K., Kamiya, T. and Anderson, R.H. What factors affect ventricular performance after a Fontan-type operation? *Journal of Thoracic and Cardiovascular Surgery*. 1995;110:405-15.

235. Sano, T., Ogawa, M., Yabuuchi, H., Matsuda, H., Nakano, S., Shimazaki, Y., Taniguchi, K., Arisawa, J., Hirose, H. and Kawashima, Y. Quantitative cineangiographic analysis of

ventricular volume and mass in patients with single ventricle: relation to ventricular morphologies. *Circulation*. 1988;77:62-9.

236. Hornung, T.S., Bernard, E.J., Celermajer, D.S., Jaeggi, E., Howman-Giles, R.B., Chard, R.B. and Hawker, R.E. Right ventricular dysfunction in congenitally corrected transposition of the great arteries. *American Journal of Cardiology*. 1999;84:1116-9.

237. Hornung, T.S., Kilner, P.J., Davlouros, P.A., Grothues, F., Li, W. and Gatzoulis, M.A. Excessive right ventricular hypertrophic response in adults with the mustard procedure for transposition of the great arteries.[see comment]. *American Journal of Cardiology*. 2002;90:800-3.

238. Derrick, G. and Deanfield, J.E. Decline in ventricular function and clinical condition after Mustard repair. *Eur Heart J*. 2004;25:1863-1864.

239. Carlgren, L.E. The incidence of congenital heart disease in children born in Gothenburg 1941-1950. *British Heart Journal*. 1959;21:40-50.

240. Hay, J.D. The management and prognosis of congenital heart disease. *Practitioner*. 1966;196:199-208.

241. MacMahon, B., McKeown, T. and Record, R.G. Incidence and life expectation of children with congenital heart disease. *British Heart Journal*. 1953;15:121-129.

242. Morris, C.D., Outcalt, J. and Menashe, V.D. Hypoplastic left heart syndrome: natural history in a geographically defined population. *Pediatrics*. 1990;85:977-83.

243. Lambert, E.C., Canent, R.V. and Hohn, A.R. Congenital cardiac anomalies in the newborn. A review of conditions causing death or severe distress in the first month of life. *Pediatrics*. 1966;37:343-51.

244. Samanek, M., Benesova, D., Goetzova, J. and Hrycejova, I. Distribution of age at death in children with congenital heart disease who died before the age of 15. *British Heart Journal*. 1988;59:581-5.

245. Campbell, M. Tricuspid atresia and its prognosis with and without surgical treatment. *British Heart Journal*. 1961;23:699-710.

246. Dick, M., Fyler, D.C. and Nadas, A.S. Tricuspid atresia: clinical course in 101 patients. *American Journal of Cardiology*. 1975;36:327-37.

247. Franklin, R.C., Spiegelhalter, D.J., Anderson, R.H., Macartney, F.J., Rossi Filho, R.I., Douglas, J.M., Rigby, M.L. and Deanfield, J.E. Double-inlet ventricle presenting in infancy. I. Survival without definitive repair. *Journal of Thoracic & Cardiovascular Surgery*. 1991;101:767-76.

248. Franklin, R.C., Spiegelhalter, D.J., Sullivan, I.D., Anderson, R.H., Thoele, D.G., Shinebourne, E.A. and Deanfield, J.E. Tricuspid atresia presenting in infancy. Survival and suitability for the Fontan operation. *Circulation*. 1993;87:427-39.

249. Moodie, D.S., Ritter, D.G., Tajik, A.J. and O'Fallon, W.M. Long-term follow-up in the unoperated univentricular heart. *American Journal of Cardiology*. 1984;53:1124-8.

250. Hoffman, J.I. Natural history of congenital heart disease. Problems in its assessment with special reference to ventricular septal defects. *Circulation*. 1968;37:97-125.

251. Rigolin, V.H., Robiolio, P.A., Wilson, J.S., Harrison, J.K. and Bashore, T.M. The forgotten chamber: the importance of the right ventricle. *Catheterization & Cardiovascular Diagnosis*. 1995;35:18-28.

252. Furey 3rd, S.A., Zieske, H.A. and Levy, M.N. The essential function of the right ventricle. *American Heart Journal*. 1984;107:404-10.

253. Uhl, H.S.M. A previously undescribed congenital malformation of the heart: almost total absence of the myocardium of the right ventricle. *Bulletin of the Johns Hopkins Hospital*. 1952;91:197-209.

254. Dalla Volta, S., Battaglia, G. and Zerbini, E. "Auricularization' of right ventricular pressure curve. *American Heart Journal*. 1961;61:25-33.

255. Sade, R.M. and Castaneda, A.R. The dispensable right ventricle. *Surgery*. 1975;77:624-631.

256. Robicsek, F. The history of right heart bypass before Fontan. *Herz*. 1992;17:199-212.

257. Rodbard, S. and Wagner, D. By-passing the right ventricle. *Proceedings of the Society of Experimental Biology and Medicine*. 1949;71:69-70.

258. Rodbard, S. Body Temperature, Blood Pressure, and Hypothalamus *Science*. 1948;108:413-415.

259. Trusler, G.A., Williams, W.G., Cohen, A.J., Rabinovitch, M., Moes, C.A., Smallhorn, J.F., Coles, J.G., Lightfoot, N.E. and Freedom, R.M. William Glenn lecture. The cavopulmonary shunt. Evolution of a concept. *Circulation*. 1990;82:IV131-8.

260. Mainwaring, R.D., Lamberti, J.J. and Uzark, K. The bidirectional Glenn procedure: Palliation of the univentricular heart. *Advances in Cardiac Surgery*. 1994;5:115-140.

261. Castaneda, A.R. From Glenn to Fontan. A continuing evolution. *Circulation*. 1992;86:II80-4.

262. Cowgill, L.D. The Fontan procedure: A historical review. *Annals of Thoracic Surgery*. 1991;51:1026-30.

263. Carlon, C.A., Mondini, P.G. and De Marchi, R. Surgical treatment of some cardiovascular diseases. *Journal of the International College of Surgeons*. 1951;16:1-11.

264. Glenn, W.W.L. Circulatory bypass of the right side of the heart. IV. Shunt between the superior vena cava and distal right pulmonary artery: report of clinical application. *New England Journal of Medicine*. 1958;259:117-120.

265. Laks, H., Mudd, J.G., Standeven, J.W., Fagan, L. and Willman, V.L. Long-term effect of the superior vena cava-pulmonary artery anastomosis on pulmonary blood flow. *Journal of Thoracic & Cardiovascular Surgery*. 1977;74:253-60.

266. Pennington, D.G., Nouri, S., Ho, J., Secker-Walker, R., Patel, B., Sivakoff, M. and Willman, V.L. Glenn shunt: long-term results and current role in congenital heart operations. *Annals of Thoracic Surgery*. 1981;31:532-9.

267. di Carlo, D., Williams, W.G., Freedom, R.M., Trusler, G.A. and Rowe, R.D. The role of cava-pulmonary (Glenn) anastomosis in the palliative treatment of congenital heart disease. *Journal of Thoracic & Cardiovascular Surgery*. 1982;83:437-42.

268. Salmon, A.P., Sethia, B., Silove, E.D., Goh, D., Mitchell, I., Alton, H., De Giovanni, J.V., Wright, J.G. and Abrams, L.D. Cavopulmonary anastomosis as long-term palliation for patients with tricuspid atresia. *European Journal of Cardio-Thoracic Surgery*. 1989;3:494-7; discussion 497-8.

269. Gatzoulis, M.A., Munk, M.D., Williams, W.G. and Webb, G.D. Definitive palliation with cavopulmonary or aortopulmonary shunts for adults with single ventricle physiology. *Heart*. 2000;83:51-7.

270. Glenn, W.W. Superior vena cava-pulmonary artery anastomosis. *Annals of Thoracic Surgery*. 1984;37:9-11.

271. Hopkins, R.A., Armstrong, B.E., Serwer, G.A., Peterson, R.J. and Oldham, H.N., Jr. Physiological rationale for a bidirectional cavopulmonary shunt. A versatile complement to the Fontan principle. *Journal of Thoracic and Cardiovascular Surgery*. 1985;90:391-8.

272. Young, W.G., Jr., Sealy, W.C., Houck, W.S., Jr., Whalen, R.E., Spach, M.S. and Canent, R.V., Jr. Superior vena cava--right pulmonary artery anastomosis in cyanotic heart disease. *Annals of Surgery*. 1963;157:894-901.

273. La Corte, M.A., Dick, M., Scheer, G., La Farge, C.G. and Fyler, D.C. Left ventricular function in tricuspid atresia. Angiographic analysis in 28 patients. *Circulation*. 1975;52:996-1000.

274. Mathur, M. and Glenn, W.W. Long-term evaluation of cava-pulmonary artery anastomosis. *Surgery*. 1973;74:899-916.

275. Bradley, S.M., Mosca, R.S., Hennein, H.A., Crowley, D.C., Kulik, T.J. and Bove, E.L. Bidirectional superior cavopulmonary connection in young infants. *Circulation*. 1996;94:II5-11.

276. Salim, M.A., DiSessa, T.G., Arheart, K.L. and Alpert, B.S. Contribution of superior vena caval flow to total cardiac output in children : A Doppler echocardiographic study. *Circulation*. 1995;92:1860-1865.

277. Boruchow, I.B., Swenson, E.W., Elliott, L.P., Bartley, T.D., Wheat, M.W., Jr. and Schiebler, G.L. Study of the mechanisms of shunt failure after superior vena cava-right pulmonary artery anastomosis. *Journal of Thoracic & Cardiovascular Surgery*. 1970;60:531-9.

278. Bargeron, L.M., Jr., Karp, R.B., Barcia, A., Kirklin, J.W., Hunt, D. and Deverall, P.B. Late deterioration of patients after superior vena cava to right pulmonary artery anastomosis. *American Journal of Cardiology*. 1972;30:211-6.

279. Kopf, G.S., Laks, H., Stansel, H.C., Hellenbrand, W.E., Kleinman, C.S. and Talner, N.S. Thirty-year follow-up of superior vena cava-pulmonary artery (Glenn) shunts.[see comment]. *Journal of Thoracic & Cardiovascular Surgery*. 1990;100:662-70; discussion 670-1.

280. Samanek, M., Oppelt, A., Kasalicky, J. and Voriskova, M. Distribution of pulmonary blood flow after cavopulmonary anastomosis (Glenn operation). *British Heart Journal*. 1969;31:511-6.

281. Rastelli, G.C., Wallace, R.B. and Ongley, P.A. Complete repair of transposition of the great arteries with pulmonary stenosis. A review and report of a case corrected by using a new surgical technique. *Circulation*. 1969;39:83-95.

282. Claxton, C.P., Jr. and Sabiston, D.C., Jr. Correction of tetralogy of Fallot following superior vena cava to pulmonary artery shunt. *Journal of Thoracic & Cardiovascular Surgery*. 1969;57:475-8.

283. Fontan, F. and Baudet, E. Surgical repair of tricuspid atresia. *Thorax*. 1971;26:240-8.

284. Kreutzer, G., Galindez, E., Bono, H., De Palma, C. and Laura, J.P. An operation for the correction of tricuspid atresia. *Journal of Thoracic & Cardiovascular Surgery*. 1973;66:613-21.

285. Ross, D.N. and Somerville, J. Surgical correction of tricuspid atresia. *Lancet*. 1973;1:845-9.

286. Bjork, V.O., Olin, C.L., Bjarke, B.B. and Thoren, C.A. Right atrial-right ventricular anastomosis for correction of tricuspid atresia. *Journal of Thoracic & Cardiovascular Surgery*. 1979;77:452-8.

287. Kitagawa, T. Evolving Fontan strategy: hemi-Fontan procedure and its clinical application. *Annals of Thoracic & Cardiovascular Surgery*. 2000;6:213-5.

288. Pridjian, A.K., Mendelsohn, A.M., Lupinetti, F.M., Beekman, R.H., 3rd, Dick, M., 2nd, Serwer, G. and Bove, E.L. Usefulness of the bidirectional Glenn procedure as staged reconstruction for the functional single ventricle. *American Journal of Cardiology*. 1993;71:959-62.

289. Mazzera, E., Corno, A., Picardo, S., Di Donato, R., Marino, B., Costa, D. and Marcelletti, C. Bidirectional cavopulmonary shunts: clinical applications as staged or definitive palliation. *Annals of Thoracic Surgery*. 1989;47:415-20.

290. Bridges, N.D., Jonas, R.A., Mayer, J.E., Flanagan, M.F., Keane, J.F. and Castaneda, A.R. Bidirectional cavopulmonary anastomosis as interim palliation for high-risk Fontan candidates. Early results. *Circulation*. 1990;82:IV170-6.

291. Lamberti, J.J. and Uzark, K.C. The Fontan operation. *Annals of Thoracic Surgery*. 1999;67:1523-4.

292. Tweddell, J.S., Litwin, S.B., Thomas, J.P., Jr. and Mussatto, K. Recent advances in the surgical management of the single ventricle pediatric patient. *Pediatric Clinics of North America*. 1999;46:465-80.

293. van Doorn, C.A. and de Leval, M.R. The Fontan operation in clinical practice: indications and controversies. *Nature Clinical Practice Cardiovascular Medicine*. 2005;2:116-7.

294. Hosein, R.B.M., Clarke, A.J.B., McGuirk, S.P., Griselli, M., Stumper, O., De Giovanni, J.V., Barron, D.J. and Brawn, W.J. Factors influencing early and late outcome following the Fontan procedure in the current era. The 'Two Commandments'? *European Journal of Cardio-Thoracic Surgery*. 2007;31:344-52; discussion 353.

295. Azzolina, G., Eufrate, S. and Pensa, P. Tricuspid atresia: experience in surgical management with a modified cavopulmonary anastomosis. *Thorax*. 1972;27:111-5.

296. Douville, E.C., Sade, R.M. and Fyfe, D.A. Hemi-Fontan operation in surgery for single ventricle: a preliminary report.[see comment]. *Annals of Thoracic Surgery*. 1991;51:893-9; discussion 900.

297. Norwood, W.I., Jr., Jacobs, M.L. and Murphy, J.D. Fontan procedure for hypoplastic left heart syndrome. *Annals of Thoracic Surgery*. 1992;54:1025-9; discussion 1029-30.

298. Douglas, W.I., Goldberg, C.S., Mosca, R.S., Law, I.H. and Bove, E.L. Hemi-Fontan procedure for hypoplastic left heart syndrome: outcome and suitability for Fontan. *Annals of Thoracic Surgery*. 1999;68:1361-7; discussion 1368.

299. Jacobs, M.L. and Pourmoghadam, K.K. The hemi-Fontan operation. *Seminars in Thoracic & Cardiovascular Surgery. Pediatric Cardiac Surgery Annual*. 2003;6:90-7.

300. Bove, E.L., de Leval, M.R., Migliavacca, F., Guadagni, G. and Dubini, G. Computational fluid dynamics in the evaluation of hemodynamic performance of cavopulmonary connections after the Norwood procedure for hypoplastic left heart syndrome. *Journal of Thoracic & Cardiovascular Surgery*. 2003;126:1040-7.

301. Pekkan, K., Dasi, L.P., de Zelicourt, D., Sundareswaran, K.S., Fogel, M.A., Kanter, K.R. and Yoganathan, A.P. Hemodynamic performance of stage-2 univentricular reconstruction: Glenn vs. hemi-Fontan templates. *Annals of Biomedical Engineering*. 2009;37:50-63.

302. Nuland, S.B., Glenn, W.W.L. and Guilfoil, P.H. Circulatory bypass of the right heart. III. Some observations on long-term survivors. *Surgery*. 1958;43:184-201.

303. Mace, L., Dervanian, P., Weiss, M., Daniel, J.P., Losay, J. and Neveux, J.Y. Hemodynamics of different degrees of right heart bypass: experimental assessment. *Annals of Thoracic Surgery*. 1995;60:1230-7.

304. Mace, L., Dervanian, P., Losay, J., Folliguet, T.A., Grinda, J.M., Abdelmoulah, S., Verrier, J.F., Santoro, F. and Neveux, J.Y. Bidirectional inferior vena cava-pulmonary artery shunt. *Annals of Thoracic Surgery*. 1997;63:1321-5.

305. Warden, H.E., DeWall, R.A. and Varco, R.L. Use of the right auricle as a pump for the pulmonary circuit. *Surgical Forum*. 1954;5:16-22.

306. Rose, J.C., Cosimano, S.J., Jr., Hufnagel, C.A. and Massullo, E.A. The effects of exclusion of the right ventricle from the circulation in dogs. *Journal of Clinical Investigation*. 1955;34:1625-31.

307. Haller, J.A., Jr., Adkins, J.C., Worthington, M. and Rauenhorst, J. Experimental studies on permanent bypass of the right heart. *Surgery*. 1966;59:1128-32.

308. Tatooles, C.J., Ardekani, R.G., Miller, R.A. and Serratto, M. Operative repair for tricuspid atresia. *Annals of Thoracic Surgery*. 1976;21:499-503.

309. Stanford, W., Armstrong, R.G., Cline, R.E. and King, T.D. Right atrium-pulmonary artery allograft for correction of tricuspid atresia. *Journal of Thoracic & Cardiovascular Surgery*. 1973;66:105-11.

310. Bowman, F.O., Jr., Malm, J.R., Hayes, C.J. and Gersony, W.M. Physiological approach to surgery for tricuspid atresia. *Circulation*. 1978;58:I83-6.

311. Yacoub, M.H. and Radley-Smith, R. Use of a valved conduit from right atrium to pulmonary artery for "correction" of single ventricle. *Circulation*. 1976;54:III63-70.

312. Gale, A.W., Danielson, G.K., McGoon, D.C. and Mair, D.D. Modified Fontan operation for univentricular heart and complicated congenital lesions. *Journal of Thoracic & Cardiovascular Surgery*. 1979;78:831-8.

313. Doty, D.B., Marvin, W.J., Jr. and Lauer, R.M. Modified Fontan procedure. Methods to achieve direct anastomosis of right atrium to pulmonary artery. *Journal of Thoracic & Cardiovascular Surgery*. 1981;81:470-5.

314. Di Carlo, D., Marcelletti, C., Nijveld, A., Lubbers, L.J. and Becker, A.E. The Fontan procedure in the absence of the interatrial septum. Failure of its principle? *Journal of Thoracic & Cardiovascular Surgery*. 1983;85:923-7.

315. Laks, H., Williams, W.G., Hellenbrand, W.E., Freedom, R.M., Talner, N.S., Rowe, R.D. and Trusler, G.A. Results of right atrial to right ventricular and right atrial to pulmonary artery conduits for complex congenital heart disease. *Annals of Surgery*. 1980;192:382-9.

316. Kreutzer, G.O., Vargas, F.J., Schlichter, A.J., Laura, J.P., Suarez, J.C., Coronel, A.R. and Kreutzer, E.A. Atriopulmonary anastomosis. *Journal of Thoracic & Cardiovascular Surgery*. 1982;83:427-36.

317. Kawashima, Y., Kitamura, S., Matsuda, H., Shimazaki, Y., Nakano, S. and Hirose, H. Total cavopulmonary shunt operation in complex cardiac anomalies. A new operation. *Journal of Thoracic & Cardiovascular Surgery*. 1984;87:74-81.

318. Vargas, F.J., Mayer, J.E., Jr., Jonas, R.A. and Castaneda, A.R. Anomalous systemic and pulmonary venous connections in conjunction with atriopulmonary anastomosis (Fontan-Kreutzer). Technical considerations. *Journal of Thoracic & Cardiovascular Surgery*. 1987;93:523-32.

319. Puga, F.J., Chiavarelli, M. and Hagler, D.J. Modifications of the Fontan operation applicable to patients with left atrioventricular valve atresia or single atrioventricular valve. *Circulation*. 1987;76:III53-60.

320. de Leval, M.R., Kilner, P., Gewillig, M. and Bull, C. Total cavopulmonary connection: a logical alternative to atriopulmonary connection for complex Fontan operations. Experimental studies and early clinical experience. *Journal of Thoracic & Cardiovascular Surgery*. 1988;96:682-95.

321. Geggel, R.L. Update on the modified Fontan procedure. *Current Opinion in Cardiology*. 1997;12:51-62.

322. Fontan, F., Deville, C., Quaegebeur, J., Ottenkamp, J., Sourdille, N., Choussat, A. and Brom, G.A. Repair of tricuspid atresia in 100 patients. *Journal of Thoracic & Cardiovascular Surgery*. 1983;85:647-60.

323. Ishikawa, T., Neutze, J.M., Brandt, P.W. and Barratt-Boyes, B.G. Hemodynamics following the Kreutzer procedure for tricuspid atresia in patients under two years of age. *Journal of Thoracic & Cardiovascular Surgery*. 1984;88:373-9.

324. DiSessa, T.G., Child, J.S., Perloff, J.K., Wu, L., Williams, R.G., Laks, H. and Friedman, W.F. Systemic venous and pulmonary arterial flow patterns after Fontan's procedure for tricuspid atresia or single ventricle. *Circulation*. 1984;70:898-902.

325. Shemin, R.J., Merrill, W.H., Pfeifer, J.S., Conkle, D.M. and Morrow, A.G. Evaluation of right atrial-pulmonary artery conduits for tricuspid atresia. Experimental study. *Journal of Thoracic & Cardiovascular Surgery*. 1979;77:685-90.

326. Penny, D.J. and Redington, A.N. Doppler echocardiographic evaluation of pulmonary blood flow after the Fontan operation: the role of the lungs. *British Heart Journal*. 1991;66:372-4.

327. Matsuda, H., Kawashima, Y., Takano, H., Miyamoto, K. and Mori, T. Experimental evaluation of atrial function in right atrium--pulmonary artery conduit operation for tricuspid atresia. *Journal of Thoracic & Cardiovascular Surgery*. 1981;81:762-7.

328. Di Donato, R.M. The Fontan operation 30 years later. *Cardiology in the Young*. 2004;14 Suppl 3:66-70.

329. van Doorn, C.A.d.L., M. R. The Lateral Tunnel Fontan. *Operative Techniques in Thoracic and Cardiovascular Surgery: A Comparative Atlas*. 2006;11:105-122.

330. Giannico, S., Corno, A., Marino, B., Cicini, M.P., Gagliardi, M.G., Amodeo, A., Picardo, S. and Marcelletti, C. Total extracardiac right heart bypass. *Circulation*. 1992;86:II110-7.

331. Nawa, S. and Teramoto, S. New extension of the Fontan principle: inferior vena cava-pulmonary artery bridge operation. *Thorax*. 1988;43:1022-3.

332. Bridges, N.D. and Castaneda, A.R. The fenestrated Fontan procedure. *Herz*. 1992;17:242-5.

333. Gaynor, J.W., Bridges, N.D., Cohen, M.I., Mahle, W.T., DeCampli, W.M., Steven, J.M., Nicolson, S.C. and Spray, T.L. Predictors of outcome after the Fontan operation: Is hypoplastic left heart syndrome still a risk factor? *Journal of Thoracic & Cardiovascular Surgery*. 2002;123:237-245.

334. Mayer, J.E., Jr. Initial management of the single ventricle patient. *Seminars in Thoracic & Cardiovascular Surgery*. 1994;6:2-7.

335. Van Praagh, R., Ongley, P.A. and Swan, H.J. Anatomic types of single or common ventricle in man. Morphologic and geometric aspects of 60 necropsied cases. *American Journal of Cardiology*. 1964;13:367-86.

336. Gewillig, M. Ventricular dysfunction of the functionally univentricular heart: Management and outcomes. *Cardiology in the Young*. 2005;15:31-34.

337. Barnea, O., Austin, E.H., Richman, B. and Santamore, W.P. Balancing the circulation: theoretic optimization of pulmonary/systemic flow ratio in hypoplastic left heart syndrome. *Journal of the American College of Cardiology*. 1994;24:1376-81.

338. Gewillig, M. The Fontan circulation: late functional results. *Seminars in Thoracic & Cardiovascular Surgery*. 1994;6:56-63.

339. Akagi, T., Benson, L.N., Green, M., Ash, J., Gilday, D.L., Williams, W.G. and Freedom, R.M. Ventricular performance before and after Fontan repair for univentricular atrioventricular connection: angiographic and radionuclide assessment. *Journal of the American College of Cardiology*. 1992;20:920-6.

340. Sluysmans, T., Sanders, S.P., van der Velde, M., Matitiau, A., Parness, I.A., Spevak, P.J., Mayer Jr., J.E. and Colan, S.D. Natural history and patterns of recovery of contractile function in single left ventricle after Fontan operation. *Circulation*. 1992;86:1753-61.

341. Senzaki, H., Masutani, S., Kobayashi, J., Kobayashi, T., Sasaki, N., Asano, H., Kyo, S., Yokote, Y. and Ishizawa, A. Ventricular afterload and ventricular work in fontan circulation: comparison with normal two-ventricle circulation and single-ventricle circulation with blalock-taussig shunts. *Circulation*. 2002;105:2885-92.

342. Rychik, J., Jacobs, M.L. and Norwood Jr., W.I. Acute changes in left ventricular geometry after volume reduction operation. *Annals of Thoracic Surgery*. 1995;60:1267-73; discussion 1274.

343. Tanoue, Y., Sese, A., Ueno, Y., Joh, K. and Hijii, T. Bidirectional Glenn procedure improves the mechanical efficiency of a total cavopulmonary connection in high-risk fontan candidates. *Circulation*. 2001;103:2176-80.

344. Papadimitriou, J.M., Hopkins, B.E. and Taylor, R.R. Regression of left ventricular dilation and hypertrophy after removal of volume overload. Morphological and ultrastructural study. *Circulation Research*. 1974;35:127-35.

345. Cheung, Y.F., Penny, D.J. and Redington, A.N. Serial assessment of left ventricular diastolic function after Fontan procedure. *Heart*. 2000;83:420-4.

346. Penny, D.J. and Redington, A.N. Angiographic demonstration of incoordinate motion of the ventricular wall after the Fontan operation. *British Heart Journal*. 1991;66:456-9.

347. Gaasch, W.H., Levine, H.J., Quinones, M.A. and Alexander, J.K. Left ventricular compliance: mechanisms and clinical implications. *American Journal of Cardiology*. 1976;38:645-53.

348. Norwood, W.I. and Jacobs, M.L. Fontan's procedure in two stages. *American Journal of Surgery*. 1993;166:548-51.

349. Garofalo, C.A., Cabreriza, S.E., Quinn, T.A., Weinberg, A.D., Printz, B.F., Hsu, D.T., Quaegebeur, J.M., Mosca, R.S. and Spotnitz, H.M. Ventricular Diastolic Stiffness Predicts Perioperative Morbidity and Duration of Pleural Effusions After the Fontan Operation. *Circulation*. 2006;114:I-56-61.

350. Szabo, G., Buhmann, V., Graf, A., Melnitschuk, S., Bahrle, S., Vahl, C.F. and Hagl, S. Ventricular energetics after the Fontan operation: contractility-afterload mismatch. *Journal of Thoracic & Cardiovascular Surgery*. 2003;125:1061-9.

351. Tanoue, Y., Kado, H., Shiokawa, Y., Fusazaki, N. and Ishikawa, S. Midterm Ventricular Performance After Norwood Procedure With Right Ventricular-Pulmonary Artery Conduit. *Annals of Thoracic Surgery*. 2004;78:1965-1971.

352. Hogg, K., Swedberg, K. and McMurray, J. Heart failure with preserved left ventricular systolic function; epidemiology, clinical characteristics, and prognosis. *Journal of the American College of Cardiology*. 2004;43:317-27.

353. Adam, A., Dixon, A.K., Grainger, R.G. and Allison, D.J. *Grainger and Allison's diagnostic radiology: a textbook of medical imaging* 5th ed. London: Churchill Livingstone; 2008.

354. Libby, P., Bonow, R.O. and Zipes, D.P. *Braunwald's heart disease: a textbook of cardiovascular medicine*. 8th ed. London: W.B. Saunders Company; 2007.

355. Chuang, M.L., Hibberd, M.G., Salton, C.J., Beaudin, R.A., Riley, M.F., Parker, R.A., Douglas, P.S. and Manning, W.J. Importance of imaging method over imaging modality in noninvasive determination of left ventricular volumes and ejection fraction: assessment by two- and three-dimensional echocardiography and magnetic resonance imaging. *Journal of the American College of Cardiology*. 2000;35:477-84.

356. Hangiandreou, N.J. AAPM/RSNA physics tutorial for residents. Topics in US: B-mode US: basic concepts and new technology. *Radiographics*. 2003;23:1019-33.

357. Bharucha, T., Roman, K.S., Anderson, R.H. and Vettukattil, J.J. Impact of multiplanar review of three-dimensional echocardiographic data on management of congenital heart disease. *Annals of Thoracic Surgery*. 2008;86:875-81.

358. Cheitlin, M.D., Armstrong, W.F., Aurigemma, G.P., Beller, G.A., Bierman, F.Z., Davis, J.L., Douglas, P.S., Faxon, D.P., Gillam, L.D., Kimball, T.R., Kussmaul, W.G., Pearlman, A.S., Philbrick, J.T., Rakowski, H. and Thys, D.M. ACC/AHA/ASE 2003 guideline update for the clinical application of echocardiography--summary article: a report of the American College of Cardiology/American Heart Association Task Force on Practice

Guidelines (ACC/AHA/ASE Committee to Update the 1997 Guidelines for the Clinical Application of Echocardiography). *Journal of the American College of Cardiology*. 2003;42:954-70.

359. Grant, R.P. Architectonics of the heart. *American Heart Journal*. 1953;46:405-31.

360. Greenbaum, R.A. and Gibson, D.G. Regional non-uniformity of left ventricular wall movement in man. *British Heart Journal*. 1981;45:29-34.

361. Mercier, J.C., DiSessa, T.G., Jarmakani, J.M., Nakanishi, T., Hiraishi, S., Isabel-Jones, J. and Friedman, W.F. Two-dimensional echocardiographic assessment of left ventricular volumes and ejection fraction in children. *Circulation*. 1982;65:962-9.

362. Carr, K.W., Engler, R.L., Forsythe, J.R., Johnson, A.D. and Gosink, B. Measurement of left ventricular ejection fraction by mechanical cross-sectional echocardiography. *Circulation*. 1979;59:1196-206.

363. Sandler, H. and Alderman, E. Determination of left ventricular size and shape. *Circulation Research*. 1974;40:1-8.

364. Mitchell, J.H., Wildenthal, K. and Mullins, C.B. Geometrical studies of the left ventricle utilizing biplane cinefluorography. *Federation Proceedings*. 1969;28:1334-43.

365. Palacios, I., Goldman, M., Aretz, T., Okada, R., Osbakken, M., Leavitt, M., Block, P.C. and Boucher, C. Comparison of contrast x-ray biplane cineangiography and technetium-99m radionuclide scans for measurement of ventricular volumes in human autopsy hearts. *American Heart Journal*. 1986;112:1032-8.

366. Pietras, R.J., Kondos, G.T. and Juska, J. Quantitative validation of cineangiographic axial oblique biplane left ventricular volume measurement. *Catheterization & Cardiovascular Diagnosis*. 1987;13:157-61.

367. Pietras, R.J., Kondos, G.T. and Kaplan, D. Quantitative validation of cineangiographic biplane axial oblique right ventricular volume measurement. *American Heart Journal*. 1987;113:321-5.

368. McGuirk, S.P., Winlaw, D.S., Langley, S.M., Stumper, O.F., de Giovanni, J.V., Wright, J.G., Brawn, W.J. and Barron, D.J. The impact of ventricular morphology on midterm outcome following completion total cavopulmonary connection. *European Journal of Cardio-Thoracic Surgery*. 2003;24:37-46.

369. Askenazi, J., Ahnberg, D.S., Korngold, E., LaFarge, C.G., Maltz, D.L. and Treves, S. Quantitative radionuclide angiocardiography: detection and quantitation of left to right shunts. *American Journal of Cardiology*. 1976;37:382-7.

370. Kriss, J.P., Enright, L.P., Hayden, W.G., Wexler, L. and Shumway, N.E. Radioisotopic angiocardiography: findings in congenital heart disease. *Journal of Nuclear Medicine*. 1972;13:31-40.

371. Parrish, M.D., Graham, T.P., Jr., Born, M.L. and Jones, J. Radionuclide evaluation of right and left ventricular function in children: validation of methodology. *American Journal of Cardiology*. 1982;49:1241-7.

372. Kurtz, D., Ahnberg, D.S., Freed, M., LaFarge, C.G. and Treves, S. Quantitative radionuclide angiocardiography. Determination of left ventricular ejection fraction in children. *British Heart Journal*. 1976;38:966-73.

373. Iskandrian, A.E. and Verani, M.S. *Nuclear cardiac imaging. Principles and applications*. 3rd ed. New York: Oxford University Press; 2002.

374. Bogaert, J., Dymarkowski, S. and Taylor, A.M. *Clinical cardiac MRI*. Berlin: Springer-Verlag Berlin and Heidelberg GmbH & Co. KG; 2005.

375. Ohnesorge, B.M., Flohr, T.G., Becker, C.R., Knez, A. and Reiser, M.F. *Multi-slice and dual-source CT in cardiac imaging: principles, protocols, indications, outlook*. 2nd ed. Berlin: Springer-Verlag Berlin and Heidelberg GmbH & Co. KG; 2006.

376. Bellenger, N.G., Grothues, F., Smith, G.C. and Pennell, D.J. Quantification of right and left ventricular function by cardiovascular magnetic resonance. *Herz*. 2000;25:392-9.

377. Lorenz, C.H., Walker, E.S., Graham, T.P., Jr. and Powers, T.A. Right ventricular performance and mass by use of cine MRI late after atrial repair of transposition of the great arteries. *Circulation*. 1995;92:II233-9.

378. Kaji, S., Yang, P.C., Kerr, A.B., Tang, W.H., Meyer, C.H., Macovski, A., Pauly, J.M., Nishimura, D.G. and Hu, B.S. Rapid evaluation of left ventricular volume and mass without breath-holding using real-time interactive cardiac magnetic resonance imaging system. *Journal of the American College of Cardiology*. 2001;38:527-33.

379. Kuehne, T., Yilmaz, S., Steendijk, P., Moore, P., Groenink, M., Saaed, M., Weber, O., Higgins, C.B., Ewert, P., Fleck, E., Nagel, E., Schulze-Neick, I. and Lange, P. Magnetic resonance imaging analysis of right ventricular pressure-volume loops: in vivo validation and clinical application in patients with pulmonary hypertension. *Circulation*. 2004;110:2010-6.

380. Baan, J., Jong, T.T., Kerkhof, P.L., Moene, R.J., van Dijk, A.D., van der Velde, E.T. and Koops, J. Continuous stroke volume and cardiac output from intra-ventricular dimensions obtained with impedance catheter. *Cardiovascular Research*. 1981;15:328-34.

381. Baan, J., van der Velde, E.T., de Bruin, H.G., Smeenk, G.J., Koops, J., van Dijk, A.D., Temmerman, D., Senden, J. and Buis, B. Continuous measurement of left ventricular volume in animals and humans by conductance catheter. *Circulation*. 1984;70:812-23.

382. Mur, G. and Baan, J. Computation of the input impedances of a catheter for cardiac volumetry. *IEEE Transactions on Biomedical Engineering*. 1984;31:448-53.

383. Valentinuzzi, M.E. and Spinelli, J.C. Intracardiac measurements with the impedance technique. *IEEE Engineering in Medicine and Biology Magazine*. 1989;8:27-34.

384. White, P.A. and Redington, A.N. Right ventricular volume measurement: can conductance do it better? *Physiological Measurement*. 2000;21:R23-41.

385. Rushmer, R.F., Crystal, D.K., Wagner, C. and Ellis, R.M. Intracardiac impedance plethysmography. *American Journal of Physiology*. 1953;174:171-4.

386. Geddes, L.A., Hoff, H.E. and Mello, A. The development and calibration of a method for the continuous measurement of stroke-volume in the experimental animal. *Japanese Heart Journal*. 1966;7:556-65.

387. Geddes, L.A. and Baker, L.E. *Principles of applied biomedical instrumentation*. 2nd ed. New York: John Wiley & Sons; 1975.

388. Baker, L.E. Principles of the impedance technique. *IEEE Engineering in Medicine and Biology Magazine*. 1989;8:11-15.

389. Penney, B.C. Theory and cardiac applications of electrical impedance measurements. *Critical Reviews in Biomedical Engineering*. 1986;13:227-81.

390. Woodard, J.C., Bertram, C.D. and Gow, B.S. Effect of radial position on volume measurements using the conductance catheter. *Medical & Biological Engineering & Computing*. 1989;27:25-32.

391. Geddes, L.A. and Baker, L.E. The specific resistance of biological material--a compendium of data for the biomedical engineer and physiologist. *Medical & Biological Engineering*. 1967;5:271-93.

392. Al-Khalidi, A.H., Townend, J.N., Bonser, R.S. and Coote, J.H. Validation of the conductance catheter method for measurement of ventricular volumes under varying conditions relevant to cardiac surgery. *American Journal of Cardiology*. 1998;82:1248-52.

393. White, P.A., Brookes, C.I., Ravn, H., Hjortdal, V., Chaturvedi, R.R. and Redington, A.N. Validation and utility of novel volume reduction technique for determination of parallel conductance. *American Journal of Physiology - Heart & Circulatory Physiology*. 2001;280:H475-82.

394. Gawne, T.J., Gray, K.S. and Goldstein, R.E. Estimating left ventricular offset volume using dual-frequency conductance catheters. *Journal of Applied Physiology*. 1987;63:872-6.

395. McKay, R.G., Spears, J.R., Aroesty, J.M., Baim, D.S., Royal, H.D., Heller, G.V., Lincoln, W., Salo, R.W., Braunwald, E. and Grossman, W. Instantaneous measurement of left and right ventricular stroke volume and pressure-volume relationships with an impedance catheter. *Circulation*. 1984;69:703-10.

396. Steendijk, P. and Baan, J. Comparison of intravenous and pulmonary artery injections of hypertonic saline for the assessment of conductance catheter parallel conductance. *Cardiovascular Research*. 2000;46:82-9.

397. Steendijk, P., Staal, E., Jukema, J.W. and Baan, J. Hypertonic saline method accurately determines parallel conductance for dual-field conductance catheter. *American Journal of Physiology - Heart & Circulatory Physiology*. 2001;281:H755-63.

398. Herrera, M.C., Olivera, J.M. and Valentinuzzi, M.E. Parallel conductance determination in cardiac volumetry using dilution manoeuvres: theoretical analysis and practical implications. *Medical & Biological Engineering & Computing*. 1999;37:169-74.

399. Cassidy, S.C. and Teitel, D.F. The conductance volume catheter technique for measurement of left ventricular volume in young piglets. *Pediatric Research*. 1992;31:85-90.

400. Boltwood, C.M., Jr., Appleyard, R.F. and Glantz, S.A. Left ventricular volume measurement by conductance catheter in intact dogs. Parallel conductance volume depends on left ventricular size. *Circulation*. 1989;80:1360-77.

401. Applegate, R.J., Cheng, C.P. and Little, W.C. Simultaneous conductance catheter and dimension assessment of left ventricle volume in the intact animal. *Circulation*. 1990;81:638-48.

402. Kornet, L., Schreuder, J.J., van der Velde, E.T. and Jansen, J.R. The volume-dependency of parallel conductance throughout the cardiac cycle and its consequence for volume estimation of the left ventricle in patients. *Cardiovascular Research*. 2001;51:729-35.

403. Salo, R.W. The theoretical basis of a computational model for the determination of volume by impedance. *Automedica*. 1989;11:299-310.

404. Wei, C.-L., Valvano, J.W., Feldman, M.D. and Pearce, J.A. Nonlinear conductance-volume relationship for murine conductance catheter measurement system. *IEEE Transactions on Biomedical Engineering*. 2005;52:1654-61.

405. Wu, C.C., Skalak, T.C., Schwenk, T.R., Mahler, C.M., Anne, A., Finnerty, P.W., Haber, H.L., Weikle, R.M., 2nd and Feldman, M.D. Accuracy of the conductance catheter for

measurement of ventricular volumes seen clinically: Effects of electric field homogeneity and parallel conductance. *IEEE Transactions on Biomedical Engineering*. 1997;44:266-77.

406. Kun, S. and Peura, R.A. Analysis of conductance volumetric measurement error sources. *Medical & Biological Engineering & Computing*. 1994;32:94-100.

407. Steendijk, P., van der Velde, E.T. and Baan, J. Single and dual excitation of the conductance-volume catheter analysed in a spheroidal mathematical model of the canine left ventricle. *European Heart Journal*. 1992;13 Suppl E:28-34.

408. Salo, R.W., Wallner, T.G. and Pederson, B.D. Measurement of ventricular volume by intracardiac impedance: theoretical and empirical approaches. *IEEE Transactions on Biomedical Engineering*. 1986;33:189-95.

409. Salo, R.W. Improvement in intracardiac impedance volumes by field extrapolation. *European Heart Journal*. 1992;13 Suppl E:35-9.

410. Baan, J., van der Velde, E.T., Steendijk, P. and Koops, J. Calibration and application of the conductance catheter for ventricular volume measurement. *Automedica*. 1989;11.

411. Steendijk, P., Van der Velde, E.T. and Baan, J. Left ventricular stroke volume by single and dual excitation of conductance catheter in dogs. *American Journal of Physiology*. 1993;264:H2198-207.

412. Hayashi, Y., Takeuchi, M., Takaoka, H. and Yokoyama, M. Measurement of left ventricular volume by dual-field conductance catheter in humans--comparison with single-field conductance catheter. *Japanese Circulation Journal*. 1996;60:85-95.

413. Szwarc, R.S., Laurent, D., Allegrini, P.R. and Ball, H.A. Conductance catheter measurement of left ventricular volume: evidence for nonlinearity within cardiac cycle. *American Journal of Physiology*. 1995;268:H1490-8.

414. Danton, M.H.D., Greil, G.F., Byrne, J.G., Hsin, M., Cohn, L. and Maier, S.E. Right ventricular volume measurement by conductance catheter. *American Journal of Physiology - Heart & Circulatory Physiology*. 2003;285:H1774-1785.

415. van der Velde, E.T., van Dijk, A.D., Steendijk, P., Diethelm, L., Chagas, T., Lipton, M.J., Glanz, S.A. and Baan, J. Left ventricular segmental volume by conductance catheter and Cine-CT. *European Heart Journal*. 1992;13 Suppl E:15-21.

416. Odake, M., Takeuchi, M., Takaoka, H., Hata, K., Hayashi, Y. and Yokoyama, M. Determination of left ventricular volume using a conductance catheter in the diseased human heart. *European Heart Journal*. 1992;13 Suppl E:22-7.

417. Asanoi, H., Ishizaka, S., Kameyama, T., Nozawa, T., Miyagi, K. and Sasayama, S. Serial reproducibility of conductance catheter volumetry of left ventricle in conscious dogs. *American Journal of Physiology*. 1992;262:H911-5.

418. O'Brien, E. and Fitzgerald, D. The history of blood pressure measurement. *Journal of Human Hypertension*. 1994;8:73-84.

419. Kurtz, T.W., Griffin, K.A., Bidani, A.K., Davisson, R.L., Hall, J.E., Subcommittee of, P. and Public Education of the American Heart, A. Recommendations for blood pressure measurement in humans and experimental animals. Part 2: Blood pressure measurement in experimental animals: a statement for professionals from the subcommittee of professional and public education of the American Heart Association council on high blood pressure research. *Hypertension*. 2005;45:299-310.

420. Lake, C.L. and Booker, P.D. *Pediatric cardiac anesthesia*. 4th ed. Philadelphia: Lippincott Williams and Wilkins; 2004.

421. Hipkins, S.F., Rutten, A.J. and Runciman, W.B. Experimental analysis of catheter-manometer systems in vitro and in vivo. *Anesthesiology*. 1989;71:893-906.

422. Patel, D.J., Mason, D.T., Ross, J., Jr. and Braunwald, E. Harmonic Analysis of Pressure Pulses Obtained from the Heart and Great Vessels of Man. *American Heart Journal*. 1965;69:785-94.

423. Attinger, E.O., Anne, A. and McDonald, D.A. Use of Fourier series for the analysis of biological systems. *Biophysical Journal*. 1966;6:291-304.

424. Hansen, A.T. Pressure measurements in the human organism. *Acta Physiologica Scandinavica*. 1949;19 (Suppl 68):1-227.

425. Ishizawa, A., Awa, S., Kaneshi, K., Koike, I. and Okamoto, A. Accuracy in Manometry during Cardiac Catheterization in Children (Quantitative Assessment of Damping of the Systems of Manometry Using Various Catheters and Connectors). *Pediatrics International*. 1980;24:315-323.

426. Gersh, B.J., Hahn, C.E.W., Prys-Roberts, C. and Cashion, J. Physical criteria for measurement of left ventricular pressure and its first derivative. *Cardiovascular Research*. 1971;5:32-40.

427. Fry, D.L. Physiologic recording by modern instruments with particular reference to pressure recording. *Physiological Reviews*. 1960;40:753-88.

428. Gardner, R.M. Direct blood pressure measurement--dynamic response requirements. *Anesthesiology*. 1981;54:227-36.

429. Schwid, H.A. Frequency response evaluation of radial artery catheter-manometer systems: sinusoidal frequency analysis versus flush method. *Journal of Clinical Monitoring*. 1988;4:181-5.

430. Nichols, W.W. and O'Rourke, M.F. *Mcdonald's Blood Flow in Arteries. Theoretic, Experimental and Clinical Principles*. 3rd ed. Philadelphia: Lippincott Williams and Wilkins; 1990.

431. Kleinman, B. Understanding natural frequency and damping and how they relate to the measurement of blood pressure. *Journal of Clinical Monitoring*. 1989;5:137-47.

432. van Genderingen, H.R., Gevers, M. and Hack, W.W. Intra-arterial pressure measurement in neonates: dynamic response requirements. *Physiological Measurement*. 1995;16:55-61.

433. Millar, H.D. and Baker, L.E. A stable ultraminiature catheter-tip pressure transducer. *Medical & Biological Engineering*. 1973;11:86-9.

434. Sugeng, L., Mor-Avi, V., Weinert, L., Niel, J., Ebner, C., Steringer-Mascherbauer, R., Schmidt, F., Galuschky, C., Schummers, G., Lang, R.M. and Nesser, H.-J. Quantitative assessment of left ventricular size and function: side-by-side comparison of real-time three-dimensional echocardiography and computed tomography with magnetic resonance reference. *Circulation*. 2006;114:654-61.

435. Bland, J.M. and Altman, D.G. Measurement error. *British Medical Journal*. 1996;313:744.

436. Parker, K.H. An introduction to wave intensity analysis. *Medical & Biological Engineering & Computing*. 2009;47:175-88.

437. Parker, K.H. A brief history of arterial wave mechanics. *Medical & Biological Engineering & Computing*. 2009;47:111-8.

438. O'Rourke, M.F. and Taylor, M.G. Input Impedance of the Systemic Circulation. *Circulation Research*. 1967;20:365-380.

439. Zimmer, H.G. and Millar, H.D. Technology and application of ultraminiature catheter pressure transducers. *Canadian Journal of Cardiology*. 1998;14:1259-66.

440. Tibby, S.M. and Murdoch, I.A. Monitoring cardiac function in intensive care. *Archives of Disease in Childhood*. 2003;88:46-52.

441. Allsager, C.M. and Swanevelder, J. Measuring cardiac output. *Continuing Education in Anaesthesia, Critical Care & Pain*. 2003;3:15-19.

442. Li, J., Schulze-Neick, I., Lincoln, C., Shore, D., Scallan, M., Bush, A., Redington, A.N. and Penny, D.J. Oxygen consumption after cardiopulmonary bypass surgery in children: determinants and implications. *Journal of Thoracic & Cardiovascular Surgery*. 2000;119:525-33.

443. LaFarge, C.G. and Miettinen, O.S. The estimation of oxygen consumption. *Cardiovascular Research*. 1970;4:23-30.

444. Ganz, W., Donoso, R., Marcus, H.S., Forrester, J.S. and Swan, H.J. A new technique for measurement of cardiac output by thermodilution in man. *American Journal of Cardiology*. 1971;27:392-6.

445. Pauli, C., Fakler, U., Genz, T., Hennig, M., Lorenz, H.P. and Hess, J. Cardiac output determination in children: equivalence of the transpulmonary thermodilution method to the direct Fick principle. *Intensive Care Medicine*. 2002;28:947-52.

446. Le Tulzo, Y., Belghith, M., Seguin, P., Dall'Ava, J., Monchi, M., Thomas, R. and Dhainaut, J.F. Reproducibility of thermodilution cardiac output determination in critically ill patients: comparison between bolus and continuous method. *Journal of Clinical Monitoring*. 1996;12:379-85.

447. Su, N.-Y., Huang, C.-J., Tsai, P., Hsu, Y.-W., Hung, Y.-C. and Cheng, C.-R. Cardiac output measurement during cardiac surgery: esophageal Doppler versus pulmonary artery catheter. *Acta Anaesthesiologica Sinica*. 2002;40:127-33.

448. Berton, C. and Cholley, B. Equipment review: new techniques for cardiac output measurement--oesophageal Doppler, Fick principle using carbon dioxide, and pulse contour analysis. *Critical Care*. 2002;6:216-21.

449. Dark, P.M. and Singer, M. The validity of trans-esophageal Doppler ultrasonography as a measure of cardiac output in critically ill adults. *Intensive Care Medicine*. 2004;30:2060-6.

450. Wyatt, D.G. Blood flow and blood velocity measurement in vivo by electromagnetic induction. *Transactions of the Institute of Measurement and Control*. 1982;4:61-78.

451. Marcus, M.L., Wilson, R.F. and White, C.W. Methods of measurement of myocardial blood flow in patients: a critical review. *Circulation*. 1987;76:245-53.

452. Louagie, Y.A., Haxhe, J.P., Buche, M. and Schoevaerdts, J.C. Intraoperative electromagnetic flowmeter measurements in coronary artery bypass grafts. *Annals of Thoracic Surgery*. 1994;57:357-64.

453. Kolin, A., MacAloin, R.N., Snow, H.D., Coster, I.R. and Stein, J.J. Dependability of the non-occlusive base line of the interrupted resonance electromagnetic blood flow meter system. *Life Sciences*. 1975;16:501-16.

454. Beldi, G., Bosshard, A., Hess, O.M., Althaus, U. and Walpoth, B.H. Transit time flow measurement: experimental validation and comparison of three different systems. *Annals of Thoracic Surgery*. 2000;70:212-7.

455. Hartman, J.C., Olszanski, D.A., Hullinger, T.G. and Brunden, M.N. In vivo validation of a transit-time ultrasonic volume flow meter. *Journal of Pharmacological & Toxicological Methods*. 1994;31:153-60.

456. Laustsen, J., Pedersen, E.M., Terp, K., Steinbrüchel, D., Kure, H.H., Paulsen, P.K., Jørgensen, H. and Paaske, W.P. Validation of a new transit time ultrasound flowmeter in man. *European Journal of Vascular and Endovascular Surgery*. 1996;12:91-96.

457. Schroeder, M.J.M.J., Perreault, B., Ewert, D.L.D.L. and Koenig, S.C.S.C. HEART: an automated beat-to-beat cardiovascular analysis package using Matlab. *Computers in Biology & Medicine*. 2004;34:371-88.

458. Al-Khalidi, A.H., Robinson-Miller, M., Eagleton, T., Farr, J.P.G., Sammons, R.L., Lewis, M.E., Townend, J.N., Bonser, R.S. and Coote, J.H. On the repeated use of combination pressure-volume catheter. *Journal of the Institute of Sterile Services Management* 2000;4.

459. Tkacova, R., Hall, M.J., Liu, P.P., Fitzgerald, F.S. and Bradley, T.D. Left ventricular volume in patients with heart failure and Cheyne-Stokes respiration during sleep. *American Journal of Respiratory & Critical Care Medicine*. 1997;156:1549-55.

460. Kass, D.A. Clinical evaluation of left heart function by conductance catheter technique. *European Heart Journal*. 1992;13 Suppl E:57-64.

461. Senzaki, H., Chen, C.H., Masutani, S., Taketazu, M., Kobayashi, J., Kobayashi, T., Sasaki, N., Asano, H., Kyo, S. and Yokote, Y. Assessment of cardiovascular dynamics by pressure-area relations in pediatric patients with congenital heart disease. *Journal of Thoracic & Cardiovascular Surgery*. 2001;122:535-47.

462. Taccardi, B., Arisi, G., Macchi, E., Baruffi, S. and Spaggiari, S. A new intracavitary probe for detecting the site of origin of ectopic ventricular beats during one cardiac cycle. *Circulation*. 1987;75:272-281.

463. Derfus, D.L., Pilkington, T.C., Simpson, E.W. and Ideker, R.E. A comparison of measured and calculated intracavitary potentials for electrical stimuli in the exposed dog heart. *IEEE Transactions on Biomedical Engineering*. 1992;39:1192-206.

464. Khoury, D.S. and Rudy, Y. A model study of volume conductor effects on endocardial and intracavitary potentials. *Circulation Research*. 1992;71:511-25.

465. Burkhoff, D., Mirsky, I. and Suga, H. Assessment of systolic and diastolic ventricular properties via pressure-volume analysis: a guide for clinical, translational, and basic researchers. *American Journal of Physiology - Heart & Circulatory Physiology*. 2005;289:H501-12.

466. Roelandt, J. and Gibson, D.G. Recommendations for standardization of measurements from M-mode echocardiograms. *European Heart Journal*. 1980;1:375-8.

467. Mogelvang, J., Thomsen, C., Mehlsen, J., Brackle, G., Stubgaard, M. and Henriksen, O. Evaluation of left ventricular volumes measured by magnetic resonance imaging. *European Heart Journal*. 1986;7:1016-21.

468. Al-Khalidi, A.H., Lewis, M.E., Townened, J.N., Bonser, R.S. and Coote, J.H. A novel and simple technique to allow detection of the position of the R-waves from intraventricular pressure waveforms: application to the conductance catheter method. *IEEE Transactions on Biomedical Engineering*. 2001;48:606-10.

469. Freedom, R.M., Nykanen, D. and Benson, L.N. The physiology of the bidirectional cavopulmonary connection. *Annals of Thoracic Surgery*. 1998;66:664-667.

470. Santamore, W.P., Barnea, O., Riordan, C.J., Ross, M.P. and Austin, E.H. Theoretical optimization of pulmonary-to-systemic flow ratio after a bidirectional cavopulmonary anastomosis. *American Journal of Physiology*. 1998;274:H694-700.

471. Lamberti, J.J., Spicer, R.L., Waldman, J.D., Grehl, T.M., Thomson, D., George, L., Kirkpatrick, S.E. and Mathewson, J.W. The bidirectional cavopulmonary shunt. *Journal of Thoracic & Cardiovascular Surgery*. 1990;100:22-9; discussion 29-30.

472. Jacobs, M.L., Rychik, J., Rome, J.J., Apostolopoulou, S., Pizarro, C., Murphy, J.D. and Norwood Jr., W.I. Early reduction of the volume work of the single ventricle: the hemi-Fontan operation. *Annals of Thoracic Surgery*. 1996;62:456-61; discussion 461-2.

473. Donofrio, M.T., Jacobs, M.L., Spray, T.L. and Rychik, J. Acute changes in preload, afterload, and systolic function after superior cavopulmonary connection. *Annals of Thoracic Surgery*. 1998;65:503-8.

474. Forbes, T.J., Gajarski, R., Johnson, G.L., Reul, G.J., Ott, D.A., Drescher, K. and Fisher, D.J. Influence of age on the effect of bidirectional cavopulmonary anastomosis on left ventricular volume, mass and ejection fraction. *Journal of the American College of Cardiology*. 1996;28:1301-7.

475. Seliem, M.A., Baffa, J.M., Vetter, J.M., Chen, S.L., Chin, A.J. and Norwood Jr., W.I. Changes in right ventricular geometry and heart rate early after hemi-Fontan procedure. *Annals of Thoracic Surgery*. 1993;55:1508-12.

476. Berman, N.B. and Kimball, T.R. Systemic ventricular size and performance before and after bidirectional cavopulmonary anastomosis. *Journal of Pediatrics*. 1993;122:S63-7.

477. Allgood, N.L., Alejos, J., Drinkwater, D.C., Laks, H. and Williams, R.G. Effectiveness of the bidirectional Glenn shunt procedure for volume unloading in the single ventricle patient. *American Journal of Cardiology*. 1994;74:834-6.

478. Selamet Tierney, E.S., Glickstein, J.S., Altmann, K., Solowiejczyk, D.E., Mosca, R.S., Quaegebeur, J.M., Kleinman, C.S. and Printz, B.F. Bidirectional cavopulmonary anastomosis: Impact on diastolic ventricular function indices. *Pediatric Cardiology*. 2007;28:372-378.

479. Williams, R.V., Ritter, S., Tani, L.Y., Pagoto, L.T. and Minich, L.L. Quantitative assessment of ventricular function in children with single ventricles using the Doppler myocardial performance index.[see comment]. *American Journal of Cardiology*. 2000;86:1106-10.

480. Rumball, E.M., McGuirk, S.P., Stumper, O., Laker, S.J., de Giovanni, J.V., Wright, J.G., Barron, D.J. and Brawn, W.J. The RV-PA conduit stimulates better growth of the pulmonary arteries in hypoplastic left heart syndrome. *European Journal of Cardio-Thoracic Surgery*. 2005;27:801-6.

481. McGuirk, S.P., Griselli, M., Stumper, O.F., Rumball, E.M., Miller, P., Dhillon, R., de Giovanni, J.V., Wright, J.G., Barron, D.J. and Brawn, W.J. Staged surgical management of hypoplastic left heart syndrome: a single institution 12 year experience. *Heart*. 2006;92:364-70.

482. Brawn, W.J. and Barron, D.J. Management and outcome in hypoplastic left heart syndrome. *Current Paediatrics*. 2004;14.

483. Barron, D.J., Brooks, A., Stickley, J., Woolley, S.M., Stumper, O., Jones, T.J. and Brawn, W.J. The Norwood procedure using a right ventricle-pulmonary artery conduit: comparison of the right-sided versus left-sided conduit position. *Journal of Thoracic & Cardiovascular Surgery*. 2009;138:528-37.

484. Cohn, L.H., ed. *Cardiac Surgery in the Adult*. 3rd ed. New York: McGraw-Hill; 2007.

485. DuBois, D. and DuBois, E.F. A formula to estimate the approximate surface area if height and weight be known. *Archives of Internal Medicine*. 1916;17:863-871.

486. Swindell, C.G., Barker, T.A., McGuirk, S.P., Jones, T.J., Barron, D.J., Brawn, W.J., Horsburgh, A. and Willetts, R.G. Washing of irradiated red blood cells prevents hyperkalaemia during cardiopulmonary bypass in neonates and infants undergoing surgery for complex congenital heart disease.[see comment]. *European Journal of Cardio-Thoracic Surgery*. 2007;31:659-64.

487. Heymann, M.A. and Rudolph, A.M. Effects of increasing preload on right ventricular output in fetal lambs in utero. *Circulation*. 1973;48:IV-37.

488. Brookes, C.I., White, P.A., Bishop, A.J., Oldershaw, P.J., Redington, A.N. and Moat, N.E. Validation of a new intraoperative technique to evaluate load-independent indices of

right ventricular performance in patients undergoing cardiac operations. *Journal of Thoracic & Cardiovascular Surgery*. 1998;116:468-76.

489. Nakazawa, M., Marks, R.A., Isabel-Jones, J. and Jarmakani, J.M. Right and left ventricular volume characteristics in children with pulmonary stenosis and intact ventricular septum. *Circulation*. 1976;53:884-90.

490. Graham, T.P., Jr., Jarmakani, J.M., Canent Jr., R.V. and Morrow, M.N. Left heart volume estimation in infancy and childhood. Reevaluation of methodology and normal values. *Circulation*. 1971;43:895-904.

491. Nozawa, T., Yasumura, Y., Futaki, S., Tanaka, N., Uenishi, M. and Suga, H. Efficiency of energy transfer from pressure-volume area to external mechanical work increases with contractile state and decreases with afterload in the left ventricle of the anesthetized closed-chest dog. *Circulation*. 1988;77:1116-24.

492. van der Velde, E.T., Burkhoff, D., Steendijk, P., Karsdon, J., Sagawa, K. and Baan, J. Nonlinearity and load sensitivity of end-systolic pressure-volume relation of canine left ventricle in vivo. *Circulation*. 1991;83:315-27.

493. Graham, T.P., Jr., Jarmakani, J.M., Atwood, G.F. and Canent, R.V., Jr. Right ventricular volume determinations in children. Normal values and observations with volume or pressure overload. *Circulation*. 1973;47:144-53.

494. Chin, A.J., Franklin, W.H., Andrews, B.A. and Norwood Jr., W.I. Changes in ventricular geometry early after Fontan operation. *Annals of Thoracic Surgery*. 1993;56:1359-65.

495. Seliem, M., Muster, A.J., Paul, M.H. and Benson Jr., D.W. Relation between preoperative left ventricular muscle mass and outcome of the Fontan procedure in patients with tricuspid atresia. *Journal of the American College of Cardiology*. 1989;14:750-5.

496. Gewillig, M. and Kalis, N. Pathophysiological aspects after cavopulmonary anastomosis. *Thoracic & Cardiovascular Surgeon*. 2000;48:336-41.

497. Scheurer, M.A., Hill, E.G., Vasuki, N., Maurer, S., Graham, E.M., Bandisode, V., Shirali, G.S., Atz, A.M. and Bradley, S.M. Survival after bidirectional cavopulmonary anastomosis: analysis of preoperative risk factors. *Journal of Thoracic & Cardiovascular Surgery*. 2007;134:82-9.

498. Frenneaux, M. and Williams, L. Ventricular-arterial and ventricular-ventricular interactions and their relevance to diastolic filling. *Progress in Cardiovascular Diseases*. 2007;49:252-62.

499. McKenney, P.A., Apstein, C.S., Mendes, L.A., Connelly, G.P., Aldea, G.S., Shemin, R.J. and Davidoff, R. Increased left ventricular diastolic chamber stiffness immediately after coronary artery bypass surgery. *Journal of the American College of Cardiology*. 1994;24:1189-94.

500. Ballweg, J.A., Dominguez, T.E., Ravishankar, C., Kreutzer, J., Marino, B.S., Bird, G.L., Gruber, P.J., Wernovsky, G., Gaynor, J.W., Nicolson, S.C., Spray, T.L. and Tabbutt, S. A contemporary comparison of the effect of shunt type in hypoplastic left heart syndrome on the hemodynamics and outcome at stage 2 reconstruction. *Journal of Thoracic & Cardiovascular Surgery*. 2007;134:297-303.

501. Jacobs, M.L. and Norwood Jr., W.I. Fontan operation: influence of modifications on morbidity and mortality. *Annals of Thoracic Surgery*. 1994;58:945-51; discussion 951-2.

502. de Leval, M.R. The Fontan circulation: a challenge to William Harvey? *Nature Clinical Practice Cardiovascular Medicine*. 2005;2:202-8.

503. Gentles, T.L., Gauvreau, K., Mayer Jr., J.E., Fishberger, S.B., Burnett, J., Colan, S.D., Newburger, J.W. and Wernovsky, G. Functional outcome after the Fontan operation: factors influencing late morbidity. *Journal of Thoracic & Cardiovascular Surgery*. 1997;114:392-403; discussion 404-5.

504. Fontan, F., Kirklin, J.W., Fernandez, G., Costa, F., Naftel, D.C., Tritto, F. and Blackstone, E.H. Outcome after a "perfect" Fontan operation. *Circulation*. 1990;81:1520-36.

505. Driscoll, D.J., Offord, K.P., Feldt, R.H., Schaff, H.V., Puga, F.J. and Danielson, G.K. Five- to fifteen-year follow-up after Fontan operation. *Circulation*. 1992;85:469-96.

506. Border, W.L., Syed, A.U., Michelfelder, E.C., Khoury, P., Uzark, K.C., Manning, P.B. and Pearl, J.M. Impaired systemic ventricular relaxation affects postoperative short-term outcome in Fontan patients. *Journal of Thoracic & Cardiovascular Surgery*. 2003;126:1760-4.

507. McCormack, J.G. Total intravenous anaesthesia in children. *Current Anaesthesia & Critical Care*. 2008;19:309-314.

508. Kelley, J.R., Mack, G.W. and Fahey, J.T. Diminished venous vascular capacitance in patients with univentricular hearts after the Fontan operation. *American Journal of Cardiology*. 1995;76:158-63.

509. de Leval, M.R. The Fontan circulation: what have we learned? What to expect? *Pediatric Cardiology*. 1998;19:316-320.

510. Redington, A.N., Penny, D. and Shinebourne, E.A. Pulmonary blood flow after total cavopulmonary shunt. *British Heart Journal*. 1991;65:213-7.

511. Kussmaul, W.G., Noordergraaf, A. and Laskey, W.K. Right ventricular-pulmonary arterial interactions. *Annals of Biomedical Engineering*. 1992;20:63-80.

512. Hsia, T.Y., Khambadkone, S., Redington, A.N., Migliavacca, F., Deanfield, J.E. and de Leval, M.R. Effects of respiration and gravity on infradiaphragmatic venous flow in normal and Fontan patients. *Circulation*. 2000;102:III148-53.

513. Gewillig, M.H., Lundstrom, U.R., Deanfield, J.E., Bull, C., Franklin, R.C., Graham Jr., T.P. and Wyse, R.K. Impact of Fontan operation on left ventricular size and contractility in tricuspid atresia. *Circulation*. 1990;81:118-27.

514. Gewillig, M., Daenen, W., Aubert, A. and Van der Hauwaert, L. Abolishment of chronic volume overload. Implications for diastolic function of the systemic ventricle immediately after Fontan repair. *Circulation*. 1992;86:II93-9.

515. Penny, D.J., Rigby, M.L. and Redington, A.N. Abnormal patterns of intraventricular flow and diastolic filling after the Fontan operation: evidence for incoordinate ventricular wall motion. *British Heart Journal*. 1991;66:375-8.

516. Fogel, M.A., Weinberg, P.M., Chin, A.J., Fellows, K.E. and Hoffman, E.A. Late ventricular geometry and performance changes of functional single ventricle throughout staged Fontan reconstruction assessed by magnetic resonance imaging. *Journal of the American College of Cardiology*. 1996;28:212-21.

517. Schulze-Neick, I., Li, J., Penny, D.J. and Redington, A.N. Pulmonary vascular resistance after cardiopulmonary bypass in infants: effect on postoperative recovery. *Journal of Thoracic & Cardiovascular Surgery*. 2001;121:1033-9.

518. Kass, D.A. and Kelly, R.P. Ventriculo-arterial coupling: concepts, assumptions, and applications. *Annals of Biomedical Engineering*. 1992;20:41-62.

519. Chaturvedi, R.R., Lincoln, C., Gothard, J.W., Scallan, M.H., White, P.A., Redington, A.N. and Shore, D.F. Left ventricular dysfunction after open repair of simple congenital heart defects in infants and children: quantitation with the use of a conductance catheter immediately after bypass. *Journal of Thoracic & Cardiovascular Surgery*. 1998;115:77-83.

520. White, P.A., Chaturvedi, R.R., Shore, D., Lincoln, C., Szwarc, R.S., Bishop, A.J., Oldershaw, P.J. and Redington, A.N. Left ventricular parallel conductance during cardiac cycle in children with congenital heart disease. *American Journal of Physiology*. 1997;273:H295-302.

521. Lewis, M.E., Al-Khalidi, A.H., Bonser, R.S., Clutton-Brock, T., Morton, D., Paterson, D., Townend, J.N. and Coote, J.H. Vagus nerve stimulation decreases left ventricular contractility in vivo in the human and pig heart. *Journal of Physiology*. 2001;534:547-52.

522. Lewis, M.E., Al-Khalidi, A.H., Townend, J.N., Coote, J. and Bonser, R.S. The effects of hypothermia on human left ventricular contractile function during cardiac surgery. *Journal of the American College of Cardiology*. 2002;39:102-8.

523. Caputo, M., Schreuder, J., Fino, C., Baan, J. and Alfieri, O. Assessment of myocardial performance with ventricular pressure-volume relations: clinical applications in cardiac surgery. *Italian Heart Journal*. 2000;1:269-74.

524. Tulner, S.A.F., Klautz, R.J.M., Engbers, F.H.M., Bax, J.J., Baan, J., van der Wall, E.E., Dion, R.A.E. and Steendijk, P. Left ventricular function and chronotropic responses after normothermic cardiopulmonary bypass with intermittent antegrade warm blood cardioplegia in patients undergoing coronary artery bypass grafting. *European Journal of Cardio-Thoracic Surgery*. 2005;27:599-605.

525. Tulner, S.A.F., Bax, J.J., Bleeker, G.B., Steendijk, P., Klautz, R.J.M., Holman, E.R., Schalij, M.J., Dion, R.A.E. and van der Wall, E.E. Beneficial hemodynamic and clinical effects of surgical ventricular restoration in patients with ischemic dilated cardiomyopathy.[see comment]. *Annals of Thoracic Surgery*. 2006;82:1721-7.

526. Tulner, S.A., Steendijk, P., Klautz, R.J., Tops, L., Bax, J.J., Versteegh, M.I., Verwey, H.F., Schalij, M.J., van der Wall, E.E. and Dion, R.A. Clinical efficacy of surgical heart failure therapy by ventricular restoration and restrictive mitral annuloplasty. *Journal of Cardiac Failure*. 2007;13:178-83.

527. Handschumacher, M.D., Lethor, J.P., Siu, S.C., Mele, D., Rivera, J.M., Picard, M.H., Weyman, A.E. and Levine, R.A. A new integrated system for three-dimensional echocardiographic reconstruction: development and validation for ventricular volume with application in human subjects. *Journal of the American College of Cardiology*. 1993;21:743-53.

528. Sapin, P.M., Schroeder, K.M., Gopal, A.S., Smith, M.D. and King, D.L. Three-dimensional echocardiography: Limitations of apical biplane imaging for measurement of left ventricular volume. *Journal of the American Society of Echocardiography*. 1995;8:576-84.

529. Gordon, E.P., Schnittger, I., Fitzgerald, P.J., Williams, P. and Popp, R.L. Reproducibility of left ventricular volumes by two-dimensional echocardiography. *Journal of the American College of Cardiology*. 1983;2:506-13.

530. Huonker, M., Konig, D. and Keul, J. Assessment of left ventricular dimensions and functions in athletes and sedentary subjects at rest and during exercise using echocardiography, Doppler sonography and radionuclide ventriculography. *International Journal of Sports Medicine*. 1996;17 Suppl 3:S173-9.

531. Parikh, S.R., Hurwitz, R.A., Caldwell, R.L. and Girod, D.A. Ventricular function in the single ventricle before and after Fontan surgery. *American Journal of Cardiology*. 1991;67:1390-5.

532. Masuda, H., Kawamura, K., Tohda, K., Shozawa, T., Sageshima, M. and Honma, M. Endocardium of the left ventricle in volume-loaded canine heart. A histological and ultrastructural study. *Acta Pathologica Japonica*. 1989;39:111-20.

533. Malagon, I., Hogenbirk, K., van Pelt, J., Hazekamp, M.G. and Bovill, J.G. Effect of three different anaesthetic agents on the postoperative production of cardiac troponin T in paediatric cardiac surgery. *British Journal of Anaesthesia*. 2005;94:805-9.

534. Seghaye, M.-C. The clinical implications of the systemic inflammatory reaction related to cardiac operations in children. *Cardiology in the Young*. 2003;13:228-39.

535. Mehlhorn, U., Geissler, H.J., Laine, G.A. and Allen, S.J. Myocardial fluid balance. *European Journal of Cardio-thoracic Surgery*. 2001;20:1220-1230.

536. Tatebe, S., Davies, M.J., Tsang, V.T. and Elliott, M.J. Perioperative monitoring of left ventricular contractility. *Journal of Thoracic & Cardiovascular Surgery*. 2001;122:1036-8.